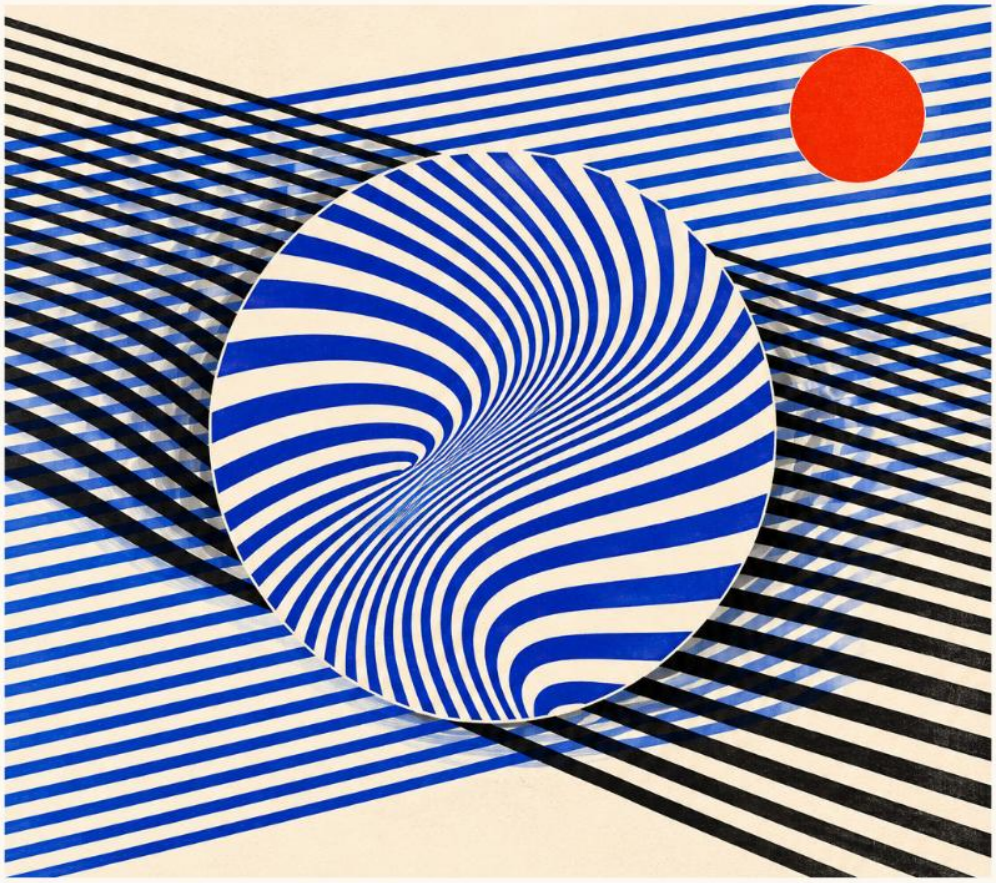
The Limit of Superposition



Eudgene Brenev
Mira Veyran

2026

The Limit of Superposition

From Superposition to Testable Hypotheses

Eudgene Brenev
Mira Veyran
2026

Preface

What This Book Is About

Quantum theory lets us calculate probabilities with great precision and control states that are difficult to reconcile with a familiar picture of separate things. Yet its practical success does not eliminate questions about the nature of a state, measurement, or the relationship between quantum description and gravity. These questions become especially interesting where distinct experimental predictions can be proposed.

The book's central subject is the search for a testable boundary between the standard quantum dynamics of an open system and an additional physical mechanism. A recurring example concerns the loss of spatial interference. The effect is concrete enough to calculate, yet complex enough to reveal the main difficulties: the environment can mimic a signal, parameters may be indistinguishable, and an idealized experiment may omit an important part of the trajectory.

The book begins with the necessary concepts and gradually moves toward contemporary research. It then considers collapse models, noise, gravitational entanglement, and physical clocks. The final part sets out working hypotheses and concepts for measurement protocols. In each area, the domain of applicability, observable quantity, and conditions under which the proposed explanation should be abandoned are essential.

An initial mathematical construction, a combination of three measurements of the decoherence rate, runs through several chapters. At first, it seems a convenient way to remove the background. An exact counterexample then emerges: ordinary random kicks can produce the same law. Further development centers on what additional information actually helps distinguish mechanisms. A general methodology thus grows out of a specific physical problem.

The book combines explanations of physical principles with tests that have been carried out. A sodium experiment with openly available data is examined through a specification of its apparatus, an environmental calculation, and a reproduction of the published analysis. A separate artificial model makes it possible to measure the false positive rate, statistical power, and interval coverage. In the gravitational sections, an ideal phase is developed into a measurement witness and a finite event count. The provenance of the data is identified in every case: our simulations are not presented as laboratory observations, and reproductions of others' results retain their attribution.

The central result of the book is methodological. An observable effect should be connected to a class of dynamical explanations, a calibration, and a decision rule. Quantitative tests are constructed for some classes; for others, exact indistinguishability is proved under limited access to the system. These results do not establish scientific priority for new physical laws. They provide a reproducible basis on which such a claim could be tested.

How to Read This Book

The first six chapters form an introduction. They suit readers familiar with the basic school-level concepts of probability, energy, and waves who do not use the quantum formalism every day. New mathematical objects are introduced through their roles in preparation and measurement. Long technical derivations are not required to follow the main argument.

The second part concerns a physical limit to superposition. The concepts become concrete: mass, branch separation, correlation length, holding time, and environmental parameters enter the discussion. Readers already comfortable with density matrices may find it useful to begin with Chapter 7 and return to the introductory definitions as needed.

The third part considers gravity and time. It does not assume that the chosen laboratory protocols have already established the quantum nature of gravity experimentally. The main task is to distinguish levels of inference: measuring a force, observing a phase, detecting entanglement, and investigating the mediator's structure answer different questions.

The final part addresses readers who want to begin calculations of their own. It gives a general spatiotemporal model a physical specification, examines the limits of its connection to collapse hypotheses, and carries out a statistical experiment with separate calibration, a search over scale, and a held-out test. The effects of finite pulses are calculated for temporal noise. The chapters show both successful recovery of an injected signal and false physical attribution when the background description is incomplete.

Formulas come with explanations of the notation and chapter-based numbering. They can usefully be read in two passes: first follow the measurement problem in the main text, then check the calculation. Numbered references point to the bibliography. The opening chapters contain complete examples with two states and two bases; the technical appendix derives formulas for likelihood, projection, and temporal noise. The glossary and running instructions let you revisit definitions and reproduce numbers without reconstructing hidden steps.

Blue and orange accents help distinguish elements; the meaning of color is specified in each figure. Teaching and design diagrams are distinguished from the apparatus of a published experiment. Objects in explanatory illustrations are not drawn to scale; quantitative relationships are specified by dimensional labels, formulas, and graphs.

Contents

Part I Fundamentals of Quantum Description

1 What quantum theory claims 6
2 States and probabilities in quantum dynamics 12
3 Measurement and environment 21
4 Entanglement and limitations on explanation 28
5 When a hypothesis changes a theory 34
6 How measurement becomes evidence 40

Part II Search for the limit of superposition

7 How to find the superposition limit 46
8 Objective collapse models 56
9 Environment as a physical model 64
10 Three measurements and the limits of their meaning 76
11 What heating and correlations add 85
12 From raw counts to a verified result 94

Part III Gravity and physical clocks

13 Why gravity is difficult to include in the quantum picture 103
14 Two masses and a test of the mediator 113
15 What does quantum time mean? 128
16 How to compare gravity models 137

Part IV Verifiable Research Program

17 Universal spatial noise hypothesis 148
18 Memory and controlled decoherence hypothesis 161
19 The limit of distinguishability and a minimal set of observations 172
20 Experimental apparatus and the full data pipeline 181
21 Results of the computational program and the limits of inference 189
What has been established and where inference ends 199
Appendix A Symbols and physical units 201
Appendix B A concise glossary 203
Appendix C Reproducing the calculations 205
Appendix D Technical derivations 207
References 210
List of figures 217

Part I Fundamentals of Quantum Description

1 What quantum theory claims

Quantum theory relates the way a system is prepared to the probabilities of the measurement results. Its unusualness is revealed even when one object can come to the detector in several ways. To understand the subsequent hypotheses, it is first necessary to establish what features of this experiment actually require explanation.

One object and many repetitions

Let's imagine a setup that releases particles one at a time. There are two available paths between the source and the screen. Each registered object leaves a local trace: a single point, a flash or an electrical impulse. After many repetitions, a distribution of hits emerges. Under certain conditions it contains alternating regions of high and low probability. These bands make up the interference pattern.

An individual point and a distribution of points answer different questions. The first shows where a particular interaction with the detector ended. The second characterizes the statistics of identically prepared experiments. Therefore, the phrase “a particle behaves like a wave” requires clarification: the wave structure appears in the rules for calculating probabilities, although the registration can be local. It is usually impossible to restore this entire structure from one hit.

One of the historical steps towards testing this behavior for complex objects was made in 1999: interference was observed for molecules C60. It is important that we were talking about the center of mass of a molecule consisting of many atoms, and not about an individual electron inside it. This result expanded the class of systems for which it was possible to implement the corresponding experiment [1]. Subsequent experiments with more massive objects are discussed in the seventh chapter.

The two-path thought experiment is useful precisely because of its simplicity. It allows you to discuss preparation, installation, and registration separately. If these stages are confused, it is easy to mistake a change in the source for a change in the laws of motion, or a feature of the detector for a fundamental limit of nature. In real work, each stage gets its own model and its own checks.

Amplitude and probability

For the two alternatives, standard quantum mechanics first adds the amplitudes. They can be complex numbers, so they cannot be identified with positive probabilities. After addition, the square of the modulus is calculated. It is at this step that a term appears that depends on the relative phase of the two contributions.

Let the amplitudes of arrival at a certain point on the screen be equal to a and b. If both alternatives participate coherently, the probability is proportional to the square of the modulus of their sum. With an independent classical choice of path, the

probabilities would add up. The difference between these procedures can be tested by varying the relative phase and observing the movement of the fringes.

The phase is not an additional probability that the object “changed its mind” to follow the chosen path. It specifies the relative position of complex amplitudes. A convenient geometric analogy is two oriented segments on a plane: the result of addition depends on both their lengths and the angle between them. The analogy explains the calculation, but does not itself tell what physical substance the wave function is made of.

With equal moduli of contributions, the relative phase can enhance the probability at one point and suppress it at another. The probability never becomes negative: the squared modulus is always non-negative. The disappearance of probability in a certain area means redistribution among acceptable outcomes while maintaining full normalization. If losses are possible, the “particle not registered” outcome should also be included in the full result set.

$$|a+b|^2 = |a|^2 + |b|^2 + 2\mathrm{Re}(a^* b)$$

(1.1) The last term is interference. The asterisk denotes the complex conjugate, and Re highlights the real part.

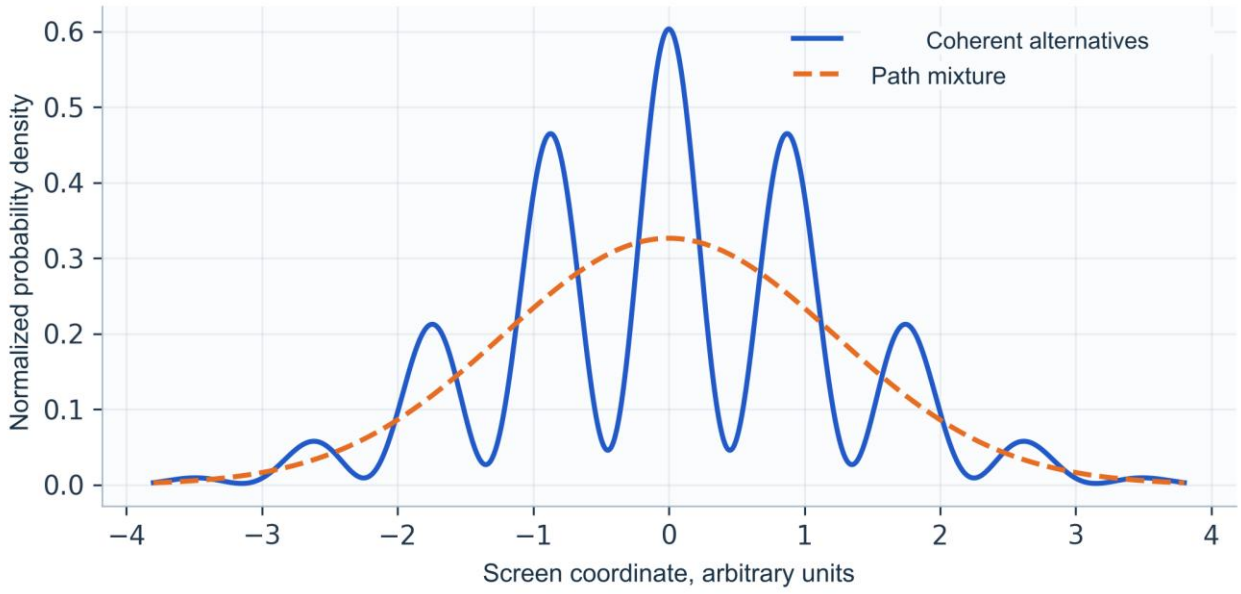


Figure 1. The addition of amplitudes creates interference fringes. Normalized model distributions are shown; their overall envelope is the same.

Superposition and ignorance

It is possible to prepare the object so that in half of the experiments the left path is open, and in the other half the right path is open. If you forget which option was chosen, you end up with a statistical mixture. In another procedure, both paths remain coherent and their relative phase is controlled. When measuring only the position before the paths are brought together, both preparations may produce the same statistics. After mixing, the difference becomes observable.

Therefore, ignorance of the result and quantum superposition are not interchangeable concepts. The system may be poorly known to the experimenter and yet be described by a mixture of states. It may also be prepared in a known pure state from which the single outcome of the chosen measurement cannot be predicted in advance. To distinguish between these cases, you need to specify which measurements are available.

There is also the opposite subtlety. What appears to be a mixture for one object may arise from the pure entangled state of a larger system. If only the object is available, some correlations remain unavailable. Its local description then does not contain all the information about the joint state. In the third chapter this transition will be shown by explicit calculation.

When the expression “an object is in two places” is used, it briefly denotes preparation with spatially separated coherent components. It should not replace the description of experiment with a picture of two classical copies, each of which has all the properties of the original body. What quantities are determined and what correlations exist is decided by the specific state.

A single trial and the expected pattern

In the two-path example, you can go straight to the numbers. Let the source prepare equal amplitudes, and before the paths converge, phase φ is established in the right branch. The combined beam comes to two outputs, indicated by plus and minus signs. The ideal setting is designed so that at zero phase the amplitudes are amplified at the plus output and cancel each other at the minus output. During phase π, the outputs change roles.

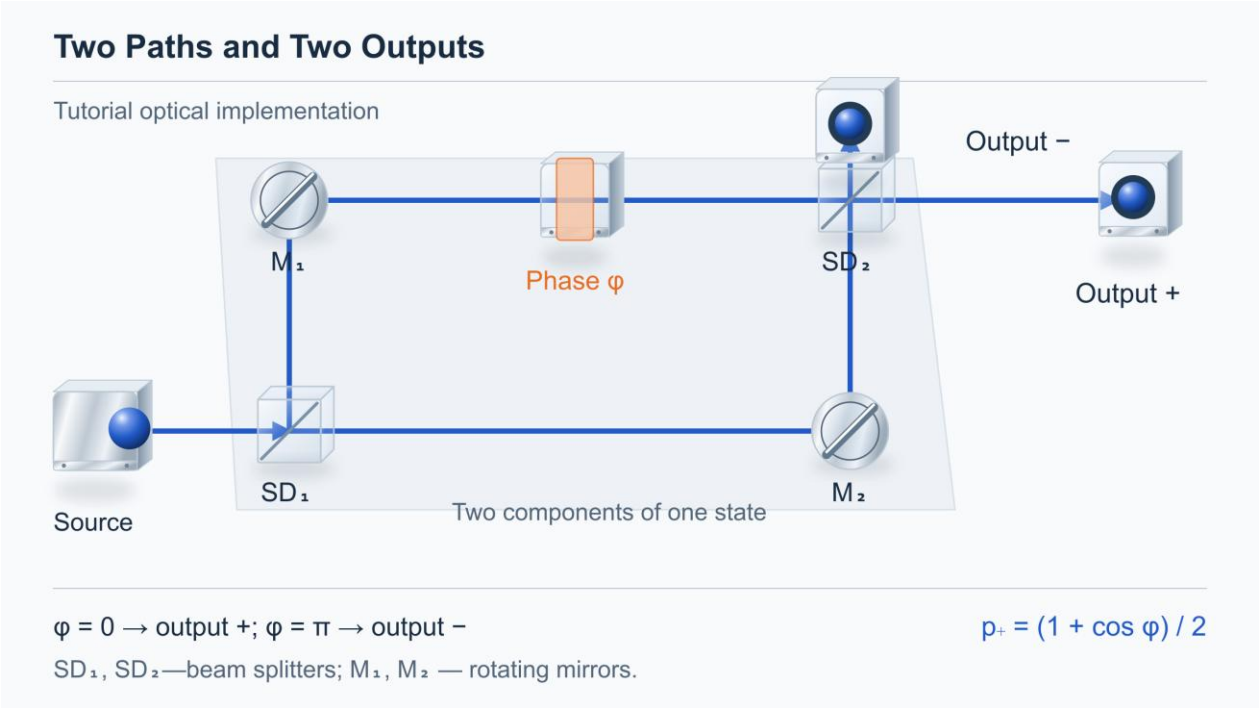


Figure 2. Training two-path interferometer: two beam splitters, two rotating mirrors, a phase element and two detectors. In the chosen convention, the ideal setting gives $p_+(\varphi) = (1 + \cos \varphi)/2$: when $\varphi = 0$ the plus output is triggered, when $\varphi = \pi$ the minus output is triggered. The blue lines represent the state components of a single object. This is a training optical circuit, not a MUSCLE sodium setup.

When $\varphi = \pi/2$ both outcomes are equally probable. For a thousand identical runs, approximately five hundred registrations are expected per output. This is a mathematical expectation, and not a promise of strictly equal integers in each series. If the runs are independent, the standard deviation of the number of registrations of one output is equal to the root of $Np(1-p)$. With $N = 1000$ and $p = 1/2$ it is about 15.8. Therefore, for example, a moderate difference between two counters does not in itself mean a breakdown of the interferometer.

Now the path is chosen randomly during preparation. In half of the runs the object is sent to the left branch, in half - to the right; there is no coherent connection between them. After perfect convergence, both outputs give the probability 1/2 at any phase. Thus, the difference between the two preparations is not visible at a single point on the detector, or even in one set of five hundred events. It appears as a distribution depending on the controlled setting.

This scene will be repeated in the book with gradually more detailed descriptions. In the second chapter, probabilities are obtained from matrices. In the third, a physical record of the path will appear in the marker. The sixth will add registration losses and exit label errors. Thanks to this, the abstract “loss of coherence” is each time associated with what events have changed and what additional dimension allows us to understand the reason.

The zero probability in the ideal formula has a precise meaning: the corresponding amplitude is set to zero in the given model. The laboratory recording may still contain background events, slight phase error, and imperfect mixing. Therefore, ideal zero is useful as a control limit for the calculation. To assess the real effect, it is necessary to

separately describe which ordinary processes create the counts in the almost dark output.

$$p_+(\varphi) = \frac{1 + \cos\varphi}{2}$$
$$p_-(\varphi) = 1 - p_+(\varphi).$$

(1.2) Probabilities of two outputs of an ideal interferometer with equal amplitudes. For an equally probable mixture of paths, both probabilities are equal to 1/2, regardless of phase.

What counts as an observation?

In a physics protocol, observation means an interaction that relates the state of a system to the distinguishable states of a device or environment. The detector is able to register an event while there is no person in the room. Data can be saved and read later. To calculate the readings of such a device, the standard formalism suffices to describe the interaction, preparation and reading.

This does not resolve all philosophical questions about consciousness and experiment. It establishes a narrower fact about the construction of the model: a separate “person looked” variable is not introduced into the equations studied here. If a physical dependence on conscious perception is proposed, it must be formulated as an independent hypothesis with its own observable consequences. Simply using the word "observer" is not enough for this.

It is especially important to distinguish between the acquisition of path information and its subsequent use. If information is physically recorded in another entity and that entity is not controlled, interference from the selected subsystem may be reduced regardless of who reads the record. The quantitative relationship between available path information and interference visibility has been explored, in particular, in Englert's work [2].

In the following, the words “observer”, “sensor” and “reading system” will refer to specific physical roles. Such language allows claims to be tested without hidden transitions between experiment and worldview. It also helps you notice when a popular explanation promises more than the measurements suggest.

The scope of the question

The success of a quantum calculation for a certain range of masses, energies and times does not prove its applicability in all possible conditions. Any experimental test has a range of sensitivity. At the same time, the lack of direct experiment with an arbitrarily large object is not evidence of a violation of the theory. In between these statements lies work to expand the measurement range.

This book focuses on spatial coherence, open quantum systems, and testable changes in dynamics. Quantum field theory, particle physics and the design of quantum computers appear where they help pose a specific question. A complete presentation of all branches of quantum physics would require a different structure and a different volume.

The main interest is the transition from general doubt to comparison of predictions. The question “is quantum mechanics complete” becomes experimental when two models, setup parameters, and data by which they can be distinguished are specified. This clarification does not reduce the fundamental nature of the problem. It shows what kind of work is needed so that the answer no longer depends only on the preferred picture of the world.

In the next chapter this conversation takes on mathematical language. For the main line of the book, a few objects are enough: a state vector, a density matrix, a rule for calculating probabilities, and an equation of motion. Each of them will be introduced through the problem it solves.

2 States and probabilities in quantum dynamics

The mathematics of quantum theory is needed to compare preparations and measurements. Symbols acquire meaning through operations that can be performed or at least precisely defined. This chapter introduces a minimal set of notation and shows what requirements a possible modification of the theory must preserve.

State vector

If a system has two distinguishable underlying states, it is convenient to denote them as zero and one. For an interferometer, these can be left and right branches; for another device the meaning will be different. Notation as a vector means that an arbitrary pure state is represented by a linear combination of selected underlying states.

The coefficients determine the amplitudes. Their squared moduli give the probabilities of the corresponding outcomes in a given basis, and normalization expresses that the sum of the probabilities is equal to one. Multiplying the entire vector by the same phase factor does not change the observed probabilities. The relative phase between components, on the other hand, may appear after changing the measurement method.

Basis is a recording method associated with the selected distinguishable alternatives. Replacing it does not create a new object in the laboratory. However, a physical operation that rotates the state relative to a fixed meter changes the statistics. It is useful to distinguish between a mathematical change of coordinates and a real impact on the system: mixing these actions often gives rise to false paradoxes.

Even for two states, a complete prediction cannot be obtained only from the probabilities of zero and one. Two preparations with the same probabilities may differ in relative phase. To detect the difference, a measurement in a different basis is needed. This capability will form the basis of state recovery and coherence testing.

$$|\psi\rangle = \alpha|0\rangle + \beta|1\rangle$$

$$|\alpha|^2 + |\beta|^2 = 1$$

(2.1) Coefficients α and β are complex amplitudes. The probabilities of 0 and 1 in the chosen basis are equal to the squares of their absolute values.

Density matrix

Not all preparation is described by one vector. The source may randomly select different pure states, but the researcher may only have access to part of the larger system. In both cases it is convenient to use the density matrix. It combines the information needed to calculate local probabilities.

For a known pure state, the matrix is obtained from the outer product of a vector and its conjugate vector. For a statistical mixture, such matrices are added with

weights equal to the preparation probabilities. The diagonal elements in the selected basis specify the probabilities of the underlying outcomes. Off-diagonal elements characterize coherent connections relative to this basis.

Two equally populated paths provide a particularly clear example. In a coherent superposition, the matrix contains off-diagonal elements. In a mixture where the path is chosen randomly and there is no phase coupling, these elements are equal to zero. Measuring the path does not differentiate between preparations because the diagonals are the same. The convergence of paths and subsequent measurement distinguishes them.

The word "off-diagonal" always refers to a specific basis. It is possible to diagonalize the matrix mathematically, but such a notation in itself does not prove that a physical collapse occurred in the experiment. The question is about changing predictions given a fixed description of preparation and reading, not about the arrangement of numbers on the page.

$$\rho = \sum_j p_j |\psi_j\rangle\langle\psi_j|$$

$$p_j \geq 0$$

$$\sum_j p_j = 1$$

(2.2) The density matrix can represent a mixture of preparations. Different decompositions of the same matrix do not have to correspond to locally distinguishable situations.

$$\rho_+ = \frac{1}{2}\begin{pmatrix} 1 & 1 \\ 1 & 1 \end{pmatrix}$$

$$\rho_{\text{mix}} = \frac{1}{2}\begin{pmatrix} 1 & 0 \\ 0 & 1 \end{pmatrix}$$

(2.3) The first matrix describes a coherent state with equal amplitudes, the second - an equally probable mixture of two basic states.

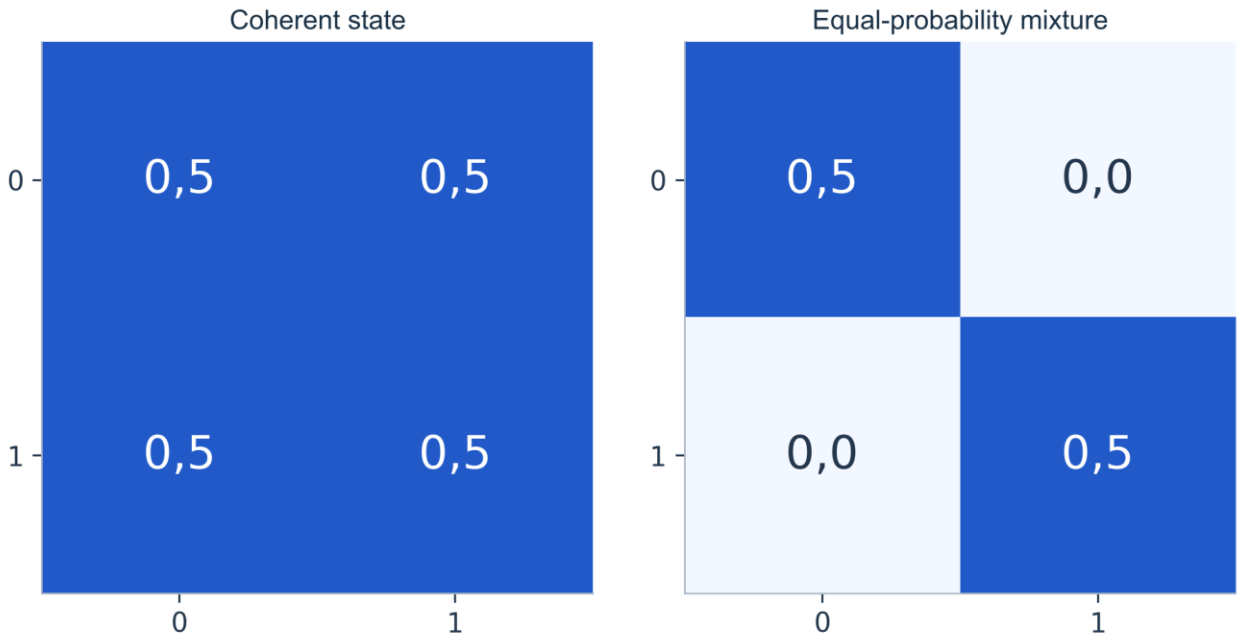


Figure 3. Matrices of two preparations with identical diagonals. Off-diagonal elements are different, so measuring in a different basis may distinguish preparations.

Rule of Probability

A measurement is defined by a set of possible outcomes and corresponding operators. In the simplest ideal case, projectors onto distinguishable states are used. For real instruments, a more general set of positive operators whose sum is equal to unity is more useful. Such a set is called a positive operator-valued measure (POVM). It allows you to take into account the finite resolution and some reading features without claiming that the device is ideal.

The probability of an outcome is calculated from the state and operator of that outcome. This rule relates an abstract matrix to the frequencies of observed events. It also shows why different states can be indistinguishable by a limited set of measurements. If the chosen operators are insensitive to differences between matrices, additional repetitions of the same experiment will not recover the missing information.

Normalization and positivity of the density matrix have a direct physical meaning. A negative probability or a sum of probabilities other than one for the full set of outcomes indicates a problem with the model or an incorrect description of the data selection. A possible new theory must explicitly explain how it obtains the acceptable probabilities. A beautiful equation of motion does not exempt you from this check.

In state reconstruction, finite statistical errors sometimes produce a formal matrix with a small negative eigenvalue. This is not automatically a violation of quantum mechanics. First, the statistical procedure, calibration, and reconstruction constraints need to be verified. Observed statistics and the result of numerical reconstruction are different levels of description.

$$p(k) = \mathrm{Tr}(\rho E_k)$$

$$E_k \geq 0$$

$$\sum_k E_k = I$$

(2.4) The operators E_k describe measurement outcomes. The trace Tr sums the diagonal elements of the product and gives the probability of the corresponding outcome.

Two bases and four probabilities

Let's consider two already written matrices, ρ_+ and ρ_{mix}, as two instructions for predicting one device. The path measurement is described by the projectors $P_0 = |0\rangle\langle 0|$ and $P_1 = |1\rangle\langle 1|$. In the accepted notation, these are diagonal matrices with a single unit. When multiplying by ρ and taking the trace, the corresponding diagonal element is isolated. Both preparations yield p(0) = p(1) = 1/2.

To measure another quantity, the paths are converged with a controlled relative phase. At zero phase, the plus output corresponds to the vector $|+\rangle = (|0\rangle+|1\rangle)/\sqrt{2}$, and the minus output corresponds to the vector $|-\rangle = (|0\rangle-|1\rangle)/\sqrt{2}$. The projector P_+ coincides with the matrix ρ_+. The trace of the square of ρ_+ is equal to one, so the coherent preparation hits the output plus with probability one. For a mixture, the trace of the product of I/2 and P_+ is equal to 1/2. The same two rows of the matrix are used here; no new physical variable was needed to make the difference.

It is useful to perform one multiplication manually. The product ρ_{mix} P_+ is equal to a matrix whose all elements are equal to 1/4. The sum of its diagonal elements is 1/2. On the contrary, $\rho_+^2 = \rho_+$, and the sum of the diagonal is equal to one. Thus, a rule with a trace turns the qualitative word “coherence” into a verifiable difference between two distributions. For outcomes, the minus probabilities are complemented to one: zero and 1/2, respectively.

Let us now introduce phase and gradual decay. For equal populations, we denote the relative coherence modulus by v, where $0 \leq v \leq 1$. A vector with right-hand amplitude $\exp(i\varphi)/\sqrt{2}$ gives the upper off-diagonal element $\exp(-i\varphi)/2$; after the selected dephasing channel it becomes $v \exp(-i\varphi)/2$. The eigenvalues of the matrix are equal to $(1\pm v)/2$. Therefore, the specified range of v both provides a valid state and limits visibility.

Measuring the path still gives two probabilities 1/2. The measurement after reduction gives $p(+) = [1+v\cos\varphi]/2$. For example, with v = 0.6 and φ = 0, the probability of exit plus is equal to 0.8, with $\varphi = \pi/2$ it is equal to 0.5, with $\varphi = \pi$ - 0.2. These are three calculated values of one state with three settings. They are not an experimental assessment of any mechanism.

This comparison also shows the limits of the method. The measured values can determine v and φ within the model, but do not tell how v is reduced. Mixing during preparation, uncontrolled phase and interaction with the environment can lead to one local matrix. To find the cause, you will need preparation conditions, time

dependencies and independent observations, which are discussed in the following chapters.

$$P_+ = \frac{1}{2}\begin{pmatrix} 1 & 1 \\ 1 & 1 \end{pmatrix}$$

$$P_- = \frac{1}{2}\begin{pmatrix} 1 & -1 \\ -1 & 1 \end{pmatrix}.$$

(2.5) These are two measurement projectors in the plus and minus basis. Their sum is equal to I, and their product is equal to zero.

$$\rho(v, \varphi) = \frac{1}{2}\begin{pmatrix} 1 & v e^{-i\varphi} \\ v e^{i\varphi} & 1 \end{pmatrix}$$

$$p_+ = \frac{1 + v\cos\varphi}{2}.$$

(2.6) The parameter v describes the relative coherence modulus for this two-level example. It does not specify a physical reason for its decrease.

Preparation	**p(0)**	**p(1)**	**p(+)**	**p(−)**
Coherent state |+⟩	1/2	1/2	1	0
Equiprobable mixture	1/2	1/2	1/2	1/2
v = 0.6 and φ = 0	1/2	1/2	0.8	0.2

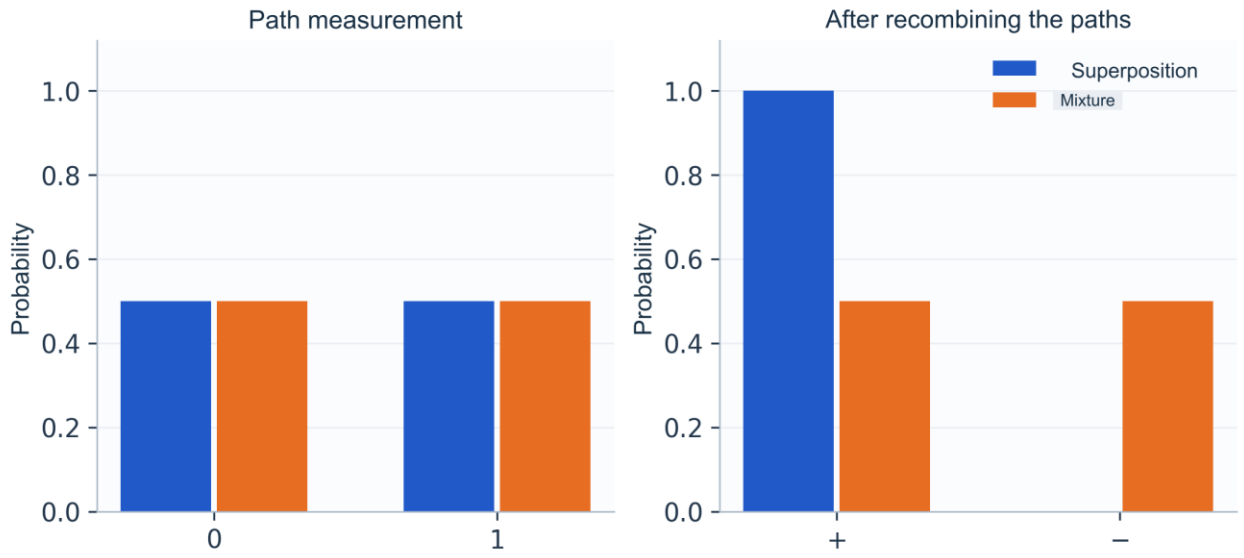


Figure 4. The two bases differentiate the two preparations in different ways. In the path basis, the probabilities are the same; after mixing, the coherent preparation and mixture give different yields. All values are calculated from the written matrices.

What happens after the result

The probabilities of the first measurement do not yet determine the state that the second device will encounter. A complete description must link each recorded outcome to a system transformation. In quantum theory, this defines a measuring instrument: for the result k, a completely positive mapping $\mathscr{J}_k$ is used, and the sum of the mappings preserves the trace. The probability of the outcome is equal to the trace of the non-normalized output state. The normalized state after selecting the result is obtained by dividing by this probability. Such a device is especially important for sequential and conditionally selected measurements. [56]

In the finite-dimensional case, the mapping can be represented by Kraus operators $M_{k\alpha}$. The additional index α takes into account physically indistinguishable variants of the same result k. The sum of $M_{k\alpha}^\dagger M_{k\alpha}$ over α gives the effect operator E_k, which was included in the probability rule. Therefore, the instrument detects the POVM, but the POVM alone is usually not sufficient to recover the instrument. This difference becomes visible already in the experiment with two states.

Let the device poorly distinguish paths. Its two operators K_+ and K_- are diagonal; the parameter μ between zero and one sets the strength of discrimination. When $\mu = 0$ both operators are proportional to unity: the record does not report anything about the path and the state does not change. When $\mu = 1$ we get projectors on the path. The intermediate case allows one to obtain part of the information while maintaining part of the coherence.

For input $|+\rangle$ and $\mu = 0.6$, each sign of the device appears with probability 1/2. After the result plus, the normalized matrix has diagonals 0.8 and 0.2, and both off-diagonal elements are 0.4. It remains pure: the determinant is zero. The result does not mean that a perfect path measurement has occurred; it changed the relative amplitudes and made one path more likely.

Let's compare two devices. The first after receiving the plus sign leaves the system in the indicated state. The second gets exactly the same entry and then swaps the paths with operator X. Its operator for this outcome is XK_+. Since $X^\dagger X = I$, the probabilities of the first sign of the two devices are the same for any input. But at the next measurement of the path, the probability of zero is 0.8 for the first and 0.2 for the second. The same set of E_k effects does not describe this difference.

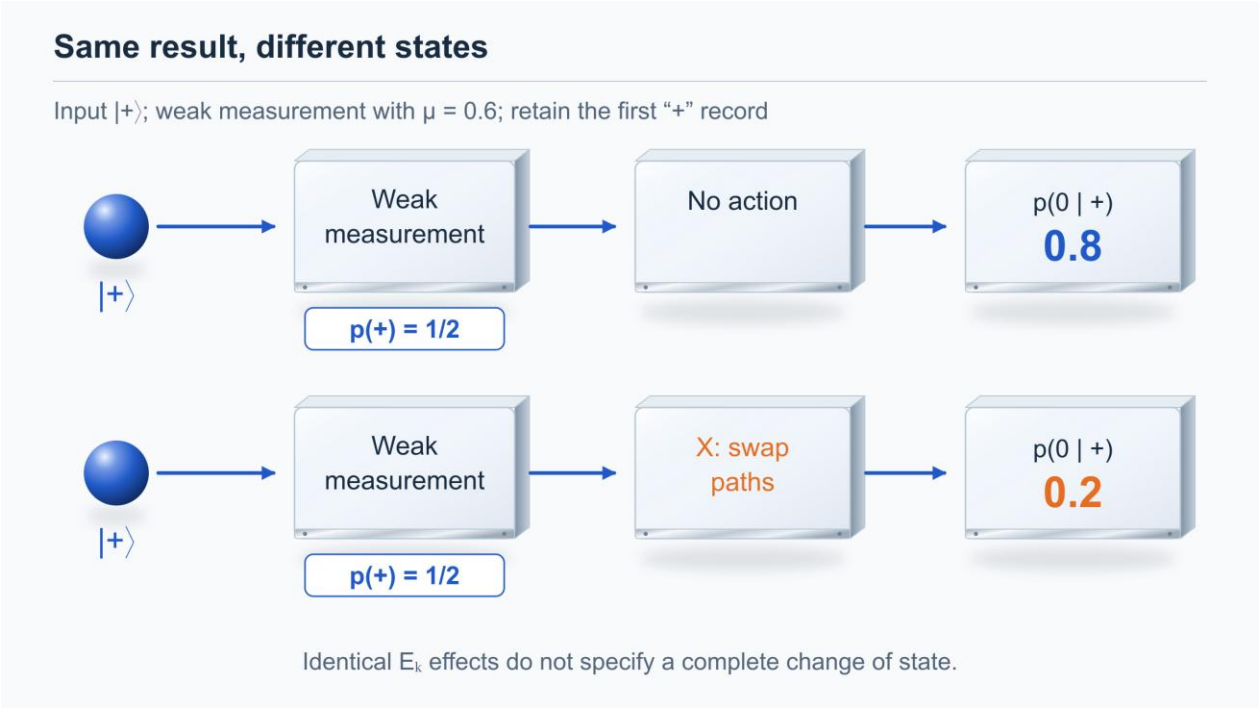


Figure 5. The two measuring instruments have the same E_k effects, but differ in what they do after recording. For input $|+\rangle$ and $\mu = 0.6$, the probability of the first entry plus is equal to 1/2. After its selection, the next result of the path 0 has a probability of 0.8 without additional action and 0.2 after physically rearranging the paths X. The coincidence of the first statistic does not determine the state after the measurement.

If a weak device's record is lost, both unnormalized output states are added together. With $\mu = 0.6$, the diagonals return to 1/2, and the coherence is multiplied by $\sqrt{(1-\mu^2)} = 0.8$. After the paths are converged, the probability of plus is equal to 0.9. Conditional prediction with a known record and unconditional prediction after removing it answer different experimental questions. This distinction will be needed when discussing the medium, continuous measurement, and the supposed objective collapse.

$$\mathcal{J}_k(\rho) = \sum_\alpha M_{k\alpha} \rho M_{k\alpha}^\dagger$$

$$E_k = \sum_\alpha M_{k\alpha}^\dagger M_{k\alpha}.$$

(2.7) The tool determines both the probability of the outcome and the unnormalized state after it. Summing all effects gives I.

$$p_k = \mathrm{Tr}\,\mathcal{J}_k(\rho)$$

$$\rho_k = \frac{\mathcal{J}_k(\rho)}{p_k} (p_k > 0).$$

(2.8) The conditional state is defined for non-zero probability outcomes. If a record is lost, the output is equal to the sum $\mathcal{J}_k(\rho)$, without additional normalization of each term.

$$K_+ = \begin{pmatrix} \sqrt{(1+\mu)/2} & 0 \\ 0 & \sqrt{(1-\mu)/2} \end{pmatrix}$$

$$K_- = \begin{pmatrix} \sqrt{(1-\mu)/2} & 0 \\ 0 & \sqrt{(1+\mu)/2} \end{pmatrix}.$$

(2.9) Two weak path measurement operators. Here 0 ≤ μ ≤ 1; their squares are summed into an identity matrix.

$$\rho_{+\text{record}} = \begin{pmatrix} 0.8 & 0.4 \\ 0.4 & 0.2 \end{pmatrix}$$

$$X\rho_{+\text{record}}X = \begin{pmatrix} 0.2 & 0.4 \\ 0.4 & 0.8 \end{pmatrix}.$$

(2.10) Two different states after the same statistics of the first result. The reversal of paths becomes discernible in the next measurement.

Closed and open system

For an idealized closed system, the evolution of the state is given by the Hamiltonian. It determines how phases change and how amplitudes are redistributed. Unitary dynamics preserves normalization and allows inverse transformation at the level of full mathematical description if the Hamiltonian and control are known.

An open system exchanges information and sometimes energy with its environment. Its state usually cannot be described by one unitary operator acting only on it. This does not mean an immediate abandonment of quantum mechanics. It is possible to describe a coupled system and then exclude unavailable degrees of freedom when calculating local probabilities.

In certain Markov approximations, the dynamics of the density matrix is written in the form established by the work of Gorini, Kossakovsky, Sudarshan and Lindblad. Its structure ensures complete positivity and preservation of the trace under appropriate conditions [8, 9]. These works characterize the class of generators; they do not claim that every real environment is memoryless.

Complete positivity means the correctness of the transformation even in the case when the system under consideration is entangled with an additional one, which is not affected by the transformation. Conventional positivity only for an isolated set of inputs may not be sufficient. This subtlety is essential when building new dynamic models: they need to be tested on composite systems.

$$i\hbar \frac{d|\psi\rangle}{dt} = H|\psi\rangle$$

(2.11) Schrödinger equation for a closed system. The constant $\hbar$ translates energy into the rate of phase change scale.

$$\dot{\rho} = -\frac{i}{\hbar}[H, \rho] + \sum_k \left(L_k \rho L_k^\dagger - \frac{1}{2}\{L_k^\dagger L_k, \rho\} \right)$$

(2.12) A Markov generator in GKSL form. Square brackets denote a commutator and curly brackets an anticommutator. Rate parameters may be included in the operators L_k.

Why formulas alone are not enough

The same form of an equation can arise from different microscopic descriptions. The additional coherence-reducing term may represent collisions, a fluctuating field, or a putative fundamental mechanism. Therefore, calling a term “collapse” does not mean establishing its origin.

For physical interpretation, it is necessary to indicate which variables it refers to, which parameters are considered universal, and how it changes under controlled changes in conditions. If the coefficient is freely chosen separately for each experiment, the model can describe the observations, but its predictive power is limited. The universal hypothesis makes a stronger requirement for consistency.

A specific example sets a convenient procedure for testing new dynamics. First, the normalized probabilities of a single measurement are calculated, then the joint probabilities of the sequence, and then environment and control are added. Approximations—point body, white noise, constant distance—are introduced at the step where they simplify the corresponding calculation. The limits of these simplifications will be shown in subsequent parts.

It is now possible to describe a measurement as the interaction of two or more quantum systems. It is in this description that the role of the environment becomes visible and the question arises of what decoherence explains and what remains beyond its immediate result.

3 Measurement and environment

The measuring device must change so that its state depends on the state of the object being studied. This simple task leads to entanglement. If the device interacts with the environment, some of the correlations become unavailable and local interference weakens. Here you can trace the entire transition without resorting to the metaphor of the human gaze.

How does a recording appear?

Let's consider a device with an initial readiness state. It is designed so that an object in state zero transfers it to one record, and an object in state one transfers it to another. For these two inputs, the operation of the device seems completely classical: each input corresponds to a specific output.

But quantum dynamics is linear. If the input is a superposition of two states, after the interaction, a superposition of two correlated combinations of object and device is obtained. The formal result contains the relationship between the object's state component and the corresponding record. You cannot replace it with one of the combinations just because the device is large.

This creates the central tension of the measurement problem. The linear model of joint interaction gives a certain state, while in each specific read a certain record is recorded. Different interpretations and modifications of the theory relate these levels of description in different ways. Before discussing them, it is necessary to understand what the instrument's environment does.

The two records must be sufficiently robust and distinguishable for the selected reading procedure. Not every short-term interaction produces a usable measurement result. If the states of the device almost coincide, information about the object is small. If they change quickly and unpredictably, the record may not persist until it is read.

$$(\alpha|0\rangle + \beta|1\rangle)|D_{\text{ready}}\rangle \longrightarrow \alpha|0\rangle|D_0\rangle + \beta|1\rangle|D_1\rangle$$

(3.1) The idealized measurement interaction relates two input states to two instrument records. Linearity preserves the superposition of joint alternatives.



Figure 6. The object interacts with the device, and information about the recording state can be propagated to the environment through further interactions. The bottom rows show joint description alternatives, rather than two simultaneously read outcomes of the same run. Decoherence in itself is not evidence of the choice of a single outcome. Conceptual scene: geometry, scale and number of environmental fragments do not define a quantitative model.

What does the subsystem see?

Let the left and right branches of the object correlate with two states of the environment. The joint state remains pure in the idealized model, but the local density matrix of the object is obtained after eliminating the medium. Its off-diagonal element is multiplied by the overlap of the two environmental states.

If the environment in both cases is almost the same, the overlap is close in magnitude to unity, and phase coupling is available to the object. If the environment can reliably distinguish paths, there is little overlap. Then the interference of the object weakens, even if the medium was not specially measured and no one read its state.

For several independent fragments of the environment, the joint overlap becomes the product of individual overlaps. For example, if each of one hundred conditional fragments has an overlap of 0.99, the product is about 0.366. With a thousand such fragments it is about 0.000043. These numbers refer to a mathematical example and not to a specific experimental setup. They show how many weak correlations can make local interference virtually impossible.

The independence of the fragments is essential here. The real environment may have spatial and temporal correlations, so a simple product is not always acceptable. It is precisely such details that become decisive when trying to separate ordinary decoherence from an additional mechanism.

$$|\Psi\rangle = \frac{|L\rangle|E_L\rangle + |R\rangle|E_R\rangle}{\sqrt{2}}$$

$$\rho_{LR} = \frac{1}{2}\langle E_R|E_L\rangle$$

(3.2) A partial trace across the medium leaves an overlap of its states in local coherence. This is a direct calculation for the selected joint state.

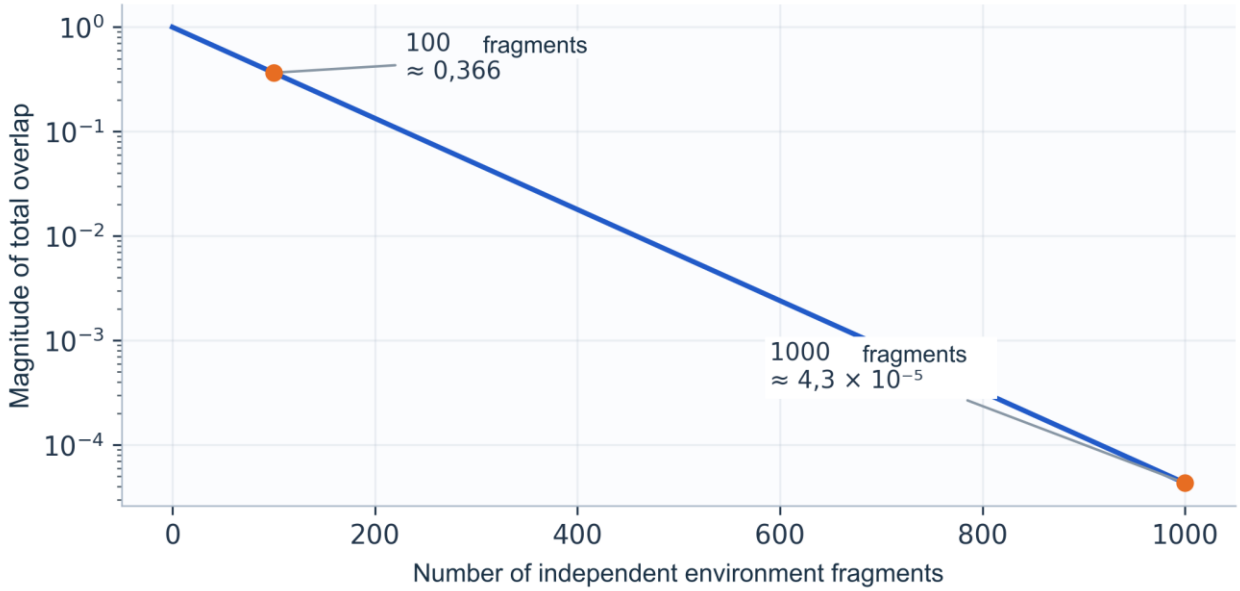


Figure 7. Mathematical example of correlation accumulation. When overlapping 0.99 for each independent fragment, the total multiplier is equal to 0.99 to the power of N.

Why are some records more durable than others?

The environment usually interacts with certain physical quantities. For example, scattered radiation can carry information about the position of an object. States that are stably correlated with the environment during such interaction play a special role in the formation of observed records.

In the work of Zurek 1981, the connection between the stable basis of the device and the Hamiltonian of its interaction with the environment was formulated explicitly. The subsequent description of environmentally induced superselection rules developed this idea [3, 4]. For this book, a specific consequence is important: the choice of stable recordings depends on the physics of communication with the environment, and not on the arbitrary preference of the experimenter.

This result helps explain why certain macroscopic records are usually available in everyday measurements. However, a statement about the stability of a certain set of states is not identical to a statement about the choice of one outcome in a separate experiment. It characterizes the dynamic structure of correlations and the suppression of observed interference between records.

The distinction becomes especially important when creating alternative models. If the added term of the equation simply reduces the off-diagonal elements of the

ensemble matrix, it does not follow that the history of a single event is completely described. For such a conclusion, it is necessary to specify additional rules or dynamics of individual states and show their connection with the ensemble description.

Reversibility and access to correlations

In an idealized closed system, unitary evolution can be inverted by a suitable inverse operator. But if an object is entangled with a huge number of uncontrolled degrees of freedom, implementing such an inversion becomes a separate physical problem. The reversibility of the equation does not mean that the laboratory has access to all the necessary variables.

Therefore, practical irreversibility can arise without fundamentally violating the unitarity of the full description. What matters in an experiment is the scale of loss of control: how much information is available, what influences are allowed, and how long the record is retained. The statement “the interference has disappeared” always refers to a certain set of available operations.

We can consider a simple model of marking a path with an additional two-level object. If the marker stores different records for the left and right branches, interference without conditioning on the marker is reduced. With suitable joint measurement, correlations can emerge in conditional subsets of the data. This does not allow arbitrary changes to the already recorded past: it is a question of which joint probabilities are analyzed.

Post-selection requires special care. Showing only a selected subset of events may provide a picture that is not present in the full distribution. The physical statement must be accompanied by a probability of being in a subset and a rule for selecting it. Otherwise, a change in statistics can easily be mistaken for a new causal effect.

Path recording and conditional interference

Let's take a marker with two orthogonal states. After perfect marking, the joint state of the object and the marker is $(|0\rangle|0\rangle+|1\rangle|1\rangle)/\sqrt{2}$. The partial trace along the marker gives the object the matrix I/2. After path convergence, any phase shift leaves the local output probabilities equal to 1/2. All phase information did not disappear from the joint description: it ceased to be available only for the object.

Now the marker is measured in plus and minus basis. For each sign the probability is equal to 1/2. With a plus sign, the conditional state of the object is $|+\rangle$, with a minus sign - $|-\rangle$. After the phase shift φ and convergence, the probability of output plus is $[1+\cos\varphi]/2$ and $[1-\cos\varphi]/2$, respectively. Two conditional interference patterns are shifted by half a period.

The sum with the correct weights returns a local prediction: half of the first curve plus half of the second is equal to 1/2 at any phase. For example, when $\varphi = 0$ the event “marker plus and object plus” has a probability 1/2, “marker minus and object plus” has a probability of zero. But all the events with the plus object still take up half

of the full series. The sort did not create additional registrations; it shared existing joint events.

For a device that reads only an object, the meaning of the marker sign is unknown. Therefore, it is not possible to know from one local record whether a marker was measured in a path basis or in a plus and minus basis. To see conditional bands, you need to compare both records and apply a predefined selection rule. This is a specific version of the difference between correlation and controlled signaling.

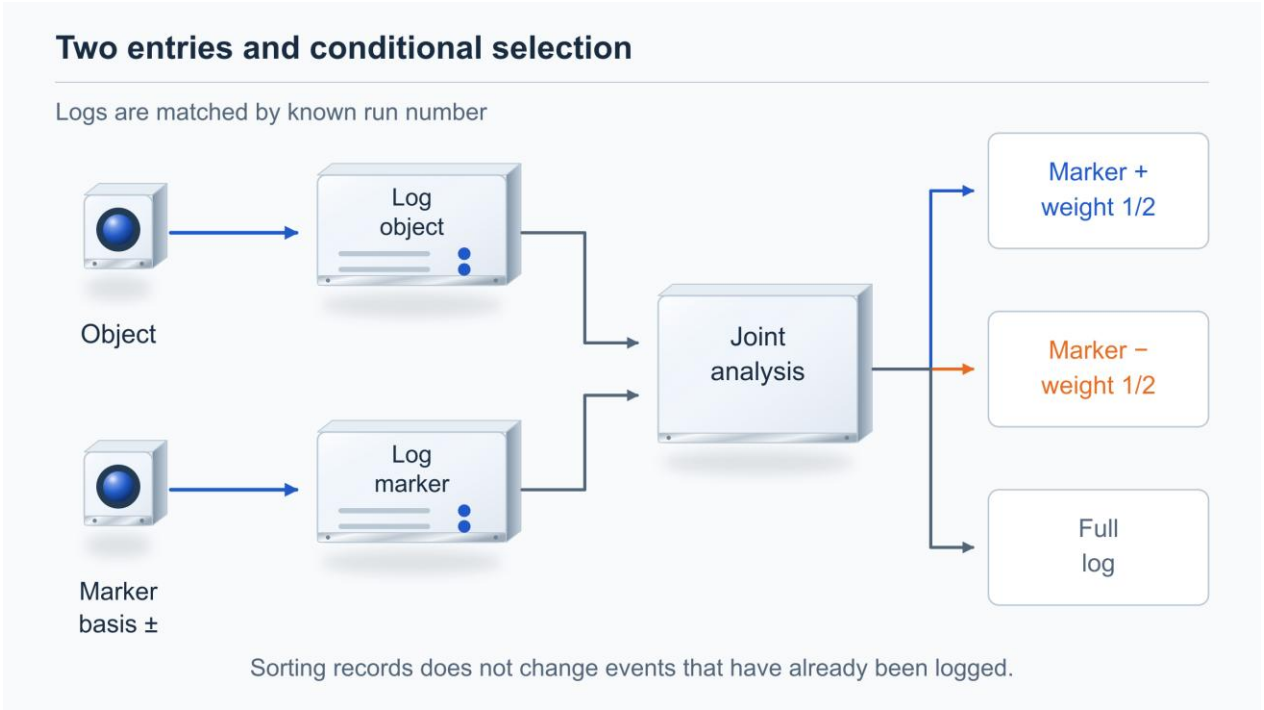


Figure 8. For conditional statistics, you need to compare the classic object and marker logs. Marker sign selection produces two subsets with weights 1/2 in the example in this chapter; the full log is saved. Neither the local entry of the object nor the subsequent sort by itself provides a controlled message or effect on an already completed run.

The intermediate marking is also calculated directly. If the marker states have real overlap c = 0.5, the local object matrix receives off-diagonal elements 0.25 and visibility v = 0.5. At zero phase, the probability of plus is equal to 0.75. Thus, a continuous decrease in the overlap of the environment sets a continuous change in the observed probabilities; ideal orthogonal entries are the limit c = 0.

In this example, restoration of conditional interference requires a specially available token. For macroscopic environments, such access may be practically impossible. Nevertheless, the model is useful: it shows which correlations were excluded by the partial trace and what exactly had to be returned to the set of observations. To argue for the restoration of coherence without taking into account the probability of selection would be to compare different statistical problems.

$$|\Psi\rangle = \frac{|00\rangle + |11\rangle}{\sqrt{2}} = \frac{|+\rangle|+\rangle + |-\rangle|-\rangle}{\sqrt{2}}.$$

(3.3) The same entangled pair is written in two bases. The first character refers to the object, the second to the marker.

$$p(x = +, m = \pm|\ \varphi) = \frac{1 \pm \cos\varphi}{4}$$

$$p(x = +|\ \varphi) = \frac{1}{2}.$$

(3.4) Joint probabilities preserve phase dependence. The sum over the unknown record of marker m eliminates it.

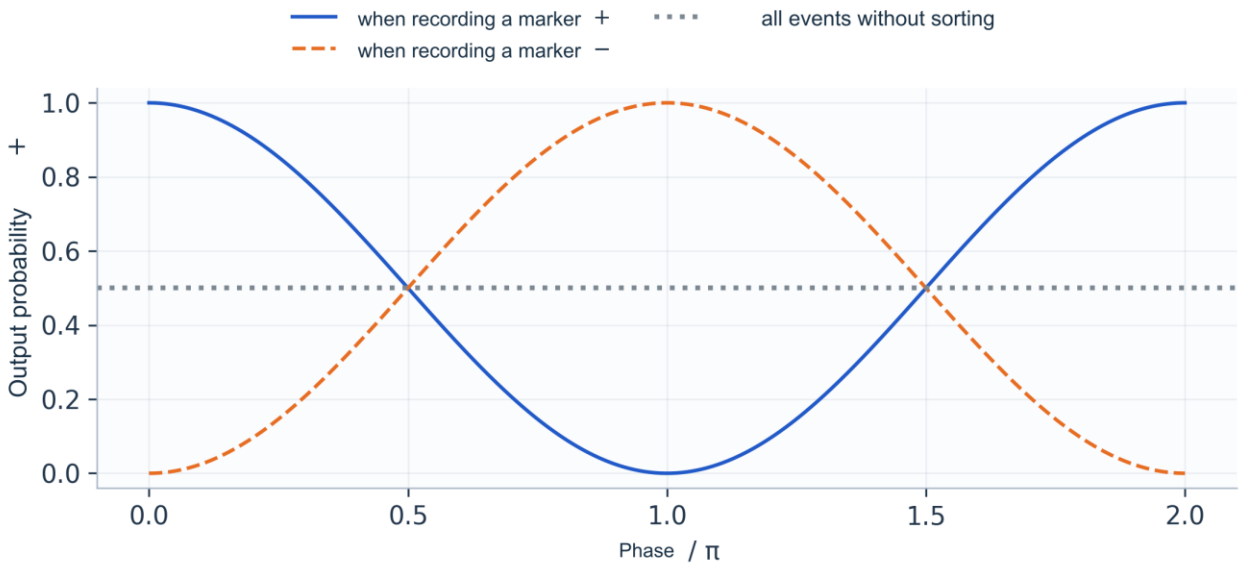


Figure 9. Conditional interference patterns for two marker records are mutually complementary. After summing with the probabilities 1/2, the complete set of events remains without stripes. This is a calculation of joint probabilities, not a change to past registration.

What remains open

Decoherence explains an important part of the transition from coupled quantum dynamics to stable local records. It allows you to calculate the suppression of interference, the influence of the environment and the selection of practically stable states. These results can be tested quantitatively.

The question of why an experiment is described as one observable outcome requires a separate indication of the accepted interpretation or modification of the dynamics. In some approaches, singularity is understood relative to the record of the observing subsystem. Others introduce additional variables or objective stochastic localization. These approaches should be assessed by their explicit assumptions and implications.

For the book's experimental program, this calculation asks a practical question: What records are available, and what prediction will emerge after averaging them? The normal environment, additional localization, and preparation errors are compared on the same set of observations. The transition to the eighth chapter will show another ambiguity: different individual stochastic histories can give one ensemble equation.

Thus there is a transition from the problem of measurement to the problem of distinguishability. Discussion of what exists in nature must be accompanied by a question about the information available. If different models give the same probabilities for all chosen measurements, those particular measurements will not resolve the dispute, regardless of their accuracy.

Entanglement with the environment has already shown that the state of a whole can contain more than local descriptions of its parts. The next chapter examines this feature directly and explains what restrictions on conventional models follow from quantum correlations.

4 Entanglement and limitations on explanation

For a composite quantum system, complete knowledge of its parts may not be enough. The observed correlations depend on the joint state. Entanglement makes this feature particularly salient and allows entire classes of explanations to be tested, but the conclusion of each such test involves certain assumptions.

When the whole cannot be decomposed into parts

Two systems are in a pure product state if the state of each can be specified separately, and the joint state is obtained by their tensor product. In this case, one part can influence another through subsequent dynamics, but the initial preparation does not contain entanglement. A mixed state is separable if it can be represented as a convex mixture of tensor products of the states of the subsystems: the weights are non-negative and add up to one.

Let's consider a pair of two-level objects in an equal superposition of joint alternatives 00 and 11. Each object individually produces a zero or a one with equal probability. But their results in this basis coincide. The coincidence itself can still be reproduced by classical correlation: the source could have distributed identical random bits in advance.

The difference arises when measuring in other bases. A coherent joint state preserves phase relationships between alternatives that are not present in a simple mixture of pre-distributed bits. Therefore, one chosen type of correlation does not provide sufficient evidence of entanglement. What is needed is a set of measurements that excludes corresponding uncomplicated explanations.

In experiments, this is often done with the help of a witness: a quantity calculated from the data for which the boundary is known for a certain class of states. Violation of the boundary produces a conclusion when assumptions about the preparation, measurements, and statistical procedure are met. The word "witness" does not imply an exemption from these assumptions.

$$|\Phi^+\rangle = \frac{|00\rangle + |11\rangle}{\sqrt{2}}$$

$$\rho_A = \rho_B = \frac{I}{2}$$

(4.1) The joint state is pure and entangled, while the local states are maximally mixed. The completeness of a joint description does not reduce to the completeness of two local descriptions.

$$\rho_{AB} = \sum_j p_j \rho_A^{(j)} \otimes \rho_B^{(j)}$$

$$p_j \geq 0, \sum_j p_j = 1.$$

(4.2) This is the definition of a separable mixed state. An entangled state is a state for which no such representation exists.

Bell's Inequality Logic

Bell's work 1964 showed the incompatibility of a certain class of local hidden parameter descriptions with quantum predictions. The Clauser, Horn, Shimoni and Holt version made the test suitable for realistic experimental setups [5, 6]. The assumptions of the model are significant, including local factorization and the independence of the choice of settings from the latent parameters in the sense used.

The simplest algebraic idea is this. Settings A and A′ are available on one side, B and B′ on the other; the result of each setting is plus or minus one. If they can be jointly assigned values in the model under consideration, the expression S for a particular set of latent parameters is always equal to plus or minus two. Indeed, one of the sums B+B′ and B−B′ is equal to zero, and the other has modulus two.

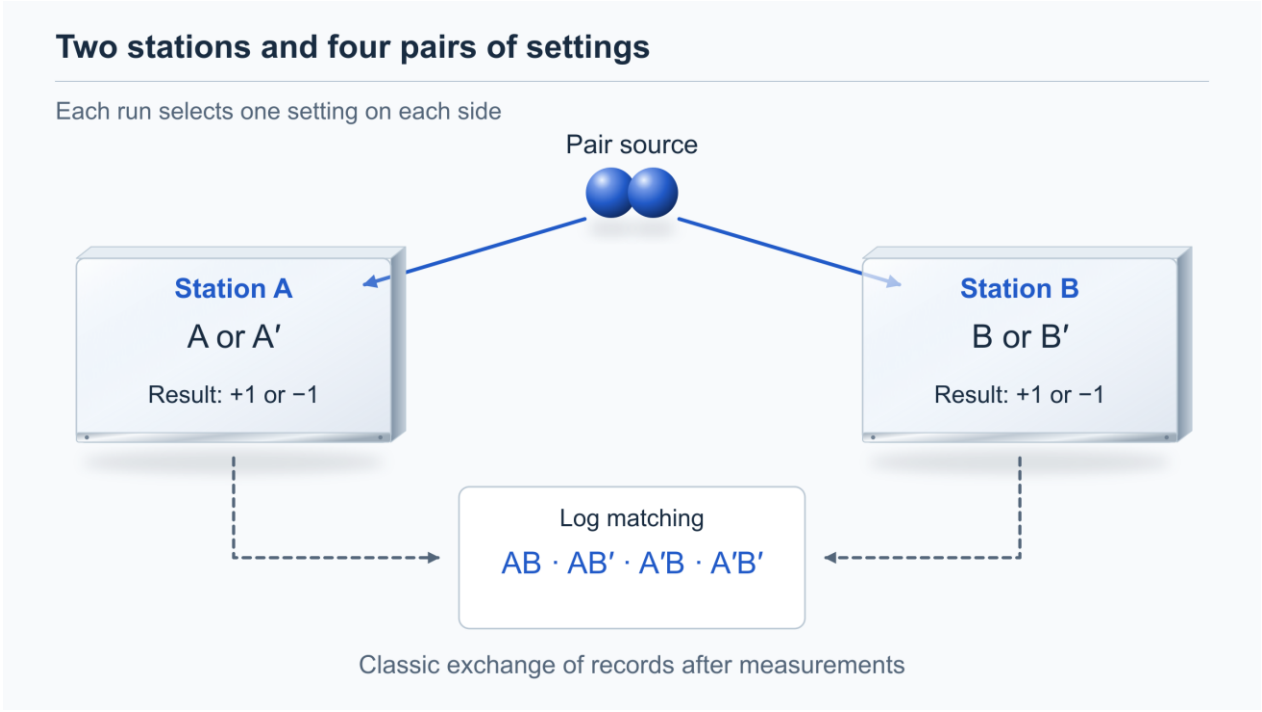


Figure 10. Logic of experiment CHSH. The source prepares a pair, each side chooses one of two settings and receives the result ±1. After measurements, the classical logs are compared for four combinations AB, AB′, A′B, A′B′. The diagram is not a reconstruction of a specific historical experiment; the conditions necessary to close experimental loopholes are discussed in the text.

Stochastic local models obey the same bound. Their additional local randomness can be included in an extended description of the hidden parameters; equivalently,

the conditional means of the results lie between −1 and +1, which preserves the CHSH limit.

After averaging over one general distribution of hidden parameters, the modulus of S does not exceed two. Quantum theory, for a suitable state and set of measurements, allows for up to two times the square root of two. The experimental task is to evaluate correlations and test boundaries, taking into account the finite statistics and the design of the experiment.

Here, an overly broad conclusion is often allowed. Violation of such an inequality does not mean that every possible reality is mathematically refuted or that any hidden parameter description is prohibited. The set of assumptions used in the conclusion is rejected. Some alternatives change locality, others discuss setting independence or the structure of causal explanation. Each of them requires separate analysis.

$$S = \langle AB \rangle + \langle AB' \rangle + \langle A'B \rangle - \langle A'B' \rangle$$

$$|S| \leq 2$$

(4.3) CHSH boundary for the corresponding class of local models. Angle brackets indicate the average product of the results for the specified pair of settings.

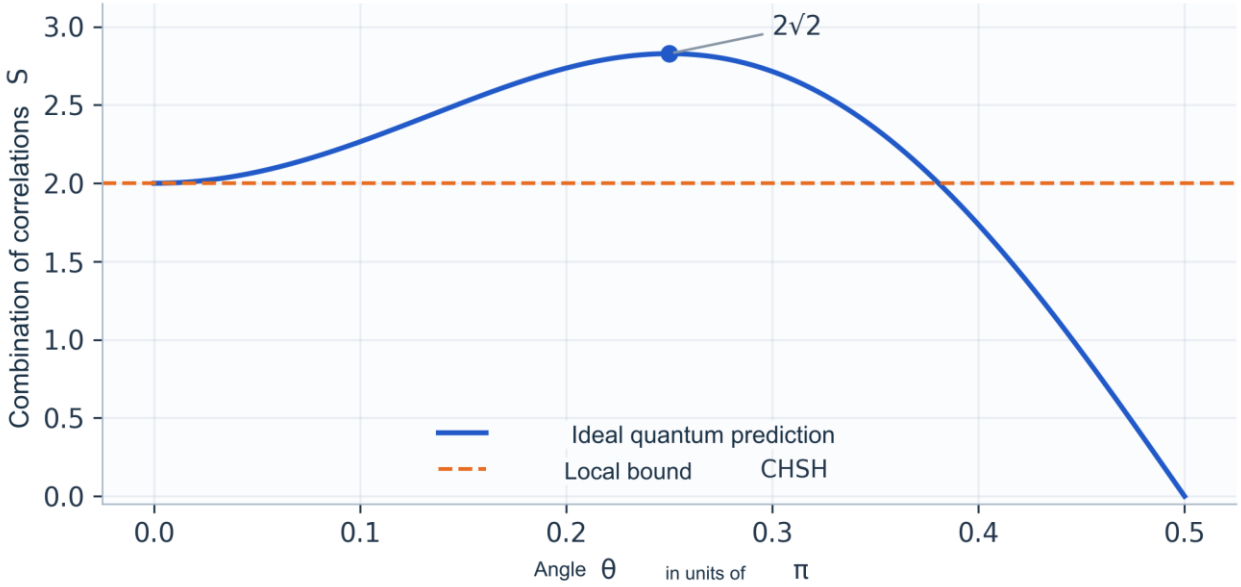


Figure 11. An illustrative relationship is S = 3 cos θ − cos 3θ for suitable ideal quantum measurements. Comparison with the boundary 2 refers to the CHSH assumptions.

What does the experiment add?

To apply an inequality, you need to be sure that the appropriate events are being compared. Incomplete recording, setting-dependent selection, or possible signal exchange between parts of the installation may change the interpretation of the observed disturbance. These problems are known as experimental loopholes.

In 2015, Hensen et al reported a test with electron spins separated by 1.3 kilometers, which together closed key locality and registration loopholes as part of

their [7] formulation. This was a specific experimental result, not a universal guarantee of the absence of any conceivable assumptions.

It is usually useful to separate the three statements. The theorem specifies the boundary under the listed conditions. The experiment evaluates the observed quantity and uncertainty. The interpretation explains which conditions and which class of models the result allows to reject. If these levels are not separated, a neat test can easily turn into an overly broad statement.

This example is especially important for later chapters. Gravity experiments also use witnesses and no-go arguments. The strength of the inference depends not only on the number at the output, but also on how physically based the model of the mediator and the structure of the interaction are. The familiar word “classical” can hide several different requirements.

Why correlation is not a controlled message channel

In standard quantum theory, the local statistics of one part are unchanged by the action of a linear, completely positive, trace-preserving channel on another part, when averaged over all remote outcomes. This follows from the partial trace of the joint state. Conditional subsets can have different local statistics, but to separate them, it is necessary to transfer records of remote results and corresponding settings.

Therefore, strong correlations do not provide automatically controlled superluminal communication. To transmit a message, the sender must select an effect such that the recipient can discern the choice from his available data. A correlation discovered only after comparing records using a normal channel does not fulfill this requirement.

This distinction must be maintained when analyzing the proposed modifications. Certain nonlinear changes in pure states can make different decompositions of the same density matrix physically distinguishable. Then the local forecast may begin to depend on remote preparation. A well-known example of such a risk for the nonlinear Weinberg extension was considered by Gisin [11].

This result in itself does not prohibit any conceivable nonlinear or stochastic model. It shows the need to test component systems and methods for preparing states. In a research program, new dynamical terms should undergo this test before discussing the intended sensitivity of the instrument.

What can you say about the wave function?

The question of whether a quantum state is a physical reality or a description of knowledge also receives limitations when formulated explicitly mathematically. In simpler terms, the question is: can two different pure quantum states reflect only different knowledge about the same physical situation? The theorem of Pusey, Barrett and Rudolph considers a class of models with physical states underlying observed probabilities and the assumption of independence of independently prepared

systems. Under these conditions, a certain form of overlapping epistemic description is incompatible with the quantum predictions of [10].

The significance of the theorem lies in the accuracy of the conditions. It does not resolve without additional arguments all disputes about the nature of reality, does not automatically select an interpretation, and does not replace the description of measurement. If a theory changes the assumption of independence of preparation or the class of admissible models itself, it needs to be examined separately.

In this book, theorems are used as restrictions on specific constructions. They help identify which assumptions will need to be revised, but do not relieve you from constructing a consistent alternative. What remains between the rejection of one postulate and a new physical theory are equations, probabilities, composite systems, and experimental predictions.

Testing one pair and the limits of three inferences

For the state $|\Phi^+\rangle$, the quantum value CHSH can be obtained manually. The Z operator distinguishes between zero and one, the X operator swaps them. For the selected pair, the averages ZZ and XX are equal to one, and the mixed averages ZX and XZ are equal to zero. On the first side, Z or X are measured; on the second - directions $(Z+X)/\sqrt{2}$ or $(Z-X)/\sqrt{2}$. Each of these directions corresponds to the observed one with the results ±1.

Four correlations are obtained: $1/\sqrt{2}$, $1/\sqrt{2}$, $1/\sqrt{2}$, and $-1/\sqrt{2}$. When adding with the last minus sign specified in CHSH, the result is $2\sqrt{2}$. The local distributions of both devices remain equally probable. This means that exceeding the boundary of two and the absence of a controlled message are compatible already in one explicit calculation. The real number S is estimated from the finite series of each pair of settings; symbolic meaning is provided only by an ideal reference point.

Three often adjacent results refer to different questions. The Bell test limits the class of causal explanations for correlations. No-signaling characterizes local statistics after averaging remote outcomes. The PBR argument refers to the overlap of descriptions of physical states given independent preparation. Substituting one conclusion for another does not strengthen the evidence, but changes the question.

It is useful to refer back to this table when reading subsequent gravitational witnesses. The observed effect is always included in the chain along with the prerequisites. If two studies use different definitions of available operations or a mediator, those definitions should be compared first and then the effect size. This preserves the possibility of a strong conclusion without expanding it beyond the limits of what has been proven.

$$A = Z,\ A' = X,\ B = \frac{Z+X}{\sqrt{2}},\ B' = \frac{Z-X}{\sqrt{2}}$$

$$S_{\Phi^+} = 2\sqrt{2}.$$

(4.4) Direct calculation of CHSH for state $|\Phi^+\rangle$. The local probabilities of each outcome ±1 are equal to 1/2.

Result	Essential Prerequisite	Valid output
CHSH [5, 6]	Local factorization and independent choice of settings in the accepted class of models	Correlations are inconsistent with the totality of these conditions
No-signaling	The local linear channel preserves the trace; remote outcomes are averaged	Local statistics do not transmit the selection of a remote operation
PBR [10]	The described class of physical conditions and independence of preparations	The corresponding overlapping description does not reproduce all quantum predictions

After discussing correlations, we can clarify what exactly the expansion of quantum theory means. Changing the picture of the world, adding variables, and changing the probabilities of observations are different research activities. The next chapter relates these to the requirements for a testable hypothesis.

5 When a hypothesis changes a theory

A new verbal explanation can change the idea of what is happening, preserving all the calculated probabilities. A physical modification that is experimentally verifiable must produce a different prediction for at least some valid experiment. It is necessary to draw a precise line between these cases.

Description of reality and observed probabilities

The two approaches can use different representations of the state of an individual system and still produce the same statistical results. Then comparing the selected measurements will not determine which representation is correct. This statement refers to the available data and does not resolve the philosophical question about the merits of the explanation.

In Everett's formulation of relative states, joint quantum dynamics are considered without a separate fundamental collapse. Bohm's approach introduces additional position variables and directional dynamics; at appropriate quantum equilibrium, the standard statistical predictions [13, 14] are reproduced. These brief characterizations do not replace a full analysis of the approaches, but show that the debate about the pattern of individual events can extend beyond a single experimental distribution.

Objective collapse models take a different tack: they typically introduce dynamics that, under certain parameters, change the observed statistics. Therefore, they can be limited by interference, diffusion or radiation. Which observable fits depends on the shape of the model, not on the general word “collapse.”

For research text, it is useful to always ask what has been added. The new variable can be a computational auxiliary quantity, an environmental parameter, or a fundamental object. The new term may describe a known effective interaction. Establishing these roles prevents new physical laws from being announced prematurely.

Minimum verifiable modification

A convenient strategy is to change one clearly stated property of the standard model. For example, add a weak spatial localization channel with intensity and characteristic length. In the limit of zero intensity, the original dynamics should be restored. This gives a comparable null model and allows us to talk about parameter limitations.

This construction does not yet explain the origin of the additional process. It is a phenomenological model: it specifies the form of the effect and the method for testing it. Its value depends on its internal consistency, its scope of applicability, and whether it can independently constrain similar background processes.

If there are too many parameters and each experiment gets its own free values, the model can fit the data without significant risk of being rejected. To avoid this, general

parameters and transfer rules between installations are set in advance. Then a new experiment can test the prediction, and not just add another coefficient.

Preferring a minimal model is not a requirement that nature be simple. This is a way to make the first conclusions visible. Once a discrepancy is discovered, the description can be expanded, but each expansion must show what new observation it explains and what additional consequences it creates.

Consistency of Probabilities and Energy

Before discussing the discovery, it is useful to check the mathematical feasibility of the dynamics. Is normalization still in effect? Does the density matrix remain positive? How does the model act on part of the entangled system? Are different ways of preparing the same condition compatible with the same subsequent prognosis?

A separate issue concerns energy. Some simple noise patterns cause heating. This may be an observable consequence, or it may indicate an area where dissipative expansion is required. One cannot simultaneously use the prediction of additional diffusion and silently ignore the associated energy effect if both follow from the same generator.

In this case, the requirement for conservation of energy must be formulated for the corresponding system. The energy of an open object can change due to its surroundings. If the added process is declared fundamental, it is necessary to explain how the energy balance of the full description makes sense. It is not always possible to reconstruct this answer from one effective equation for a subsystem.

Relativistic compatibility should also be handled with care. A nonrelativistic model may be useful in its field, but without a separate construction it cannot be considered a complete theory of space and time. A successful low-energy test tests a certain mode and certain parameters.

Example of checking a probability rule

Another way of extension is related to Born's rule. In an idealized three-path formulation, standard addition of amplitudes creates pairwise interference terms. The combination of probabilities that subtracts all single and paired contributions should vanish if one consistent amplitude model applies to the configurations being compared.

In 2010, Sinha and co-workers used a three-slit photonic experiment to limit higher-order interference. In their formulation, the observations were consistent with the standard rule, and the work gave a quantitative limit for the possible deviation [12]. It should be read as a concrete test with finite precision, and not as a proof of the formula under all physical conditions.

The algebraic reduction is transparent: the square of the sum of the three amplitudes contains the squares of the moduli and three pairwise cross terms. By subtracting the corresponding two-path expressions and returning the single

contributions, each of these terms cancels out. This conclusion is based on the consistency of the alternatives between which the comparison is made.

All quantities in combination must have a common absolute normalization - for example, the probability of registration per one identically prepared input particle, taking into account the stability of the flow. It is impossible to separately renormalize each slot configuration by the number of passing particles: then other conditional probabilities are compared, for which the above reduction does not have to hold.

In a real optical setup, closing the slit may change the propagation boundary conditions and the detector may have a nonlinear response. Then a non-zero experimental combination requires calculation of the usual physics of the installation itself. It would be a mistake to substitute different physical situations into an idealized identity and call the remainder a violation of the rule of probability.

$$I_3 = P_{ABC} - P_{AB} - P_{AC} - P_{BC} + P_A + P_B + P_C - P_\emptyset$$

(5.1) Third order combination. The indices denote the available alternatives, and the last term takes into account the background without them. The null prediction refers to an explicitly specified ideal model.

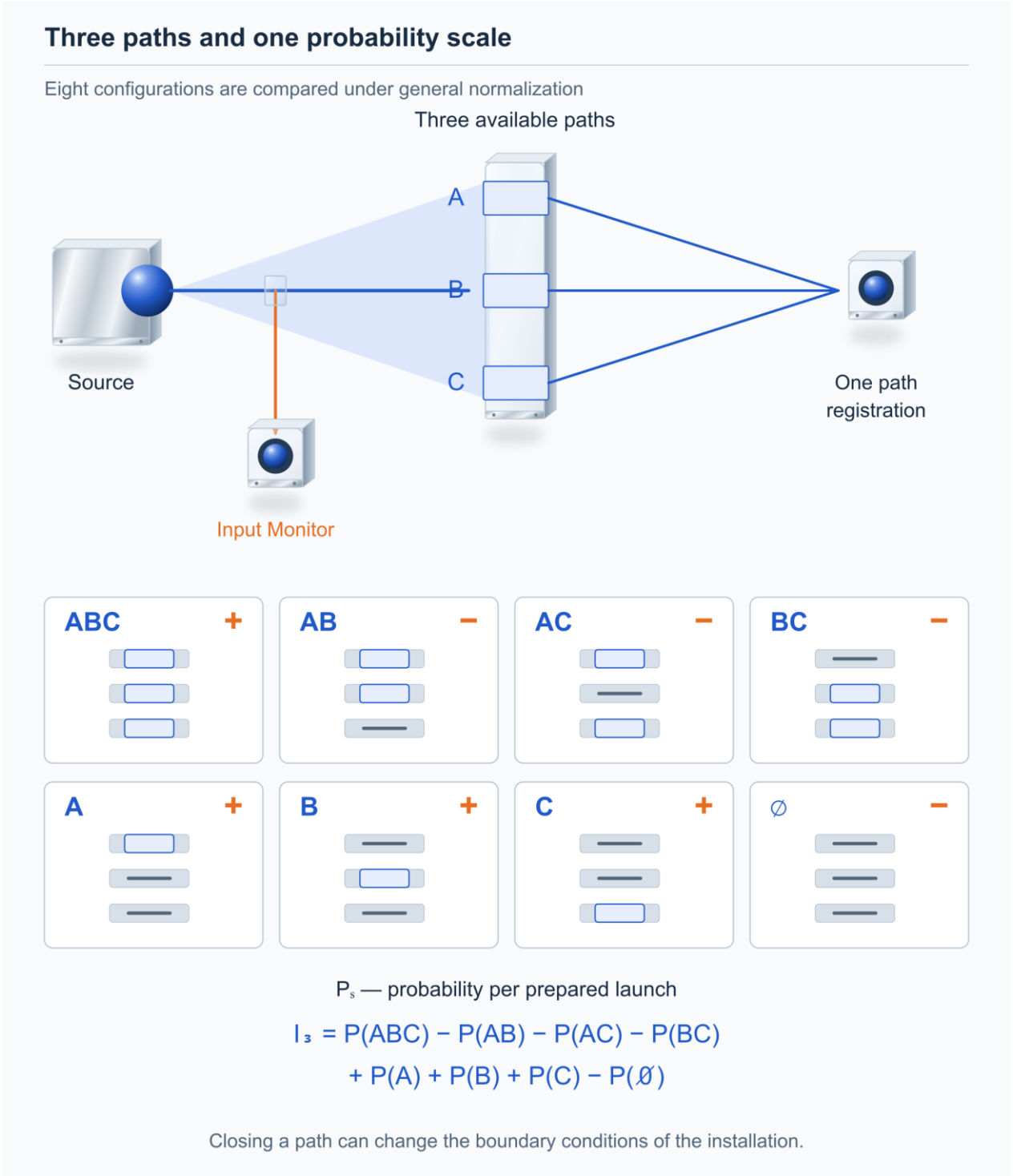


Figure 12. Training three-path setup and eight available path configurations. The notation P(S) in the figure corresponds to P_s in the text: the probability is normalized to one prepared run, with a general control of the input flow. Combination signs I_3: $+ABC$, $-AB$, $-AC$, $-BC$, $+A$, $+B$, $+C$, $-\varnothing$. Closing the slit can change the boundary conditions, so a non-zero experimental residual requires analysis of the detector setup and response.

How is novelty checked?

A new recording of a known equality does not in itself constitute a scientific discovery. After obtaining the formula, it is necessary to compare it with the literature, check equivalent notations and establish which conditions have already been considered. Sometimes the result turns out to be a known special case; sometimes the useful contribution lies in application to another physical setting.

The most compelling claim for a new contribution indicates a precise difference from nearby work. For example, the previously omitted background correlation is taken into account, the discriminability limit is found for a limited set of controls, or a new way to check the universality of parameters is shown. Such a statement can be criticized in detail.

The working hypotheses of the last chapters are compared with the nearest published designs. Models, calculations performed and failure conditions are given for them. The mere fact of independently obtaining a formula does not establish historical priority. Therefore, the status of the result is indicated separately: reproduction, educational development of a known model, stability test, or proposal for further physical testing.

What exactly does the calculation add?

A research result is conveniently described by three related questions: what assumption is being tested, what has been calculated, and what conclusion stands up to that calculation. For example, the three-point rate combination in Chapter Ten eliminates the constant and quadratic background at general coefficients. It can be displayed in full and verified with numbers. But the word "excludes" refers to the two forms indicated, and not to all the usual mechanisms of decoherence.

Replacing a constant separation with a real trajectory changes the optimum of this combination. The result adds quantitative information about the specified protocol. It remains useful even without proposing a new fundamental law. Similarly, the replication of the published-data analysis in the twelfth chapter establishes that a particular estimate can be recovered from the available materials. It does not turn another research team's measurement into a new experimental discovery by this book's authors.

The statistical program in the last chapters tests at the next level: how often the procedure is wrong and what it predicts for new settings. Here, the result is not only the parameters of the best-fit curve, but also false detection rates, sensitivity to weak signals, and robustness to background changes. A comparison with nearby works in chapter 21 shows which elements are already known and where the exact subject remains for independent verification.

This sequence allows for a meaningful negative result. If two models give the same dynamics for all permitted operations, the calculation may determine that it is impossible to separate them in this protocol. The research question is then corrected by adding access to the environmental record, another object, or an independent

calibration. Increasing the number of repetitions does not replace changing the problem if the difference in probabilities is strictly zero.

Result	What it establishes	What is missing for the next step?
Algebraic background reduction	Insensitive to specified functions with general parameters	Checks for other physical background forms
Optimum for trajectory	Best contrast in selected profile family	Number of events, control errors and statistical criterion
Replicating a publication	Reproducibility of a specific external assessment	Independent difference and its quantitative result
Calibrated Numerical Test	Error rates under explicitly simulated conditions	Confirming assumptions and testing them with actual experiment

The next step is to move from the probability calculated by the theory to the data produced by the device. This relationship includes calibrations, finite statistics, and environmental parameters. Without it, even the correct equation does not turn into a reliable test.

6 How measurement becomes evidence

The theory predicts the distribution of data under given conditions. An experiment measures a finite number of events using an imperfect instrument. The comparison of these two levels requires an explicit observation model and a pre-formulated question: what alternative is the result capable of eliminating.

Visibility of interference

In a simple interference experiment, the dependence of the frequency of events on the phase is recorded. Visibility characterizes the depth of modulation. It can be determined through the maximum and minimum of the ideal pattern, but in real analysis it is often more reliable to fit the full model to the distribution of counts, taking into account the background and response of the detector.

The same loss of total particle number does not necessarily reduce normalized visibility. If both pathways are equally attenuated and selection is independent of phase, the number of events falls, but the ratio of the modulated part to the average part may be maintained. On the contrary, an additional incoherent background can reduce visibility without a fundamental loss of phase relationships of the object under study.

That is why the model separately takes into account source intensity, registration probability, background count and coherence. If you reduce them to one free coefficient, the calculation may be convenient, but the physical interpretation of the coefficient becomes ambiguous.

To convert visibility to decay rate, you need the original visibility. Its uncertainty is transferred to the estimate of rate. If the initial contrast itself depends on the distance between branches or on the time of the sequence, the assumption of constant normalization can create an artificial dependence similar to the desired effect.

$$V = \frac{I_{\max} - I_{\min}}{I_{\max} + I_{\min}}$$

$$\widehat{\Gamma} = -\frac{1}{T} \ln \frac{V}{V_0}$$

(6.1) The first formula sets ideal visibility. The second estimates a constant decay rate given a known initial visibility and a suitable exponential accumulation model.

The entire trajectory matters

The interferometer arms usually first separate, then move for a while and finally converge. Additional localization is in effect throughout the entire sequence. Therefore, the signal depends on the temporal profile of the distance and not just on the maximum separation.

If the instantaneous rate is proportional to the square of the distance, the accumulated attenuation depends on the integral of this square over time. Two trajectories with the same maximum distance and the same total duration may produce different results. The branches in one can remain separated for a long time, the other reaches its maximum only for a short time.

For a saturating spatial kernel, the situation is more varied still. Increasing separation far beyond the characteristic scale may barely change the instantaneous rate, whereas increasing the holding time continues to accumulate the effect. These dependencies help select an experiment, provided that the other sources of loss are also modeled over the full sequence.

When comparing multiple configurations, you need to determine which settings are actually saved. Changing geometry can change heating, control fluctuations, and convergence efficiency. Formal reduction of the common background only works for that part that is physically common.

$$-\ln\frac{V}{V_0}=\int_0^T \Gamma[d(t)]dt$$

(6.2) General form of accumulation for time-local rate. With environment memory, more complex functional of the entire history may be required, which is discussed later.

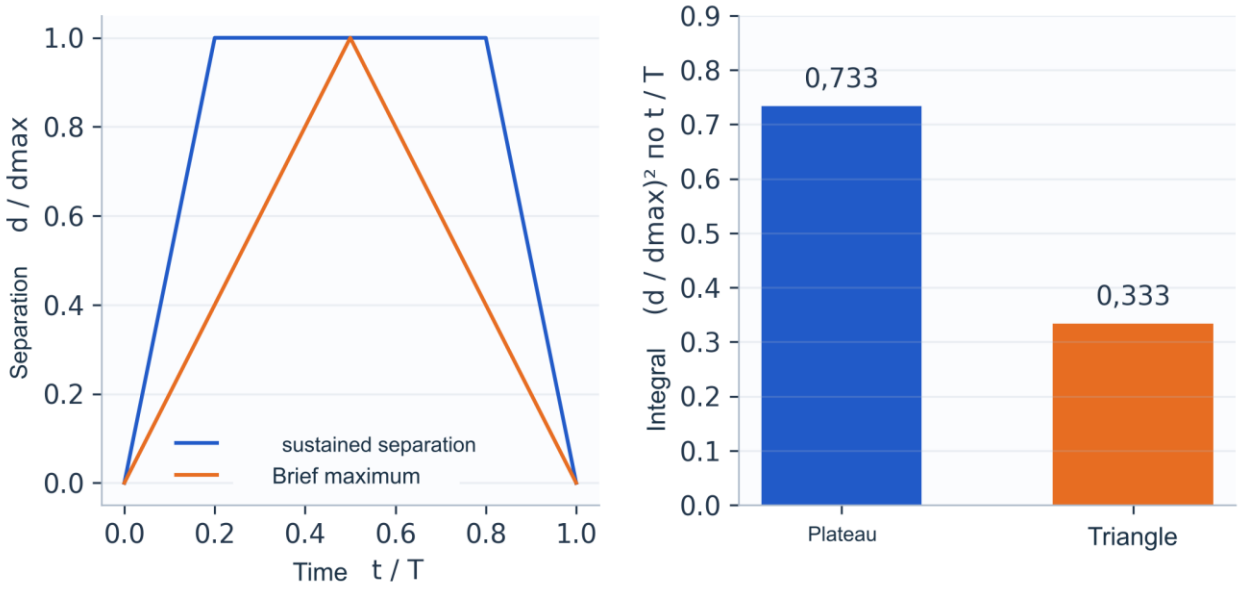


Figure 13. The same maximum separation and duration give different accumulated attenuation. In the quadratic mode, the integral of the square of the entire trajectory is decisive.

From state to three detector records

Consider a device that prepares one system in each pre-known run and allows no more than one registration. The two ideal outputs are labeled plus and minus; Additionally, the “no registration” outcome is retained. Such accounting is possible, for example, with a separately known number of preparations. If the number of input objects is unknown, a flow model is required, and the multinomial formulation below does not carry over without modification.

Let us denote the visibility to the detector by V, and the probability of registration by η. Let the device independently change the exit label to the opposite one with probability ε upon a registered event. We assume equal efficiencies of the two outputs, no phase dependence of losses, and no additional dark counts. These terms describe the teaching device; they are not declared properties of all interferometers.

For the plus output, two incompatible ways of obtaining a record are added up: the correct reading of the real plus and the erroneous label of the real minus. Therefore, the probability of the written plus is equal to $\eta[(1-\varepsilon)p_{+}+\varepsilon(1-p_{+})]$. The minus written down receives the remaining part of η, and the omission receives the probability $1-\eta$. The sum of the three probabilities is identically equal to one. The value of η reduces the size of the registered sample; ε reduces the difference between outputs.

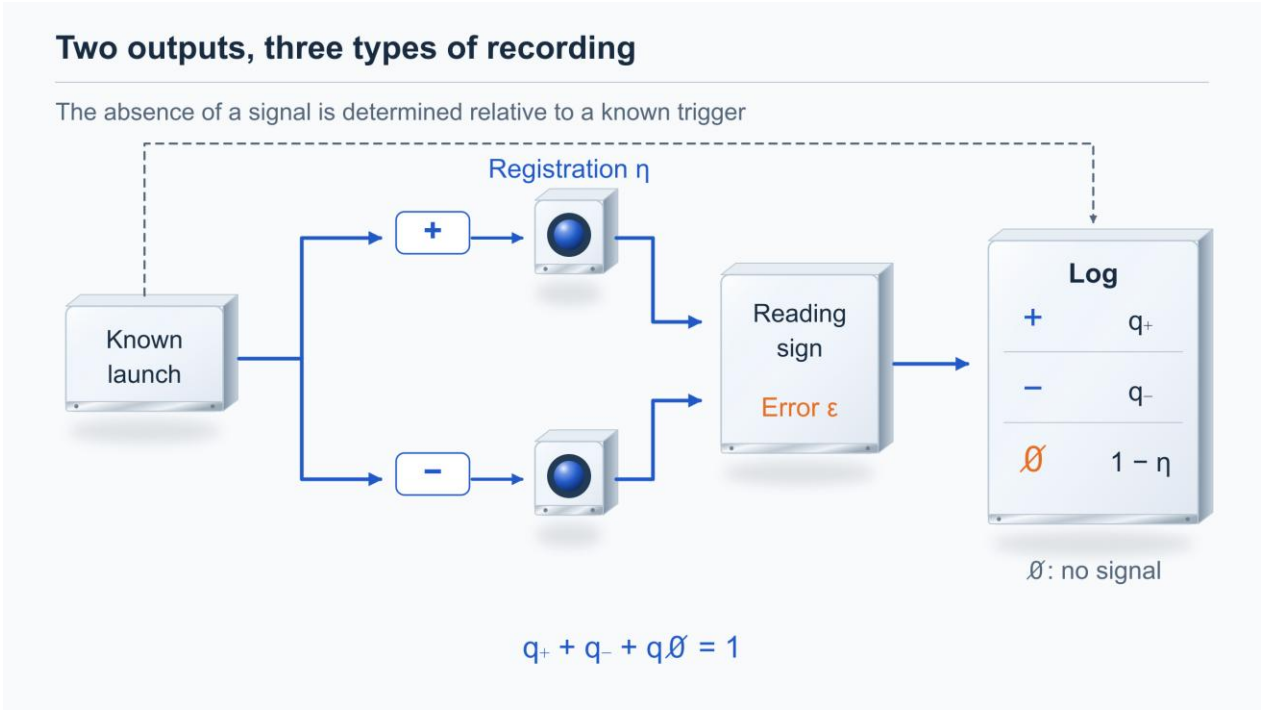


Figure 14. After a known startup, the system has two physical outputs. Efficiency η specifies the share of registrations, ε is the probability of error of the recorded sign. Three categories appear in the log: plus, minus and no signal Ø with probability 1 − η. The dotted line shows the log's association with a known run. Ø is not a third physical detector; symmetrical phase-independent losses by themselves do not reduce conventional visibility.

Let's take V = 0.8, η = 0.6 and ε = 0.02. With phases 0, π/2 and π, the mathematical expectations indicated in the table are obtained for thousands of preparations for each setting. Fractional values are acceptable precisely because they are expectations. A particular series contains random integers. At the central phase, 300 pluses, 300 minuses and 400 passes are expected; the complete record contains useful loss information even where the contrast of the two outputs is zero.

After conditional selection of recorded events, the observed visibility is equal to $(1-2\varepsilon)V = 0.768$. If the reading error is taken to be physical decoherence, an extra attenuation exponent $-\ln(0.96) \approx 0.04082$ will be assigned. For a sequence lasting one second, this would look like incremental rate 0.04082 s^{-1}. At the same time, no new mechanism was introduced into the system state.

The efficiency of η is reduced in the conditional plus probability only due to the assumed independence of losses from phase and outcome. It still affects statistical accuracy: with a fixed number of preparations, fewer useful events remain. If η depends on the hidden trajectory or changes between outputs, simply dividing by the total number of detected particles can distort the shape of the curve. The omission outcome then needs to be modeled along with the recorded outcomes.

For N preparations, the likelihood has a multinomial form. Calibration series with a known input limit ε, and the comparison of the number of preparations and registrations limits η. Their uncertainties cannot be considered to have disappeared after one preliminary measurement: they are transferred to the estimate V or included in the joint likelihood. This small example prepares the full analysis of chapters 19–21, where unknown background and physical signal parameters are determined simultaneously.

$$q_+ = \eta\left[\varepsilon + (1-2\varepsilon)\frac{1+V\cos\varphi}{2}\right]$$

$$q_- = \eta - q_+$$

$$q_\emptyset = 1-\eta.$$

(6.3) Probabilities of three records with independent losses and symmetric label error. Here 0 ≤ η ≤ 1 and 0 ≤ ε ≤ 1/2.

$$\mathcal{L} = \frac{N!}{n_+!\,n_-!\,n_\emptyset!}\,q_+^{n_+}q_-^{n_-}q_\emptyset^{n_\emptyset}$$

$$n_+ + n_- + n_\emptyset = N.$$

(6.4) Likelihood for one phase setting. For independent settings, such factors are multiplied; calibration data is added with its own multipliers.

Phase	Pluses expected	Minus counts expected	Misses expected
0	530.4	69.6	400
π/2	300	300	400
π	69.6	530.4	400

Parameter and physical reason

Let the observed rate be represented by the sum of two non-negative contributions. If they have the same dependence on all available settings, the data determines only the sum. No matter how many times the experiment is repeated, a separate determination is impossible without additional information. This is the structural non-identifiability of the model.

Another case occurs when the dependencies are slightly different, but the difference is small compared to the noise. Then separation is possible in principle,

but the selected number of measurements is not enough. This is a practical problem of sensitivity. It can be improved by observation time, more accurate calibration, or a good choice of settings.

It is necessary to distinguish between these cases before promising a new experiment. Increasing the accuracy helps when there is a small non-zero difference in predictions. For an exact match, you need to change the set of observations or independently constrain some of the parameters. This logic underlies the three-point example and its counterexample in Chapter Ten.

In problems with multiple parameters, it is useful to see how each prediction changes with a small change in the parameter. If two changes always shift all observations in the same way, it is difficult to separate them locally. But even the independence of such shifts at one point does not guarantee global uniqueness of the solution: another suitable set may exist far in the parameter space.

The signal is checked on data without a signal

To assess the reliability of the procedure, it is necessary to simulate situations in which there is no additional mechanism. These data are then analyzed in the same way that is intended to be applied to the experiment. If a procedure often finds a positive signal, it needs to be revised, no matter how convincing one good chart looks.

Testing only on data generated by the same ideal model used for fitting is especially dangerous. Such experiment confirms the functionality of the program in convenient conditions, but weakly tests its resistance to errors in the description of the environment. Scenarios with modified noise shape, drift, and realistic calibration uncertainty are needed.

The options and settings chosen after reviewing the data affect the statistical interpretation. If among many configurations only the most unusual one is shown, you need to take into account the search itself. This applies to the selection of the characteristic length, and to the choice of the time window, and to the selection of the most beautiful interference pattern.

Deferred configurations provide additional verification. The model is selected according to one part of the conditions, after which it predicts another without reconfiguring the fundamental parameters. The success of such a test is stronger than a simple coincidence on the data already used in the setup, although it still belongs to the studied class of alternatives.

Three types of calculated result

The book contains analytical conclusions, numerical model examples and results of published experiments. Their status varies. The analytical conclusion establishes the consequence of the listed assumptions. A numerical example shows the behavior of the selected model and helps to detect errors or estimate scale. Experimental data links the calculation to a physical device.

Model graphs and numerical series in the book are directly designated as calculated; their parameters and random number generators are available in the attached code. The reproduction of published measurements in chapter 12 has a different status: an external set of experimental data is used, its origin and the limits of the repeated analysis are indicated. Comparing these two types of material allows you to see where the physical device is being tested and where the properties of the analytical procedure are being tested.

Published restrictions must also be read in context. The upper bound of the parameter depends on the model, background assumptions and the statistical procedure adopted. It is not equal to measuring the zero value with absolute precision. A new noise source can weaken the constraint, and independent calibration can sometimes make it stronger.

A test prepared in this way can produce several useful outcomes. It may reveal a reproducible misfit of the original model, narrow the parameter range, or show the inadequacy of the selected observations. Each outcome becomes meaningful if it is clear what was compared and what conditions were used.

Now the basic concepts and matching rules have been defined. The second part of the book moves on to modern experiments and models that try to test the physical limit of superposition. It gives the general question of the quantum boundary specific masses, spatial scales, and sources of uncertainty.

Part II Search for the limit of superposition

7 How to find the superposition limit

The question of the boundary of the quantum world becomes physical only after it is specified which system must preserve the superposition, how long it must retain it, and what observation will confirm this preservation. The phrase “a large object behaves quantumly” leaves too many uncertainties. Quantum can be one internal transition, collective excitation or movement of the center of mass. To test the assumed spatial localization, these cases are not equivalent. The beginning of the study therefore looks modest: a specific degree of freedom is selected and it is established what exactly the device can say about it.

What does it mean to place an object in superposition?

Let us imagine a particle whose motion is controlled in such a way that two spatial alternatives can later meet again. As long as alternatives exist, one cannot observe them separately and simultaneously require that all the original interference be preserved. The test works differently: the control changes the relative phase, and the distribution of the final results responds to this change. If detection frequencies change regularly, the observation contains information about the mutual consistency of the alternatives. Simply not knowing which path an ordinary particle has taken does not in itself create such a phase dependence. However, the stripe pattern still needs to be compared with suitable classical models of the device.

This last caveat is especially important for grids and periodic masks. A sequence of holes can create flow inhomogeneity without spatial quantum coherence. Therefore, a convincing experiment tests the dependence of the signal on the control parameters, and not just the existence of a beautiful pattern. In January 2026, the group of Sebastian Pedalino and co-authors reported the interference of sodium nanoparticles containing more than seven thousand atoms and having a mass of more than 170 thousand daltons. The experiment expanded the area of the tested spatial superposition, but did not detect its violation. Testing a specific mass and geometry does not establish a universal limit to the applicability of quantum theory. [15]

Four scales instead of one mass

To plan a study, it is useful to mentally decompose the experiment into four scales: the mass of the object, the distance between the alternatives, the time of their existence, and the spatial structure of the body itself. Mass determines sensitivity only together with other parameters. A heavy particle whose positions differ by an extremely small amount may be a less sensitive probe of a particular pattern than a light particle with a larger separation. Similarly, long-term retention of almost identical branches does not have to replace short-term retention of clearly distinguishable ones. The answer depends on how the proposed mechanism differentiates the distributions of matter.

Body size adds its own difficulty. If the hypothetical noise is consistent across the entire object, the contributions of its various parts can add up together. If the correlation length is small compared to the size, different regions begin to respond differently. Replacing the complex mass structure with a single point then changes the prediction. A practical conclusion can be obtained even before detailed calculations: the table of the prospects of experiments should contain information about density and shape, and not just one column with mass. A ranking based on the number of atoms is convenient for reporting the result, but is not sufficient for choosing the next experiment.

A simple analogy with measuring terrain helps here. It is pointless to evaluate the sensitivity of a ruler without the size of the irregularities that need to be distinguished. In a quantum experiment, the role of this size is played, among other things, by the correlation length of the influence being studied. A probe whose settings never cross the appropriate spatial scale can only see a local approximation to the law. Several different physical dependencies within a narrow range become almost identical. Increasing the number of repetitions reduces statistical error, but does not always eliminate this geometric ambiguity.

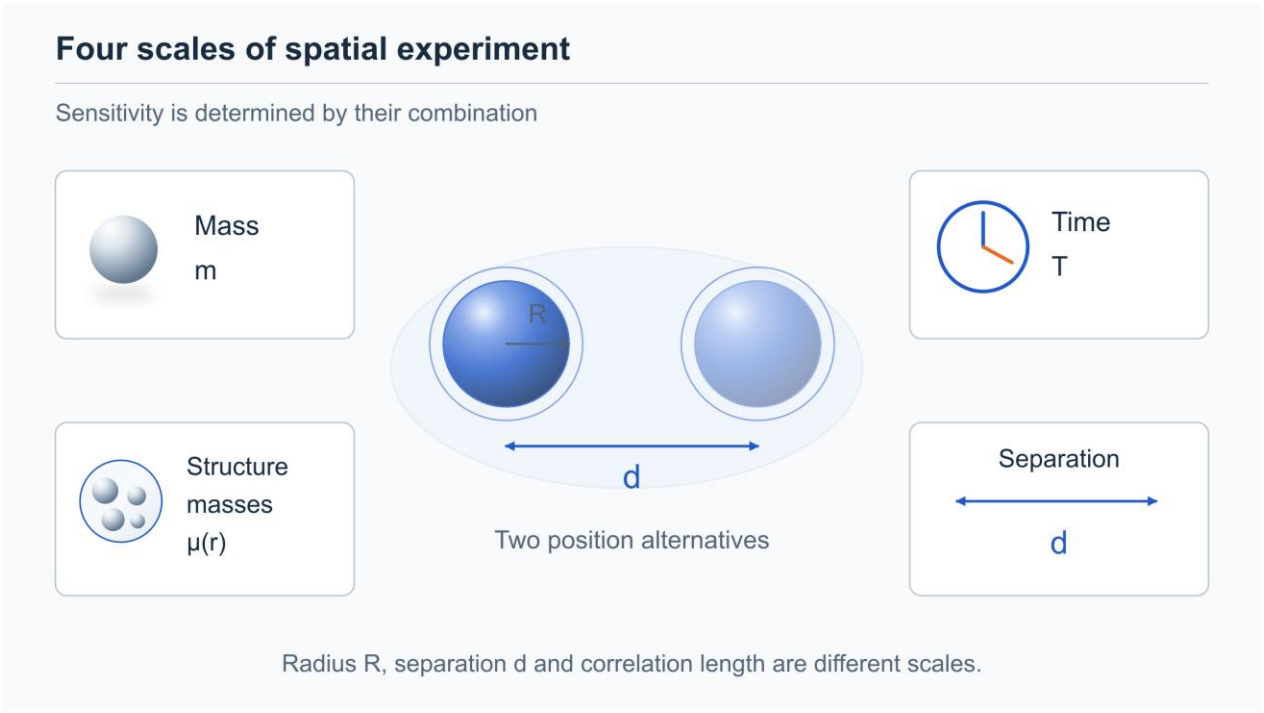


Figure 15. Four characteristics of spatial experiment: mass m, duration T, separation of alternatives d and mass structure μ(r). The body radius R is shown separately from the distance between the centers of the alternatives. The two translucent positions refer to one state, not two independent classical particles. Dimensions are relative; the figure does not report new records and does not depict the correlation length as a field boundary.

What does visibility measure?

It is convenient to characterize an approximately sinusoidal interference signal by visibility: the ratio of the difference between the maximum and minimum values to their sum. This value lies between zero and one with a normal positive signal. It

answers the question of how pronounced the alternation of light and dark areas or high and low registration frequencies is. On its own, it does not explain the reason for the weakening. Imperfect preparation, velocity spread, phase fluctuation, particle loss, and physical destruction of coherence can change the observed contrast in different ways, sometimes simultaneously. Therefore, a reference visibility is needed for the same control sequence.

In a thought experiment, one can assume that the reference visibility is precisely known and write down the exponential decay at a constant rate. In the actual procedure, the reference visibility is also measured or calculated with error. If the separation of branches changes over time, each part of the trajectory contributes its own share of losses. The maximum distance between branches does not replace the movement history. Two experiments that reach the same maximum separation may accumulate very different losses because one lingered in that state and the other quickly moved through it. This difference should be included in the model before comparison with the data.

$$V = \frac{I_{\max} - I_{\min}}{I_{\max} + I_{\min}}$$

$$-\ln \frac{V}{V_0} = \int_0^T \Gamma(d(t))dt.$$

(7.1) The first formula determines the visibility of a suitable interference signal. The second describes the additional attenuation for a given separation trajectory d(t), if the time-local rate model Γ is applicable and the reference visibility V_0 is correctly defined. This is a working approximation and not a universal property of all open systems.

How lack of effect becomes a result

Suppose the model predicts an almost complete disappearance of interference, and the instrument consistently observes a noticeable contrast. If the background and preparation are checked, the relevant model parameters can be eliminated. This is a meaningful answer, although no new particle or force has been found. It shows what the mechanism we are looking for cannot be. But the negative result has a conditional form: the parameter range is excluded under certain assumptions about noise, mass distribution and time dynamics. To replace such a formulation with the statement “there is no collapse” means losing most of the knowledge gained.

Another way uses side effects of the proposed mechanism. In March 2026, the XENON collaboration published a search for spontaneous X-ray emission in XENONnT data. No significant signal was detected; new restrictions are established on the studied Markov variants of continuous spontaneous localization (CSL) and Dieuchy-Penrose (DP) models. For CSL, the limit $\lambda/r_C^2 < 3.0 \times 10^{-3}$ s^{-1} m^{-2} at the confidence level 90 % was obtained. This form of the limit is applicable for a correlation length rC of no more than approximately 10^{-5} m; the conclusion relates to the white noise used and the radiation model adopted. It cannot be transferred to an arbitrary spectrum without recalculation or declared to be the exception of all objective collapses. [16]

The calculation of radiation also depends on the internal structure of the substance. A preprint by Manti et al. for germanium and xenon examined atomic correlations that change the low-energy spectrum of the predicted emission. In the region 1–100 keV, a simple dependence inversely proportional to the photon energy no longer replaces the calculation of a specific material. This is a theoretical refinement of the signal model, not a detection of collapse; To obtain a new numerical limit, it is necessary to reprocess the experimental data. [68]

Such results require discipline in further modeling. A beautiful numerical example with parameters already excluded is acceptable as an educational illustration, if this is clearly indicated. To forecast a real discovery, you need to start with areas that are compatible with the current restrictions in the selected version of the model. Otherwise, high sensitivity appears on paper only because the calculation is looking for an effect, the absence of which has already been shown by another experiment. Checking the available parameter area precedes promises of the power of the new installation.

An experiment as a comparison of explanations

A well-designed test compares multiple explanations of the same entries. The first includes conventional quantum dynamics, medium and apparatus. The second adds a certain change in fundamental dynamics. At the same time, it is useful to consider a third thing: a more complete version of the usual background. If an additional parameter improves the description, this may indicate either a new mechanism or the original model being too poor. A separate plot with small residuals does not allow one to choose between these cases.

Therefore, the experimental program must contain changes in conditions in advance. A decrease in pressure tests one set of assumptions, a change in temperature another, and a redistribution of mass a third. Not every change will be convenient, but physically independent changes are especially valuable. They force the explanation to make new predictions while maintaining the same fundamental parameters. The superposition boundary, if it exists, must appear consistently in such a system of checks. The next chapter specifies which laws can be applied to this requirement.

Compare degrees of freedom and verification methods

The table of experimental platforms is only useful when the same words represent the same measurement tasks. The mass of the vibrational mode, the total mass of the molecule and the mass of the atom in the interferometer refer to different objects of description. For a mode, the effective mass and coordinate amplitude are important; for a molecular beam - the distribution of masses and the history of separation of the center of mass. The internal spin superposition by itself does not determine the difference in spatial mass densities. Therefore, each row of the table begins with a degree of freedom, and not with a record number of atoms.

One published set of MUSCLE measurements is then used as a single numerical reference - the second grating power scan for sodium clusters from April 22 2025. The publication was published in 2026; the date of data recording and the date of the article indicate different events. Information from another mode of the same installation does not replace the parameters of the selected set. This choice allows you to link trajectory calculations, sample processing, and model constraints to a single source. [15, 63]

To compare the types of platforms, it is enough to indicate what test they make possible. The beam interferometer directly tests the spatial interference of transmitted particles. A levitating mechanical object allows for detailed control of movement and heating, but achieving the ground state is not the same as preparing two widely separated branches. Correlated mechanical noise opens up another observation channel and requires its own consideration of geometry. These possibilities complement each other: they should be compared based on the predictions of one selected model. [20, 29]

Platform	Observed value	What is required for the spatial test
Atomic interferometer	Phase and contrast of the center of mass movement	Separation history, duration, interactions and frequency of events
Molecules and clusters	Distribution of transmitted particles and fringe harmonics	Mass, shape, velocities, grating photophysics and losses
Levitating object	Vibrational coordinate, motion spectrum, heating	A certain state of motion; for interference - preparing and bringing together branches
Related mechanical systems	General and difference correlations	Mass form factor, spacing, mechanical response and common background

Specification of the selected measurement set

From the original table and program description, the distance between the gratings 0.98375 m, the period 133 nm, the average speed 158 m/s and its Gaussian width 9 m/s are taken. The nominal center of the mass filter is 170 kDa. Weighting the published mass spectrum into the window adopted by the authors gives 168.940 kDa. This number refers to a specific selection rule in the open source. The effective center 172 kDa indicated in the main text of the article refers to its description of the distribution; these numbers should not be silently mixed in the same calculation. Open archive entries are used sequentially to replicate Chapter Twelve. [15, 63]

With these parameters, the de Broglie wavelength is 14.949 fm, and the Talbot wavelength is 1.18327 m. The flight between the first and third gratings lasts 12.4525 ms. This is the evolution time of an individual particle inside the interferometer; it does not coincide with either the second accumulation of counts in one position or with the total duration of the series recording. Separating these three times is necessary to calculate decoherence and statistical error.

In the harmonic description of a symmetric interferometer, the characteristic maximum separation for the first harmonic is hL/(mvd). For the selected inputs it is 110.574 nm. The grating period 133 nm serves as a geometric scale and does not automatically replace this calculated separation. The latter depends on mass and velocity, so in the full calculation the signal is averaged over their distributions. One monochromatic example is useful for checking dimensionality; the final macroscopicity estimate then uses the published averaging.

The radius 4.101 nm in the table is calculated for a homogeneous sphere with a bulk sodium density of 971 kg/m³. It is not an independent measurement of the shape of each particle. Pressures and temperatures are taken from the installation description and supplement to the article. The gas in the chamber is around room temperature, and the internal temperature of the clusters is estimated to be approximately 80 K; substituting one temperature for another would lead to a different estimate of scattering and radiation. [64]

The open table contains 95 scans at 41 position, with a step of 15 nm and a registration time of one second per position. The amount is 3895 seconds, or 64.92 minutes of net accumulation. This value does not include moving, setting up, pumping out or self-calibrations. Registered 10 772 714 counts. The fraction relative to the corresponding reference signals without gratings is 0.13612. This is the relative passage of the entire measuring path, and not the absolute quantum efficiency of the detector.

The last difference shows what the completed specification should be: the number is given along with the procedure for obtaining it and the limits of interpretation. Missing absolute efficiency cannot be recovered by dividing two values if both already contain unknown losses. For mode comparisons, the normalized response may be sufficient; Additional flow and detector measurements will be required to predict the performance of the new facility.

$$\lambda_{\mathrm{dB}} = \frac{h}{m v}$$

$$L_T = \frac{d_g^2}{\lambda_{\mathrm{dB}}}$$

$$T_{13} = \frac{2L}{v}.$$

(7.2) d_g is the grating period, L is the distance between adjacent gratings. Index 13 means the span from the first to the third grating; T_{13} = 12.4525 ms for selected inputs.

$$\Delta x^{(1)}_{\max} = \frac{hL}{m v d_g}$$

$$R = \left(\frac{3m}{4\pi \rho_m}\right)^{1/3}.$$

(7.3) The first formula specifies the characteristic separation of the first harmonic; the second converts mass into radius at the assumed uniform density ρ_m. These are different geometric characteristics.

Parameter	Meaning	Origin
Nominal mass	170 kDa	Mass window in the archive [63]
mass after weighing	168.940 kDa	Calculation from published mass spectrum
Speed and its width	158 and 9 m/s	Open analysis inputs [63]
Period and distance	133 nm; 0.98375 m	Inputs of the same configuration [63]
Time between G_1 and G_3	12.4525 ms	2L/v
Chamber pressure	Less than 9×10^{-9} mbar; in the calculation 9×10^{-9}	Description of operating mode [15, 64]
Gas/cluster	300 K / about 80 K	Different physical temperatures [64]
Sphere size	Radius 4.101 nm	Density 971 kg/m³ - assumption
Recording capacity	3895 positions; 10 772 714 counts	Direct file counting [63]
Net accumulation	3895 s	Sum of registration times; not full experiment time

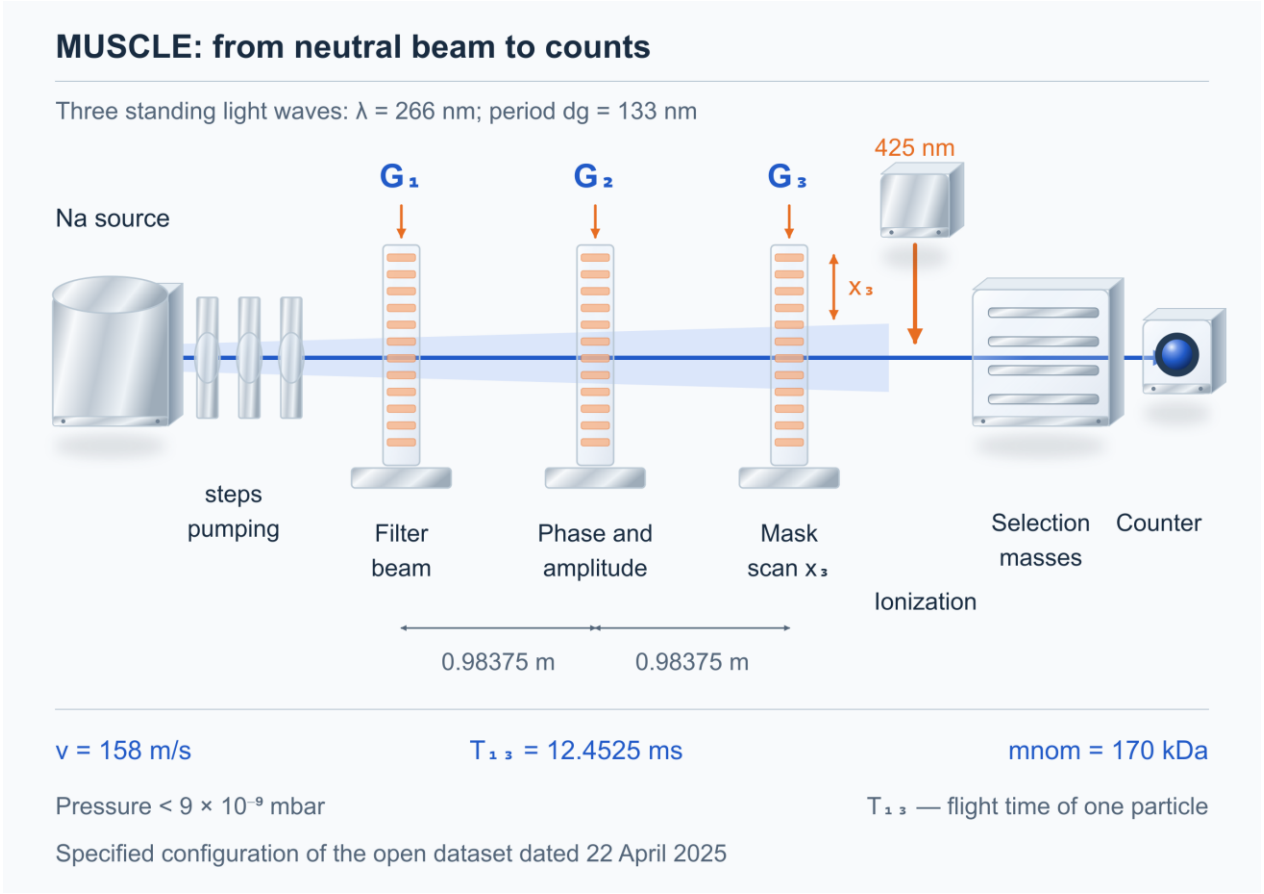


Figure 16. Measuring path of the sodium experiment: neutral clusters pass through three standing ultraviolet waves with a period of 133 nm; after the third grating, ionization, mass filtration and registration are performed. The diagram is functional, not to scale. Specification values refer to the selected published set; The time of flight of a particle differs from the time of accumulation of counters. According to data [63] and description [15].

Constraint Map with Explicit Model

For a spatial test, it is useful to construct a boundary in the plane of intensity λ and length rC. Each point on such a map means a given modification of the dynamics. The same limit of visibility usually gives significantly different restrictions at different lengths: on small scales the structure of the body is significant, on large scales there is poor discrimination of close branches. The map is therefore more informative than the singular number λ for an arbitrarily chosen rC.

As a transparent example, we take a mass-proportional Markov CSL, a homogeneous sphere with specification parameters and the condition of maintaining at least 78% of the reference contrast. The latter value is used in the supplementary material for the interferometric comparison. Here it is transferred to a clearly limited monochromatic setting with the first harmonic and a finite radius. The resulting line is a sensitivity estimate reproduced by formulas, and not a new confidence limit obtained by repeated full processing of all calibrations. [17, 64]

For rC = 100 nm, this formulation gives λ about 7.51×10^{-9} s^{-1} at the boundary of the specified condition. The reference mass in normalization is equal to one dalton. The number answers the question what intensity would give an additional attenuation

index −ln(0,78) for the chosen trajectory. It does not indicate that such intensity has been detected, nor does it establish the likelihood of a false exclusion.

The same figure shows the published white noise bound XENONnT $\lambda/rC^2 < 3.0 \times 10^{-3}$ s^{-1} m^{-2} at the confidence level 90%. Its greater rigor in this model does not turn interferometry into an unnecessary experiment: the observation channels test different manifestations of the mechanism and depend on different frequency assumptions. When the spectrum changes, the radiative and interferometric responses must be recalculated. The statistical statuses of the two lines are different and are indicated separately. [16, 24]

It makes sense to design a future protocol in a model space that is still compatible with the relevant constraints. If a training calculation uses a stronger effect for clarity, its amplitude remains a simulation parameter. To claim an achievable fundamental test would require a general model of the spectrum, body, trajectory, and all observables used.

$$\lambda_{\max}(r_C) = \frac{-\ln R_{\min}}{K(r_C)}$$

$$R_{\mathrm{CSL}} = e^{-\lambda K(r_C)}.$$

(7.4) K(rC) is calculated by integrating the selected mass kernel along the trajectory. Here Rmin = 0.78 is an explicitly accepted condition for an illustrative line, not an independent level of statistical significance.

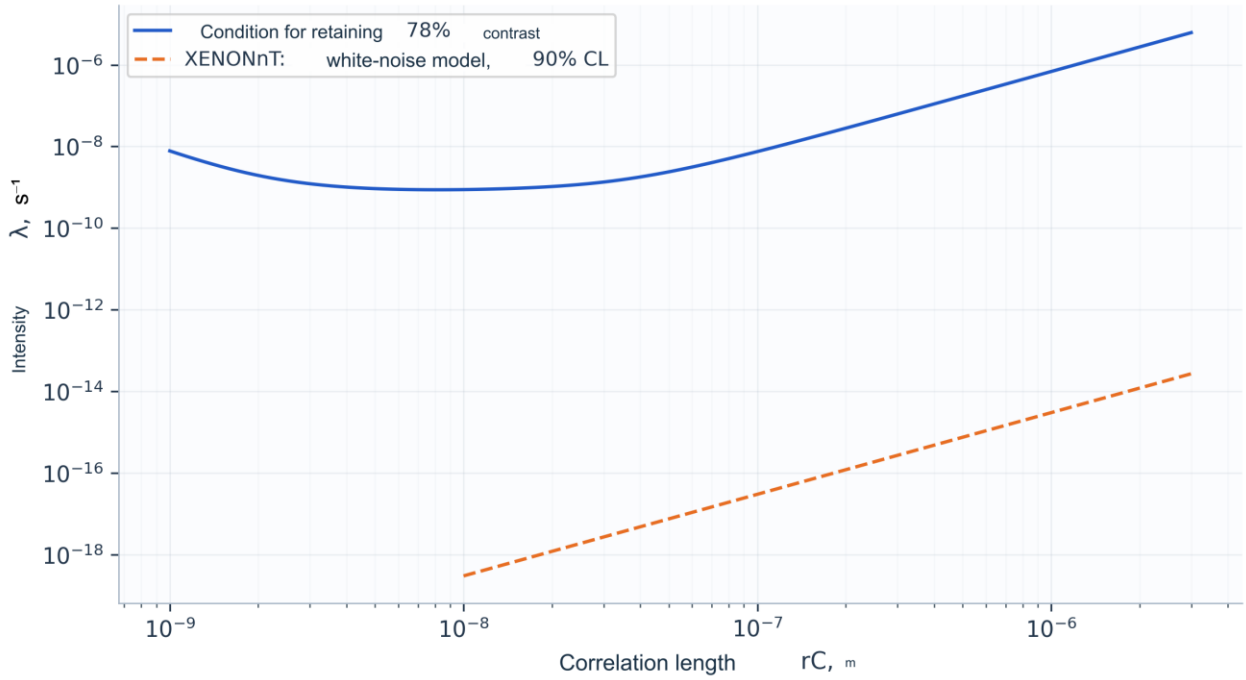


Figure 17. Calculated line of condition R ≥ 0.78 for specification geometry and published boundary XENONnT. The first line is illustrative, the second has the declared level 90% CL; both belong to the specified white noise model. These lines cannot be transferred to an arbitrary spectrum. [16, 64]

Comparing platforms becomes meaningful when mass is accompanied by geometry, timing, and registration model. The selected sodium set then goes through

media evaluation and re-analysis of the raw readings. This allows each step of the reasoning to be checked and the distinction between the published measurement, the model calibration and the calculated consequence to be maintained.

8 Objective collapse models

Objective collapse suggests that the reduction of the set of spatial alternatives is due to a physical law that operates regardless of whether anyone is looking at the device. Such a hypothesis becomes testable when it specifies dynamics and parameters. Talking about spontaneous choice of position is not enough: it is necessary to explain which states are localized, how quickly this happens and what happens to the energy. Different answers lead to different theories, although in popular exposition they are often grouped under one name.

What changes in the law of motion

Ordinary unitary development transfers the pure state of a closed system from one form to another, preserving its norm and purity. The collapse model adds special dynamics. At the level of individual states, it can be random and nonlinear, and after averaging, it can give a linear equation for the density matrix. These two descriptions answer different questions. The first describes the putative history of a particular condition; the second allows you to calculate frequencies of results from a large number of repetitions. They cannot be replaced without explanation.

In the work of Ghirardi, Pearl and Rimini 1990, continuous spontaneous localization was formulated through stochastic evolution compatible with the symmetry of identical particles. The goal was to preserve familiar microscopic predictions and quickly suppress some macroscopic superpositions. This is an original theoretical construct and not an established experimental mechanism. It shows an important possibility for research: to propose a universal dynamic that differs from the standard one and is therefore testable. [21]

When reading such a model, it is useful to distinguish between three levels of statements. The law for the density matrix determines the observed ensemble probabilities. An additional rule for individual states determines the expected pattern of events. Finally, the connection of this picture with a single perceived result requires its own argumentation. While the calculation has proven the damping of off-diagonal elements, it has not yet proven all three levels at once. Such caution does not invalidate the model; it helps to see which issue is truly resolved.

Two spatial localization parameters

In the mass-proportional version of CSL, it is convenient to isolate the intensity λ and the length r_C. The first sets the frequency scale for the reference mass, the second sets the spatial resolution of the mechanism. If two alternatives are almost the same relative to r_C, the impact does little to differentiate them. When the separation is large enough, the discriminability becomes saturated. For a compact body whose dimensions are much smaller than r_C, the law contains the square of the ratio of the body mass to the reference mass of the nucleon. This effective form and

the connection with the collisional decoherence equation are explicitly discussed by Nimmrichter et al. [17]

The compact body formula allows us to construct the first dimensional checks. λ has the dimension of inverse time, the mass ratio is dimensionless, and the argument of the exponential is also dimensionless. Therefore Γ really is a rate. With zero separation, it becomes zero: coinciding positions cannot be distinguished by spatial localization. When the separation is small, the expansion of the exponential gives the square of the distance; when the separation is large, it gives a constant limit. These properties are more useful than memorizing a single coefficient: they immediately detect many errors in new calculations.

$$\Gamma_{\mathrm{CSL}}(d) = \lambda\left(\frac{m}{m_0}\right)^2\left[1 - \exp\left(-\frac{d^2}{4r_C^2}\right)\right]$$

$$R \ll r_C.$$

(8.1) Here m is the mass of a compact rigid object, m_0 is the selected reference mass of the nucleon, d is the separation of spatial alternatives. The formula refers to a specific mass-proportional CSL with white noise. R characterizes body size; for an extended object, this approximation is replaced by a calculation based on mass density.

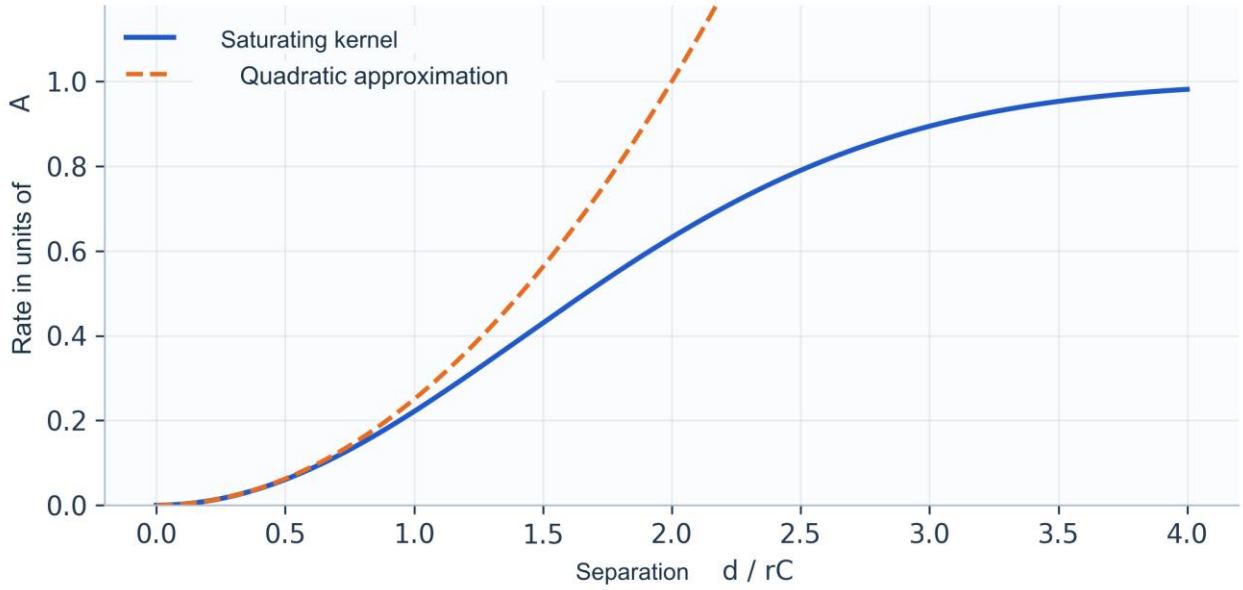


Figure 18. The compact spatial model moves from quadratic behavior to saturation. The quadratic approximation is only applicable for small d/rC.

Why body shape is included in the theory

A real object has mass distributed in space. Two bodies of equal mass can have the same center, but different shells, voids and internal layers. If the model is sensitive to the distribution of matter at scale r_C, it should distinguish between these cases. A convenient language for calculation is the spatial Fourier transform of mass density. It shows how much an object contains irregularities of a given size. The weight of

each heterogeneity is then determined by the correlation kernel of the model. This calculation is called taking into account the form factor.

Testing edge cases provides simple control. As the body size tends to zero, the form factor should turn into total mass, and the integral should return a compact formula. When moving parts of a large body apart, the contributions of their mutual correlation should correctly disappear when the distance exceeds the corresponding scale. Simply multiplying the point result by the number of atoms usually does not replace this procedure. The number of atoms and the square of the total mass arise from different assumptions about the consistency of the contributions.

This difference opens up an opportunity for experiment design. Changing the geometry can change the signal under study at an almost constant total mass. But it simultaneously changes mechanical modes, interactions with surfaces, and sensitivity to external fields. This means that the geometric gain should be assessed together with the changed background. An object that maximizes the formal collapse term does not necessarily provide the most compelling comparison with ordinary physics.

To verify such a calculation, you can explicitly specify the mass density and the selected Fourier transform convention. In the notation below, the wave vector k has the dimension of inverse length, and the converted density has the dimension of mass. Gaussian weight suppresses spatial inhomogeneities at too small a scale. The cosine multiplier compares the original and shifted distributions. In the point limit, the transformed density is m, and the ordinary Gaussian integral returns the formula from the previous section. This is a convenient analytical test of the implementation: an error in the normalization of the integral will immediately violate the point limit.

$$\tilde{\mu}(\mathbf{k}) = \int d^3 r\, \mu(\mathbf{r}) e^{-i\mathbf{k}\cdot\mathbf{r}}.$$

(8.2) μ(r) is the mass density of the rigid body. A transformation without a normalization coefficient before the integral is adopted; μ̃(0) = m.

$$\Gamma(\mathbf{d}) = \frac{\lambda r_C^3}{\pi^{3/2} m_0^2} \int d^3 k\, e^{-r_C^2 k^2} |\tilde{\mu}(\mathbf{k})|^2 [1 - \cos(\mathbf{k}\cdot\mathbf{d})].$$

(8.3) The final geometry is enabled through the mass form factor in the specified mass-proportional CSL convention. Two identically oriented copies of one rigid body are considered, differing in the transfer d. For the superposition of different orientations, a more general calculation of the difference in distributions is required.

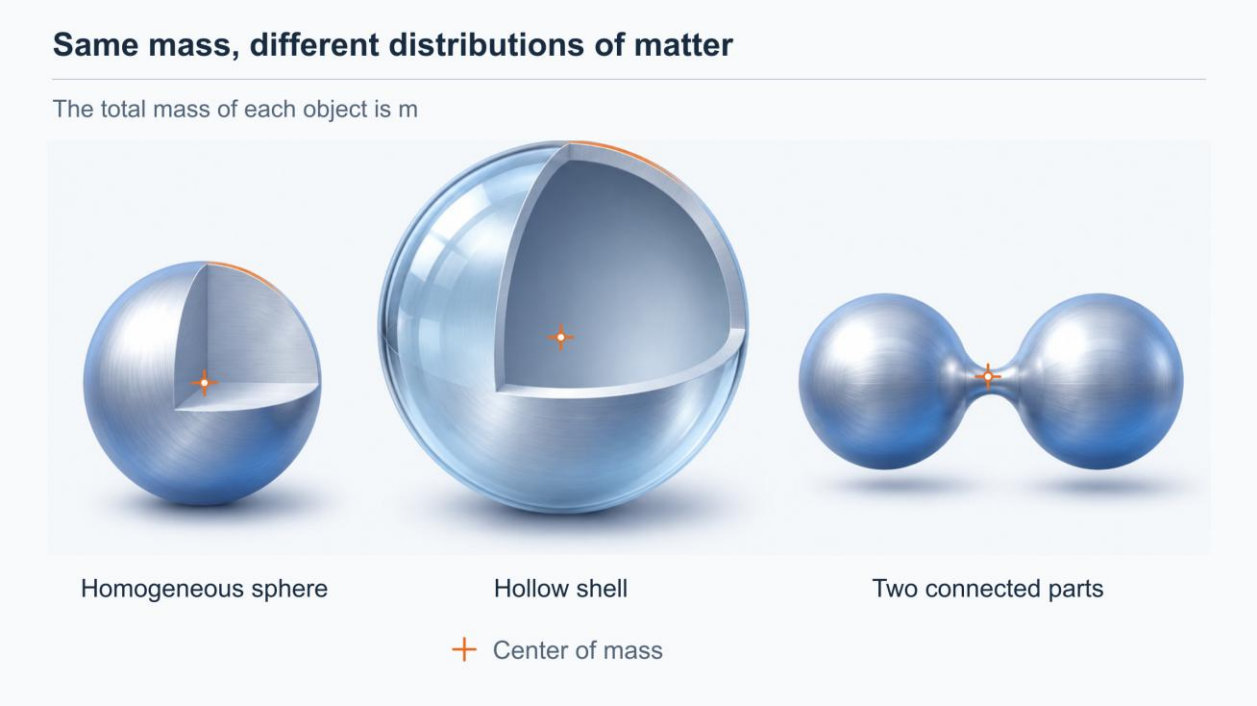


Figure 19. Three possible distributions of one total mass m: a homogeneous sphere, a hollow shell and two connected compact parts. Orange marks indicate the centers of mass of full bodies. The cuts reveal the structure conditionally, without implying the removal of the substance. The dimensions and densities of structures can vary: equal mass does not require equal outer radii or densities. The scene illustrates the geometry, not the calculated form factor.

Two stories of one ensemble

The difference between individual history and ensemble law can be seen in a two-level system without spatial integrals. Let $H = 0$, and B is a bounded dimensionless self-adjoint operator. For specific numbers, we then take $B = Z$ with eigenvalues ± 1. The parameter κ is positive and has the dimension of inverse time. Two normalized stochastic evolutions are compared.

In the first evolution, the noise changes phase in a unitary manner. Its exact solution at constant B is equal to $\exp(-i\sqrt{\kappa}\, B\, W_t)|\psi_0\rangle$. In the stochastic notation, a deterministic term $-\kappa B^2 dt/2$ appears, although each finite transformation is unitary. It is necessary when using Ito's rule: the contribution of the quadratic variation dW^2 is of order dt. Without this term the norm would erroneously change.

In the second evolution, the noise multiplies the deviation of B from its current mean b_t. The average is calculated from the same individual normalized wave function, so the equation is nonlinear. This type of stochastic equation arises, in particular, for the state caused by recording an ideal continuous measurement. The relationship between record, conditional state, and averaged equation is developed in detail in the continuous measurement literature. [57]

Let us denote the individual projector by $P = |\psi\rangle\langle\psi|$. When calculating dP, you need to keep three terms: $d|\psi\rangle\langle\psi|$, $|\psi\rangle d\langle\psi|$ and $d|\psi\rangle d\langle\psi|$. The latter contains dW^2 and gives the usual contribution of the order of dt. For both equations, the deterministic part

after reduction is κ(BPB−{B²,P}/2). The terms with b_t in the second case cancel out precisely in this part.

The stochastic parts remain different. In the unitary case they contain the commutator −i√κ[B,P]dW, in the conditional case - √κ(BP+PB−2b_tP)dW. When averaging over the physical probability measure of Wiener increments, their average contribution is equal to zero. Therefore, both constructions give the same matrix ρ with the same linear equation of motion.

Equality of ensemble dynamics does not make individual stories equal. In the first evolution, the populations of the eigenstates of B do not change. In the second, the entry gradually distinguishes between these states and changes the conditional populations. The ambiguity of the stochastic description under the single Lindblad equation also appears in the models of spatial motion considered by Hofmann and Drossel. [28]

$$d|\psi\rangle = \left[-\frac{\kappa}{2}B^2 dt - i\sqrt{\kappa}B dW\right]|\psi\rangle.$$

(8.4) Random unitary phase in Ito form. W is a real Wiener process; the mathematical expectation dW is zero.

$$d|\psi\rangle = \left[-\frac{\kappa}{2}(B-b_t)^2 dt + \sqrt{\kappa}(B-b_t)dW\right]|\psi\rangle$$

$$b_t = \langle\psi|B|\psi\rangle.$$

(8.5) Normalized nonlinear stochastic evolution. In the continuous measurement model, W describes the random remainder of the record after subtracting its conditional average, and not the instrument reading itself.

$$\dot{\rho} = \kappa\left(B\rho B - \frac{1}{2}\{B^2,\rho\}\right) = -\frac{\kappa}{2}[B,[B,\rho]].$$

(8.6) General ensemble equation of both constructions. It is obtained by the direct Ito product rule under the specified restrictions.

How populations differ and visibility coincides

Let the initial state be |+⟩ and B = Z. With a random unitary phase, the probability of path zero in each history remains 1/2. The relative phase between paths changes by an amount proportional to W_t. Averaging exp(−2i√κ W_t) over a Gaussian quantity with variance t gives exp(−2κt). Therefore, the ensemble visibility fades, although no individual story chooses one of the paths.

For the second evolution it is convenient to follow z = ⟨Z⟩. Direct application of the stochastic equation gives dz = 2√κ(1−z²)dW. There is no deterministic shift in mean z. However, individual trajectories go to regions around +1 or −1, where the noise coefficient becomes small. This corresponds to the conditional preferential population of one of the two eigenstates.

In this example, the eigenstate of Z does not change during the measurement. The recording distribution can be generated without time sampling error. In dimensionless time τ = κt, the auxiliary sign h is chosen with probabilities 1/2; then

Y(τ) = 2hτ + B_τ, where B_τ is a Wiener process with variance τ. The conditional z is equal to tanh(2Y). The sign of h here serves as a way to sample the exact distribution of the measurement record. It is not introduced as a proven hidden physical variable of a quantum system.

For τ = 1/2, the total ensemble visibility of both structures is equal to exp(−1) ≈ 0.367879. At τ = 1 it is equal to exp(−2) ≈ 0.135335. In the above calculation, this is tested separately for 160 000 independent implementations of each type at four times; deviations of the means are consistent with their statistical uncertainty. The figure shows different conditional populations and the matching ensemble forecast. It represents a simulation of given laws.

To observe a conditional trajectory means to have access to a specific measurement record and to accept a model of its relationship with the system. If the entry is deleted, the same ρ remains. If a record is available, the composition of observations has changed, and joint statistics of the system and record need to be compared. Therefore, demonstrating different stochastic paths is not a new solution to the measurement problem and does not prove objective collapse. It shows what additional structure is missing in one ensemble equation.

For a spatial model, the conclusion is transferred as a requirement to the description: it is necessary to name the localization operator, the rule of individual evolution and the available observations. Bilevel calculation does not replace mass proportional CSL; it allows one to check the logical transition from its ensemble law to a statement about individual events.

$$dz = 2\sqrt{\kappa}(1 - z^2)dW$$

$$z(0) = 0$$

$$p_0 = \frac{1 + z}{2}.$$

(8.7) Conditional population for continuous measurement Z at H = 0. In the random unitary construction, z is identically equal to zero for the same initial state.

$$\rho(t) = \frac{1}{2}\begin{pmatrix} 1 & e^{-2\kappa t} \\ e^{-2\kappa t} & 1 \end{pmatrix}$$

$$V(t) = e^{-2\kappa t}.$$

(8.8) Coincident ensemble matrix. Its diagonals are constant, and off-diagonal elements decay in both models.

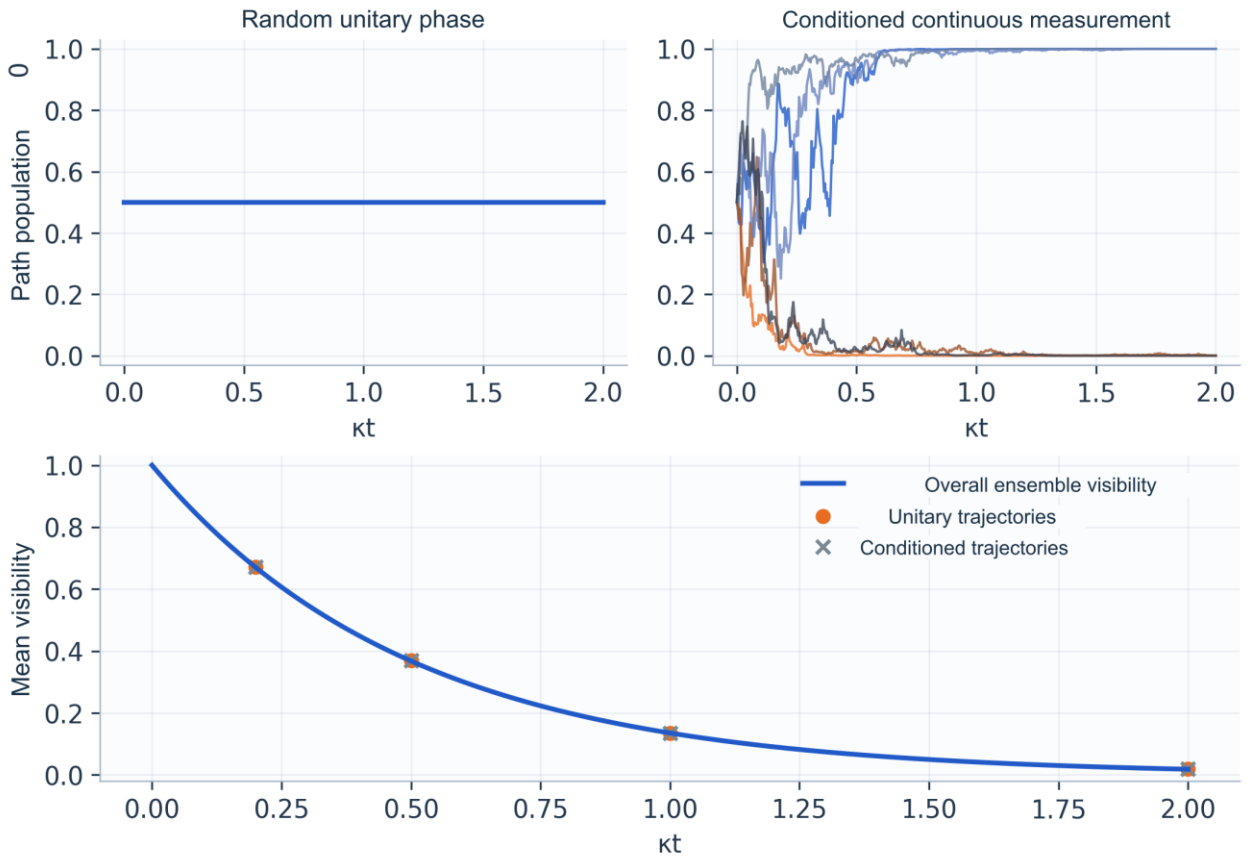


Figure 20. Different individual descriptions give one ensemble. In the case of a random unitary phase, the population of the path is unchanged; with conditional continuous measurement it changes. The bottom panel compares precise visibility with independently modeled averages; This is model data.

Gravitational motivation and its limits

Another way relates the instability of the superposition to the difference between the two mass distributions and the corresponding gravitational fields. Gyöchy in 1989 proposed a dynamical model with a gravitational measure of mass fluctuations. Penrose in 1996 discussed a different line of reasoning: the difficulty of matching time evolution for superposed geometries and the characteristic time scale being inversely proportional to the gravitational energy of the difference. The similarity of the emerging assessments explains the common combined name, but does not make both initial constructions completely identical. [22, 23]

If we denote the difference between two mass densities by δμ, the Newtonian energy of such a difference is given by a double spatial integral. For smooth densities, it allows comparison of geometries. When replacing matter with point sources, caution is required at short distances: short-wavelength contributions may become uncertain. Therefore, the smoothing or other physical limit is part of the model and not a harmless technical detail. Changing this assumption can change heating predictions and constraints.

Estimating time through energy does not replace the complete law. It does not automatically tell which stochastic history is realized, how the probabilities are

updated, or how a consistent relativistic version is constructed. The research text should indicate whether only scale estimation or specific regularized dynamics is used. Otherwise, one formula imperceptibly begins to represent several divergent hypotheses.

$$E_G = \frac{G}{2}\int d^3r\, d^3r' \frac{\delta\mu(\mathbf{r})\delta\mu(\mathbf{r}')}{|\mathbf{r}-\mathbf{r}'|}$$

$$\tau \sim \frac{\hbar}{E_G}.$$

(8.9) This notation expresses the common Newtonian estimate for a smooth or explicitly regularized mass density difference. Numerical conventions and smoothing must be specified separately. The relation $\tau \sim \hbar/E_G$ has the status of a model estimate, and not an experimentally established universal collapse time.

White noise and memory

White noise is an idealization in which correlations over time are extremely short and the spectral density remains constant in the frequency range under consideration. This makes the equations simpler, but expands the content of the hypothesis: the same law actually relates very different frequencies. If the effect has a memory time, its high-frequency part may be weakened. Then the limitation obtained for one type of radiation is not automatically transferred to mechanical motion at significantly lower frequencies.

Carlesso, Ferialdi and Bassi examined how non-interference tests of collapse models depend on the spectrum of colored noise. Their work demonstrates the need to explicitly specify spectral assumptions when comparing constraints. [24] It does not follow from this that arbitrary complication makes the model protected from verification. Every added feature or scale must be constrained by data. If the spectrum can be freely rearranged after each experiment, the hypothesis gradually loses its predictability.

For a first research program, it is reasonable to select a small family of spectra with a limited number of parameters and test the robustness of the inference to alternative families. The resulting constraint will already be a universal statement, but it can be verified and reproduced. The next step is to construct an equally explicit model of the environment. You cannot demand precision from a proposed new law and at the same time describe the usual sources of loss with the vague word “noise.”

9 Environment as a physical model

When looking for new dynamics, it is easy to turn the environment into a residual category: everything that prevents you from seeing the desired effect is called noise. This is not enough for fundamental experiment. Gas, thermal photons, electric fields and control instability operate according to different laws. They depend on different parameters and leave different records. Understanding these differences allows us not only to reduce interference, but also to construct controls for changes where explanations diverge. This is where the abstract problem about the boundary of the quantum world turns into concrete research work.

Separate particle loss and coherence loss

Let the number of registered particles decrease after changing the setting. This does not mean that the remaining particles have lost the mutual consistency of spatial alternatives. Part of the flow could escape the detector, collide with a wall, or change the charge. With a different setting, the number of particles may be almost the same, but the interference will be weakened due to random phase shift. The third possibility is that the velocity distribution has expanded and different interference patterns no longer coincide when averaging. These cases require different corrections and produce different test predictions.

It is therefore useful to model the entire registration process: preparation, completion, survival and final readout. If the analysis uses only particles that make it to completion, selection also becomes part of the physical model. For example, the impact may remove some speeds or dimensions more strongly. The remaining ensemble no longer represents the original distribution. Fitting one general visibility is then able to attribute the collapse to a change in sample composition. This is not a rare logical subtlety, but a general consequence of conditional statistics: the result depends on which events are included in the denominator.

In a computational model, it is convenient to test such a difference on artificial data. First, obviously ordinary physics and a known loss mechanism are specified. This data is then processed using a simplified procedure. If the procedure reliably returns a non-zero fundamental parameter, an analysis problem has been detected. It needs to be corrected, and not explained away by a false effect with a new theory. Such a test is especially useful before receiving real data, when expectations are not yet tied to a specific schedule.

Collision as information transfer

A gas molecule can carry away information about the position of an object through the post-scattering state. To an observer who does not register the surrounding gas, this will appear as a decrease in spatial coherence. In 2003 Hornberger et al measured the weakening of fullerene interference with increasing residual gas pressure and quantitatively correlated the observation with collision decoherence.

Thus, the environment acted as a controlled physical participant in the experiment, and not an arbitrary explanation for the inconvenient result. [26]

If momentum transfer in a collision is random, the two spatial alternatives acquire different relative phases. The difference depends on the product of momentum and separation. A very small separation is barely resolved by that event; a large separation may be almost fully resolved. This reasoning already shows that environmental decoherence need not grow quadratically at every distance. The quadratic law is often only the first term of an expansion around coincident positions.

The overall result for a sequence of independent random shocks is expressed through the characteristic distribution function of the transmitted impulse. In such a recording, saturation of spatial rate occurs naturally, without changing quantum mechanics. This formalism is developed in detail in Vacchini's work on collisions and Lévy processes. [18] The conclusion is significant for the research problem: the shape of the visibility loss curve in itself does not assign a fundamental origin to the impact. You need to know what shapes the measured environment allows.

Warm object in a cold chamber

Wall temperature, gas temperature, and internal particle temperature are different quantities. Even if the chamber is cold and well evacuated, the particle can store internal energy and emit photons. Radiation changes the state of the medium, and the availability of position information depends, in particular, on the wavelength. You cannot replace this entire process with one temperature taken from the nearest sensor. The model should indicate exactly what temperature is being measured and how it is related to the state of the flying object.

Hackermüller et al. in 2004 demonstrated the loss of interference of C_{70} molecules upon thermal radiation. This is an experimental example of how the internal state of a complex object affects the observed spatial coherence. [25] For the new protocol, a practical requirement follows: a change in preparation power or flight time must be checked not only as a change in the spatial trajectory, but also as a possible change in the thermal history.

Hidden connections between control knobs are especially dangerous. Increasing the distance between branches may require a stronger optical pulse. This pulse can heat the particle, and heating can change the emission and contrast. Loss versus distance will appear in the data, although the immediate cause is related to preparation. An additional sequence helps to break this ambiguity, which changes the invested energy while maintaining the trajectory, or the trajectory with comparable energy. The possibility of such control must be clarified at the design stage.

Phase instability and limited recovery

Random phase can make the average interference pattern almost flat. In this case, an individual trigger can remain well defined if a record of the disturbing field is available. Conditional processing taking this record into account sometimes restores contrast. The point of restoration is not to undo a fundamental event that has already

taken place, but to change the available information about the usual dynamics. However, such success relates to the registered source and does not prove that all the loss of coherence in the installation is of the same nature.

And the opposite conclusion is false: the failure of restoration does not yet prove objective collapse. The recording might not be accurate enough, the control pulses might be too slow, or the medium might contain inaccessible degrees of freedom. Therefore, a statement about restoreability is always accompanied by a description of permitted actions and their accuracy. The theoretical possibility of completely reversing closed-loop dynamics and the practical ability of a laboratory to perform this reversal are different questions.

Accuracy of language is especially important when modeling individual trajectories. Different stochastic representations of the same ensemble equation can paint completely different histories of the wave function. Hofmann and Drossel showed this with a model particle in a noisy potential: the same loss of phase coherence did not provide the same localization in different representations. [28] Therefore, the animation of a shrinking packet is not an independent experimental proof of collapse.



Figure 21. A generalized transparent chamber connects physical sources of losses with parts of the measurement path. Gas scattering, thermal radiation, phase disturbance, and drift away from the recording area are shown separately. The temperatures of the particle, gas and walls differ. A collision does not necessarily remove the particle from the sample. The color of conventional photon waves does not determine their wavelength. The scene is not a reconstruction of MUSCLE and does not set a quantitative budget.

How does a background get the right to be called verified?

A validated background model is not required to list every possible influence in the universe. It must clearly define the area in which its parameters are measured and provide correct responses to the intended control changes. The statement “residual gas is negligible” is only useful in conjunction with pressure, composition, uncertainties and calculation of the corresponding contribution. Likewise, the absence of visible drift in a short recording does not establish its absence during a long data set. The model becomes more reliable by checking its predictions, rather than by increasing the list of terms.

For later analysis, it is useful to separate the parameters into several roles without turning these roles into physical entities. Some define the law under study, others characterize the environment, and others describe registration. They may all be uncertain, but not all should fit freely into one curve. Some parameters are determined by individual measurements. For the remaining ones, acceptable ranges are set and it is checked how the output changes when they are expanded. If the conclusion disappears after a small reasonable adjustment to the background, it should be considered fragile.

Finally, the remainder after subtracting the background is also the result of a calculation with an error. It may be negative, correlate between settings, or depend on the selected processing method. One cannot first treat the background as an exact quantity and then treat the remainder as a direct observation of a new force. The correct way is to transfer the uncertainty of all essential components into the final comparison. The next chapter shows how a specially selected combination of measurements can simplify this task, and where its capabilities end.

Gas budget in numbers

For the configuration specified in the seventh chapter, the gas contribution can be calculated using the scattering estimate in the supplement to the work by Pedalino and colleagues. It expresses the rate of complete decoherence in a distinguishable collision in terms of pressure, temperature, the molecule's most probable speed, and the van der Waals interaction coefficient C_6. The residual-gas composition in this estimate is a model assumption: the authors explicitly state that the interferometer chamber lacked a calibrated composition analyzer. [64]

A mixture with partial pressures is used: 4.6×10^{-9} mbar for water, 1.4×10^{-9} mbar for helium and 3.0×10^{-9} mbar for hydrogen. The sum is equal to the upper working pressure estimate 9×10^{-9} mbar accepted for calculation. The C_6 coefficients are calculated in the Slater-Kirkwood approximation using the static polarizabilities given in the source: 9.4 Å³ per sodium atom, 1.5 Å³ for water, 0.2 Å³ for helium and 0.8 Å³ for hydrogen. The electronic numbers in this estimate are also fixed by the source.

With a mass of 168.940 kDa and a flight time of 12.4525 ms, the calculation gives the rates of 8.339 s^{-1}, 1.804 s^{-1} and 7.979 s^{-1}, respectively. Their sum is equal to

18.122 s⁻¹, and the total contrast preservation multiplier is 0.79798. The closeness to the estimate around 0.79 from the supplementary material serves as a check of units and scale. The difference in the last percentages should not be interpreted as a new effect: the mass, speed and composition in such a calculation are given with much more significant physical assumptions.

The rates add up because independent Poisson scattering channels are adopted here. Visibility multipliers, on the other hand, are multiplied. This is the same law in two representations: the logarithm of the product turns each mechanism into a separate contribution. This representation is convenient for the budget, since it shows which parameter changes the final loss the most.

Hydrogen at a lower partial pressure makes a contribution comparable to water: not only the density of the gas is important, but also the speed of the molecules. Therefore, it cannot be concluded from one vacuum gauge reading that the gas correction is known. It is necessary to know the composition and applicability limit of the adopted scattering model. The latter assumes that the colliding particles remain in the detection angle; if the detector removes them, the ensemble selection changes together.

$$\Gamma_g \simeq \frac{8 p_g}{k_B T_g}\left(\frac{C_6^2 v_g^3}{\hbar^2}\right)^{1/5}$$

$$R_g = \exp\!\left[-T_{13}\sum_g \Gamma_g\right].$$

(9.1) The estimate is applied under the prerequisites for long-range scattering specified in the source. When substituting, pressure is converted to pascals: 1 mbar = 100 Pa. T_{13} is the total time from the first to the third grating.

Component	Partial pressure, mbar	Γ, s⁻¹	Multiplier R
H_2O	$4{,}6 \times 10^{-9}$	8.339	0.90137
He	$1{,}4 \times 10^{-9}$	1.804	0.97778
H_2	$3{,}0 \times 10^{-9}$	7.979	0.90541
Sum/product	$9{,}0 \times 10^{-9}$	18.122	0.79798

Partial pressures are a published compositional model, not three independent measurements of a given set. The results were recalculated based on specification entries.

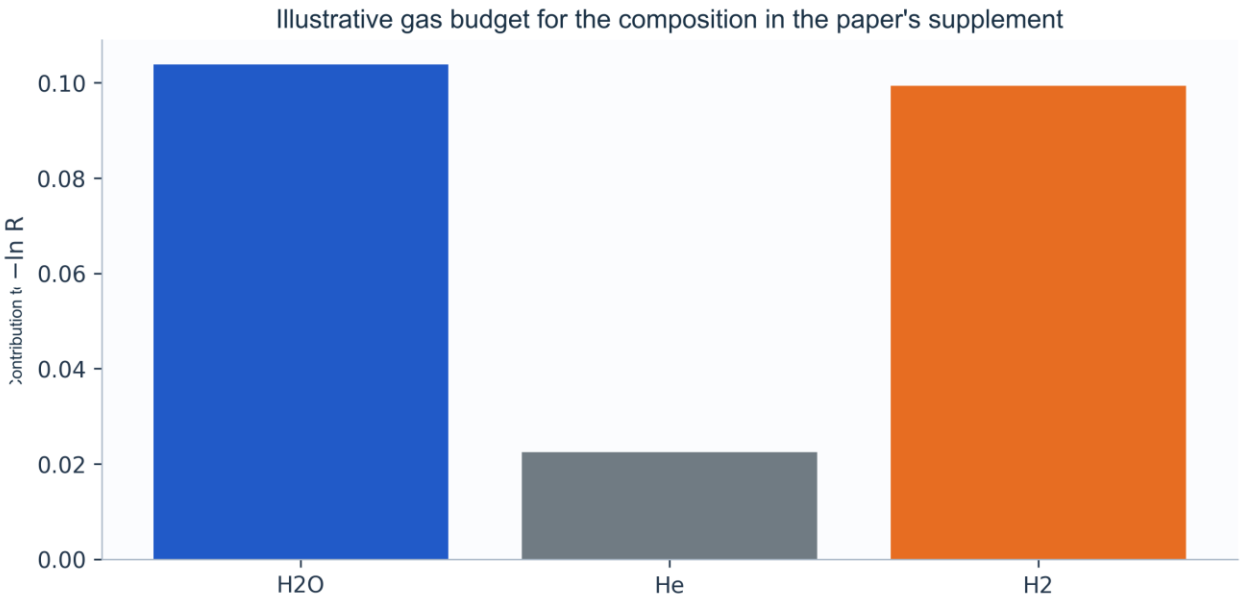


Figure 22. Contribution of the components of the selected residual gas model to the contrast loss index. Composition taken from supplementary material but not independently measured in this kit. The calculation was repeated according to the specification parameters. [64]

Composition uncertainty changes conclusion

To evaluate the role of an unknown composition, one can leave the total pressure unchanged and consider extreme variations within the same set of substances. If all the pressure is attributed to helium, we get Rg = 0.86550; for water - 0.81615; for hydrogen - 0.74223. These edges do not indicate that the chamber is actually filled with pure gas. They show the range allowed by the model itself without additional information about component proportions.

This change is much larger than the small remainder that we would like to attribute to fundamental dynamics. The observation condition 78% reference visibility is compatible with some conventional gas compositions. If the nominal mixture is considered accurate, then after dividing it a factor of approximately 0.97747 remains. With a different permissible composition, this remainder may decrease, disappear, or change sign in the logarithmic representation. A nonzero correction after subtracting a single background does not yet define a new mechanism.

It is convenient to transfer systematics into analysis through the parameters of partial pressures with a limit on their sum. Then a separate experiment on composition or pressure change really narrows down the many explanations. Substituting a single convenient composition with zero error artificially increases the accuracy of the fundamental parameter. For a new experiment, the priority may be to calibrate the gas composition rather than an additional hour of collecting the same interference samples.

Even with a fixed composition, uncertainties remain in the polarizability and applicability of the cross section. In the above model, Γ is proportional to $pC_6^{2/5}T_g^{-7/10}$ if the gas velocity is expressed in terms of its temperature. Small

relative changes are therefore transferred with different coefficients. This allows you to decide in advance which auxiliary parameter should be measured more accurately, without assigning equal importance to all inputs.

$$\frac{\delta \Gamma}{\Gamma} \simeq \frac{\delta p}{p} + \frac{2}{5}\frac{\delta C_6}{C_6} - \frac{7}{10}\frac{\delta T_g}{T_g}.$$

(9.2) Linear sensitivity refers to one gas component and $\nu_g \propto \sqrt{T_g}$. This is a transfer of small changes, not a formula for adding independent standard errors: the latter requires a covariance matrix.

Phase requires the covariances of three gratings

The shift of the stripes is determined by a combination of movements of the first, second and third gratings. The overall motion of the entire structure is not equivalent to three independent vibrations. For Gaussian displacements, it is convenient to introduce the effective displacement $X_{eff} = \delta x_1 - 2\delta x_2 + \delta x_3$. Then the contrast is set by the dispersion of this particular combination, and not by the average reading of one accelerometer.

If all three movements are independent and have the same variance σx^2, the variance X_{eff} is equal to $6\sigma x^2$. With a completely common synchronous shift, the combination becomes zero. The real installation lies between such limits, and its frequency correlations are important. The numerical coefficient in front of σx^2 cannot be transferred from one mechanical model to another without checking the definition of amplitude and cross-correlations.

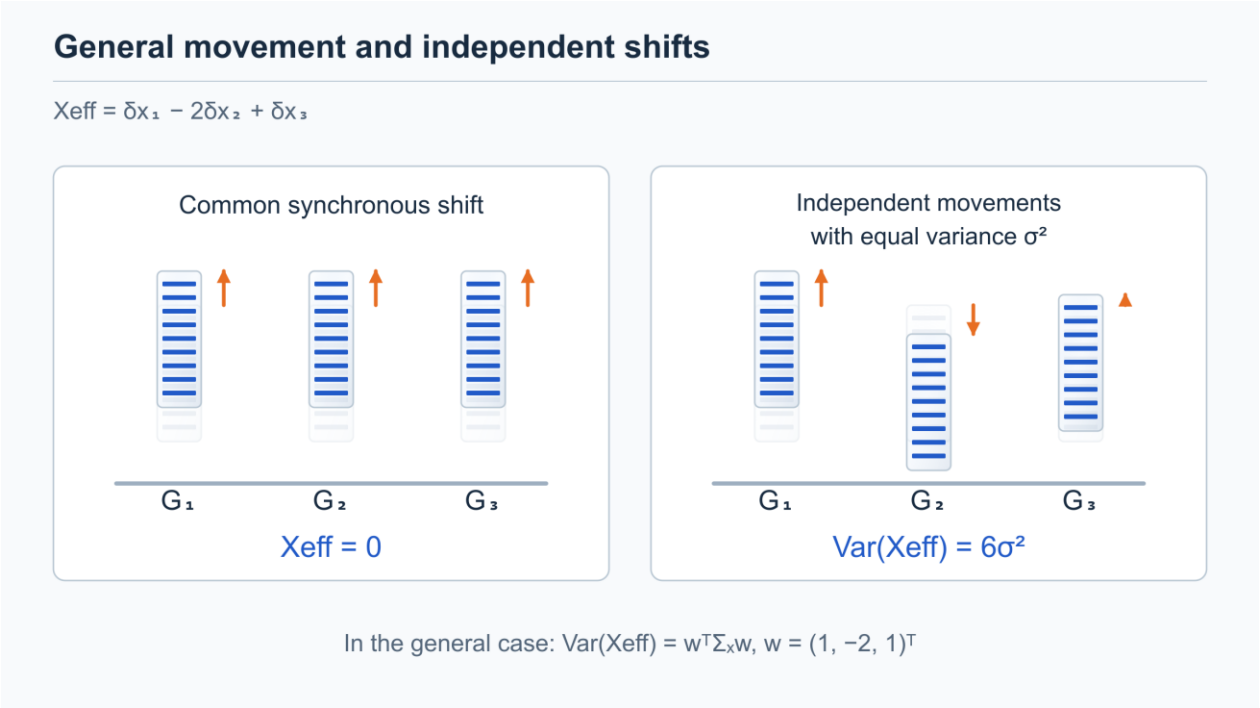


Figure 23. The effective displacement of the three gratings is equal to Xeff = δx₁ − 2δx₂ + δx₃. Equal effective movements are reduced; three independent movements of the same dispersion σ² give Var(Xeff) = 6σ². In the general case, a covariance matrix Σₓ is needed. The displacements must be compared with the moments of interaction of the flying particle; General mechanical support alone does not guarantee compensation for random vibration. Shown are model limits, not measured amplitudes.

To obtain the visibility ratio 0.78 by phase averaging alone, a standard deviation Xeff of about 14.922 nm is required. In the particular case of three independent equal displacements, this corresponds to σx about 6.092 nm for each grating. If we first assume the nominal gas factor 0.79798, a σeff of about 4.519 nm is sufficient for the remaining ratio 0.97747. These numbers are equivalent noise levels calculated from the selected loss; they are not the result of vibration measurements.

Therefore, two explanations for one decrease in contrast cannot be completely multiplied and called the total budget. If the gas already accounts for almost all of the loss, the additional phase amplitude must be estimated along with it. Otherwise, the same loss is counted twice. In a valid model, gas intensity and phase dispersion are constrained by independent controls, and the remaining uncertainty is transferred to the overall probability of the data.

The estimate of about 7 nm given in the supplement to the article corresponds to the coefficient $8\pi^2$ in the attenuation index; for the independence of the three lattices explicitly assumed here, the coefficient is equal to $12\pi^2$ and the result is 6.09 nm. Equality of mean square biases alone is not enough to identify models: covariance is required. No specific unspecified correlation is attributed to the source authors here. [64]

$$\delta\phi = \frac{2\pi}{d_g}\,\mathbf{w}^{T}\delta\mathbf{x}$$

$$\mathbf{w} = (1,-2,1)^{T}.$$

(9.3) The weight of the second grid differs from the weights of the first and third. The overall shift cancels out because the sum of the weights is zero.

$$R_{\phi} = \exp\!\left[-\frac{1}{2}\left(\frac{2\pi}{d_g}\right)^{2}\mathbf{w}^{T}\,\Sigma_{x}\,\mathbf{w}\right].$$

(9.4) Σ_x is the covariance matrix of grating displacements averaged according to the time of flight. The formula assumes a Gaussian random phase and includes cross-correlations.

Heat and registration in one measuring path

For the internal temperature of sodium clusters around 80 K, the authors estimate thermal radiation as an insignificant source of contrast loss; A similar conclusion was made for Rayleigh scattering on gratings and evaporation of atoms. In the nominal budget, therefore, the thermal multiplier Rth = 1 is adopted. This is the use of a published physical estimate and not an independently measured upper limit. When another particle is heated, the string must be recalculated from its frequency-dependent optical response. [64]

Temperature should not be substituted into the ideal black body law without checking the optical model. A particle with a radius of a few nanometers is much smaller than the characteristic thermal wavelengths, and its absorption and emission are determined by the material and geometry. The geometric area by itself does not define the spectrum. Therefore, the reliability of the thermal budget is based on the model of the interaction of light with the selected object, and not on the presence of a numerical thermometer in the table.

Registration adds another mechanism for reducing observed visibility. If a constant dark background D is added to a sine wave with average level S, the amplitude of the fringes remains the same, but the average level becomes S + D. The measured visibility is multiplied by S/(S+D). If the background has already been subtracted, this correction cannot be reapplied.

The average sampling frequency in the selected archive is 2765.78 s⁻¹. The article indicates the range of electronic dark counts 15–100 s⁻¹. If such an unsubtracted constant contribution were present at this average frequency, the corresponding visibility multiplier would be between 0.99458 and 0.96384. This is a calculation of sensitivity to background processing. The open archive itself does not provide grounds to automatically consider each of these amendments implemented at each point. [15]

In contrast to a constant dark background, a uniform loss of the proportion of useful particles with a constant composition reduces the number of events, but not necessarily visibility. Its price is manifested through statistical error and the duration of accumulation. If losses depend on speed, mass or position, they also change the

averaged distribution. These cases require different coefficients in the response model and should not be combined into one unnamed performance parameter.

$$V_{\mathrm{recorded}} = V_{\mathrm{signal}} \frac{S}{S + D}.$$

(9.5) The formula describes the addition of a constant non-interfering background D to the useful average signal S. It does not describe all types of losses and is not reapplied after the same background has been correctly subtracted.

Budget Element	Numerical reference	Status
Residual gas	R = 0,79798	Calculation for the specified model composition
Composition at the same pressure	R from 0.74223 to 0.86550	Extreme variants of a mixture of three gases
Gravity and rotation	R > 0,99	Authors' rating for leveled installation [64]
Thermal radiation	Nominally R = 1	Published estimate at about 80 K; not measured exact unit
Phase averaging	σeff = 4.519 nm after nominal gas	Equivalent noise for ratio 0.78, not new calibration
Dark Counts	Multiplier 0.96384–0.99458	Conditional calculation if the specified background is not subtracted
Accumulation	3895 s; 10.773 Msample	Measured archive data; rebuilds not included

What control reduces major uncertainty?

The drawn up budget allows you to formulate a specific solution for the next measurement. In the accepted gas model, an unknown fraction of hydrogen changes the contrast by an amount comparable to the entire residue under consideration. Control of composition and pressure dependence therefore directly tests one of the main explanations. Additional interference scans in constant mode reduce the random error, but do not eliminate this physical degeneracy.

For mechanics, it is useful to record the phase-sensitive motion combination, or an equivalent calibration of the vibration transmission to the strip. The low signal of an individual accelerometer does not determine all the correlations of the three gratings. Dark series and control of mass selection are useful for registration; they should be carried out under conditions comparable to the main recording. For heat, the test must change the internal state of an object with a known geometry and a controlled optical response.

These actions do not provide an abstract list of precautions, but a measuring sequence. First, the residue of interest is fixed, then parameters that can absorb it

are found, after which independent control of these parameters is selected. In Chapter Nineteen, the same logic will be expressed in terms of the joint probability of initial events and tested on ensembles of artificial data.

The calculated budget shows both the magnitude of losses and the limit of knowledge about their composition. For the selected sodium set, ordinary gas already gives a decrease in contrast of the desired scale, and a small phase or registration correction noticeably changes the remainder. Therefore, subsequent statistical analyzes must include calibrations while maintaining the distinction between the measured quantity, the estimated mechanism, and the counterfactual.

10 Three measurements and the limits of their meaning

For the first calculation, it is useful to choose a problem that can be solved before the big simulation. Suppose you want to check whether the loss dependence on branch separation contains curvature that is missing in the simple background model. This task is much narrower than proving objective collapse, but it allows one to accurately demonstrate the effect of the method. Neither the spatial localization formula nor the differences between neighboring values are a new discovery. The value of the example is its transparency: it shows what assumptions are being made, what is destroyed by the combination of measurements, and what alternatives remain.

Working model and meaning of each term

An idealized experimental section is considered, in which the branches are held at a constant distance for the same amount of time. The device estimates the additional rate of loss of visibility after taking into account the reference contrast. In a certain non-zero range of distances, the background is approximated by the sum of the constant and quadratic parts. Added to it is the saturable dependence characteristic of the compact mass-proportional CSL. The intensity of this term is denoted by A. Such a notation specifies the task of distinguishing between two functional forms, and not the complete law of installation.

The constant part has a local empirical meaning. For example, some background process may already be saturated at all distances under study. It is impossible to continue such an approximation to exactly matching positions without checking: the physical rate of pure spatial decoherence should disappear with zero separation. Similarly, the coefficient of the quadratic part is assumed to be common for all three settings. If changing the trajectory simultaneously changes temperature or charge, this assumption may be violated.

$$\Gamma(d) = b_0 + b_2 d^2 + A\left[1 - e^{-d^2/(4r_C^2)}\right]$$

$$A = \lambda\left(\frac{m}{m_0}\right)^2.$$

(10.1) b_0 and b_2 describe the background in the selected range; A and r_C specify the added saturable term. The compact CSL limit discussed in chapter 8 is used. The record does not claim that the entire environment has such a simple appearance.

Distances are selected by their squares

The usual difference between two measurements removes the constant background, but retains the quadratic one. To eliminate both, it is convenient to choose three distances so that their squares form an arithmetic progression. To do this, take d_0, $\sqrt{2}\,d_0$ and $\sqrt{3}\,d_0$. Then the first and third rate values are added, and twice the second is subtracted. Any straight line in the variable d^2 disappears. The

method does not know the origin of this straight line: it destroys the corresponding form in the same way for hardware correction and physical impact.

Substituting the saturated term gives a short expression. It is negative at positive intensity and finite non-zero distance. With a very small separation, the saturable dependence is itself almost quadratic, so the combination suppresses it too. With an extremely large separation, all three values almost become saturated and the combination disappears again. The greatest absolute contrast occurs between these limits. This is the geometric reason for the optimum; it is understandable before differentiation.

After replacing the exponent with a new variable, the problem is reduced to the maximum of a cubic polynomial on the interval. It turns out u = ln 3 and the absolute value 4A/27. This result helps to select an area to scan if the scale r_C is assumed to be known. When r_C is unknown, a single setting cannot be declared optimal for all possible mechanisms. You should explore the range and take into account that finding the most expressive area from the data itself changes the statistics of the statement.

$$d_j = \sqrt{j}\, d_0 \ (j = 1,2,3)$$

$$u = \frac{d_0^2}{4 r_C^2}$$

$$Q = \Gamma(d_1) - 2\Gamma(d_2) + \Gamma(d_3) = -A e^{-u}(1 - e^{-u})^2.$$

(10.2) Q is the second difference in the square of the distance. The constant and quadratic backgrounds cancel algebraically with common coefficients.

$$|Q|_{\max} = \frac{4A}{27}$$

$$u_* = \ln 3$$

$$d_{0,*} = 2 r_C \sqrt{\ln 3}.$$

(10.3) This is the maximum of the absolute model contrast at a fixed A, and not automatically the maximum of experimental significance.

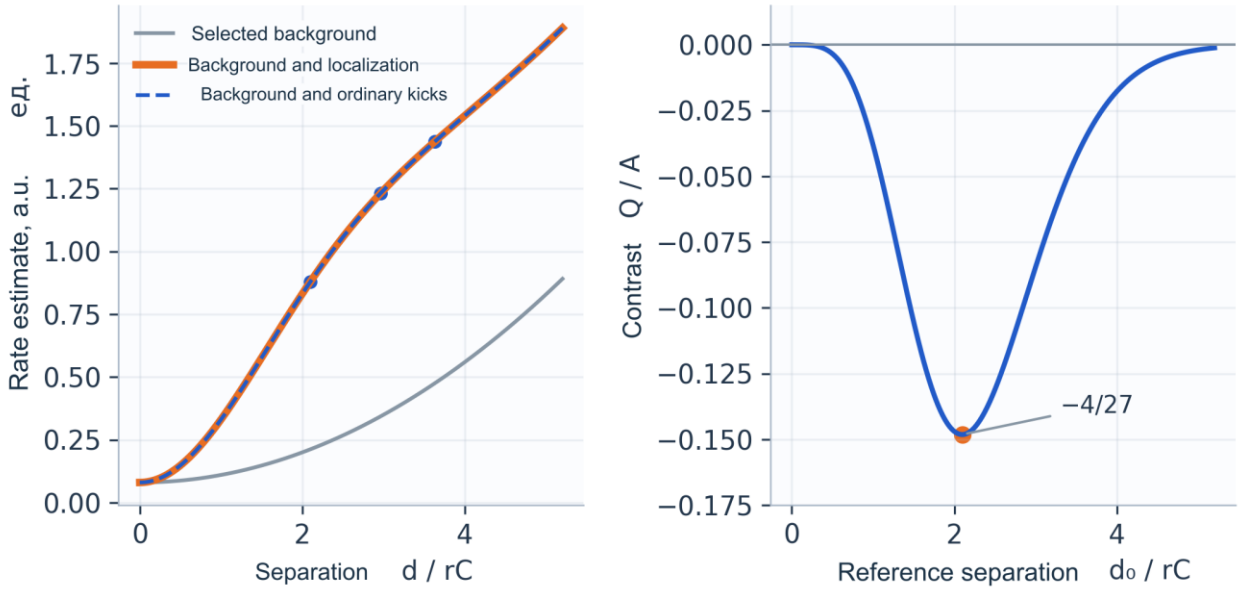


Figure 24. Three measurements cancel the constant and quadratic background. However, the saturable curves of localization and suitable normal noise coincide; contrast does not establish cause by itself.

What price was paid for background reduction

Combining measurements reduces sensitivity to certain systematic effects, but does not create data for free. Every rate estimate has an error. With independent equal variances, the variance of Q is six times the variance of the individual estimate. If the errors are correlated, the result is determined by the full covariance matrix. The overall equal correction may be reduced, but drift that affects successive settings differently may increase. The order of the data set therefore becomes part of the design rather than a neutral technical detail.

In real experiment, the errors are usually not the same. With strong attenuation, little information about the contrast remains, and the rate is determined worse. In addition, the logarithm transformation may make the error distribution skewed. Therefore, the maximum of absolute Q does not have to coincide with the maximum of the signal-to-uncertainty ratio. To make the final choice of setting, you should simulate the initial readings and evaluate the statistics using the procedure that will be applied to the experiment.

There is also a physical cost of approximation. If the $b_4 d^4$ term is present in the background, it contributes $2b_4 d_0^4$ to Q. Therefore, a non-zero response establishes a deviation from the chosen linear relationship in d^2. It does not say which of the additional terms created it. The background check should cover precisely those nonlinearities that are capable of simulating the desired sign and scale. Increasing the accuracy of measurements without such verification may only make an erroneous explanation more confident.

A simple control consists of repeating three settings in different time orders. If the value of Q varies markedly depending on which setting was performed first, the underlying assumption of a general stationary background is called into question. An additional fourth point can help separate the parameters, but with b_0, b_2, A and r_C

unknown, four points are generally not enough to independently test the entire four-parameter model. For such a check, additional or previously deferred configurations are required. When choosing between repetitions and a new point, it is the gain in distinguishability that is evaluated. More adjustments are justified when testing an assumption on which a physical derivation depends.

$$\mathrm{Var}(Q) = \mathbf{w}^{T}\,\Sigma\,\mathbf{w}$$

$$\mathbf{w} = (1, -2, 1)^{T}.$$

(10.4) Σ is the covariance matrix of the three rate estimates. With independent identical errors σ², Var(Q) = 6σ²; given general drift, this simplification may not be correct.

Separating and recombining the branches

Let us replace the constant distance with three consistent trajectories $d_j(t) = \sqrt{j}\, d_0\, f(t)$, where j = 1, 2, 3, and the same profile f(t) varies from zero to one. The total duration T is the same. For each setting, the average accumulation rate $-\ln(V/V_0)/T$ is estimated. Let b_0 and b_2 be truly general, as in the original example, and the time-local compact model is preserved.

The background reduction now occurs at each moment of time: the sum of the weights is zero, and the sum of the weights multiplied by $d_j^2(t)$ is also zero. Integration does not violate the identity. However, the saturated term must be integrated as a whole. The maximum distance in itself does not determine what fraction of the time the system spent in the sensitive region of the spatial kernel.

In the first profile, f = 1 throughout the idealized sequence; the previous result $2\sqrt{\ln 3}$ is returned. In the second, the branches diverge linearly for the first half of the time and linearly converge for the second. For this triangular profile, the average of any function of f is equal to the integral of this function over f from zero to one. Thus, the optimum is found by one-dimensional quadrature without modeling individual time steps.

It turns out $d_0/r_C \approx 3.060183$ and the maximum average contrast modulus 0.0785904 A. Both numbers differ from the result of constant retention. If the distance 2.096294 r_C is left for the triangular movement, only 0.0591464 A is obtained. Increasing the maximum spread here compensates for the time spent at short distances.

You can also leave half the time for holding the maximum, and the remaining half is equally distributed between linear spreading and mixing. The contrast will be the half-sum of the results of the two profiles at one d_0. The optimal ratio is then approximately 2.252402, and the maximum modulus is 0.1052741 A. The table gives three points of one continuous family of sequences.

These optima refer to absolute contrast with a known r_C and a fixed duration. Adding real constraints on acceleration, cycle time, loss, and readout error changes the selection problem. However, the integral example serves a specific testing role: when the profile changes, the code must reproduce these limits before it is trusted with a more complex trajectory.

$$\overline{Q} = -\frac{A}{T}\int_0^T e^{-u(t)}[1 - e^{-u(t)}]^2 dt$$

$$u(t) = \frac{d_0^2 f^2(t)}{4r_C^2}.$$

(10.5) Average three-point combination in the full sequence. Constant and quadratic backgrounds cancel with a common time profile and common coefficients.

$$\frac{|\overline{Q}_{\triangle}|}{A} = J_1(\alpha) - 2J_2(\alpha) + J_3(\alpha)$$

$$J_k(\alpha) = \frac{\sqrt{\pi}}{\alpha\sqrt{k}}\,\mathrm{erf}\left(\frac{\alpha\sqrt{k}}{2}\right).$$

(10.6) Closed notation for a triangular trajectory; $\alpha = d_0/r_C$. For very small α, numerical quadrature or expansion is more reliable than direct subtraction of almost equal terms.

Hold time fraction	Optimal d_0/r_C	Maximum $\|\bar{Q}\|/A$
0 - triangular trajectory	3.060183	0.0785904
1/2 - separation with a plateau	2.252402	0.1052741
1 - permanent separation	2.096294	0.1481481

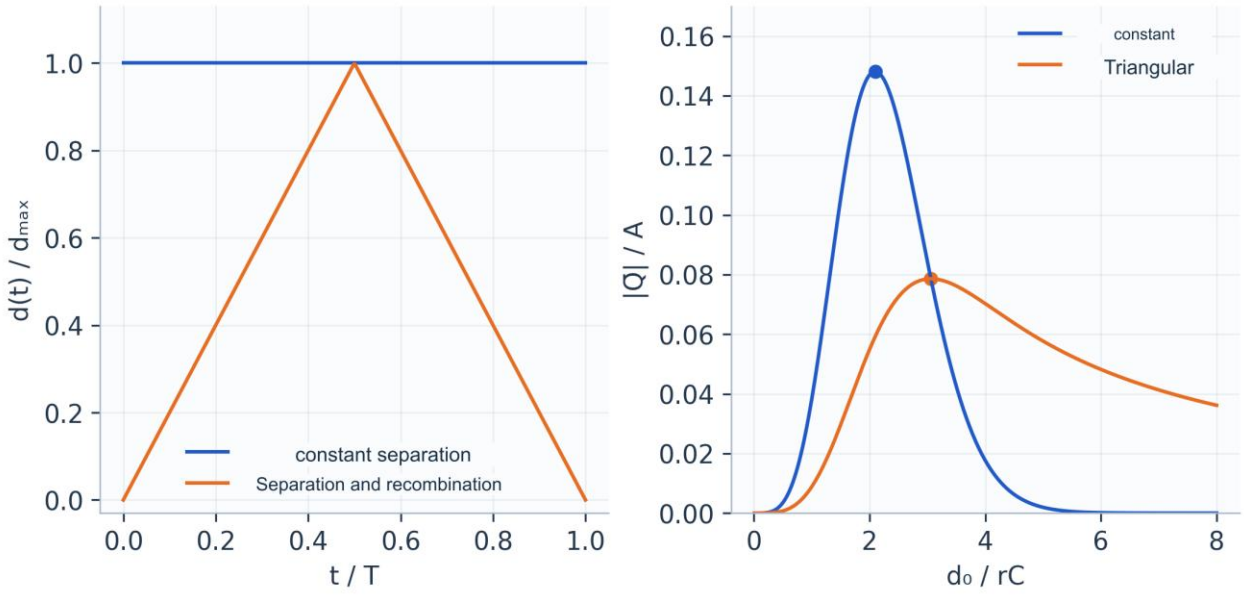


Figure 25. The time profile changes the spatial optimum. For the same duration, constant hold gives a maximum at $d_0/r_C \approx 2.0963$, triangular spread and reduction - at 3.0602. The average contrast module in a given model is maximized.

What remains of the background when there is a geometry error?

Algebraic combination uses given distances, whereas installation implements distances with uncertainty. Let us denote the deviation of each trajectory by $\delta d_j(t)$. Substitution into the quadratic background and expansion to first order gives a remainder proportional to the integral $d_j(t)\delta d_j(t)$. Therefore, the assessment of geometry is included in the physical conclusion even with a completely accurate count of events.

Consider constant relative errors ε_j throughout the sequence, so that the actual profile is equal to $(1+\varepsilon_j)d_j(t)$. If all ε_j are the same, the squared distances still form the desired family and the quadratic background cancels exactly. Such a general scaling error changes the physical meaning of the estimated r_C and the magnitude of the saturated signal, but does not itself create the remainder of the quadratic background. General additive distance error, on the other hand, does not have this automatic protection.

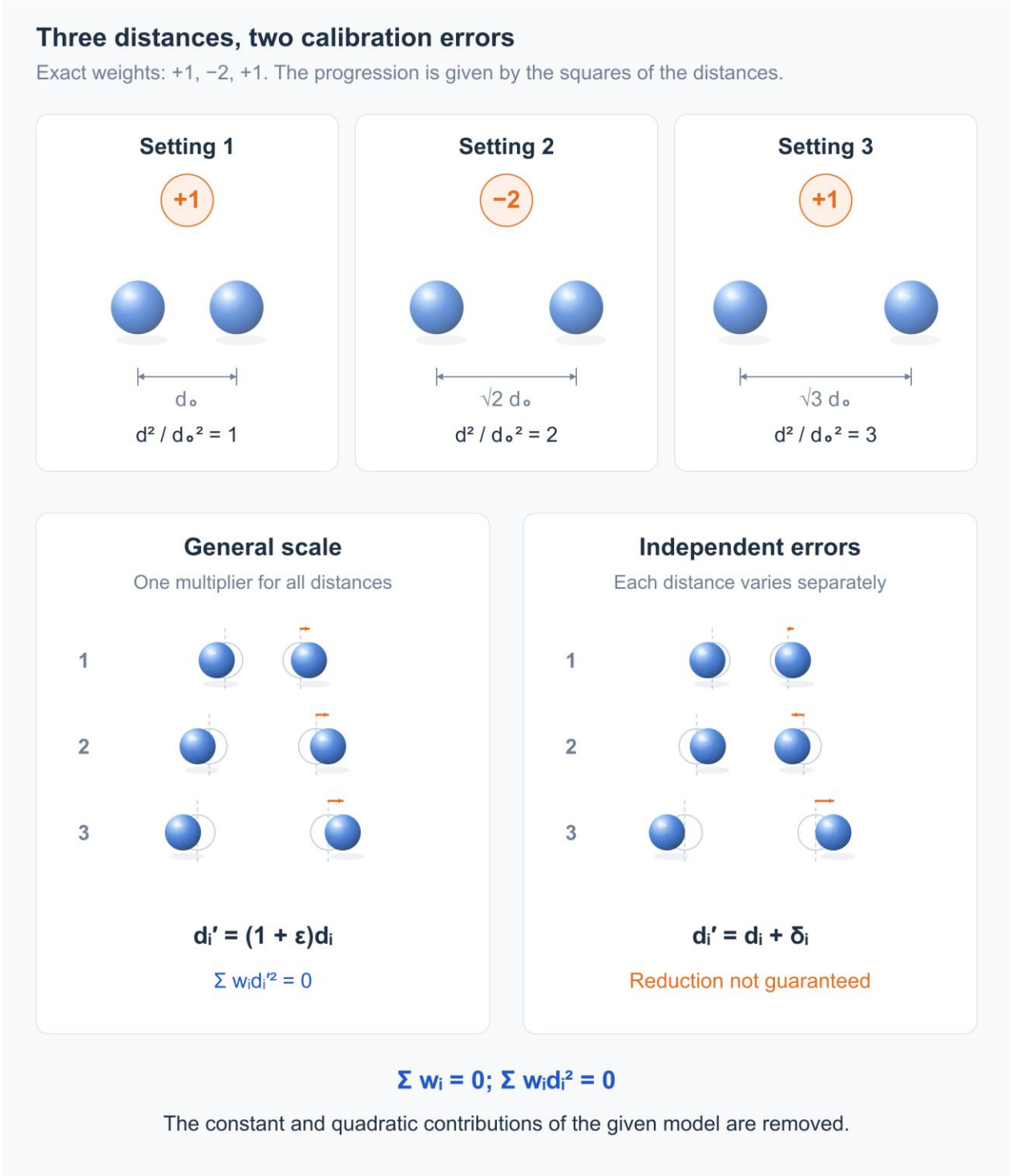


Figure 26. Three spatial settings with distances d_0, $\sqrt{2}\,d_0$ and $\sqrt{3}\,d_0$ and weights +1, −2, +1. Their weighted sum reduces the constant and quadratic background. The general multiplicative scale error preserves this reduction; independent distance errors generally leave a remainder. The gray marks show the reference geometry, the blue marks show the two branches. The displacements are schematically enlarged for clarity. The illustration is for a given calibration model.

For independent small ε_j with the same standard deviation σ_ε, the variance of the remainder is determined by the sum $1^2+4\cdot2^2+3^2 = 26$. For a triangular profile, the average f^2 is equal to 1/3. The resulting formula clearly shows why the words “the geometry is known with an accuracy of one percent” are not enough: both the scale of the background coefficient and the error correlations between settings are important.

Let's take the training values $A = 1\ s^{-1}$, $b_2 r_C^2 = 0.1\ s^{-1}$, $\sigma_\varepsilon = 0.01$ and the triangular optimum. The standard uncertainty of the first order residual background is $0.03183\ s^{-1}$, while the modulus of the desired combination is $0.07859\ s^{-1}$. The geometric uncertainty alone reaches about 40.5% of this signal. Direct modeling of 180 000 error sets gives $0.03181\ s^{-1}$ and is consistent with linear transfer.

This uncertainty is calibration uncertainty and not ordinary counting noise. Additional registrations in the same unknown geometries are not required to reduce it. More precise determination of relative distances, joint geometry estimation, or independent control settings are needed. In full statistical analyses, calibration covariances should be preserved so that the overall scale error is not erroneously replaced by three independent errors.

$$\delta\overline{Q}_{\mathrm{bg}} = \frac{2b_2}{T}\sum_{j=1}^{3} w_j \int_0^T d_j(t)\delta d_j(t)dt + O(\delta d^2)$$

$$\mathbf{w} = (1,-2,1).$$

(10.7) Transfer of small trajectory error to three-point background. For constant division, the integral returns the familiar expression $2b_2\Sigma w_j d_j \delta d_j$.

$$\sigma_{Q,\mathrm{bg}} = \frac{2b_2 d_0^2}{3}\sqrt{26}\sigma_\varepsilon.$$

(10.8) Formula for a triangular profile and independent equal relative distance errors. For correlated errors, their full covariance matrix is used.

Exact imitation by ordinary kicks

There is a stronger ambiguity than a small unknown fourth-order term. Let us consider ordinary unitary shocks that randomly impart momentum to a particle. Let the shock times obey a Poisson process with frequency ν, and the impulses be independent and Gaussian. In each run, if the complete shock record is known, the state develops unitarily. No additional rule for selecting one position is introduced in this model.

When averaging over an unknown record, the relative phases are lost. The characteristic function of the Gaussian distribution gives the exponential of the square of the distance. The choice of momentum dispersion $\hbar^2/(2r_C^2)$ and frequency $\nu = A$ reproduces the same saturable kernel, and therefore the same Q. This is a direct calculation within the framework of the well-known formalism of random momentum transfer. The equivalence of an efficient compact CSL and a collision generator has been noted in the primary literature. [17, 18]

The strength of the example lies in the accuracy of the match. This is not just a matter of an insufficient number of points or a large instrument error. If the entire available reduced generator matches, any observations determined by these single-particle dynamics in a given model remain ambiguous. Heating also does not become an automatic salvation: the same diffusion of the impulse gives the same heating. Additional information should change the physical setting, for example limiting the influence of the environment to independent measurements.

$$\Gamma_{\text{kick}}(d) = \nu\left[1 - \int dq P(q) e^{iqd/\hbar}\right]$$

$$P(q) = \frac{e^{-q^2/(2\sigma_q^2)}}{\sqrt{2\pi\sigma_q^2}}$$

$$\sigma_q^2 = \frac{\hbar^2}{2r_C^2}.$$

(10.9) For a symmetric Gaussian distribution, the integral is real and equal to $\exp[-d^2/(4r_C^2)]$. At ν = A, the rate coincides with the saturated term. This is a model counterexample of the uniqueness of the signature, and not a statement that any real gas has exactly this distribution.

What can you say after such a test?

If Q is compatible with zero, this limits the added curvature in the examined region at the achieved accuracy. If Q is persistently nonzero, the simple background approximation is insufficient or there is an additional effect. Next, a comparison of physical models that are capable of creating this effect is required. Neither result equals a definitive answer about the nature of the measurement. However, both are useful: the first narrows down the parameters, the second indicates which explanation needs to be developed.

The integral calculation already shows the price of the real time profile and geometric calibration. Its application to an extended object additionally requires the form factor from chapter 8 and the registration model from chapter 6. When increasing numerical complexity, it is the simple limits—constant hold, triangular motion, and general scale error—that serve as test cases.

Three measurements cancel out two interfering terms, and matched trajectories preserve this reduction over time. The magnitude of the effect and the accuracy of the geometry are calculated separately. A precise counterexample with random shocks shows why the next step is to test the joint physical predictions and their discriminability limit.

11 What heating and correlations add

An additional observable is useful when it requires the explanation to make a new consistent prediction. Heating, rotating, and moving multiple probes together really enhances testing. But the number of graphs is not equal to the number of independent evidence. If two mechanisms already define the same total available dynamics, another consequence of this dynamics will not separate them. Therefore, we first need to understand what new physical information each measurement brings, and then evaluate its accuracy.

One reason and two manifestations

The simplest example relates spatial decoherence to momentum diffusion. An impact that randomly changes the impulse can simultaneously blur the relative phase of spatial alternatives and increase the average square of the impulse. In a one-dimensional model, both effects are expressed through a single coefficient D_{pp}. This relationship is especially convenient for testing: fitting the interference loss already determines the amount of additional heating expected. To freely choose two coefficients instead of one would be to test a different, less stringent model.

Let the additional term of the equation have the form of a double commutator with a coordinate. In coordinate representation, it multiplies the density matrix by the square of the position difference. Therefore, the decay rate for separation d is D_{pp} $d^2/\hbar^2$. To obtain the change in second moment of momentum, the same generator is applied to the operator p_x^2. The canonical commutator gives double the diffusion coefficient. Dividing by twice the mass converts the result to the rate of growth of kinetic energy along the chosen axis.

This conclusion is a direct consequence of the written equation, and not a separate experimental law. It is useful precisely as a conditional equality: if losses and heating are explained by one such term, their quantities are related. Inconsistency indicates an incomplete model or an error in identifying additional contributions. Consistency indicates that the test is passed, but does not establish the unique nature of the impact.

$$\frac{d\rho}{dt} = -\frac{i}{\hbar}[H, \rho] - \frac{D_{pp}}{\hbar^2}[x, [x, \rho]]$$

$$\Gamma(d) = \frac{D_{pp} d^2}{\hbar^2}.$$

(11.1) One-dimensional Markov momentum diffusion is assumed. Γ refers to the contribution of the specified diffusion term; other coherence losses are taken into account separately.

$$\left.\frac{d\langle p_x^2\rangle}{dt}\right|_{\text{diff}} = 2D_{pp}$$

$$\left.\frac{d\langle E_x\rangle}{dt}\right|_{\text{diff}} = \frac{D_{pp}}{m}$$

$$\Gamma(d) = \frac{md^2}{\hbar^2}\left.\frac{d\langle E_x\rangle}{dt}\right|_{\text{diff}}.$$

(11.2) $E_x = p_x^2/(2\text{m})$ is the kinetic energy of one coordinate, not the total three-dimensional energy. The additional contributions of one mechanism are compared. The influence of the Hamiltonian, cooling and other sources must be taken into account separately.

When the coupling is no longer simple

The quadratic dependence cannot be transferred to any distance. For the saturated model from the previous chapter, the diffusion approximation corresponds to a small separation relative to r_C. At larger distances, the loss of coherence saturates, while heating characterizes the other side of the same oscillator. Applying a small-scale equality far beyond its derivation creates an imaginary contradiction. Therefore, before comparing two observables, it is necessary to check that both are calculated in compatible approximations.

Another subtlety appears in the installation with cooling. The observed energy may remain constant, although additional diffusion is present: its contribution is compensated by energy removal. The stationary dispersion or overall balance is then tested rather than the non-zero slope of temperature over time. If the model includes dissipation, the formula for pure heating also changes. The conclusion “the temperature does not rise, therefore there is no collapse” without an appropriate balance is not physically determined.

For colored noise, different measurements are sensitive to different parts of the spectrum. Long-term free movement, mechanical resonance and high-frequency radiation use different filters. They cannot be reduced to a single intensity number without specifying the spectral model. [24] However, it is precisely this distinction that can be useful: multiple bands limit the ability to adjust the spectrum. A strong program tests a single family of spectra across all data, rather than assigning each instrument the independent intensity of one supposedly universal process.

Heating beyond the quadratic approximation

For Gaussian shocks from the tenth chapter, the energy growth can be derived without decomposing the spatial kernel. Each push replaces the impulse p_x with p_x+q. With a symmetric distribution of q, the average cross term $2p_xq$ disappears, and the square of the momentum on average increases by the dispersion of the shock. The Poisson frequency A translates the increment of one event into a rate.

With a dispersion q equal to $\hbar^2/(2r_C^2)$, we obtain an increase in one-dimensional kinetic energy $A\hbar^2/(4mr_C^2)$. This result is compatible with the exact saturable rate $\Gamma(d) = A[1-\exp(-d^2/(4r_C^2))]$ for any d in the compact model. In the isotropic three-dimensional version, the same contributions of the three coordinates give a three times greater increase in the total kinetic energy.

Therefore, it is useful to compare not only individual numbers, but also the ratio that eliminates A. The quantity $md^2\dot{E}_x/(\hbar^2\Gamma)$ is equal to $u/(1-\exp(-u))$, where $u = d^2/(4r_C^2)$. For small d, it tends to unity—the diffusion equality of the beginning of the chapter returns. At $d = 2r_C$ it is approximately equal to 1.582. The discrepancy with unity in this mode does not refute the saturated model: it shows the limit of the quadratic approximation.

Let us now set up a fully numerical simultaneous example. Let us choose the reference length L and the parameters $A = 0.5\ s^{-1}$, $r_C = L$. The two average rates at $d = L$ and $d = 2L$ are equal to 0.1105996 and 0.3160603 s^{-1}, respectively. It is convenient to express the energy observable as $H = 4mL^2\dot{E}_x/\hbar^2$; its value is $0.5\ s^{-1}$. All three numbers are accurate model expectations, not random experimental readings.

For comparison, we set the training standard errors 0.005, 0.005 and 0.02 s^{-1} and assume their independence. Pure quadratic diffusion has one coefficient B: it predicts $\Gamma(d) = Bd^2/(4L^2)$ and $H = B$. Minimizing the sum of squared normalized deviations over the three observables gives $B = 0.3332979\ s^{-1}$. The predictions of such a model cannot simultaneously approach both spatial values and energy growth at the chosen weights.

The minimum weighted discrepancy is 111.12. This is a diagnostic number calculated on mathematical expectations for assigned errors. It is not the p-value of the actual discovery and does not justify the achievability of these installation errors. Its purpose is to show the specific gain of a joint prediction. The full procedure on random initial events and its statistical calibration are discussed in the last part of the book.

The outcome depends on the class of alternatives. This set of observations separates the saturable kernel from the specified pure quadratic model. But Gaussian Poisson shocks with the same A and r_C reproduce all three expectations exactly. Heating strengthened the functional form test while maintaining the original ambiguity of the physical origin.

$$\dot{E}_x = \frac{A\hbar^2}{4mr_C^2}$$

$$\frac{md^2\dot{E}_x}{\hbar^2\Gamma(d)} = \frac{u}{1-e^{-u}}$$

$$u = \frac{d^2}{4r_C^2}.$$

(11.3) Precise energy growth of a compact Gaussian pulse generator and its relation to spatial loss of coherence. $\dot{E}_x$ refers to one coordinate.

$$\widehat{B} = \frac{\sum_i y_i g_i/\sigma_i^2}{\sum_i g_i^2/\sigma_i^2}$$

$$\mathbf{g} = (1/4, 1, 1)$$

$$\mathbf{y} = (\Gamma(L), \Gamma(2L), H).$$

(11.4) Joint weighted fitting of a single quadratic diffusion parameter. The given σ_i serve as training scales and not as measured characteristics of the device.

Observable	Saturable kernel	Best quadratic model	Training error
Γ(L), s⁻¹	0.110600	0.083324	0.005
Γ(2L), s⁻¹	0.316060	0.333298	0.005
H, s⁻¹	0.500000	0.333298	0.020

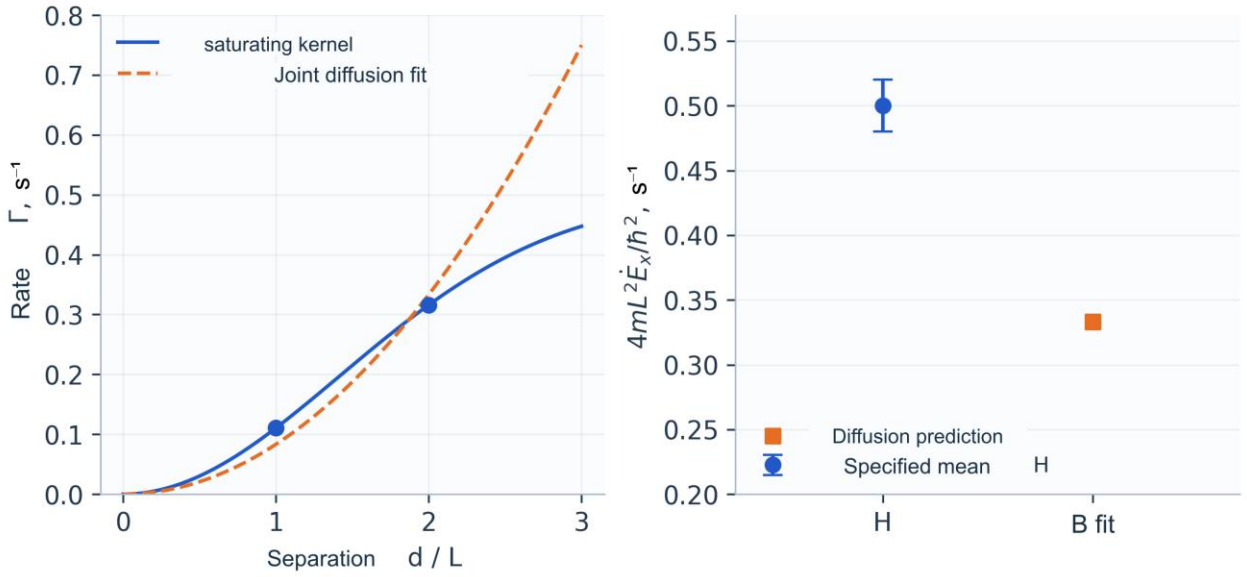


Figure 27. A joint comparison of two spatial rates and heating. Quadratic diffusion with one selected coefficient does not reproduce all given averages of the saturated kernel under training errors. Precise Gaussian shocks reproduce them completely.

Why rotation is of particular interest

Translational motion reacts to the total force, rotational - to the moment of force relative to the selected axis. These are different ways to weigh the spatial distribution of exposure. If noise is associated with mass structure, a body of complex shape may produce different ratios of translational and rotational fluctuations. Equal total mass does not mean equality of such relations. Therefore, orientation and internal geometry are able to add information that is not present in a single center-of-mass measurement.

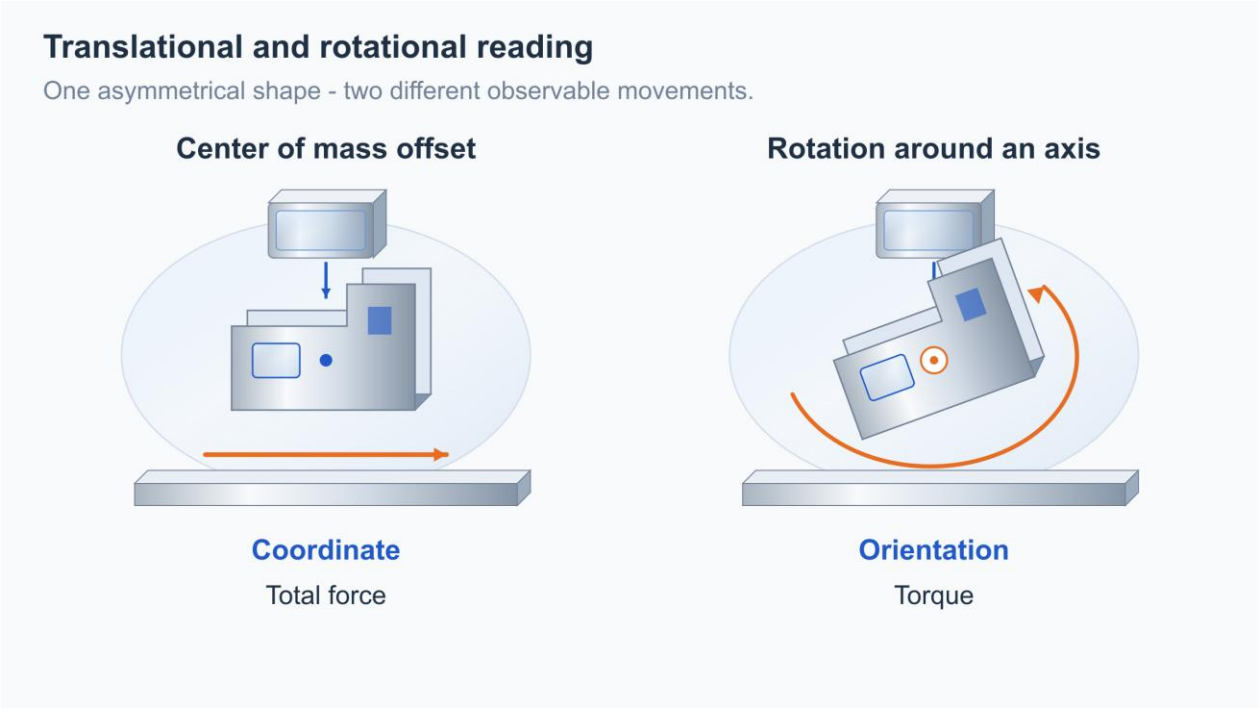


Figure 28. Translational and rotational reading of one asymmetric body. In the first case, the change in the coordinates of the center of mass is measured, in the second, the change in orientation relative to the selected axis. The total force and moment of forces provide different information about the spatial structure of the impact. The sensors and camera are shown conceptually; The figure is not a diagram of a specific implemented device.

In 2025, Altamura, Vinante, and Carlesso used LISA Pathfinder rotational noise data to refine constraints on the CSL. The work shows that an already recorded movement can contain additional verification information if you select another observable and correctly recalculate its connection with the model. [20] This does not imply universal superiority of rotational measurements: comparison depends on shape, axis, frequency range and background.

For our own calculation, a natural task is to find a response ratio that is robust to some general uncertainties. But here, too, the reduction of parameters requires verification. If the translational and rotational modes have different temperatures, losses, or calibration errors, the formally simple coefficient may not be reliable. First, a joint mechanical model is derived, then the useful combination is calculated. The reverse order can hide significant differences under a beautiful dimensionless quantity.

Two probes and common noise

If the stimulus has a spatial correlation length, two adjacent probes can move in concert. With greater distance, consistency may weaken. Bedingham and Ulbricht in 2015 considered correlated diffusion of two particles in CSL and proposed using it to test the spatial scale of the model. This is an existing direction, not a new idea for this program. [27] The practical value lies in the transition from the noise amplitude to its dependence on the relative position.

Coincident fluctuations in themselves do not constitute entanglement. General vibration of the base, electric field or unstable laser also create correlations. Therefore, it is necessary to measure the dependences on distance, orientation, charge and connection with a common support. Sometimes a differential channel suppresses a homogeneous disturbance; sometimes part of the desired signal is suppressed along with it. The word "common" does not indicate which of these cases is implemented. The answer is provided by a spatial impact model.

The two sensors can also be correlated via the measuring system. If a common amplifier or computational processing transfers the error of one channel to another, a connection of recordings without a corresponding connection of physical movements is found. Independent readout and control channels are useful, but their independence must also be verified. The requirement here is simple: an observed correlation acquires physical significance only after the path along which it could have arisen has been established.

It is convenient to compare the movement of the sum and difference of coordinates of identical probes. With equal mechanical responses, the common in-phase impulse strengthens the sum channel, and in the difference channel it is reduced. Independent shocks give a different ratio of dispersions. This simple reasoning shows where additional information comes from. But for unequal responses, it is initially necessary to bring the channels to a common physical scale. Otherwise, an imperfect reduction in the overall technical noise can be mistakenly taken for the intrinsic fluctuations of the mechanism under study. The instrumental transfer function is part of the correlation test.

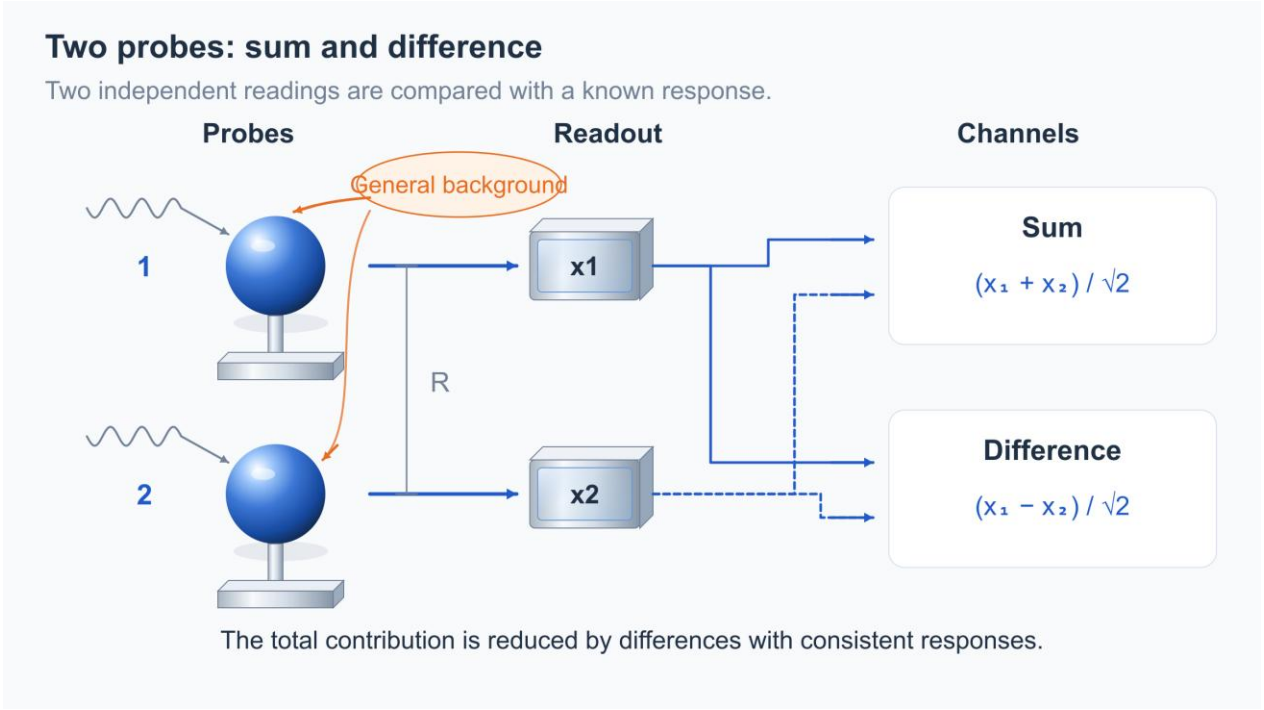


Figure 29. Two probes with independent reading provide sum and difference channels $(x_1 \pm x_2)/\sqrt{2}$. The total contribution reduces into differences only when the mechanical responses and gains are consistent. Local noise and the overall recording path require separate calibration. Correlation of records does not in itself mean entanglement.

The number that the second probe adds

Let's consider two identical probes in one-dimensional training mode. Their momentum increments have zero means and a covariance matrix $2D\,dt$, where the diagonal elements of D are equal to D_0 and the off-diagonal elements are equal to cD_0. Positivity of the covariance requires $-1 \le c \le 1$. This example specifies the acceptable classical joint noise; it has not yet been identified with a specific CSL mass kernel.

Let us introduce the normalized total and difference impulses $p_+ = (p_1+p_2)/\sqrt{2}$ and $p_- = (p_1-p_2)/\sqrt{2}$. The growth rates of their variances are equal to $2D_0(1+c)$ and $2D_0(1-c)$. When $c = 0$ the two channels receive the same contribution. At $c = 1$, the total noise completely disappears from the difference channel. Negative correlation, on the contrary, strengthens the difference channel.

If the growth rate ratio measured within this model is four, we obtain $c = 0.6$. The D_0 scale cancels out, so the ratio limits a different effect property than the absolute amplitude of a single probe. But the equality of the mechanical transfer functions and the independence of the readout are prerequisites for the calculation here. For example, an undetected gain difference leaks common noise into the difference record.

To physically test the distance dependence, it is necessary to derive c(R) from the selected interaction and probe geometry. In the mass model, it is impossible to arbitrarily replace the force correlation with the Gaussian spatial localization function itself: the transition from potential to force introduces derivatives, and the final shape

of the body introduces additional weights. Data from two probes add information only after such a connection between the observed relationship and a physical law.

$$\frac{d\mathrm{Var}p_{\pm}}{dt} = 2D_0(1 \pm c)$$

$$\mathcal{R} = \frac{1+c}{1-c}$$

$$c = \frac{\mathcal{R}-1}{\mathcal{R}+1}.$$

(11.5) Ratio for two equal responses and isolated added noise. Pulse correlation in itself is not evidence of entanglement.

Joint test and its boundary

Dey, Barker and Datta's preprint 2026 proposed limiting CSL through a change in the differential mode dispersion of two nanoballs under Coulomb coupling. The authors also consider resistance to certain color extensions. This is a theoretical proposal with given parameters and assumptions, and not a report of a detected collapse. [29] To evaluate such schemes, it is necessary to check not only the calculation of sensitivity, but also the compatibility of the proposed modes with existing restrictions.

The strongest test requires that a single set of parameters account for loss of coherence, incremental diffusion, and spatial correlations. If this is not possible, the selected model is rejected or refined. If possible, the number of acceptable explanations is reduced, but may not become equal to one. In particular, an exactly equivalent noise generator will continue to reproduce all of its own consequences. Discrimination then requires new information about the environment, its recording, or connections between systems that the original single-particle test did not capture.

Thus, the goal of expanding experiment is not to accumulate impressive graphs, but to increase the number of independent constraints. Sometimes a new observable adds almost no information. Sometimes a comparatively crude measurement destroys a degeneracy that millions of repetitions of basic experiment have not eliminated. This can only be determined in advance through a joint model and an explicit check of its identifiability. This is the subject of the next chapter.

When further runs of the same experiment cannot help

The exact discriminability limit can be formulated for the entire protocol. Let two models have the same initial reduced state and the same quantum channels between measurements for each allowed control. Let the preparation and reading instruments also coincide. Then the probability of any sequence of records is obtained by the same composition of mappings, and therefore coincides for both models.

The proof does not require assuming identical individual histories. At the first step, the unnormalized states for each possible record are matched. Using the same next channel preserves equality. Repeating this reasoning gives equality of probabilities

for any finite history. If the subsequent setting is selected based on the previous results, for each already specified history the selection rule is also the same, and the conclusion is saved.

The condition of identical channels for all allowed controls is essential. The coincidence of one free decay curve does not prove it. For a memory environment, coincidence of simultaneous states is also not enough: interventions can reveal differences in multi-temporal statistics. Therefore, what is considered here is the general Markov reduced law with identically enabled control, and not any pair of models that accidentally gives a similar graph.

In the compact white noise example, the CSL-like oscillator and the matched Gaussian pulse oscillator are the same. If all operations affect only the system being described, a new way to measure another function of its state does not establish the origin of the noise. Additional information must go beyond this equivalence: for example, independently constrain the flow of impulses, observe the available record of the environment, or verify the consistent spatial relationships of multiple systems.

This limit is useful for choosing the next experiment. It allows you to separate two tasks in advance: increasing sensitivity to different distributions and obtaining new physical information, without which the distributions coincide. The first is solved by statistics and management within the protocol. The second requires expanding the object being checked along with its model.

$$p(\mathbf{y}\mid\mathbf{u}) = \operatorname{Tr}\big[\mathcal{J}_{y_n,u_n}\Phi_{u_{n-1}}\cdots\mathcal{J}_{y_1,u_1}\Phi_{u_0}(\rho_0)\big].$$

(11.6) Probability of a sequence of outcomes as a composition of channels Φ and instruments $\mathcal{J}$. The coincidence of each element of the composition of the two models ensures the coincidence of the complete protocol.

Heating and correlations make research more rigorous by forcing one hypothesis to account for multiple consequences at once. They do not exempt you from analyzing equivalent models. A useful next experiment is selected based on how much ambiguity it is able to resolve, rather than on the number of sensors added.

12 From raw counts to a verified result

Testing a theory becomes reproducible when the transition from recorded events to the resulting constraint can be traced. This chapter first refines the statistical model and then re-calculates it using the published sodium experiment. It shows which numbers actually follow from the archive, what assumptions are included in the processing, and what remains outside the resulting output.

From an appealing effect to distinguishability

Let us present two explanations for the slight decrease in contrast. In the first, the additional loss depends mainly on the mass. In the second, it is associated with heating, which in the existing installation also increases when working with more massive particles. Given the existing data, both models may look equally convincing. A simple continuation of the series by mass can preserve ambiguity. It may be more useful to measure at the same mass and different thermal histories if the setup allows these conditions to be varied independently.

This reasoning expresses the idea of identifiability. A parameter is identifiable when its different values cannot be fully compensated for by changing other valid parameters, preserving all observed predictions. If compensation is possible, the algorithm may return a narrow uncertainty estimate only due to hidden limitations, such as the background being too rigidly fixed. Therefore, before a large data set, it is necessary to find out which combinations of parameters are generally distinguishable by the selected protocol.

Local verification uses derived predictions across parameters. If a change in one parameter shifts all the expected data almost as much as a change in another, the directions in the prediction space are almost identical. This is a warning about degeneration. However, local analysis does not guarantee global discriminability: distant parameter areas can also produce similar data. It is useful to combine derivatives with direct search for alternative good solutions.

What should a computational model contain?

The simulation input is not only fundamental parameters. We need trajectories, mass and velocity distributions, environmental characteristics, preparation errors, and a readout model. It is advisable to output the original data type: numbers of events, positions of hits, or time series. Modeling ready-made visibility is sometimes convenient, but can hide bias in its estimation. If an experiment first collects samples and then extracts contrast, the test must reproduce both steps.

Formally, what is required is the probability of the data given the parameters and setting. The law under study is denoted by the parameters θ, background and calibration - η, control - u. This notation reminds us that the inference about θ depends on the uncertainty of η. Their joint fitting, profiling or Bayesian averaging are different statistical procedures. None of them eliminate the need to check the

physical meaning of acceptable values. The algorithm does not learn on its own that the temperature cannot change arbitrarily between adjacent runs.

In 2024, Laing and Bateman developed a Bayesian formulation for near-field interference tests of collapse models, incorporating external decoherence and choice of control parameters. [19] This is an important existing landmark: the idea of optimizing the experiment through statistical inference is no longer novel. The possible contribution of the new program should be a specific extension, such as robustness to environmental model error, sharing of independent observables, or a new practically achievable regime.

$$p(\mathcal{D} \mid \theta, \eta, u).$$

(12.1) This is the probability of possible data $\mathcal{D}$ given the parameters of the dynamics under study θ, the environmental and recording parameters η and the selected control u. The usefulness of the following experiment is determined by how different such distributions are for competing explanations.

False discovery test

Before the actual experiment, the analysis should be tested on data in which the new dynamics are obviously absent. In this case, the data generator should be slightly richer than the model used in processing. You can add slow drift, weak nonlinearity in the background dependence, or an imprecisely known size distribution. If a small plausible deviation systematically creates the impression of a detected collapse, the method needs to be improved. Testing on your own ideal data confirms only internal consistency, but not resistance to reality.

Effects of known magnitude are then added to the artificial data. It is important to check whether the parameter recovers, how often the intervals contain the true value, and where the sensitivity disappears. Such additions do not constitute experimental confirmation of the hypothesis. They show the capabilities of the procedure under given assumptions. The results should be described as a prediction and accompanied by a list of factors not included in the simulation.

The zero intensity boundary requires special attention. If the parameter is by definition non-negative, conventional approximations for symmetric errors may perform poorly near zero. Additionally, choosing the most salient distance, frequency, or time window after reviewing the data increases the likelihood of randomly striking variation. Therefore, the search range and decision rule are either specified in advance or included in the modeling of the statistics of the entire procedure. Otherwise, the significance of a single point does not describe the significance of the study.

The results of such computational tests should be kept separate from experimental observations. Each artificial sample has a known generation law, which means it allows you to check a specific analysis failure. It does not confirm that nature chose this law. A useful report therefore contains both successful recovery and failure modes. For example, if the range of distances is too narrow, the two models may be

virtually indistinguishable even in a perfect simulation. Showing this area upfront is more helpful than hiding it behind one favorable example with a lot of contrast.

Cost and information

Practical optimization must take into account the cost of measurement. One mode gives a large signal, but requires a long readjustment and has a low rate of successful launches. The other is weaker in each individual event, but allows you to quickly collect independent data and carry out calibrations more often. Comparing amplitudes only misses this exchange. You need a goal expressed in terms of information or precision with limited time, number of particles and available control set.

For a consistent result, it is useful to evaluate not only the most favorable background parameters, but also a reasonable range of uncertainty. A tuning that is excellent when the temperature is only known with certainty may be poor when the temperature drifts slightly. A more moderate protocol sometimes maintains discriminability throughout the acceptable range. Thus, the challenge of sustainable design arises: to select an experiment that remains meaningful despite the foreseen errors of knowledge.

There are also physical limitations. You cannot optimize each setting independently if they are linked in a real installation. Mass affects preparation, geometry affects mechanical response, and retention time affects the likelihood of survival. The admissible set of controls must describe these connections. Otherwise, the program will find a mathematical maximum in the region where the object cannot be prepared or counted. The feasibility check is included in the calculation itself, and is not added to the beautiful result later.

The archive as a definition of a repeatable experiment

The basis is the open set of Pedalino and co-authors with DOI 10.5281/zenodo.17502163, associated with the Nature article 649, 866–870. Its measuring part contains scans from April 22 2025, a table of powers and reference signals, as well as mass spectra. The archive contains programs for extracting visibility, calculating macroscopicity, and the Talbot-Lau module. Materials are distributed under CC BY license 4.0. [15, 63]

To repeat, the archive itself is first recorded. The checksum MD5 of the original ZIP is equal to 7917961b27676f4e9df3af6d3b01c374; it matches the repository entry. This identifier distinguishes specific bytes from subsequent page updates. Next, the source files are saved without changes, and execution is carried out in a separate working copy. Library versions and exact commands are given in the accompanying instructions for the calculations.

Next, elementary checks of the structure are performed: the table specifies 95 names, each corresponds to a file with a 41 position, the counters are non-negative, the displacement units are converted from nanometers to meters. The real powers of the three grids for each launch are taken from the table. Using average power alone

instead of these lines would change the probability of passing and would no longer be a repeat of the issued procedure.

The entire set contains 3895 numerical points and 10 772 714 counts. These are two different volumes: one point represents the accumulation of many events at a given position. The integration in all selected lines is equal to one second, so the count and numerical frequency coincide only due to the specific accumulation time. For another table, this equality would have to be replaced by explicit multiplication by time.

Internal control files allow the processing to be repeated independently of the literature description, but do not turn all calibrations into precise physical facts. For example, the reference flux is measured separately and is used in the published likelihood as a fixed number. A more complete analysis could include the uncertainty of this measurement. Reproducing the original procedure preserves its conditions and specifies them exactly.

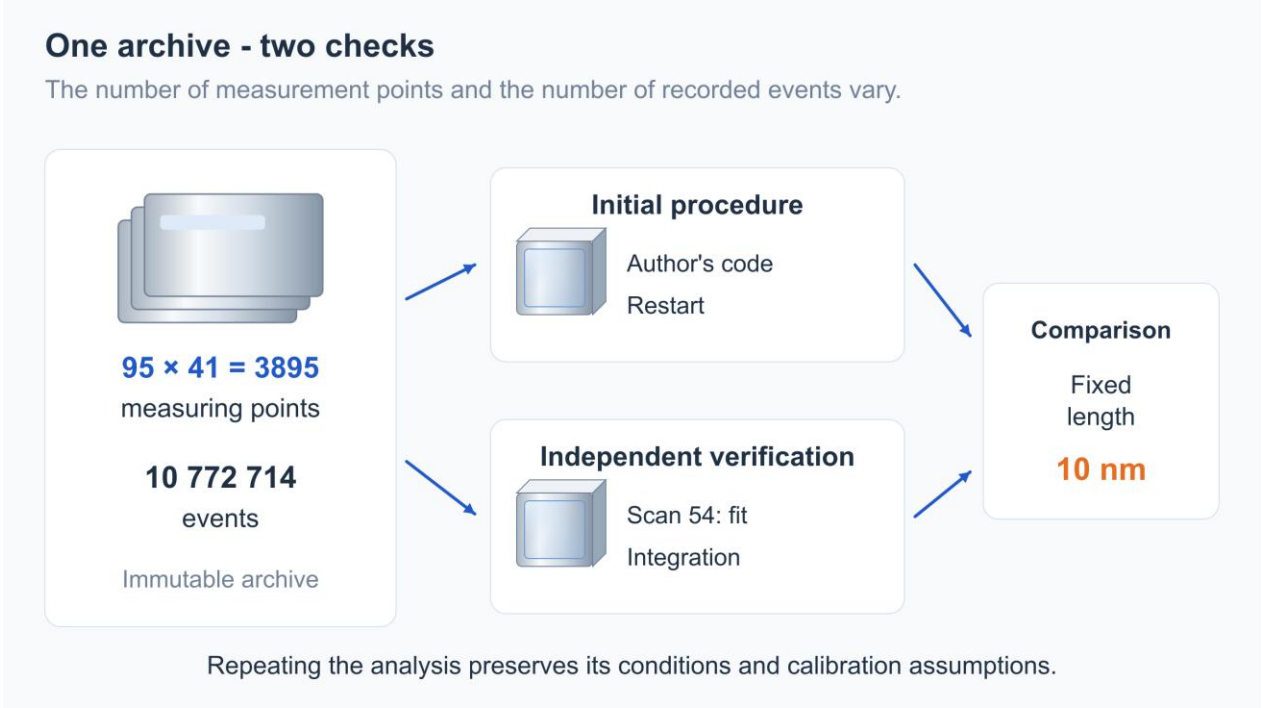


Figure 30. There are two ways to verify the published sodium set: rerunning the author's open procedure and independent verification of individual calculations. The archive contains 95 scans at 41 position, that is, 3895 measurement points, and 10 772 714 registered events. The independent branch includes the selected scan 54 and the integration test; the length in the issued procedure is fixed to 10 nm. This is a replication of the analysis under its calibration assumptions, not a new experiment or a complete re-evaluation of the calibrations.

One scan and independent visibility extraction

To see data before complex output, scan Sodium_int_powerscan_54 is selected. The selection rule is specified through the setting: this is the line with the power of the second array closest to 15.2 mW. Maximum contrast search was not used. The actual power is 15.252 mW. In 41 position the 132 283 count is registered.

With a known period, the signal can be written as the sum of a constant term, cosine and sine. This notation is linear in three coefficients, so the minimum of the sum of squares can be found using ordinary linear algebra. The coefficients are then translated into visibility and phase. This is an independent path to the same sinusoidal description, which is convenient to compare with the nonlinear fit.

For the selected scan, the average count level 3217.865 per position, visibility 0.07320 and its residual standard error 0.00814 were obtained. The phase is −2.58149 rad at the accepted origin. The figure shows actual readings and its own fit; the vertical segments √n give only a visual Poisson scale. The visibility error estimate is calculated from the residual covariance matrix of the linear regression.

This result refers to one pre-selected row, not the maximum visibility across the entire article. The variation between runs, drift and power changes do not disappear after a beautiful fit of one sine wave. All data provided and the full response of each setting are important in the final analysis.

For a small number of events, the amplitude recovered as the positive modulus of the two noise coefficients has a biased distribution. A simple symmetrical error is then insufficient. Here, high scores allow the linear fit to be used as a transparent description of the selected scan; The fundamental constraint below is reproduced based on the original counters, not just the extracted visibility.

$$n(x) = a + b\cos(2\pi x/d_g) + c\sin(2\pi x/d_g)$$

$$V = \frac{\sqrt{b^2 + c^2}}{a}.$$

(12.2) Linear fit determines a, b, c. The transition to visibility is nonlinear, so its error is obtained by transferring the full covariance of these coefficients.

$$\phi = atan2(-c, b)$$

$$\mathrm{Var}(\widehat{V}) \simeq (\nabla V)^T \mathrm{Cov}(\widehat{a}, \widehat{b}, \widehat{c})\, \nabla V.$$

(12.3) The phase is determined relative to the beginning of the grating displacement. The dispersion formula is a local approximation; near zero amplitude the full distribution should be used.

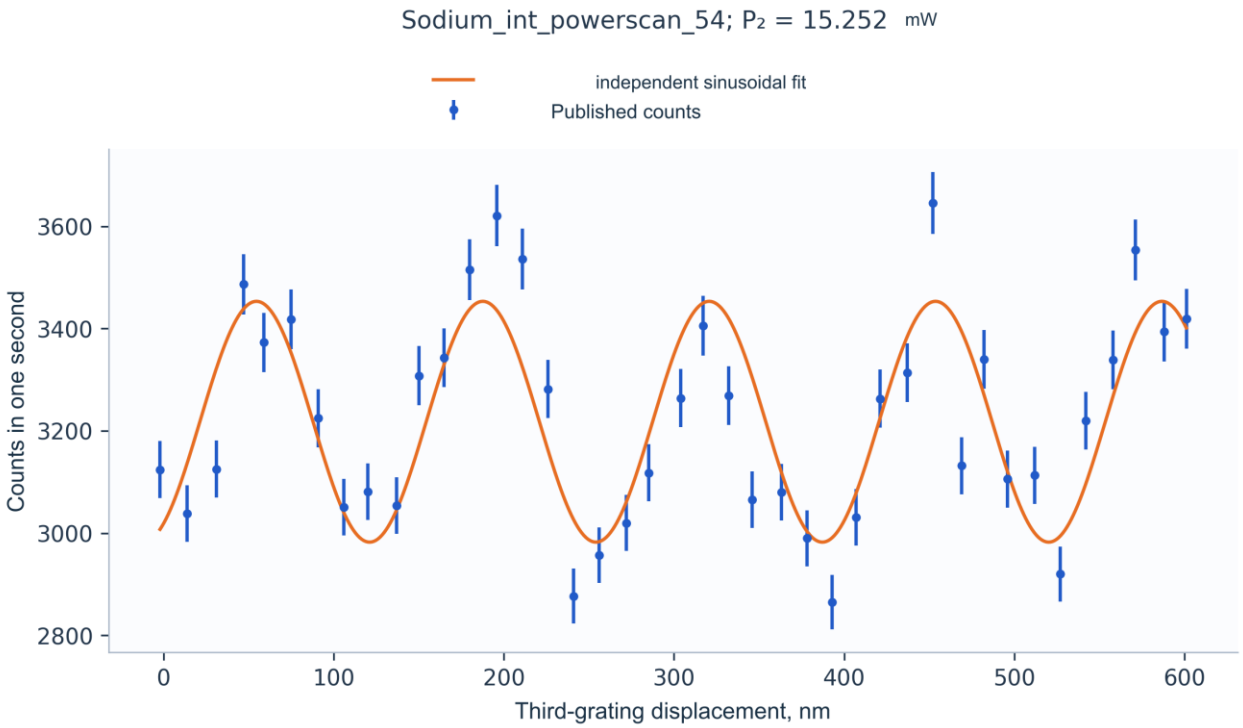


Figure 31. Published scan samples 54 and independent linear sinusoidal fit. The choice was made based on the proximity of the power to 15.2 mW. Received V = 0.07320 ± 0.00814; the error is described in the text. Data from Pedalino et al, CC BY 4.0; processing and drawing were done for this book. [63]

How the probability of registration depends on the modification

The original procedure considers a family of minimal macrorealistic modifications. Its classicalization time τe is normalized to the electron mass; the length ħ/σq determines the spatial scale. These designations cannot be directly equated to the intensity and length of another CSL convention. To transfer, it is necessary to compare the generators themselves and the normalization of masses. [65, 66]

First, the quantum probability of the passage of three gratings is calculated, taking into account their amplitude and phase action. The non-zero harmonic is then multiplied by a modification factor depending on the trajectory and mass form factor. Averaging is done over velocities and masses, as in the released module talbotlau.py. In the chosen procedure, the spatial scale is fixed at ħ/σq = 10 nm, the published setting used for the final assessment.

For a point with a recorded number c and a separately measured reference signal C_0, the author's analysis uses a conditional likelihood of binomial form on the probability of passing S. The reference signals are 17.5–26.5 thousand samples per second and are conventionally fixed as the number of trials; their measurement uncertainty is not common in this replication. The term that does not depend on τe does not affect the shape of the posterior distribution and can be omitted. The key operation is to sequentially add the logarithms of the probabilities of all points. At the same time, the phase −2.48 rad and calibration dependencies from the archive are recorded.

The posterior distribution is obtained by multiplying the likelihood by the Jeffreys prior density of the selected model. Time τe is considered on a logarithmic grid of 400 points from 10^{14} to 10^{16} seconds. Logarithmic grid - a method of placing nodes; it does not by itself specify a uniform density in log τe. When normalizing, the intervals of exactly the variable with respect to which the density is determined are used.

The lower fifth percentile τ_5 means that 5% of the probability in the adopted posterior density lies below it. It is used to construct the measure of macroscopicity. This is Bayesian inference within the stated model and calibration. It is not a universal frequentist probability that quantum mechanics is wrong, and it does not establish the existence of an additional collapse mechanism.

$$\log L(\tau_e) = \sum_i [c_i \log S_i(\tau_e) + (C_{0i} - c_i)\log(1 - S_i(\tau_e))] + \text{const.}$$

(12.4) The probability S_i includes control, averaging over distributions, and selected modification. The C_{0i} reference numbers in this replication are treated the same as in the released analysis.

$$p(\tau_e \mid \mathcal{D}) = \frac{L(\tau_e)\pi_J(\tau_e)}{\int L(\tau_e)\pi_J(\tau_e)d\tau_e}$$

$$\int_0^{\tau_5} p(\tau_e \mid \mathcal{D})d\tau_e = 0.05.$$

(12.5) π_j is the selected Jeffreys density. The lower quantile is calculated from the normalized density, and not from its maximum value.

The reproduced published estimate

Unmodified Macroscopicity_April2025.py and talbotlau.py were executed on the original data. The calculation gave $\tau_5 = 2.842065516 \times 10^{15}$ s and $\mu = \log_{10}(\tau_5/1\text{ s}) = 15.453634$. In the Methods section of the article, 2.84×10^{15} s and $\mu = 15.45$ are indicated; in the annotation the number is rounded to 15.5. The coincidence is within the rounding limits given by the authors. [15, 63]

Additionally, the Kullback–Leibler divergence between the final density and the corresponding Gaussian approximation is reproduced: 0.001267708. The article shows 1.27×10^{-3}. Here this value characterizes the shape of the resulting distribution; it does not replace the probability of false discovery of new physics.

To separate the physical result from the way the quantile was read, the density was independently normalized by trapezoidal integration and the position of 5% interpolated between adjacent nodes. We obtained $\tau_5 = 2.827503744 \times 10^{15}$ s and $\mu = 15.451403$. The difference in μ is approximately 0.00223 and is less than the accuracy with which the result is given in Methods. This is a test of the numerical quantile extraction on the same grid, rather than an independent physical calibration.

The measure μ is the logarithm of the limited time in a certain class of modifications. It is not equal to the number of worlds, the degree of consciousness of an object, or the universal percentage of its quantumness. Its meaning is determined by the selected family of dynamics, mass normalization, and statistical limitation

procedure. Comparisons of μ between trials are meaningful when this construct is used consistently. [65, 66]

The result shows that the published numerical procedure can indeed be reconstructed from the open set. At the same time, repetition of the source code and independent construction of the physical description solve different problems. The first checks data availability, calculation compatibility, and the published number. The second must vary calibrations, alternative backgrounds, and the probability model itself. For the last problem, a separate controlled numerical experiment is constructed in subsequent chapters.

Magnitude	Publication	Recalculation
Number of points	3895	3895
Lower 5%-quantile τ_5	2.84×10^{15} s	$2.842065516 \times 10^{15}$ s
μ in the Methods section	15.45	15.453634
KL to Gaussian density	$1{,}27 \times 10^{-3}$	$1{,}267708 \times 10^{-3}$
μ with CDF interpolation	Not a separate published result	15.451403 - sampling check

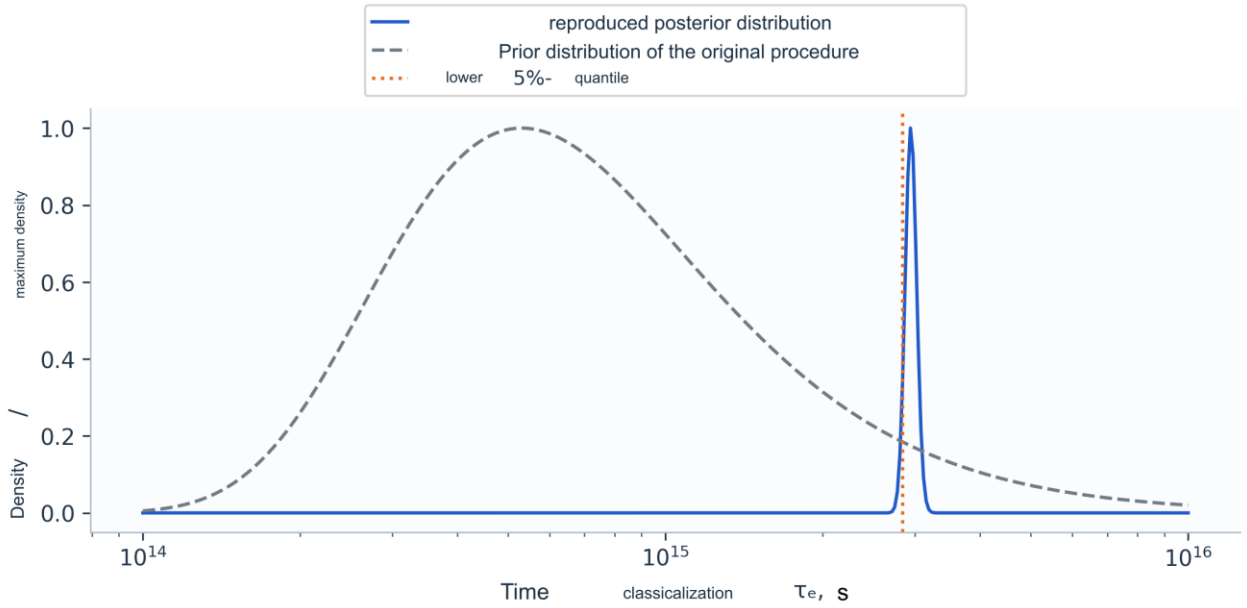


Figure 32. The result of repeated execution of the open author's procedure: a posteriori time density of classicalization and its lower five percent quantile. Densities are normalized to their own maxima only for the figure. Data and initial procedure [63], own design.

What exactly is verified by repetition

The comparison performed saves the settings of the released procedure. It confirms the calculation at a fixed length 10 nm, a given mass window, phase and photophysical dependencies. Finding a maximum over all spatial lengths and re-

evaluating all calibrations together would be different analyzes with a different parameter space. Their result cannot be attributed to the repetition described simply because the original article discusses a broader program.

The seventh and ninth chapters show why this limitation matters. The gas composition, grating vibrations, and treatment of the dark background can change the estimated residual loss. A result obtained with one calibration does not demonstrate insensitivity to those parameters. Testing that requires additional data or an explicitly bounded sensitivity analysis. General measurement theory requires a claim to include the conditions actually used.

In the computational application, the original measurements are separated from the artificial series. Real files retain names, checksums, and attributions; artificial series preserve the initial number of the generator and the generation law. This separation allows both the published experiment and the statistical method to be tested without turning a successful simulation into a fictitious observation of nature.

After replication, the choice of next step becomes concrete. You can change one calibration relationship and measure the shift in the result; source and transmission can be jointly assessed; you can compare two designs at the same time. In chapters 19–21, tests of full search, restoration of the introduced signal, interval coverage and prediction of new conditions are performed on a model for which the true parameters are known. Here this model receives real experimental support and a clear transfer limit.

The open sodium archive gives a reproducible external result: μ = 15.453634 in the released procedure, consistent with the published rounding. The usefulness of this check is the traceable relationship between the files, the probabilities and the number. The next level of research requires similar transparency across uncertain calibrations and competing backgrounds; The last part of the book is devoted to it.

Part III Gravity and physical clocks

13 Why gravity is difficult to include in the quantum picture

A stone falls, an atom interferes, a clock changes tempo at different heights. Each of these processes has a working physical description. The difficulty appears when the source of gravity becomes an object whose position cannot be replaced by one classical trajectory. What field is created by mass in superposition? What happens to geometry if matter itself obeys quantum dynamics? Getting to these questions requires precision: the familiar phrase about the incompatibility of two great theories hides several different problems.

Joint use does not mean unification

In a conventional quantum problem, space specifies the position of the device, time marks the sequence of operations, and the state describes the system under study. You can refine the source trajectory, the shape of the external field, and the detector settings while maintaining this calculation organization. In the general theory of relativity, geometry itself is involved in dynamics: the distribution of energy affects distances and the running of clocks. Therefore, when combining descriptions, not only the formula of force changes. The question arises about the physical quantities in relation to which the state is generally defined.

In this case, quantum mechanics and gravity are regularly used in the same calculation. It is enough to add the known terrestrial potential to the Hamiltonian of an atom to calculate the gravitational contribution to the phase of its wave function. In this approximation, the Earth plays the role of an external source. The calculation answers the question about the movement of quantum matter in a given field. It does not yet tell what states are permissible for the gravitational field itself and how it reacts to quantum changes in the source.

The difference is easy to see through thought experiment. If a heavy ball is previously placed on the left, the motion of an atom can be calculated next to it. If the ball is pre-set to the right, a different calculation will result. But a state of the ball that maintains coherence between two positions requires specifying how the interaction acts on both branches and on their mutual phase. Substituting the average position of the ball does not have to reproduce this dynamic. The average coordinate value does not contain all the information about the quantum state.

Three independent goals follow from this. One can study quantum matter in a classical field, construct consistent dynamics of a classical field and quantum matter, or quantize gravitational degrees of freedom. Their predictions sometimes coincide in an accessible manner. Coincidence does not make the approaches identical, just as the same speed of two cars does not mean the same engine design. The experiment must look for the value for which the coincidence ceases.

Working theory at low energies

Often the problem is formulated too sharply: as if quantizing gravity always leads to meaningless infinities. A more precise statement concerns the predictive power of the theory at arbitrarily high energies. If we consider Einstein's ordinary action as the ultimate quantum theory at all scales, new necessary parameters emerge. However, this does not prevent it from being used in a limited area of applicability, consistently taking into account corrections based on their smallness.

This approach is called effective field theory. John Donohue's paper 1994 shows how to separate low-energy quantum contributions from unknown high-energy physics and obtain specific long-range corrections. This is a serious limitation for popular claims: the claim that quantum gravity cannot calculate anything at all is false. However, an effective description does not claim to provide a complete picture of the earliest stages of the Universe or the inner regions of singularities. [30]

Efficiency here means control over accuracy. If a long wave is being studied, details of the source device that are significantly smaller than its length can be included in the calculation only through several parameters. As energy increases, more details need to be taken into account. A similar principle allows one to calculate the flow of water without tracking every molecule. The analogy concerns the organization of approximations; it does not prove that space consists of some specific microscopic medium.

For processes with characteristic energy E, the natural dimensionless indicator of quantum-gravitational smallness can be composed of G, Planck's constant and the speed of light. It shows why conventional laboratory energies are far from the regime of strong quantum corrections to geometry. However, a weak correction to the usual force and the ability of the force to transmit quantum coherence are different signs. The second can sometimes be verified through the accumulation of phase and correlation, without approaching the Planck energies.

$$\epsilon_G(E) = \frac{GE^2}{\hbar c^5} = \left(\frac{E}{E_{\mathrm{P}}}\right)^2$$

$$E_{\mathrm{P}} = \sqrt{\frac{\hbar c^5}{G}}.$$

(13.1) This is a dimensional estimate for processes where E specifies the relevant energy scale. It does not replace the calculation of a specific experiment and does not mean that any experiment due to the quantum nature of gravity must reach the Planck energy.

What field does an indeterminate source create?

The most obvious fork appears when choosing a field source. In the semiclassical approximation, the geometry can be determined by the average value of the energy distribution of quantum matter. When describing a quantum messenger, the interaction acts on the state of the composite system and is capable of connecting the degrees of freedom of two objects. In the first case, averaging is included in the law

of connection itself; in the second, it appears later, when a specific observation result is calculated. Rearranging these operations can change the prediction.

Let's imagine two remote packages of one massive object. If the field is determined by the average density, the probe system responds to a certain source distribution. If coherent interaction alternatives are maintained, the trial system may become associated with the source position. It is important not to replace this distinction with a picture of two halves of a substance. A spatial superposition, a classical mixture, and a literally separated mass may all have the same average density but different available information.

It does not follow from this that any record of an average source is automatically logically impossible. It is necessary to specify the entire theory: the rule of state evolution, measurement probabilities, field response and permissible interventions. Changing one equation without adjusting the others can create nonlinearity, dependence of predictions on the method of mixture preparation, or problems with information transfer. Such properties are tested on composite systems, and not by the external similarity of the formulas to Einstein's equations.

There are also hybrid approaches, where classical quantities are random and associated with a quantum system. In the class of consistent classical-quantum dynamics studied by Oppenheim et al., the connection is accompanied by a constraint between the decoherence of the quantum sector and the diffusion of the classical one. This is a theoretical condition for a specific mathematical class, not an observation of space-time fluctuations. Its value lies in the fact that the assumption of classical geometry comes at a quantitative cost in the form of additional noise. [43]

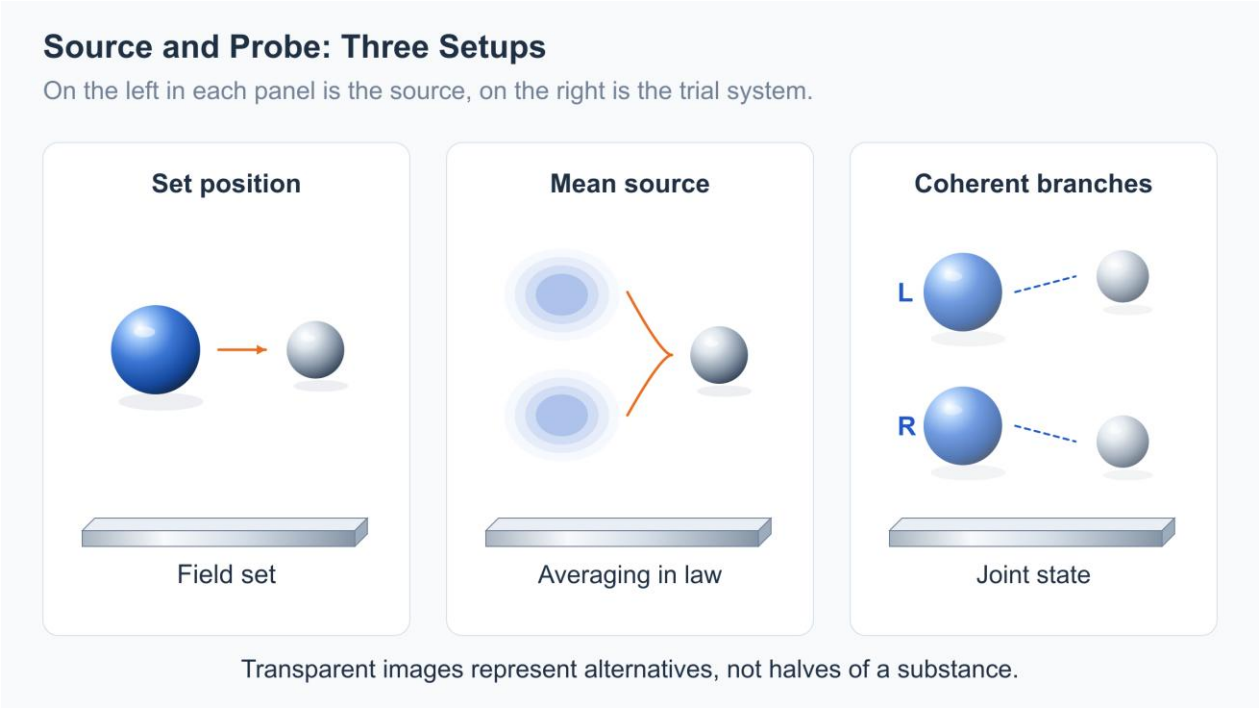


Figure 33. Three formulations of the source and probe problem: motion in a given field, the field of an unconditional average source, and the joint dynamics of coherent alternatives. In the middle panel, the blue areas represent the density distribution; on the right - state components and correlation with the probe. Transparent images do not mean half of the substance. The arrows indicate the relationship in the model, not the direction of the force. The scheme distinguishes between models without announcing the experimental choice of one of them.

What the experiment with an average source verified

The average source question has an experimental history. In 1981 Page and Geilker reported a result incompatible with Einstein's simplest semiclassical equations. The strength of this example is to test a certain rule for how the field relates to quantum matter. The authors formulated it as indirect support for the quantization of gravity, rather than as a definitive proof. [61]

The content fork can be restored on a simple diagram. Let the quantum result determine which of the two macroscopic source configurations will be realized. If we average both configurations unconditionally and then declare this average to be the only physical source, we get one prediction for the test device. If its reading correlates with a particular recorded configuration, a different rule is required. What is of decisive importance is which state is used after registration and what exactly is considered the source in a particular experiment.

Therefore, the experimental argument cannot be transferred to any model in which the word “classical” appears. Stochastic classical field, conditional post-measurement dynamics, and unconditional mean field represent different constructs. For the next test, it is necessary to write down their rules for preparation, averaging and registration in advance. This necessity connects the gravitational problem with the problem of measurement, discussed in the third chapter.

Small masses in a difficult experiment

The gravitational signal increases with mass, but a massive object is more difficult to hold in a controlled superposition. Its internal degrees of freedom, thermal radiation, collisions with residual gas, and communication with supports create additional interaction channels. Decreasing distance increases gravity while increasing the requirements for suppressing electromagnetic forces. Therefore, the task does not boil down to choosing the heaviest possible body and the closest neighbor. It is necessary to preserve exactly those properties by which the models differ.

A demonstration experiment by Westphal et al measured the gravitational coupling of gold spheres with a radius of about a millimeter and a mass of about ninety milligrams. The work was published in Nature in 2021. This is a demonstration of a sensitive measurement of the classical attraction of small sources; it did not create the claimed gravitational entanglement of two massive superpositions. This result is important as mastery of the measurement mode, but its scientific meaning cannot be expanded to confirm the quantum intermediary. [31]

In a complete experiment, several skills must be met: preparing the state, maintaining coherence for a sufficiently long time, controlled interaction and reliable reading of correlations. The success of each stage separately does not guarantee the success of the joint protocol. For example, a cooling device may introduce holding noise, or a packet separator may introduce unwanted interaction between objects. Installation parameters form a coupled problem, where improving one characteristic sometimes worsens another.

This explains the value of a preliminary calculation. It is able to show which characteristic is really limiting the experiment: temperature, distance drift, random charge, reading time or number of repetitions. Without such analysis, one can spend years perfecting a component that does little to improve the distinguishability of theories. A good model helps formulate a measurable goal for the engineer while making explicit the assumptions on which the fundamental conclusion depends.

Numerical budget for geometry and preparation

It is useful to move from the list of difficulties to the budget of one calculation. The next chapter uses two masses of 10^{-14} kg, center distance $d = 450$ μm, branch spacing $s = 250$ μm and exposure $t = 2$ s. This is a training configuration: its parameters are not declared as jointly achieved installation characteristics. Here it is needed to translate mass and geometry errors into entangling phase errors, and then see what control is required to interpret the result. Here, Δ denotes the sum of the phases of the LL and RR branches minus the sum of the phases of LR and RL; the next chapter will show why this combination defines entanglement.

For point Newtonian energy, the phase modulus is proportional to $m_1 m_2 t s^2/[d(d^2-s^2)]$. The small change in each input is multiplied by the corresponding logarithmic derivative. Therefore, one micrometer of error in d and one micrometer of error in s have different prices. As s approaches d, the derivatives increase: the

signal increase is accompanied by an increase in sensitivity to geometry. This is a property of the model, and not a disadvantage of the measuring device.

The table provides illustrative independent standard uncertainties. When calculating derivatives, an exact four-branch formula was used, without the approximation of small s/d. Each row shows the contribution to the standard uncertainty Δ. Quadratic addition gives about 0.00399 rad, or 1.59% of the phase modulus. If the calibrations are correlated, their full covariance matrix is needed instead of this addition. General image scale error, for example, changes d and s simultaneously.

The uncertainty of constant calibration and the random variation from run to run have different effects. The first expands the range of permissible prediction. The second can additionally blur the phase in the average state. The number from the table cannot be automatically substituted into the decoherence index. To do this, it is necessary to measure the time statistics of the drift and determine which fluctuations are common to two objects and four branches.

The assumption of fixed packets also requires physical implementation. Free packages are expanding; holding potential and control change their forms and phases. For Gaussian packets with a known width, one can average the Newtonian potential over the coordinate distributions or numerically propagate the entire state. The precondition for narrowness—the width is substantially less than the smallest distance d−s—only specifies the region where such averaging can be a small correction. It does not replace packet movement checking.

In the future, visibility v will characterize the coherence of each two-branch subsystem after preparation, exposure and mixing. The use of a single v is only permissible after checking that these channels are identical. The reading error will be entered separately. This division makes it possible to understand whether the quantum resource itself has decreased or whether the ability to register it has deteriorated.

$$\frac{\delta \Delta}{\Delta} = \frac{\delta m_1}{m_1} + \frac{\delta m_2}{m_2} + \frac{\delta t}{t} + \left(\frac{2}{s} + \frac{2s}{d^2 - s^2} \right) \delta s - \left(\frac{1}{d} + \frac{2d}{d^2 - s^2} \right) \delta d .$$

(13.2) Linear propagation of small parameter changes. For standard uncertainties with covariance Σ, use $\sigma^2\Delta = J\Sigma J^{T}$, where J is the string of derivatives of Δ with respect to the inputs.

Illustrative phase uncertainty budget

Input	Accepted uncertainty	Contribution to σΔ, rad
Mass of the first body	1 %	0.002511
Mass of the second body	1 %	0.002511
Distance d	0.5 μm	0.001086
Spacing s	0.5 μm	0.001453
Interaction time t	1 ms	0.000126

These are the uncertainties specified for the calculation, and not a report on the achieved accuracy of the experimental platform.

Why a weak outside connection can be decisive

The gravitational interpretation is determined not by the absolute smallness of the extraneous force, but by its relationship to the beneficial effect. For two identical masses of 10^{-14} kg, one elementary charge on each object gives Coulomb energy of the same geometric form 1/r, but approximately $3.46 \cdot 10^{10}$ times greater than Newtonian. This comparison does not assume that the charge is actually present: the cost of such a preparation error is calculated.

If both residual charges could be continuously reduced, the requirement for a Coulomb contribution below one percent of the gravitational one would correspond to a magnitude of each charge of less than approximately $5.4 \cdot 10^{-7}$ elementary charge. For an isolated body, this is not a description of the available fractional value of its free charge. The number shows the need for a neutral state and independent control of electromagnetic interactions. The zero sum of charges does not yet exclude dipole moments, inhomogeneous surface potentials and polarization.

Calibration must check exactly the combination of phases of the four branches. A field that acts equally on one object in all states of the second gives a local phase and can be removed by choosing the reading axis. A connection that depends on the states of both objects can create the same entangling combination as gravity. Therefore, measuring the average acceleration and demonstrating low background noise does not yet exclude a non-gravitational source of correlations.

Control series can be organized by changing the distance, orientation, shielding and charge preparation conditions. Each change requires its own model: the screen is capable of suppressing electrostatic coupling while adding fluctuation or mechanical coupling. In the final analysis, geometric calibrations and verified boundaries of extraneous interactions must accompany the entanglement witness. Otherwise, the quantum nature of the final state will be established, but not the reason for its occurrence.

$$\frac{|U_C|}{|U_G|} = \frac{|q_1 q_2|}{4\pi\varepsilon_0 G m_1 m_2}.$$

(13.3) The ratio refers to point charges and masses with the same distance. For extended neutral objects, a different electromagnetic model is required.

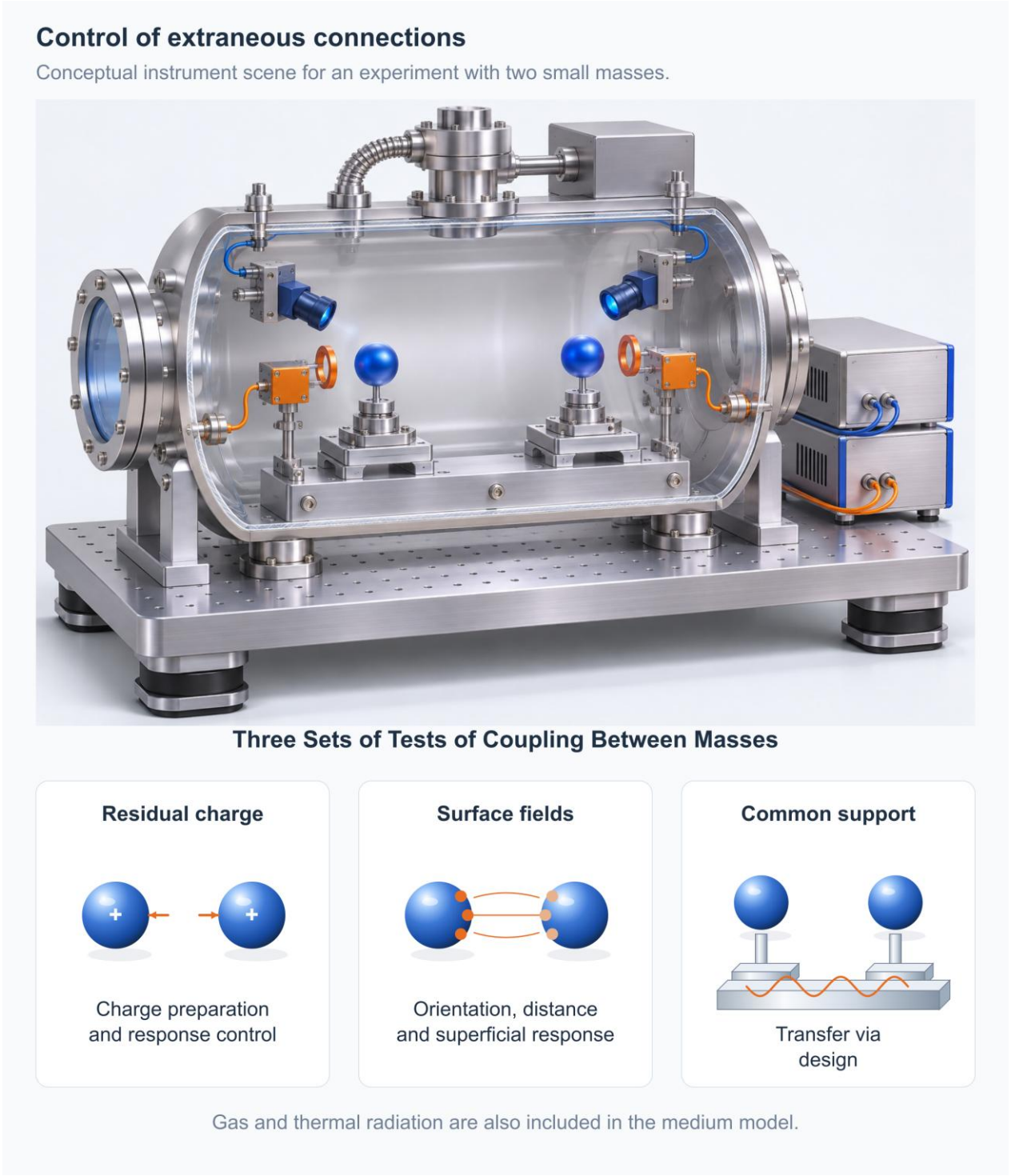


Figure 34. Conceptual map of control of extraneous connections between two small masses. Artist's section view showing individual local controls and overall mechanical design; enlarged circuits highlight residual charge, surface fields, and transmission across supports. Gas and thermal radiation are also included in the medium model. The implementation is shown conditionally: the figure does not confirm the achievement of the required superposition or gravitational entanglement and does not specify a quantitative drawing.

Levels of an answer

The first possible answer concerns the interaction itself: the observed signal is consistent with the gravitational force in the chosen range. The next one concerns the quantum state of matter: after interaction, entanglement or other predetermined property arises. A stronger conclusion concerns the mediator: the data exclude some class of classical modes of communication of interaction. Even further back are statements about field quanta, its relativistic dynamics and the final microscopic theory of geometry.

Between these levels additional arguments are needed. To conclude about the mediator, it is necessary to exclude other connections between the bodies and check the initial independence of their states. To draw a conclusion about gravitons, it is necessary to clarify what exactly is meant by field quanta and what mode is being studied. Choosing a fundamental theory requires an observable on which competing options diverge. One successful correlation curve does not automatically carry all this content.

This procedure does not reduce the importance of laboratory experiments. On the contrary, it allows you to determine in advance the achievable result. Elimination of a broad but specific family of models can change the direction of research even if no definitive theory is selected. The new noise constraint is also meaningful: it forces the alternative dynamics to respond to several dimensions at once. Science advances when the space of possible explanations is reduced and the next decisive experiment becomes clearer.

14 Two masses and a test of the mediator

Let the two small masses first be prepared independently. Each is capable of being in a coherent superposition of two spatial positions. They are left to interact, after which the measurement results are compared. Outwardly, the experiment resembles the study of a very weak force. Its fundamental question goes deeper: can an interaction create a state that can no longer be described by the independent states of the two participants?

From four alternatives to one state

In 2017, the Bose and Marletto-Vedral groups proposed using gravitational entanglement as evidence of the nonclassical properties of the mediator. In Bose et al.'s version, spatial states are coupled to spins, allowing the desired correlations to be read out through spin measurements. These are experimental proposals and theoretical arguments. Their publication does not in itself mean that gravitational entanglement has been documented. [32, 33]

For educational calculations, it is enough to leave two clearly distinguishable positions of each mass: L and R. Spatial wave packets are assumed to be narrow compared to the distances between interacting objects. The initial state contains four combinations: LL, LR, RL and RR - with the same amplitude modules. Independent preparation specifies the product of two states; at the beginning there is no entanglement.

In each combination, the distance between the masses is different, so the gravitational potential energy is also different. During exposure, different branches gain different phases. If these phases can be completely decomposed into the separate contribution of the first object and the separate contribution of the second, the state remains a product. If such a decomposition is not possible, entanglement arises. Consequently, it is not just the magnitude of the accumulated phase that is important, but its dependence on two positions at once.

In the simplest model, the positions during exposure are fixed, the movements during separation and convergence of packets are insignificant, and there are no losses. This is a deliberately limited description. It allows you to check algebra and order of magnitude. When designing an experiment, phase must be integrated along real trajectories, including control intervals, and additional interactions must be included in the same calculation as gravity.

$$|\psi(t)\rangle = \frac{1}{2} \sum_{a,b \in \{L,R\}} e^{i\phi_{ab}} |a\rangle_1 |b\rangle_2$$

$$\phi_{ab} = \frac{G m_1 m_2 t}{\hbar r_{ab}}.$$

(14.1) The positive sign of the phase follows from the negative Newtonian energy U = −Gm₁m₂/r and the evolution factor exp(−iUt/ħ). When the distance changes, the value t/r is replaced by the integral of 1/r(τ) over time.

A phase combination that cannot be removed locally

Let arbitrary phases be added to the state of the first object, depending only on L or R; the same thing was done with the second one. Such operations change individual coefficients, but do not create interactions between objects. After subtracting them, one essential combination of four phases remains. It is equal to the sum of the phases of identical marks minus the sum of the phases of different marks. It is this value that determines the entanglement of an ideal state with equal moduli of coefficients.

The conclusion can be verified without resorting to the image of invisible intermediary particles. The state coefficients form a two-by-two matrix. For the product of two vectors, its determinant is zero. Here the determinant is proportional to the difference of two complex numbers: one contains the sum of the phases LL and RR, the other - the sum of LR and RL. Their modules are the same, so the difference is determined only by the angle between them.

A convenient measure of the entanglement of the pure state of two two-level systems is called concurrence; below it is denoted C. A value of zero corresponds to the product, one to maximum entanglement. The formula shows the periodicity of the effect: increasing time does not always increase C. The phase can go through a maximum and return to a state that is again a product. Therefore, one poorly chosen duration does not allow us to conclude that the interaction does not create entanglement at all.

$$\Delta = \phi_{LL} + \phi_{RR} - \phi_{LR} - \phi_{RL}.$$

(14.2) Δ does not change when independent phases α_a and β_β are added: their contributions cancel each other in this combination.

$$C = 2|a_{LL}a_{RR} - a_{LR}a_{RL}| = \left|\sin\frac{\Delta}{2}\right|.$$

(14.3) The last equality uses $a_{a\beta} = \exp(i\varphi_{a\beta})/2$. It refers to a pure state, orthogonal branches and equal initial amplitudes. For a mixed state, this short formula is not applicable.

Geometry matters more than strength

For a clear example, the centers of the initial positions are separated by a distance d, and both masses are shifted along the same line by the same amount s between the branches. Then two combinations have distance d, one is d+s, the other is d−s. The substitution gives the exact expression within the point mass model. If s is much less than d, there remains a dependence on the square of s and the inverse cube of d.

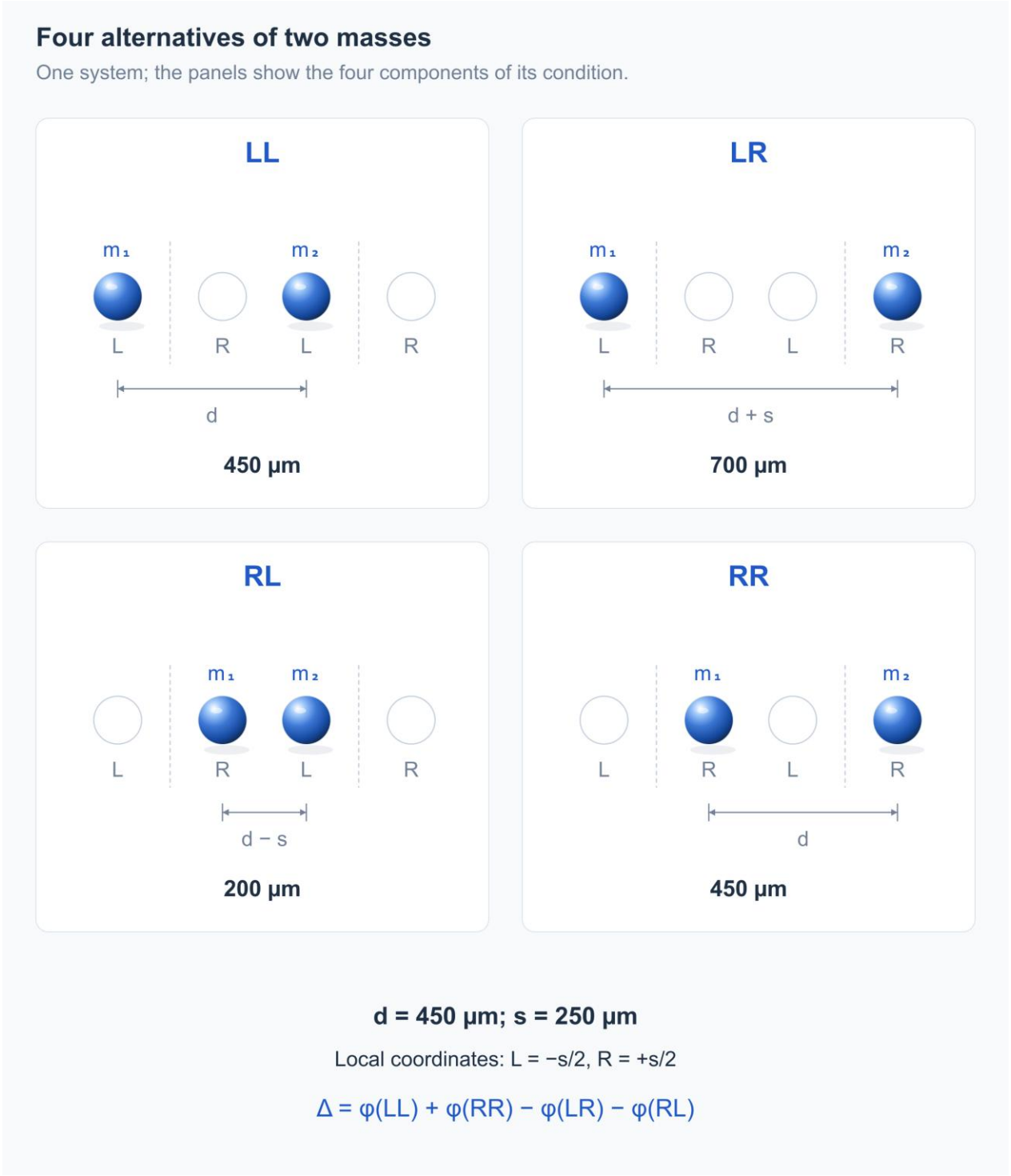


Figure 35. Four components of the two-mass model with the general orientation of local coordinates L=−s/2 and R=+s/2. In branches LL and RR the distance is d, in LR - d+s, in RL - d−s. For training d=450 μm and s=250 μm these are 450, 700, 200 and 450 μm. Gray marks show both available local positions, blue spheres show the selected alternative for each panel. These are components of one state; the mass of each body in each branch remains total. The distances between the centers are proportional to the indicated values, the diameters of the spheres are arbitrary.

The result has a physical meaning. Almost identical acceleration of all branches mainly gives local phase shifts, which in themselves do not connect objects. The entangling part is sensitive to differences in interactions between alternatives. Therefore, the same average force for different geometries can give a different useful signal. The choice of package placement is part of a fundamental measurement, not just a matter of ease of installation.

You can substitute conditional values not stated as realized experiment: $m_1 = m_2 = 10^{-14}$ kg, d = 450 μm, s = 250 μm and exposure 2 s. The exact formula gives the modulus Δ about 0.25 radians and C about 0.13 in the complete absence of decoherence. The small s approximation is no longer particularly accurate here, since the s/d ratio is more than half. The example shows why a beautiful asymptotic formula needs to be checked before engineering conclusions.

A long interaction time increases the phase, but at the same time gives the medium more time to destroy coherence. Decreasing the distance increases sensitivity to measurement error. For extended bodies, integration over mass distributions is required; Deviations in shape, orientation and proximity of surfaces are especially significant. For non-overlapping spherically symmetric bodies, the Newtonian energy coincides with the energy of the point masses at the centers. Therefore, the size does not always require correction, but the condition of symmetry must be justified.

$$\Delta = \frac{G m_1 m_2 t}{\hbar}\left(\frac{2}{d} - \frac{1}{d+s} - \frac{1}{d-s}\right) = -\frac{2 G m_1 m_2 t s^2}{\hbar d (d^2 - s^2)}.$$

(14.4) Requires d > s and no overlap of physical bodies. For $s \ll d$, the denominator can be replaced by $\hbar d^3$; the sign depends on the labeling of the branches and does not affect C.

$$U_{ab} = -G \int d^3x\, d^3y\, \frac{\varrho_{1a}(\mathbf{x})\varrho_{2b}(\mathbf{y})}{|\mathbf{x}-\mathbf{y}|}.$$

(14.5) Here ϱ denotes the mass density, and the subscripts a and b denote the positions or orientations of the corresponding branches. This energy replaces the point expression when the shape and distribution of mass are significant.

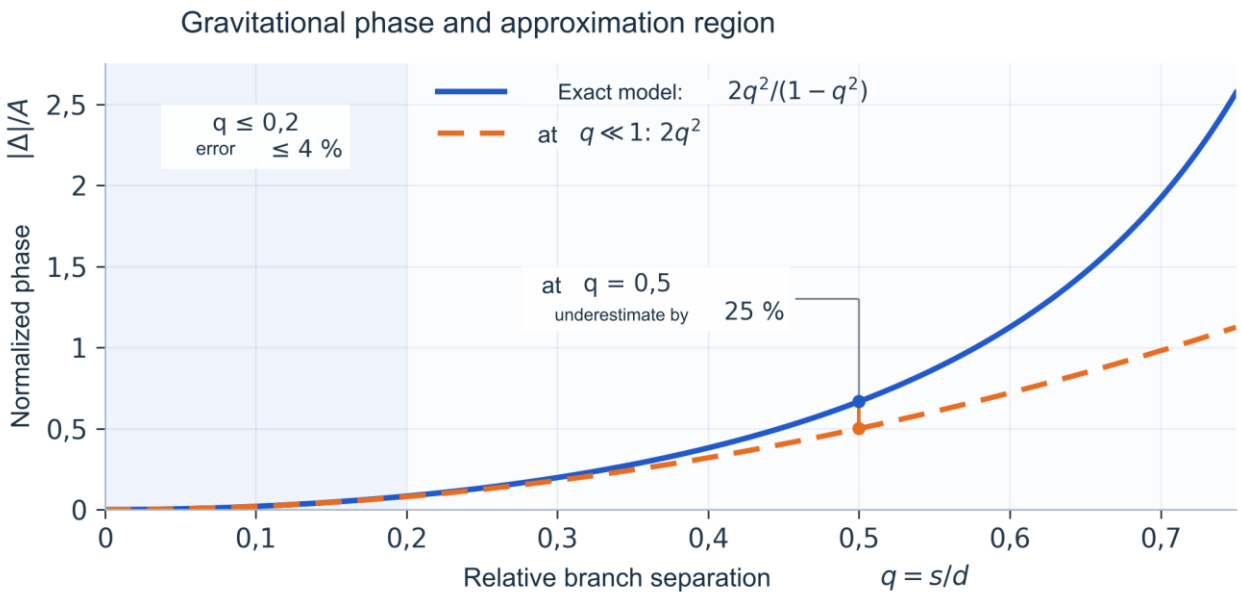


Figure 36. Calculation of the normalized gravitational phase for point masses at a fixed $A = Gm_1m_2t/(\hbar d)$. Solid line: $|\Delta|/A = 2q^2/(1-q^2)$, where $q = s/d$; dotted line: approximation $2q^2$ for $q \ll 1$. The relative underestimation of the exact value is equal to q^2: for $q = 0.2$ it is 4%, for $q = 0.5$ it is 25%. This is an illustrative model, not experimental data.

What remains after interaction with the environment?

The actual result is described by the density matrix. Its diagonal elements give the probabilities of the branches, and the non-diagonal elements contain the coherence between them. Random phase noise can reduce the latter without changing the probability of positions. Therefore, four approximately identical hit frequencies do not say anything about the preservation of the superposition. We need measurements in other bases, access to interference, or a pre-substantiated witness to entanglement.

In a simple pure decoherence model, the matrix element receives a phase factor and attenuation. But you cannot arbitrarily assign a convenient rate to each pair of branches: the aggregate transformation must preserve the physical permissibility of the state. It is more reliable to derive noise from specific random forces or from a correct open system equation. If state transitions, particle loss, or heating additionally occur, the exponent alone for off-diagonal elements is no longer sufficient.

Even with a valid model, losses can affect data selection. If only successful registrations are analyzed, you need to indicate what determines success. Selection can change the type of observed correlations. The same applies to detector calibration and preparation errors. A proper calculation relates the source parameters to the probabilities of raw outcomes, including omissions, and then constructs an estimate of entanglement and its uncertainty.

The absence of observable entanglement has several possible reasons: the interaction does not create it, the environment erases it too quickly, the chosen witness is not sensitive enough, or there are still few measurements. These options are separated by additional settings and control series. A negative result is useful

when formulated as excluding a particular range of predictions. Without a sensitivity estimate, the phrase "entanglement not found" conveys almost nothing about gravity.

$$\rho_{ab,cd}(t) = \rho_{ab,cd}(0)\exp\{i[\phi_{ab}(t) - \phi_{cd}(t)] - \Gamma_{ab,cd}t\}.$$

(14.6) This is a tutorial form for stationary Markovian pure phase noise with physically consistent rates Γ. It is not a universal model of the environment and does not prove the mechanism of objective collapse.

Explicit state matrix under phase noise

The transition to a mixed state can be performed without additional undefined coefficients. It is convenient to first select the local phase readout axes. Any four phases are decomposed into a common phase, two separate turns and an interacting part. If $z_L = 1$ and $z_R = -1$, the latter is equal to $\Delta z_\alpha z_\beta/4$. The general phase is unobservable; local rotations are determined by calibration and compensated during measurement.

After this operation, the pure state is written as $\exp(i\Delta Z_1 Z_2/4)|{+}{+}\rangle$. Here $|+\rangle = (|L\rangle+|R\rangle)/\sqrt{2}$, and Z distinguishes two branches. Compensation does not create entanglement: it is the product of two local operations. However, compensation error changes the values of specific measurement correlations. Therefore, the axes cannot be independently fitted on the same sample on which the significance of the witness is then declared. For such adjustment, a separate training series or statistical accounting of the search will be required.

Let each object independently pass through the pure phase decay channel. The diagonals of the one-particle matrix are preserved, and the off-diagonal elements are multiplied by v from zero to one. In a two-particle matrix, an element that differs in the label of one subsystem receives a multiplier v, and an element that differs in two labels receives v^2. This is the tensor product of two admissible channels, so the positivity of the entire state is ensured by the construction.

Below is the matrix in order LL, LR, RL, RR. It contains identical diagonals, but this is not enough to determine its quantum properties. When v = 0, a completely mixed state of four branches is obtained. At v = 1, a pure phase example is restored. Intermediate values describe a continuous degradation of coherence with constant position detection probabilities.

For stationary local phase noise we can set $v = \exp(-\gamma t)$. This definition of rate γ refers to the damping of a single-particle off-diagonal element. It does not include object loss, preparation asymmetries, or random transitions between branches. When such processes are significant, the matrix must change according to their individual channels.

$$\phi_{ab} = \phi_0 + \alpha z_a + \beta z_b + \frac{\Delta}{4} z_a z_b$$

$$\phi_0 = \frac{1}{4} \sum_{a,b} \phi_{ab}.$$

(14.7) α = (φLL+φLR−φRL−φRR)/4 and β = (φLL−φLR+φRL−φRR)/4. Rotations exp(−iαZ₁) and exp(−iβZ₂) remove local components.

$$\rho_v = \frac{1}{4} \begin{pmatrix} 1 & v e^{i\Delta/2} & v e^{i\Delta/2} & v^2 \\ v e^{-i\Delta/2} & 1 & v^2 & v e^{-i\Delta/2} \\ v e^{-i\Delta/2} & v^2 & 1 & v e^{-i\Delta/2} \\ v^2 & v e^{i\Delta/2} & v e^{i\Delta/2} & 1 \end{pmatrix}.$$

(14.8) The matrix refers to orthogonal branches equal to the original amplitudes, compensated local phases and identical independent phase decay channels.

Three settings for an entanglement witness

The matrix of two two-level systems has a strict check: partial transposition over the second subsystem must preserve positivity for the separable state. In the two-by-two dimension this condition is also sufficient for separability. In higher dimensions the last statement is no longer true. [59] For the family under consideration, the spectrum is calculated explicitly, and only one of its elements can become negative.

Let us denote $C_0 = |\sin(\Delta/2)|$. Negativity, that is, the sum of the moduli of negative eigenvalues of a partially transposed matrix, is equal to $\max[0,(v^2+2vC_0-1)/4]$. Therefore, the threshold is given by the equality $v^2+2vC_0 = 1$. For the original geometry it is $v = 0.88256848$. If the interaction time is two seconds and $v = \exp(-\gamma t)$, entanglement requires $\gamma < 0.06245945\ s^{-1}$. This is the boundary of a certain state model.

A full tomography is not necessary here. Let us introduce X, Y and Z as Pauli matrices in the branch basis and fix in advance $q = \text{sign}[\sin(\Delta/2)]$. Three settings are enough: measure X for both objects, then Y for the first and Z for the second, then Z for the first and Y for the second. From the three correlations, the indicator S is constructed. For negative Δ from the example given, $q = -1$, therefore all three measured correlations are added.

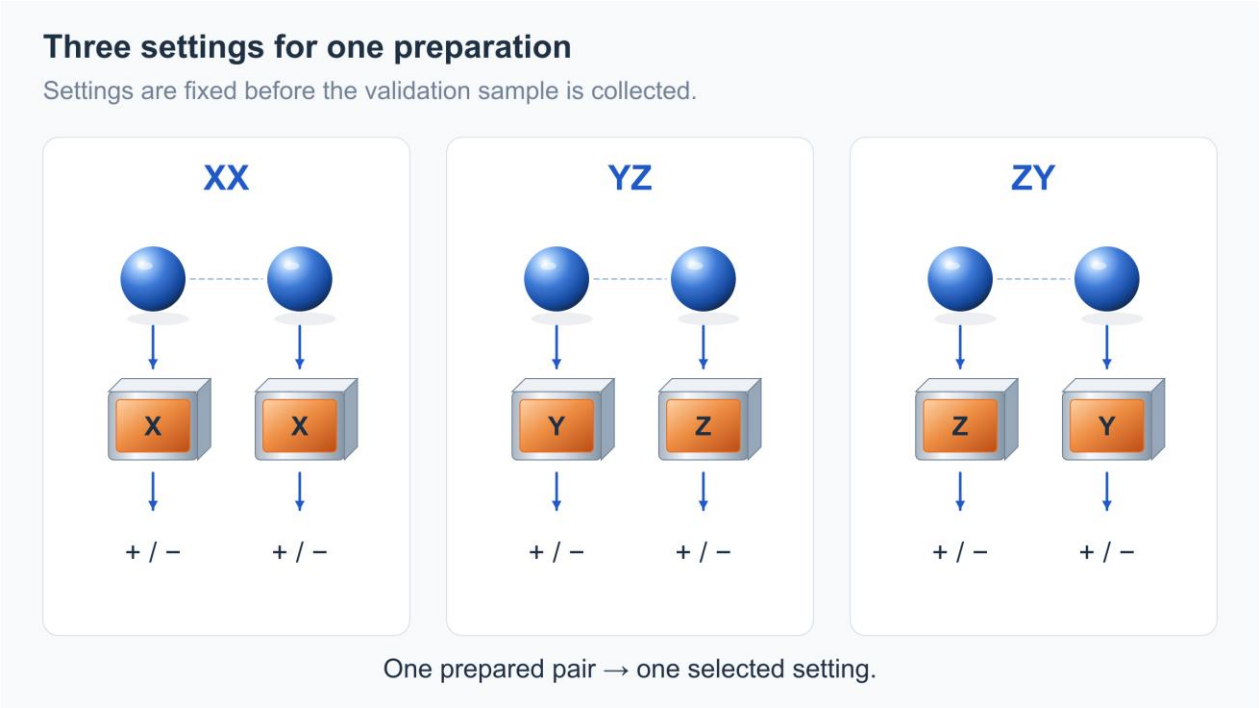


Figure 37. The same preparation is repeated for the three pre-selected settings XX, YZ and ZY. Each pair is registered in one setting and gives one of four pairs of characters. Incompatible axes are not measured simultaneously on the same pair. The diagram explains how the witness is read; a conclusion about the nature of the mediator requires additional premises and control of other connections.

The boundary $S \leq 1$ applies to any separable two-qubit state, not just the selected noise family. For a product state, correlations have the form of products of the components of the local Bloch vectors r and s. Then $S = r^T T s$, where T rearranges the two coordinates and possibly changes their signs. The spectral norm T is equal to one, and the lengths of the Bloch vectors do not exceed one. Hence $S \leq 1$. A mixture of product states preserves inequality due to linearity.

For a given matrix, $\langle XX \rangle = v^2$ and $\langle YZ \rangle = \langle ZY \rangle = -v \sin(\Delta/2)$. Therefore $S = v^2 + 2vC_0$, and this particular witness reaches the same threshold as the partial transposition criterion. This coincidence is due to the symmetry of the family. For an arbitrary mixed state, the absence of a violation $S \leq 1$ does not prove separability: another witness may be more sensitive.

The scope of mathematical verification here is clear. The property of two selected degrees of freedom is measured. To draw a conclusion about a gravitational intermediary, independence of the initial preparation and control of other communication channels are additionally required. Local change of axes is not physically capable of creating false entanglement, but an unknown or data-driven axes selection procedure can distort the statistical estimate.

$$\operatorname{spec}(\rho_v^{T_2}) = \left\{ \frac{1 + v^2 \pm 2v|\cos(\Delta/2)|}{4}, \frac{1 - v^2 \pm 2v|\sin(\Delta/2)|}{4} \right\}.$$

(14.9) Both pairs contain two values. The first pair is non-negative; the minimum value of the second determines the threshold for this family.

$$S = \langle X \otimes X \rangle - q(\langle Y \otimes Z \rangle + \langle Z \otimes Y \rangle)$$

$$W = \frac{I - X \otimes X + q(Y \otimes Z + Z \otimes Y)}{4}.$$

(14.10) For any separable state, S ≤ 1 and ⟨W⟩ ≥ 0. The violation S > 1 indicates entanglement; q is selected before data analysis.

$$\nu_{\mathrm{crit}} = \sqrt{1 + C_0^2} - C_0$$

$$\mathcal{N} = \max\left(0, \frac{\nu^2 + 2\nu C_0 - 1}{4}\right).$$

(14.11) C_0 characterizes the ideal pure state. Negativity N and concurrence C_0 are different measures; they cannot be identified for the noise state.

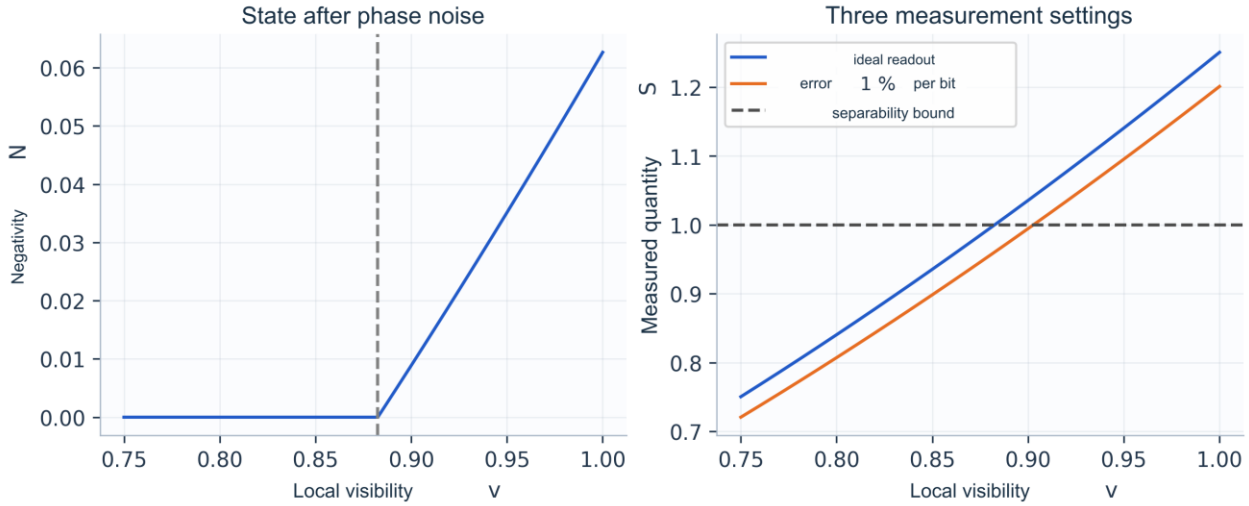


Figure 38. The entanglement boundary in the two-branch model. On the left is the negativity of the mixed state, on the right is the three-tuning indicator S with ideal reading and error 1 % per registered sign. With the accepted geometry, the state threshold is ν = 0.882568, and the threshold of a direct witness with such an error is ν = 0.902822. This is a calculation of a given model, not a measurement.

From state to four detector outcomes

Each of the three settings yields four pairs of binary outcomes: ++, +−, −+, and −−. The correlation follows directly from their frequencies: equal signs contribute +1 and opposite signs contribute −1. The full likelihood requires all four probabilities because the single-particle means in the XX setting are also nonzero. Reducing the data to one measure is convenient for the witness, but must not lead to loss of the original record.

For measurement A for the first object and B for the second, the probability of the pair a,b is equal to a quarter of the sum of unity, two single-particle averages and the correlation term. In the selected axes, $\langle X_1 \rangle = \langle X_2 \rangle = \nu \cos(\Delta/2)$, while the Y and Z averages are zero. Therefore, most XX outcomes, when well prepared, have a ++ sign, although the other two settings remain close to uniform.

Let us introduce a simple, separately verifiable registration response: each recorded sign independently changes to the opposite one with probability ε. At η = 1−2ε single-particle averages decrease by η times, correlations by η² times. This is a symmetrical error model, the same for all axes. An asymmetric detector requires two error probabilities per object and its own response matrix for each setting.

With v = 0.95 and ε = 0.01, the expected recorded value is 1.095301. Even a slight deterioration in reading is noticeable: with v = 0.90 the state is still entangled according to PPT, but the recorded indicator is already less than one. The threshold for this unconverted witness increases from 0.882568 to 0.902822. Therefore, “a state contains entanglement” and “a given reading method reveals it” are different quantitative conditions.

In this example, registration errors are not subtracted from the correlations: the criterion is applied directly to the raw characters. Given the symmetric model adopted, this is equivalent to a local weakening of the Bloch vectors, which does not create entanglement. Inversion of the poorly known response matrix could artificially increase S; it is only acceptable if calibration uncertainty is included in the analysis.

Object losses require another outcome variable. The table below is based on a correctly prepared and registered pair. Such a convention is acceptable if a successful event is declared before the selection of measuring axes or the independence of selection from the setting and hidden result is justified by a separate model. If the probability of registration depends on the outcome, the four conditional frequencies do not form a complete test: it is necessary to include gaps in the likelihood and test for selection effects.

$$P(a,b\mid A,B)=\frac{1}{4}[1+a\langle A\otimes I\rangle+b\langle I\otimes B\rangle+ab\langle A\otimes B\rangle],\ a,b=\pm1.$$

(14.12) This is the Born rule for the projectors (I+aA)/2 and (I+bB)/2. With symmetric registration error, the means are replaced by η ⟨A⟩ and η ⟨B⟩, and the correlation by η² ⟨AB⟩.

$$S_{\mathrm{reg}}=\eta^2(v^2+2vC_0)$$

$$v_{\mathrm{crit,reg}}=\sqrt{C_0^2+\eta^{-2}}-C_0.$$

(14.13) Threshold refers to the direct use of recorded correlations without response correction. If the right side is greater than one, this witness is not available for this reading.

Probabilities of outcomes for v = 0.95 and ε = 0.01

Settings	P(++)	P(+−)	P(−+)	P(−−)
XX	0.928525	0.033310	0.033310	0.004856
YZ	0.278568	0.221432	0.221432	0.278568
ZY	0.278568	0.221432	0.221432	0.278568

In each line the sum is equal to one with rounding accuracy. All values are calculated from the model, not measured.

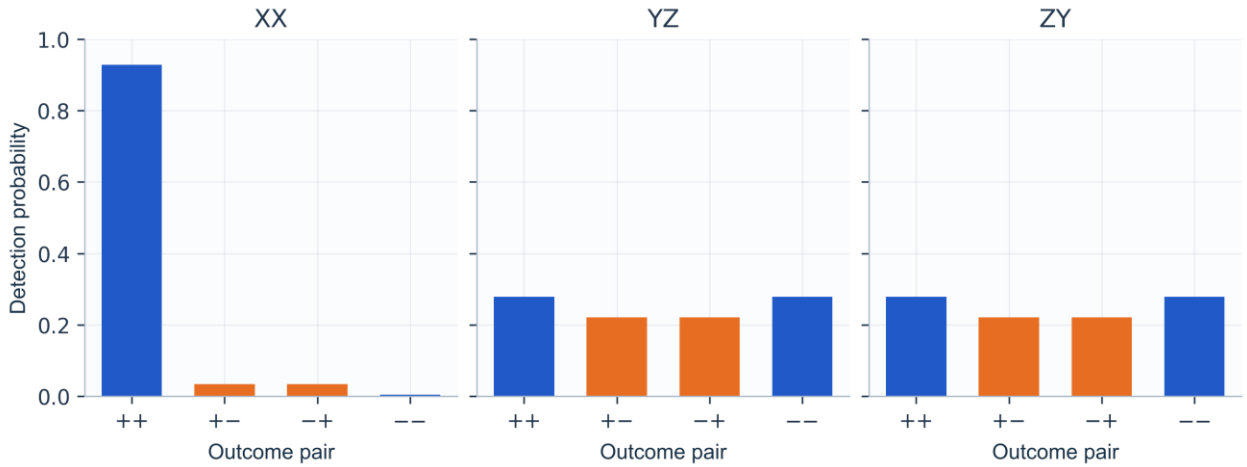


Figure 39. Calculated probabilities of four outcomes in settings XX, YZ and ZY with ν = 0.95 and reading error 1 % per sign. Irregularity XX also contains information about single-particle averages. All four outcomes are kept on record for later analysis.

How many repetitions are enough in this model?

The number of repetitions can be related to specified error probabilities. Suppose each setting is repeated n times, with pairs prepared independently in the same way, and with the settings, the sign of q, and the stopping rule fixed before data collection. Each product of signs lies between −1 and 1. Hoeffding's inequality gives a conservative bound without a Gaussian approximation to the estimator's distribution. [62]

For the sum of three correlations, the probability of overestimating its true value by h does not exceed $\exp(-nh^2/6)$. Since the separable states have $S \le 1$, it is sufficient to require that the estimate exceed one by the root of $6\ln(1/\alpha)/n$. Then the probability of false declaration of entanglement does not exceed α under the accepted conditions. The overall factor of six arises from three independent groups of measurements with limited binary outcomes.

Detection probability also matters for planning. Let the expected excess be $\delta = S_{reg} - 1$. To ensure both an upper bound α on false detection and a lower bound $1-\beta$ on power, it is sufficient to choose n at least as large as the expression below. It applies the same concentration bound to underestimation of the signal. Setting the threshold exactly at the expected mean would not provide that guarantee: roughly half the runs would fall below the mean.

For $\delta = 0.095301$, $\alpha = 0.01$ and $\beta = 0.05$, this results in $n = 9929$ pairs per setting, for a total of 29 787 registered pairs. The threshold is 1.052753. This estimate is intentionally conservative. A more efficient test on full four-output distributions may require less data, but its advantage should be established by its own calibration.

In a reproducible simulation with a fixed initial state of the random number generator, samples are obtained from the table. They give the correlations 0.871085, 0.132037 and 0.103636, that is, the estimate $S = 1.106758$. The corresponding upper

bound on the probability of such an excess in a separable state is $6.44 \cdot 10^{-9}$. This is the result of an artificial sample from a given model; it is not a registration of gravitational entanglement.

Additional 20 000 model runs yielded a detection fraction of 99.80% with a 95 Wilson percentage interval of approximately 99.73–99.85%. For the selected boundary separable product with 1/3 correlations and ideal readout, the false discovery rate was 0.065%, with a range of about 0.038–0.111%. This series tests the implementation on a specific null state. The guarantee for the entire accepted class is given not by it, but by the derived boundary.

Independence and uniformity of preparation are essential here. If the three settings are measured in long blocks with a varying source, drift can change their distributions differently. The settings should be mixed or the time dependence explicitly modeled. Likewise, stopping after the first successful exceed changes the test procedure. Sequential collection requires a predetermined consistent criterion.

The number of registered pairs also cannot be immediately translated into operating hours without an exit model. If a valid pair is obtained with probability pgodn and the full cycle lasts τcycle, the average acquisition time is estimated as 3nτcycle/pgodn, with additional time for calibrations. This formula allows us to substitute real platform parameters while maintaining the distinction between statistical sufficiency and engineering feasibility.

$$\Pr(\widehat{S} - S \geq h) \leq e^{-nh^2/6}$$

$$\widehat{S} > 1 + \sqrt{\frac{6\ln(1/\alpha)}{n}}.$$

(14.14) The boundary refers to three preselected settings with n independent identically distributed pairs per setting. Correlations are calculated as the average of the produced signs.

$$n \geq \frac{6}{\delta^2}\left(\sqrt{\ln(1/\alpha)} + \sqrt{\ln(1/\beta)}\right)^2$$

$$\delta = S_{\mathrm{reg}} - 1 > 0.$$

(14.15) Sufficient volume for a false detection rate not higher than α and power not lower than 1−β in this model. It is not a universal minimum number of repetitions.

One simulated sample of 9929 pairs per setting

Settings	++	+−	−+	−−
XX	9250	320	320	39
YZ	2787	2159	2150	2833
ZY	2755	2195	2255	2724

Initial state of the generator 20261113. The archive contains all inputs and a recalculation program.

Dispute over what exactly will be proven

The informational argument relies on the prohibition of creating entanglement from independent states only by local operations and the exchange of classical messages. However, when applied to gravity, it is necessary to justify why the supposed classical mediator actually belongs to this class of processes. The meaning of the words "local" and "classical", the composition of the subsystems and the available communication channels become part of the statement. The theorem remains valid under its premises; the debate is about which physical models these premises cover.

In the article 2025 by Aziz and Howl, a mechanism was proposed in which the description of matter by means of quantum field theory allows, according to the authors, to obtain entanglement in a classical gravitational field. The work raised technical objections. Therefore, it is considered as a controversial theoretical argument, and not as an established fact about the ability of classical gravity to entangle bodies. [34]

In the reviewed version of the August 7, 2026 preprint by Gundhi, Infantino, and Bassi, the criticism relates to the transition of particles between objects and the choice of state space partitioning. The authors argue that with such a partition, entanglement arises from free evolution, and when transitions are prohibited, the wave function remains factorized. Therefore, it is necessary to establish which subsystems are entangled and by what physical process their correlations are created: the mere presence of the gravitational potential in the calculation is not enough. [35]

Di Biagio, in the October article 2026, emphasizes the information-theoretic meaning of locality in the corresponding prohibition theorems and the need to quantitatively compare models. Schneider, Huggett and Linnemann defend the impossibility of classical gravitational mediation in the Newtonian limit they consider. These works use different premises and definitions; their conclusions cannot be declared a direct contradiction without comparing the classes of models under consideration. A scientific conclusion requires tracing what is considered an intermediary and what connections between subsystems are allowed. [36, 44]

Another position was formulated by Fan, Vedral and Marletto in 2026. They examine claims of entanglement in collapse models of gravity and point to violations of the locality assumption in these constructions. According to their analysis, the corresponding correlations do not refute the original witness when its conditions are maintained. This argument refers to a specific design of models, and does not eliminate the need for their quantitative comparison. [60]

The table compares the different levels of approval. Information locality limits the ways of transmitting information between selected subsystems; spatiotemporal locality refers to the organization of interactions in spacetime. Direct two-particle potential and explicit eigenvariable mediator are also not interchangeable descriptions for any no-go argument. Finally, changing the division into subsystems changes the very question of what entanglement is established between. For a

particular experiment, these decisions enter the model before correlations are analyzed.

Background to the discussion of gravitational entanglement

Approach	Essential Prerequisite	Valid output
Mediator's witness [33]	Independent samples; communication only through an intermediary; local operations in the accepted information sense	Entanglement eliminates the classical middleman in this class of processes.
Aziz and Howl [34]	Quantum field description of matter at classical potential	The authors state entanglement; it is necessary to determine the subsystems and the source of correlations.
Gundhi et al [35]	Particle transport and the selected state space partition are checked	According to the authors' analysis, transfer has an effect even with free evolution; When carry is prohibited, factorization is preserved.
Di Biagio [36]	Informational and spatiotemporal locality are separated	A general conclusion about the field requires checking the applicability of the theorem and comparing the dynamics.
Schneider et al [44]	Classical mediation in the considered Newtonian limit	The impossibility of such entanglement in the specified class is defended.
Feng et al [60]	The locality of collapse structures is checked	The stated counterexamples violate the witness premise, according to the authors' analysis.

The table records the subject of disagreement rather than ranking positions as a complete consensus.

Other signatures of a quantum mediator

An additional way was proposed by Hanif et al: look for the inevitable disturbance of the source when measuring the field created by it. In their design, several interferometers make it possible to separate a certain classical phase change from the desired measurement effect. This is a theoretical proposal in its own right that can complement tests of entanglement. It also requires control of physical connections and does not turn any observed noise into a sign of quantum gravity. [37]

The question of gravitons is even stricter. Mitrakos and co-authors, in paper 2026, analyze under what assumptions entanglement through the Newtonian potential supports the inference about field quanta. Of particular importance in their research are delay effects and the distinction between instantaneous potential as an approximation and superluminal transmission of controlled information. The result relates to a theoretical analysis and not to the detection of individual gravitons. [38]

The general research strategy emerges from these differences. One experiment can reliably exclude several methods of classical transmission of interaction, another can test the response to a measurement, and a third can limit additional noise. The joint picture is stronger than a separate beautiful signal if the same model parameters are used for all measurements. At the next step, another participant in each such comparison arises: the clock, according to which interactions are assigned and phases are read.

To interpret a witness, it is necessary to record the initial state, division into subsystems, permissible connections and measurements. It is these conditions that determine the strength of the physical inference.

15 What does quantum time mean?

Any phase calculated in the previous chapter contains interaction time. It seems that this is the simplest value: just look at the clock. But a clock is also a physical system. Their readings have an error, depend on movement and field, and at a fairly subtle level are described by a quantum state. The question of time begins with this practical detail and only then leads to broader hypotheses about the structure of the world.

Parameter in the equation and instrument reading

In the Schrödinger equation, time is usually an external parameter. This is the number by which the states of the system are compared. A clock in a laboratory, on the other hand, has a device: an oscillation, a transition between energy levels, a signal phase, and a recording method. It is acceptable to consider them ideal as long as the time inaccuracy is significantly less than the inaccuracies that are important for the task. When this limit is reached, the description of the clock must be included in the measurement model.

It should not be concluded from this that quantum theory prohibits the measurement of time. It can describe the time the event was registered, the duration of the process, and the operation of the physical clock. The difficulties concern the universal time operator with predetermined properties and its relation to the Hamiltonian. A specific measurement is usually specified by a broader set of positive operators, each corresponding to a possible reading. The absence of one universal construct does not mean the absence of measurable temporary quantities.

It is useful to separate three questions here. First: what is the accuracy of a particular device? Second: is it possible to record dynamics through correlations with some subsystem called a clock? Third: is there a fundamental external parameter of time in the final theory of nature? The answer to the first does not automatically solve the second, and a successful mathematical construction for the second does not prove a definite answer to the third. Mixing these levels often turns interesting work into an overly loud message.

In a gravitational experiment, the difference has direct significance. If two parts of the installation use different clocks, it is necessary to indicate how their readings are compared. If a body in superposition is associated with internal vibration, the trajectories and readings may be correlated. Then the phrase “maintain the same amount of time” needs a physical definition. In a weak field, these questions are often solved by ordinary approximations; proximity to experiment does not make them any less fundamental.

Dynamics as a conditional dependence

Page and Wootters proposed in 1983 that change be described in terms of correlations between the clock subsystem and the rest of the system. The composite

state in such a design can be stationary, and the conditional state of the system can depend on the clock readings. This is a certain way of organizing a quantum description. Its existence does not prove that the real Universe is necessarily in the chosen stationary state, nor does it eliminate all questions about quantum gravity. [39]

The meaning of the convention is familiar from ordinary statistics. To know the position of the train at ten o'clock, the combined position and clock information are needed. In the quantum case, joint data is given by the state of two subsystems and the rules for their measurement. Conditional probability is determined by dividing the probability of the joint outcome by the probability of the corresponding clock reading. Therefore, the statement about dynamics must refer to the available correlations, and not to an observer located outside the Universe.

For the simplest analytical example, we can take a clock and a system that are not interacting at the moment, and subordinate their joint state to the condition of zero total energy after choosing its reference point. The reference clock state of zero reading must contain a superposition of energies. The eigenstate of the Hamiltonian changes only to the overall phase and does not allow the readings to be distinguished. The motion of the reference state under the action of the clock Hamiltonian defines a family of phase states labeled t.

This reading can be described by a covariance measurement: the evolution of a clock for a certain duration shifts the markers of its outcomes by the same amount. In the design under consideration, the measurement effects have rank one and are proportional to the projections onto the clock phase states. These states do not have to be mutually orthogonal. The clock family, the t-label measure, and the normalization are chosen in concert so that the effects form POVMs—positive operators whose sum or integral is equal to unity. This is an additional design condition, and not a property of an arbitrary superposition of energies. The projection of the joint pure state gives the conditional vector of the system.

In this test there is no birth of movement from one word “entanglement”. The structure of the clock subsystem, energy spectra, special correlation and the rule for choosing a conditional state are essential. An arbitrary pair of entangled objects does not have to form a good clock. The energy constraint itself is a prerequisite for the teaching model here; it is not derived from a complete theory of the Universe and should not be presented as its established law.

$$P(a \mid t) = \frac{\mathrm{Tr}[(E_t \otimes M_a)\rho_{CS}]}{\mathrm{Tr}[(E_t \otimes I)\rho_{CS}]}.$$

(15.1) E_t describes the clock reading, M_a is the result of measuring the system, ρCS is the joint state. The denominator must be non-zero. This formula determines the conditional probability and does not itself determine the dynamics.

$$(H_C + H_S)|\Psi\rangle = 0, |t\rangle_C = e^{-iH_C t/\hbar}|\chi_0\rangle_C, |\widetilde{\psi}(t)\rangle_S = \langle t|_C \Psi\rangle.$$

(15.2) χ_0 is the reference phase state of the zero reading, not the energy eigenstate. When reading rank one, E_t is proportional to $|t\rangle\langle t|$ with proper POVM normalization. A tilde marks an unnormalized conditional vector; in this construction its norm is constant. Specific patterns of

clock interaction and reading can alter conditional dynamics; The very finiteness or non-orthogonality of the clock states does not define a universal correction.

$$i\hbar\frac{d}{dt}|\widetilde{\psi}(t)\rangle_S = -\langle t|_C H_C|\Psi\rangle = H_S|\widetilde{\psi}(t)\rangle_S.$$

(15.3) Equality follows directly from the definition of clock states and restrictions on the total energy. This is a test of the workings of an idealized mechanism, not a proof of the fundamental absence of time.

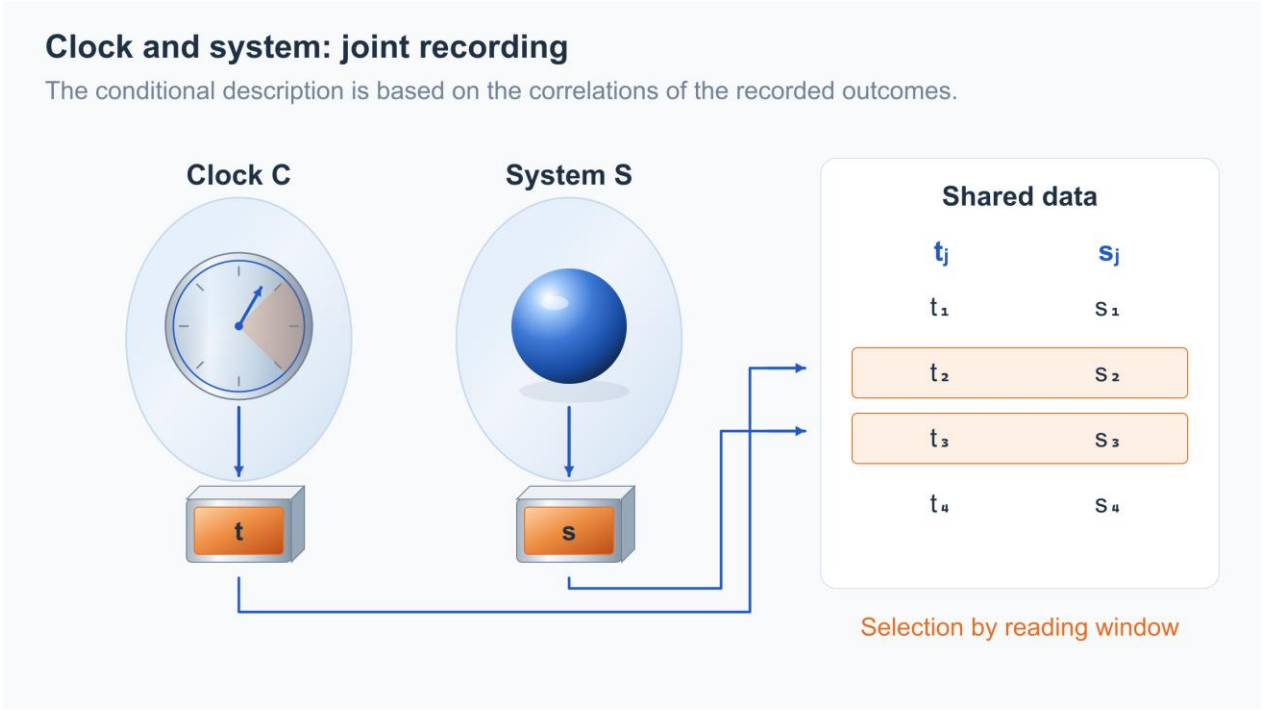


Figure 40. A conditional description of the system is constructed from joint records about the system S and the clock subsystem C. Selecting a window of indications means selecting the corresponding joint results; the symbols t_j and s_j denote recording fields rather than the experimental sample. The clock scale illustrates phase reading, without the assumption that all marks are perfectly legible. There is no separate role for the conscious observer in this scheme.

Normalized measurement of two-level clocks

Now we can calculate all the probabilities of the small clock. Let the states $|0\rangle$ and $|1\rangle$ be separated by energy $\hbar\omega$. The clock Hamiltonian is equal to $\hbar\omega|1\rangle\langle 1|$, and the system has the same energy interval with the origin shifted by $-\hbar\omega$. Then the total energy of both components of the state $(|01\rangle + |10\rangle)/\sqrt{2}$ is equal to zero. The choice of energy onset does not change either the measurement probabilities or the relative phases.

The clock indication is set by the state $|t\rangle = (|0\rangle + e^{-i\omega t}|1\rangle)/\sqrt{2}$. After the period T = 2π/ω it is repeated. To obtain a measurement on one period, you need not just a $|t\rangle\langle t|$ projector, but a $E(t) = (2/T)|t\rangle\langle t|$ effects density. The integral of E(t) over a period is equal to the identity matrix: diagonal elements integrate into ones, and oscillating non-diagonal ones give zero.

For a continuous result, the probability of a single accurate label is zero; the probability density and the probability of a finite interval have a physical meaning. Since the reduced state of the clock is equal to I/2, the reading density is constant and equal to 1/T. Meanwhile, the conditional state of the system changes with the label. Multiplying the joint vector by the clock bra gives an unnormalized vector with the squared norm 1/2; after normalization, $(e^{i\omega t}|0\rangle + |1\rangle)/\sqrt{2}$ remains.

Measuring the system in the $|+\rangle$, $|-\rangle$ basis gives $P(+|t) = [1+\cos(\omega t)]/2$ and $P(-|t) = [1-\cos(\omega t)]/2$. When t = 0 the result is plus with probability one; after a quarter of the period, both outcomes are equally likely; after half the period it turns out to be minus with probability one. After the full period, the probabilities return. Thus, the dependence on the reading is visible in one normalized example without changing the overall steady state.

However, just recording such a dependence does not make the watch ideal. The overlap of two phase states is equal to $\cos^2[\omega(t-t')/2]$. Only marks that differ by half a period are orthogonal. Close marks cannot be accurately distinguished by one measurement, and the same mark after one or several cycles generally corresponds to the same state. Counting cycles requires additional memory, which no longer fits in the two-level model.

Moreva et al.'s 2014 experiment used polarization entangled photons to illustrate the Page–Wutters mechanism. The measurements demonstrated the difference between the general stationary description of the prepared state and the conditional evolution relative to the selected clock subsystem. This is a real laboratory result about the implementation of the model. It is not experimental proof that cosmological time is entirely generated by entanglement. [40]

The practical purpose of such models is to test operational statements. You can specify exactly what is being measured, what conditional probabilities are obtained, and how the response changes as the clock gets worse. The words “inner observer” here do not require consciousness, the experience of duration, or the special status of a person. They denote access to certain correlations. The observer can be an ordinary physical memory associated with the device.

$$|\Psi\rangle = \frac{|0\rangle_C|1\rangle_S + |1\rangle_C|0\rangle_S}{\sqrt{2}}, H_C = \hbar\omega|1\rangle\langle 1|, H_S = \hbar\omega(|1\rangle\langle 1| - I).$$

(15.4) With this choice $(H_C+H_S)|\Psi\rangle = 0$. This is the condition of a specific model with a selected energy origin.

$$|t\rangle = \frac{|0\rangle + e^{-i\omega t}|1\rangle}{\sqrt{2}}, E(t) = \frac{2}{T}|t\rangle\langle t|, \int_0^T E(t)dt = I, T = \frac{2\pi}{\omega}.$$

(15.5) E(t) is the density of POVM effects, which has the dimension of inverse time. The probability of an interval is obtained by integrating the density over this interval.

$$|\psi(t)\rangle_S = \frac{e^{i\omega t}|0\rangle + |1\rangle}{\sqrt{2}}$$

$$P(+|\,t) = \frac{1+\cos\omega t}{2}$$

$$|\langle t \mid t'\rangle|^2 = \cos^2\frac{\omega(t-t')}{2}.$$

(15.6) The conditional vector is normalized. The clock-reading density for a given joint state is 1/T, so the conditional probabilities are obtained by simply dividing the joint density by 1/T.

A finite reading window and the cost of resolution

A real logger groups results into intervals. For a window of width w around mark t_0, the corresponding effect is equal to the integral E(t) over this window. At the period boundary, the window continues in a circle: the labels 0 and T indicate one state. In the chosen joint state, its probability is w/T. The conditional state of the system is obtained by averaging the phase states inside the window, and not by arbitrarily replacing time with its middle.

Integrating the cosine gives the appearance sinc(ωw/2), where sinc(x) = sin(x)/x. If the window width is T/4, it is equal to 0.900316. Therefore, the maximum probability of plus decreases from one to 0.950158, and the minimum increases from zero to 0.049842. With the width of the full period, the cosine averages to zero and both outcomes become equally probable. This is the loss of available phase information during coarse readout.

Increasing the number of repetitions more accurately determines the already blurred probability, but does not restore the lost label of a single event. To improve the time resolution, you need to change the measurement itself or the resources of the clock subsystem. It is useful to distinguish between two errors: the uncertainty in the estimated frequency, which decreases with the number of recordings, and the physical blurring of the response, which remains with infinite sampling.

This model provides another control for decoherence studies. If the contrast reduction is associated with a finite time window, changing its width should change the effect according to the calculated relationship. If visibility does not respond to the predicted extent, the brute force explanation is not sufficient. As with spatial noise, the mechanism is tested by changing the control rather than by matching a single curve.

$$P(+|\,t \in [t_0 - w/2, t_0 + w/2]) = \frac{1}{2}\left[1 + \frac{\sin(\omega w/2)}{\omega w/2}\cos(\omega t_0)\right].$$

(15.7) The formula assumes a uniform density of clock readings within the period, a rectangular window and a circular continuation near its border. When w→0 the conditional probability of the exact label is restored.

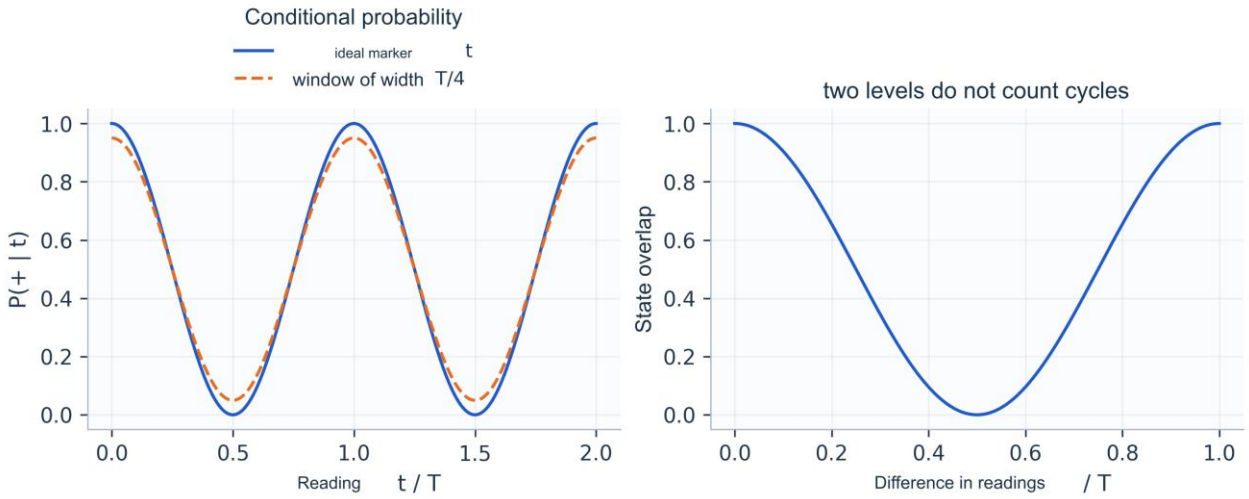


Figure 41. Conditional probabilities of two-level clocks. On the left is the ideal dependence P(+|t) and its averaging over a window of width T/4. On the right is the overlap of phase states. It shows the non-orthogonality of close readings and the repetition of one state after a period.

Why two clock readings require a new protocol

A one-time conditional distribution does not yet specify the sequence of actions with the clock. To calculate two readings, it is necessary to determine which state the first measurement leaves. This is the same question about the measurement instrument that came up in chapter two. Different physical instruments may have the same E(t) effects and different consequences for the next registration.

To be specific, consider the $K(t) = \sqrt{2/T}|t\rangle\langle t|$ instrument. It implements the specified POVM, since the integral K†(t)K(t) is equal to I. After the first result t_1, the clock is in the state $|t_1\rangle$, and the system is in its conditional state $|\psi(t_1)\rangle$. The joint state is now the product. Consequently, the correlation structure on which the original stationary example was built has already changed.

This instrument specifies an external laboratory operation on a prepared pair. It is not required to maintain the zero total energy constraint imposed on the original state. For a closed relational model, the device and memory must be included in the overall description of interaction and energy limitation. The example of the two readings therefore serves as a test of the distinction between the POVM effect and the measurement instrument, rather than as an objection to the stationary conditional formalism.

If the same measurement is immediately repeated without intermediate dynamics, the density of the second result is $[1+\cos\omega(t_2-t_1)]/T$. It is not concentrated at the point $t_2 = t_1$. A matching label is most likely in terms of density, but the result is distributed over the entire period. The reason lies in the non-orthogonality of the phase states and the design of the selected instrument, and not in a random jump in external time.

Moreover, after the first reading, re-measuring only the clocks does not change the separate state of the system already separated from them in this instrument. Therefore, the conditional probability of a system plus remains $P(+|t_1)$, and does not

automatically turn into $P(+|t_2)$. Substituting the second label into the one-time formula would give an incorrect prediction for the described sequence.

If free dynamics, memory interaction, or some other measurement is included between readings, the joint rule changes. Then the Hamiltonians, durations, registration operators and selection conventions must be specified. Studies of measurement events regarding quantum clocks just show that operationally different designs can coincide in the ideal limit and diverge for clocks with finite resources. [41]

Thus, conditional time has precise computational meaning, but requires a physical protocol. In one case, the correlations of many identically prepared pairs are compared; another traces the sequential history of one pair. The identity of these tasks cannot be assumed by default. For the experimental testing of time hypotheses, the description of what the instrument does after the first reading is as essential as its energy spectrum.

$$K(t) = \sqrt{\frac{2}{T}}|t\rangle\langle t|$$

$$p(t_2 \mid t_1) = \frac{2}{T}|\langle t_2 \mid t_1\rangle|^2 = \frac{1+\cos\omega(t_2-t_1)}{T}.$$

(15.8) Density refers to two immediate sequential readings by the same specified instrument, with no evolution between them. Its integral over the second period is equal to unity.

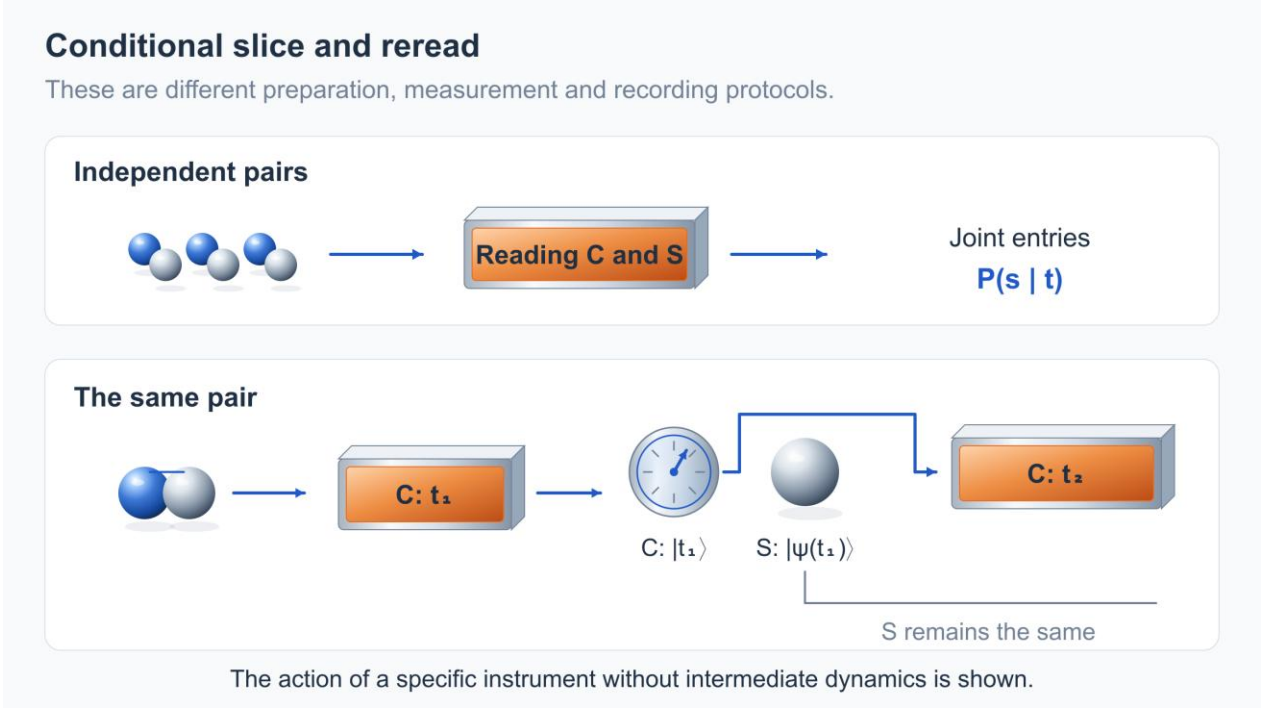


Figure 42. A single conditional slice of many identically prepared pairs and two readings of one pair are different protocols. For the instrument selected in the text, the first reading leaves the product of $|t_1\rangle$ and $|\psi(t_1)\rangle$. In the absence of intermediate dynamics, subsequent reading of only the clock does not automatically put the system into a state corresponding to t_2. The figure refers to a specific external laboratory operation.

When clock inaccuracy is like decoherence

Let's consider a more familiar case: an ideal system evolves unitarily, but the instrument reports the time with an error. One T reading corresponds to a distribution of possible durations. Then the state averaged over this distribution may have less coherence than the state at a precisely known time. No additional fundamental destruction of the superposition is required for this. Insufficient information about the accumulated phase is sufficient.

For the Gaussian error, the calculation is particularly simple. The phase between two energy levels is proportional to their difference and time. Averaging the complex exponential over a Gaussian distribution gives an additional real factor. The larger the energy gap and time scatter, the more the corresponding off-diagonal elements are smoothed out. If the scatter is constant, it is a fixed readout blur; if it increases with duration, the picture may resemble increasing decoherence.

This effect must be taken into account when searching for new physical noise. Coincidence with exponential decay does not mean that spacetime is random at a fundamental level. Generator instability, timing, frequency drift, and electronic delays must be independently assessed. At the same time, one cannot simply declare any damping to be a clock error: the explanation must be quantitatively consistent with its calibration and with several energy discontinuities in the system.

Hausmann, Schmidhuber and Castro-Ruiz, in paper 2025, compared two ways of describing measurement events relative to quantum clocks. In the ideal limit they are consistent, and with limited clock resources they can describe different operational situations and lead to different properties of evolution. This shows the importance of an explicit measurement model. The work does not establish the discreteness of time and does not turn any non-unitarity of the conventional description into a violation of quantum mechanics. [41]

$$\overline{\rho}(T) = \int dt\, p(t \mid T) e^{-iHt/\hbar} \rho(0) e^{iHt/\hbar}.$$

(15.9) p(t|T) specifies the classical duration uncertainty at the reading T. A training model of instrument error is used here; full-fledged quantum clocks may require a more general description.

$$\overline{\rho}_{mn}(T) = \rho_{mn}(0) e^{-i\omega_{mn}T} \exp\left[-\frac{\omega_{mn}^2 \sigma_t^2}{2}\right]$$

$$\omega_{mn} = \frac{E_m - E_n}{\hbar}.$$

(15.10) The result was obtained for a Gaussian time distribution with mean T and variance σ_t^2. The attenuation multiplier reflects phase averaging; it is not independent evidence of objective collapse.

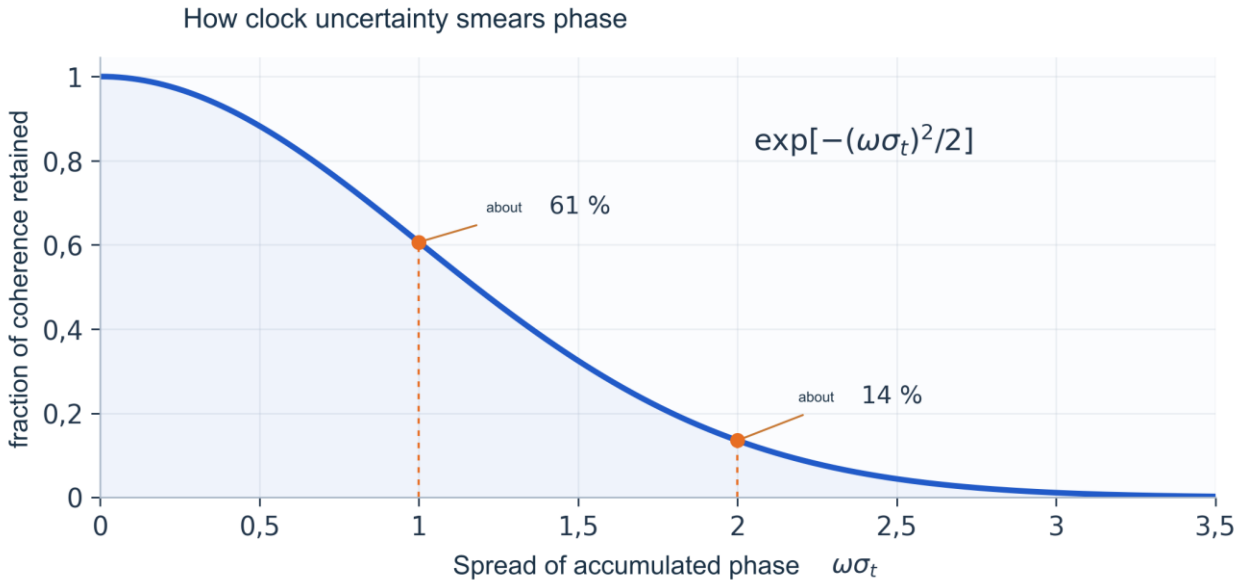


Figure 43. Illustrative calculation of phase averaging over Gaussian time uncertainty with standard deviation σ_t. For coherence with angular frequency ω, the retained factor is $\exp[-(\omega\sigma_t)^2/2]$. At $\omega\sigma_t = 1$ it is about 0.61, at $\omega\sigma_t = 2$ it is about 0.14. The constant σ_t describes a fixed readout blur; separate dynamics of loss of coherence do not follow from this curve.

Time change and direction of time

Obtaining the dependence of a state on a clock reading does not mean explaining why the past leaves records and the future does not. This is a question of the direction of processes, available information and initial conditions. The equation may allow a parameter to change in both directions, while the actual preparation of experiment and the formation of stable memory create a pronounced asymmetry. Conventional quantum time and the thermodynamic arrow of time are related, but are not the same statement.

Likewise, uncertainty about the order of events should not automatically be interpreted as an opportunity to change the recorded past. To assert such an effect requires identification of events, frames of reference, available interventions, and recording statistics. The unusual structure of correlations can be physically important without a paradoxical reading. In time studies, it is especially useful to start with the question: what sequence of instrument readings would distinguish the proposed model from the usual one?

Time is included in the uncertainty budget along with distances, masses and states. A stable discrepancy with such a model provides grounds for testing more general laws of clocks and interactions. The next chapter will integrate these sources of uncertainty into a single model comparison.

16 How to compare gravity models

After deducing the gravitational phase, I want to immediately plot a graph and see the boundary between the classical and quantum worlds. However, one plot usually only answers the question about the selected parameters of the selected model. A scientifically significant result requires a different scale of testing: is at least one valid competing model capable of reproducing the entire set of measurements with the same accuracy?

The model should produce probabilities

The names "quantum gravity" and "classical gravity" are too broad for direct statistical comparison. Each must be replaced by a specific evolution rule, input state, and set of read operations. The Hamiltonian specifies part of the dynamics, but itself does not contain preparation errors, losses, or detector response. The prediction for the experiment is the probabilities of the recorded outcomes under the specified settings.

The simplest quantum hypothesis involves an effective Newtonian interaction between quantum coordinates and an independently valid model of the medium. The alternative may include position measurement, classical transmission of the result and reverse action creating an average force. The third hypothesis may use an averaged field source. Each design has its own prerequisites. For comparison, they need to be stated before fitting, including restrictions on the free parameters.

Calibration information must remain common to competitors. If the distance is measured with a certain error, one model cannot use its exact value, and another can not arbitrarily change it for the sake of a successful coincidence. The permissible values of temperature, charges, frequencies and registration efficiency form a single set of auxiliary parameters. Differing hypotheses should arise from dynamics, not from unequal rules for dealing with uncertainty.

Even before a complex simulation, a control limit is useful. When interaction is turned off, independently prepared systems must behave independently if the environment does not bind them. At zero time, the model should return a prepared state. When the ideal clock assumption is removed, phase errors should appear consistently. These tests do not prove physical correctness, but they can detect an error that would otherwise appear to be a new fundamental property.

The same force with different noise

Average strength is particularly weak as a sole criterion. It is possible to build different mechanisms that equally change the average impulse of the body. In this case, the distribution of momentum, correlations with another body and the rate of loss of coherence will differ. Therefore, measuring attraction does not complete the validation of the model. It fixes one of its characteristics, after which the remaining observables must agree with the same set of parameters.

In the Caffrey-Taylor-Milburn model, the gravitational coupling of two mechanical systems is represented through continuous measurement and classical feedback. This design reproduces the interaction with additional decoherence and heating and does not create entanglement of independent states. This is a certain model of a classic channel. Its exclusion would not automatically exclude all logically possible non-quantized descriptions of geometry. [42]

The relationship between force and noise makes the alternative testable. If a measurement has to be amplified to obtain the required force, its inverse effect changes. If the measurement is weakened, the information used in feedback is degraded. In a specific model, these contributions provide a quantitative trade-off. Therefore, it is impossible to independently reduce all noise to zero while maintaining the same classical transmission of interaction. It is the joint constraint that needs to be checked.

More general constraints between decoherence and diffusion are explored by Oppenheim et al. for consistent classical-quantum dynamics. When applied to gravity, this motivates the comparison of matter coherence with fluctuations of the classical sector. The applicability of the result depends on the adopted mathematical class and the form of communication. The words “the most general theory” without listing these premises should not replace the calculation of a specific observable. [43]

Minimum noise of a given classical channel

For a quantitative comparison, one must first distinguish between complete positivity and classical mediation. The non-negative matrix D ensures the admissibility of a particular noise generator. It does not prevent the added Hamiltonian from creating entanglement. The simplest counterexample is $D = 0$ and the interaction Kx_1x_2: the evolution is unitary and completely positive, but the appropriate product of spatial superpositions becomes entangled.

In the symmetric linear Caffrey-Taylor-Milburn model, the position of each object is continuously measured, and the classical result is used for the force of feedback on the other object. Let us denote the positive measurement force by μ; it has the same units as the K coefficient. The measurement contribution to the double commutator coefficient is proportional to μ, and the feedback noise contribution is proportional to K^2/μ. Decreasing one increases the other. [42]

In the normalization adopted here, the coefficient before the sum $[x_j,[x_j,\rho]]$ is equal to $\mu/(2\hbar)+K^2/(8\hbar\mu)$. The minimum in μ is found at $\mu = |K|/2$ and is equal to $|K|/(2\hbar)$. Comparison with the definition of a generator in terms of D gives $D_{11} = D_{22} = \hbar|K|/2$, $D_{12} = 0$. Thus, strength and noise floor are related; choosing an arbitrarily small D for the same K no longer describes this classical channel.

The coefficient K is obtained from the Newtonian energy at small displacements around the distance d. The constant term does not affect the dynamics; linear terms and individual quadratic contributions enter into the local forces and frequencies. The cross term has the form Kx_1x_2, where $K = 2Gm_1m_2/d^3$ with consistent coordinate

orientation. The sign may change when one axis is redefined; The minimum noise depends on the modulus K.

This construction does not claim to classify all hybrid theories. It specifies a specific alternative with the same Newtonian interaction in the linear mode and the obligatory additional noise. For the narrow branches considered, its predictions can be checked directly: the state matrix is obtained from the same phase solution, but with a certain local damping K. This calculation is especially useful because it does not require judging classicality by the name of the equation.

$$a(\mu) = \frac{\mu}{2\hbar} + \frac{K^2}{8\hbar\mu} \geq \frac{|K|}{2\hbar}$$

$$\mu_{\text{opt}} = \frac{|K|}{2}.$$

(16.1) Here a is the coefficient before $[x_j,[x_j,\rho]]$, and μ is the strength of the continuous measurement in the normalization of this model. This is not the rate γ from the phase decay model.

$$H_{\text{int}} = K x_1 x_2$$

$$K = \frac{2Gm_1m_2}{d^3}$$

$$D_{11} = D_{22} = \frac{\hbar|K|}{2}, D_{12} = 0.$$

(16.2) The minimum D values apply to a symmetrical linear measurement and feedback channel. As they increase, the channel remains noisier; reduction is not a valid free adjustment of the same design.

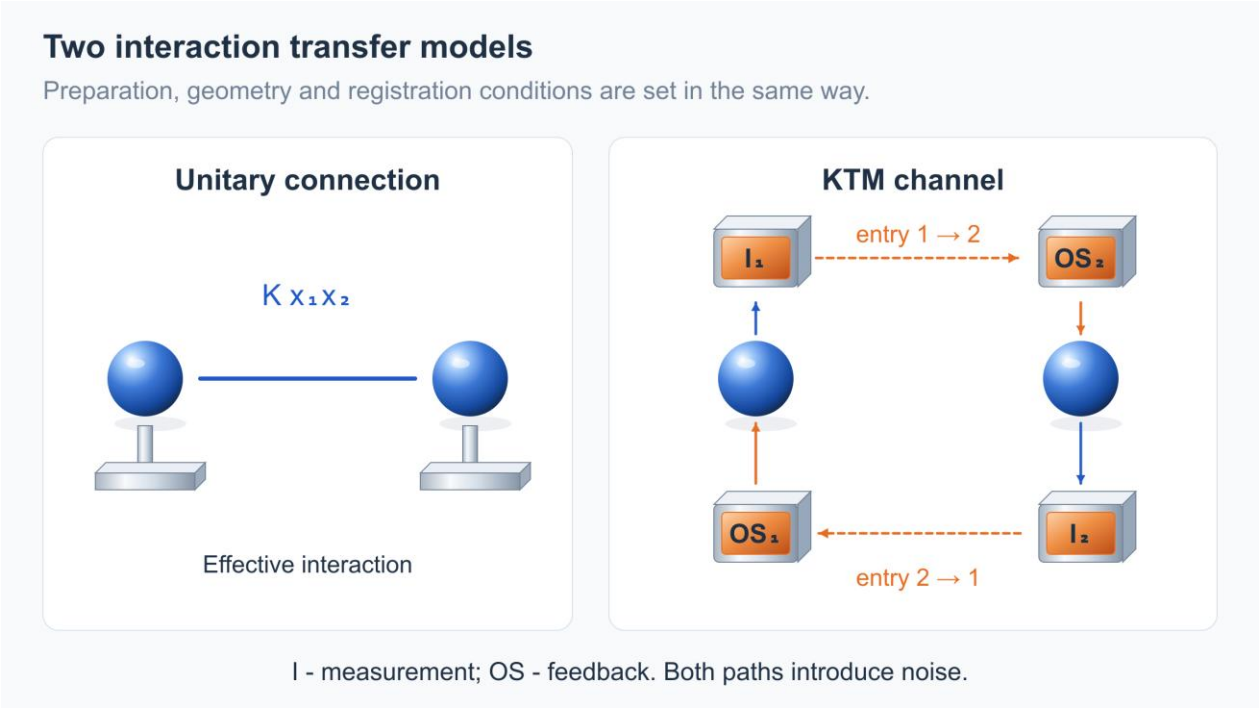


Figure 44. Comparison of effective unitary coupling and a specific KTM closed-loop measurement channel. In the lower and upper tracts on the right, each object is measured, and classical recording is used to influence the other. Measurement disturbance and feedback noise form a joint constraint; they cannot be independently eliminated while maintaining this force pattern. The scheme does not classify all possible classical-quantum theories.

Correlated noise of two masses

In chapter 11, the relationship between decoherence and diffusion was considered for one body. For two masses, a new testable quantity appears: the correlation of the random forces acting on them. In the Markov white noise model, it is included in the real symmetric matrix D. The diagonal elements describe the intrinsic diffusion of each pulse, and the cross element D_{12} describes the joint change of the pulses. This is a standard extension of the same open system generator.

The matrix D must be positive semidefinite. For two masses this means non-negative diagonal elements and a constraint on the square of the cross-factor. Therefore, the overall random force cannot be adjusted independently of the noise of individual bodies. If the proposed set of coefficients violates this condition, it does not define a physically valid channel of this form. Such restrictions are especially useful when correlated noise attempts to explain an observed residual.

The action of the generator in coordinate representation gives the rate of decay of each coherence through the difference of two spatial configurations. Between LL and RR the displacements of both bodies are in the same direction, and between LR and RL they are in the opposite direction. With positive D_{12}, the first coherence decays faster, the second slower; when negative, the sign of the difference changes. Measuring both rates allows you to check the cross-coefficient, which cannot be determined from the separate attenuation of one mass.

The same D_{12} sets the increase in the covariance of impulses. This means that the correlations of movements and the contrast of joint spatial alternatives must be consistent with one matrix D. For equal distances s, the difference between the two indicated rates is proportional to $4D_{12}s^2/\hbar^2$. This is a consequence of the standard generator and a consistency checker, not a new law in its own right. With a finite packet width and changing trajectories, an appropriate calculation of the entire sequence is required.

The coincidence of these dependencies does not yet establish the origin of the noise: the same matrix can be produced by different physical sources. Additional changes to geometry, distance and control spectrum are needed. Complete exclusion of correlated backgrounds without a basis can create a false sense of signal uniqueness. Allowing an arbitrary new matrix for each series, on the contrary, destroys predictability. The model being tested uses common parameters and constraints from independent calibrations.

$$\mathcal{L}_D(\rho) = -\frac{1}{\hbar^2}\sum_{i,j=1}^{2} D_{ij}[x_i,[x_j,\rho]]$$

$$D = D^T \geq 0.$$

(16.3) The noise part of the Markov generator is shown; Hamiltonian dynamics are added separately. D is a real matrix with the dimension of the squared impulse divided by time. For two masses, $D_{11} \geq 0$, $D_{22} \geq 0$ and $D_{11}D_{22} \geq D_{12}^2$ are required.

$$\Gamma_{ab,cd} = \frac{\delta\mathbf{x}^T D \delta\mathbf{x}}{\hbar^2}$$

$$\delta\mathbf{x} = \begin{pmatrix} x_{1a} - x_{1c} \\ x_{2b} - x_{2d} \end{pmatrix}.$$

(16.4) The decay rate refers to the density matrix element between two narrow spatial configurations (a,b) and (c,d) with fixed coordinates. The positive semi-definiteness of D guarantees the non-negativity of all such rates, connecting them with each other.

$$\left.\frac{d\mathrm{Cov}(p_i,p_j)}{dt}\right|_D = 2D_{ij}$$

$$\Gamma_{LL,RR} - \Gamma_{LR,RL} = \frac{4D_{12}s^2}{\hbar^2}.$$

(16.5) The last equality assumes the same separations s for both masses and the same direction from L to R. The first formula describes only the contribution of a given noise generator; interactions and other processes may also change covariances.

A common regime for two kinds of dynamics

In the large four-branch example of chapter 14, the s/d ratio is 250/450. Small spatial decomposition underestimates the exact phase by approximately 30.9%. Therefore, comparing its exact phase with the KTM linear channel would confuse the differences between the theories with approximation error. For the joint calculation,

s/d = 0.05 was chosen here: d = 450 μm and s = 22.5 μm. The masses are kept equal to 10^{-14} kg.

Now the relative difference between the linear phase and the exact four-branch phase is equal to 0.25%. Both dynamics use exactly the linear Hamiltonian, the same preparation $|++\rangle$, the same local axes and the same recording response. Local branches are considered fixed and narrow. The assumption of their retention is not derived from free evolution; it is part of the idealized protocol being compared.

If each object's branch coordinates are ±s/2, the interaction phase is $\Delta_{lin} = -Ks^2t/\hbar$. The minimum KTM noise multiplies the single-particle coherence by $v_{KTM} = \exp[-|K|s^2t/(2\hbar)]$. Hence $v_{KTM} = \exp(-|\Delta_{lin}|/2)$. This additional factor is absent in the unitary hypothesis. Any independently justified shared phase background can then be applied equally to both dynamics.

A check immediately follows from the formula: putting $x = |\Delta_{lin}|/2$, we obtain $S_{KTM} = \exp(-2x)+2\exp(-x)|\sin x| \le 1$, since $|\sin x| \le \sinh x$ for $x \ge 0$. For a given family, the model does not cross the witness boundary at any interaction time. This is a direct conclusion from its dynamics, and not an assumption made in the registration procedure.

$$\Delta_{lin} = -\frac{Ks^2t}{\hbar}$$

$$v_{KTM} = \exp\left[-\frac{|K|s^2t}{2\hbar}\right] = e^{-|\Delta_{lin}|/2}.$$

(16.6) Both formulas use one small spatial parameter. For an exact four-branch Newtonian phase $\Delta_{exact} = \Delta_{lin}/[1-(s/d)^2]$.

$$S_{KTM} = e^{-2x} + 2e^{-x}|\sin x| \le 1$$

$$x = \frac{|\Delta_{lin}|}{2}.$$

(16.7) The inequality follows from $e^x - e^{-x} = 2\sinh x$ and $|\sin x| \le \sinh x$. Adding equal local phase noise and symmetric registration errors does not increase S for this family.

Numerical comparison of force, coherence, and correlations

For the selected masses and distances $K = 1.46487\cdot10^{-28}$ N/m. The total driving force is equal to $3.29595\cdot10^{-32}$ N. The two hypotheses do not differ in these quantities. Their difference arises in the joint state and diffusion: the minimum KTM channel has $D_{11} = D_{22} = 7.72404\cdot10^{-63}$ kg²·m²/s³ and adds the value $\hbar|K|t$ to the dispersion of each pulse.

The table first shows the ideal limit with no common background attenuation and no recording errors. At a two-second exposure, the effect is small: the ideal measure of entanglement of a unitary model is about 0.000703. Increasing the computational time increases the divergence of the correlations, but simultaneously makes the experimental assumptions about retention and coherence stricter. The line with 200

seconds demonstrates the dynamic dependence of the model; it does not mean that such a superposition has already been prepared and stored in the laboratory.

The phase is the same in both columns. In the unitary case, S = 1+2|sin(Δlin/2)|. In the KTM case, the required damping keeps S at or below unity. At 200 seconds, the values are approximately 1.140527 and 0.999784. The second value's proximity to the boundary does not indicate a hidden small violation: the sign of the deviation is checked by the analytical inequality in the preceding section.

Momentum dispersion provides an additional check. At the same interaction time, the channel adds about $3.09 \cdot 10^{-60}$ $kg^2 \cdot m^2/s^2$ to each local dispersion. The intrinsic noise crossover is zero, since $D_{12} = 0$. The overall movement covariance, however, may vary due to interaction and initial condition. Therefore, the zero cross element of the noise matrix cannot be identified with the absence of all pulse correlations.

Heat, witness and force must be analyzed with the same mass and geometry. If, in a real installation, the unknown background completely obscures the predicted diffusion, the corresponding energy test loses sensitivity. The witness may still be useful if the local coherence and readout are good enough. Sharing observations is valuable because it tests the consistency of the mechanism rather than guaranteeing the superiority of each channel in every situation.

$$\Delta \mathrm{Var}(p_j)\big|_{\mathrm{KTM}} = 2D_{jj}t = \hbar |K| t$$

$$\Delta \mathrm{Cov}(p_1, p_2)\big|_{D} = 0.$$

(16.8) Only the direct contribution of the noise generator is shown. These quantities do not include motion, holding potentials, and additional media channels.

Two dynamics with a common linear geometry

t, s	|Δlin|, rad	C_0	vKTM	Sunit	SKTM
2	0.001406	0.000703	0.999297	1.001406	0.9999999998
20	0.014064	0.007032	0.992993	1.014064	0.9999997698
200	0.140643	0.070263	0.932094	1.140527	0.9997839124

C_0 refers to the pure unitary model. For KTM, the state is mixed, so this number is not its measure of entanglement.

Choose settings by their distinguishability

Suppose, at the same time, two hypotheses predict the same visibility of interference. Increasing the number of repetitions will refine the match, but will not necessarily help select an explanation. It is more useful to change the setting at which the dependencies diverge: time, packet separation, mass, or control pulse sequence. The correct question to ask the simulation is which new measurement reduces the range of compatibility of the hypotheses the most.

For preliminary calculations, several observables can be collected into a vector: phase, visibility, spin correlations and the width of the momentum distribution. Then estimate how far one model's prediction is from the opponent's closest prediction, taking into account all allowed auxiliary parameters. The distance must take into account errors and their correlations. Two visually different curves may be statistically indistinguishable, but a small, consistent difference may be informative.

Minimizing the opponent’s parameters is fundamental. Comparison with one inconvenient set of numbers checks only this set. A strong result survives the alternative's attempt to select the most favorable values within independently valid bounds. Moreover, the boundaries cannot be expanded after each unsuccessful forecast without a physical reason. Otherwise, the hypothesis turns into a way to rewrite any data and loses testability.

The quadratic measure below is useful when the errors are approximately Gaussian and the covariance is known. It serves a design rather than a universal declaration of significance. Rare acquisitions, nonlinear estimates, and parameters at the edge of the feasible region require full likelihood and calibration of statistics on simulated data. The decision threshold depends on the entire procedure, including the choice of settings and the number of options tested.

$$\mathcal{D}^2(\mathbf{u}) = \min_{\theta \in \Theta_B} [\mathbf{f}_A(\mathbf{u}) - \mathbf{f}_B(\mathbf{u}, \theta)]^T \Sigma^{-1} [\mathbf{f}_A(\mathbf{u}) - \mathbf{f}_B(\mathbf{u}, \theta)].$$

(16.9) u specifies the experimental settings, f is the vector of predictions, θ is the allowed parameters of alternative B, Σ is the covariance of expected errors. This is an indicator of the distinguishability of the selected models in the selected approximation, and not a new physical constant.

Comparison taking into account the common calibration area

To test the robustness of the difference, one can allow the adversary model to select the most favorable parameters within a predefined region. For example, at t = 200 s three common inputs are introduced: the scale of interaction a, the visibility of the external phase background vbackground and the error probability of one registered sign ε. It is assumed that independent calibration limited them to the intervals 0.98–1.02; 0.98–1.00 and 0.005–0.015, respectively. In this calculation, the intervals are given as conditions of the problem and are not derived from the actual installation.

The reference unitary model uses a = 1, vbackground = 0.99 and ε = 0.01. For the KTM alternative, values within the same intervals are allowed to be freely chosen; its obligatory multiplier exp(−|aΔlin|/2) additionally multiplies vbackground. All predictions are translated into four probabilities for each of the three settings. This compares outcome distributions rather than reconstructed measures of entanglement with different assumptions.

Minimizing the average Kullback-Leibler divergence over the settings gives 0.00610171 nat for the registered pair. The best KTM prediction found is at the boundary of the region: a = 0.98, vbackground = 1 and ε = 0.005. It uses the most favorable settings for preserving correlations, but the distributions still do not match.

The calculation was repeated from several starting points; this is a test of numerical stability in a given small region.

Positive divergence is also supported by an optimizer-independent argument. The reference model gives a recorded S = 1.074900, while the considered channel cannot exceed one even with a perfect readout. Therefore, there is no exact coincidence of distributions in this family. Numerical minimization estimates the size of the mismatch; the witness establishes its presence.

Information distance is not a probability of error and should not be converted into a "sigma number" without a statistical procedure. It shows the expected difference in the mean log-likelihoods under the chosen tuning distribution. A finite sample requires initial event numbers, a decision rule, and its calibration. One such complete example for a witness has already been given in chapter 14; Here another problem is solved - the stability of physical predictions to resolved gauge uncertainty.

$$\overline{D}_{\mathrm{KL}} = \min_{\theta\in\Theta} \frac{1}{3} \sum_{u\in\{XX,YZ,ZY\}} \sum_{a,b} P_A(a,b\mid u) \ln \frac{P_A(a,b\mid u)}{P_B(a,b\mid u,\theta)}.$$

(16.10) Θ is the total predefined calibration region. The settings here have equal weight; for other resources and frequencies of use, their weights must be changed.

An area where this protocol stops helping

It is convenient to represent the influence of the medium in the plane of interaction time t and external dephasing rate γbackground. For the unitary model, v = exp(−γbackgroundt), and the recorded exponent for a given reading error is $\eta^2[v^2+2v|\sin(\kappa t/2)|]$, where $\kappa = |K|s^2/\hbar$. The line S = 1 separates the region where a given witness has a positive margin and the region where increasing the number of repetitions will not in itself create a violation.

At a very short interaction time, the phase is small, and the final reading error already reduces the original correlations. Therefore, even perfect coherence does not guarantee an accessible witness for short periods of time. With a long interaction time, the phase resource increases only to certain maximums, while the accumulated background continues to reduce visibility. As a result, there is a region of useful times, which narrows with increasing γ background and may disappear.

The graph is plotted for the same ratio s/d = 0.05 and registration error 1 % per sign. The KTM alternative uses the same external background, so its curve remains on the other side of the border. If the unitary hypothesis turns out to be below the limit, this means that this witness is insufficient. Complete distributions or observations of pulsed diffusion may still vary; To establish complete indistinguishability, the entire selected data set must be compared.

This result completes the computational formulation at its own level: the dynamics, preparation, measurements, calibration region and the reason for the loss of sensitivity are specified. Transferring to an experiment requires substituting the actual characteristics of retention, background interactions, and event output. In this case, it is already clear which parameters must be measured and which conclusion

allows each outcome. Further extension of the model makes sense when it meets the specific constraint of this map.

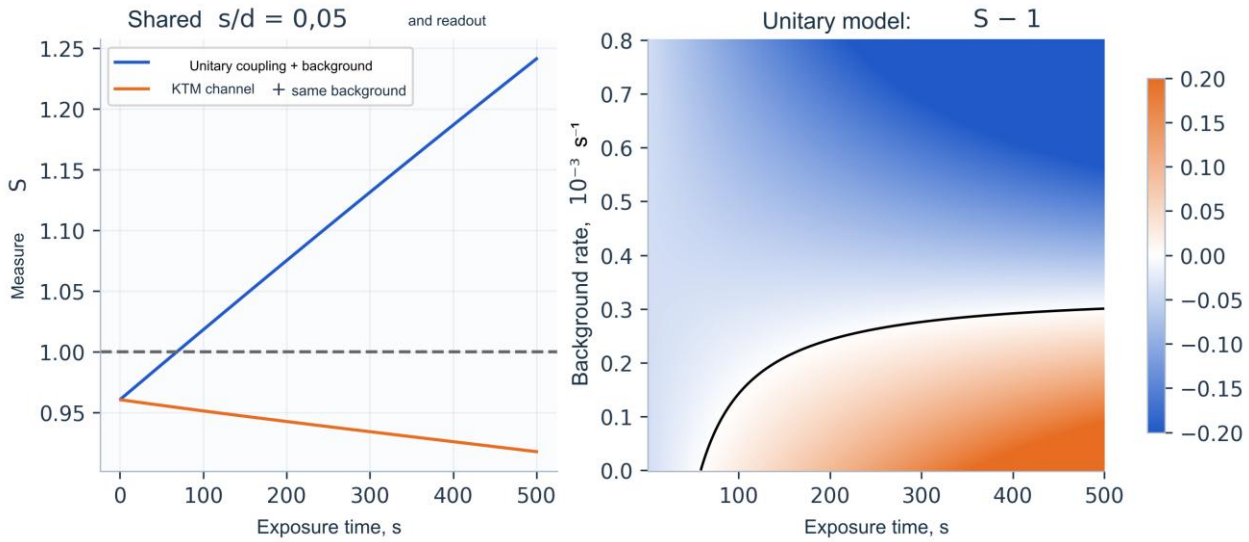


Figure 45. Comparison of two dynamics with general s/d = 0.05 and reading error 1 % per sign. On the left, the same external phase background γbackground = 5·10⁻⁵ s⁻¹ is applied to the unitary coupling and the KTM channel. On the right is the map S−1 for the unitary model; the black line is the threshold of a specific witness. Long excerpts illustrate model dependence and are not declared to be realized characteristics.

From simulation to reproducible results

The calculations in this chapter are implemented in the attached program gravity_v02.py. One set of inputs produces phase tables, outcome probabilities, minimum model divergence, and a threshold map. The program also checks the spectrum of the partially transposed matrix at the 651 point, normalization of probabilities and two-level clock POVM. The coincidence of the analytical and matrix spectra is controlled by absolute tolerance; this separates model prediction from computational errors.

Physical constants, the initial state of the random number generator, calibration intervals and simulated samples are stored along with the results. The artificial sample numbers are separated from the dynamics parameters. Therefore, the same set of observations can be analyzed using another criterion without taking the previously reconstructed measure of entanglement as the original data. Simulated readings are not designated experimental.

Independent tests include the positivity of the conventional state matrix, the sum of the probabilities, the known net limit, and the analytical inequality for KTM. The derivatives of the geometric budget are verified by finite differences. The information distance profile is calculated from several starting points. For a point model, these are sufficient checks of the stated numbers; end-packet propagation or retention dynamics will require their own convergence checks.

The result contains a positive example of violation of the witness bound, its finite statistics, and the area of desensitization. These three parts answer different

questions: is the effect possible in the model, is the selected number of events sufficient, and what characteristics of the device erase it. Their joint presentation makes the computational example complete, keeping open the question of the implementation of the corresponding conditions.

When no difference becomes the answer

In the comparison performed, a region was found where the unitary Newtonian coupling and a specific feedback measurement channel give incompatible correlations for general geometry, preparation and registration. This is the result about the selected dynamics. It does not automatically apply to any description that calls a field classical, and does not establish the attainability of assumed durations and background levels.

On the other side of the line S = 1, this witness no longer gives a positive result, even if its average is determined infinitely accurately. For this tool, this is a meaningful boundary. Complete indistinguishability would be a stronger statement: it would require the coincidence of all available distributions after allowing for allowed parameters. Distinguishing between these two cases helps determine the next step—improving the readout, measuring diffusion, or changing the geometry.

Fundamental inference gains precision when the input state, dynamics, detector outcomes, and class of excluded alternatives can be named. The next part of the book applies the same logic to spatial noise and managing temporal correlations. The point of the extension is that the new measurements check the general physical parameters and are not replaced by the independent fitting of each series.

The gravitational experiment becomes a test of the basis of the theory when not only the expected signal is known, but also the limits of its interpretation. Strength, phase, coherence, noise, and clock readings must make one consistent prediction. Then even a small measurable effect can significantly change the set of acceptable physical explanations.

Part IV Verifiable Research Program

17 Universal spatial noise hypothesis

The universal law accepts a numerical commitment: parameters found in one series must predict the other. In this chapter, the mass model is transformed into the joint likelihood of two objects. A complete example of initial readings is discussed in chapter 19, and checking the error rate is in chapter 21.

What exactly is suggested to be checked?

The working hypothesis is as follows: after quantitatively taking into account the available interactions with the environment, there is an additional component of the loss of spatial coherence, the parameters of which are common to various material objects. In its simplest form, it is associated with the mass distribution and is specified by the intensity and spatial scale of correlations. The word “universal” means the same coupling law, and not the same decay rate for a molecule, a nanoparticle, and a mechanical resonator. Their masses, shapes and movements are different, so the observed effects must also be different.

Historically, continuous spontaneous localization has already been formulated as a stochastic change in quantum dynamics. The work of Ghirardi, Pearl and Rimini 1990 relates to the foundations of this program [21]. The direction proposed here does not take credit for such an idea. Its possible contribution should be sought in the method of joint verification, the selection of independent observations, and the demonstrable robustness of the inference to environmental models. The scientific novelty of a particular protocol must be established by separate comparison with the literature.

One isolated setting allows too much freedom of explanation. An unaccounted electric field, residual gas or temperature error may appear as an additional parameter. When moving to another installation, such circumstances usually require a new description. The universal hypothesis, on the contrary, makes a commitment: the fundamental parameters found cannot be arbitrarily reconfigured for each device. It is allowed to change the measured properties of the object and known equipment parameters; the general law remains the same.

One pair of parameters for different bodies

A convenient initial parameterization uses intensity λ and length r_C. At this stage they are the coordinates of the model being tested. Their existence is not supposed to be proven. For each experiment, its own prediction is calculated, and it includes the mass distribution, trajectories of state branches, observation time and recording method. The joint analysis should find one region of acceptable values of λ and r_C consistent with all selected observations.

This requirement is stronger than the phrase “there is a little noise left in all experiments.” Residues can arise for various reasons and have no common structure. The generality is checked quantitatively. If one series requires an increase in

intensity with a constant scale, and another excludes such an increase with reliably taken into account errors, a conflict appears. It cannot be hidden by averaging incompatible estimates. First, possible errors of a specific experiment are examined, then the universal model itself is revised.

A pre-selected range of applicability is also needed. A nonrelativistic model of a rigid body is not required to describe the birth of particles, strong gravitational fields, or the destruction of the object itself. Such restrictions are acceptable if written before comparison with the data. They become a problem when they are added after every failed prediction. A research program must distinguish between honest refinement of an approximation and an endless expansion of the conditions under which a hypothesis is supposed to operate.

Geometry instead of mass alone

The reasoning “a heavier object should lose coherence faster” is only useful as a first approximation. When relating noise to mass density, the entire spatial structure of the body is significant. Its different sections may be located within the same correlation area or far beyond its borders. Therefore, a compact object and an elongated structure of the same mass can give different predictions. It is this difference that provides an additional check that is missing from a simple plot against mass.

For a rigid body, we introduce the density $\mu(\mathbf{x})$ and its Fourier transform $\tilde{\mu}(\mathbf{k}) = \int d^3x \mu(\mathbf{x}) e^{-i\mathbf{k}\cdot\mathbf{x}}$. The following expression specifies a specific Gaussian localization model when two identical distributions are shifted by the vector $\mathbf{d}$. It is used as a working definition for further calculations. All factors are written out so that for a point mass distribution the spatial law of chapter 10 is obtained. The formula has the dimension of reciprocal time.

If the dimensions of the body are small compared to r_C, in the significant region of the integral it is possible to replace $\tilde{\mu}$ with the total mass. The usual quadratic amplification appears. When the size increases, such a replacement ceases to be legal. It is then necessary to take into account the actual shape, heterogeneity, orientation and possible internal movements. A form error can simulate a violation of universality. Therefore, comparisons between different bodies must use measured geometric data, and not just the nameplate mass.

$$\Gamma_\mu(\mathbf{d}) = \frac{\lambda r_C^3}{\pi^{3/2} m_0^2} \int d^3k e^{-r_C^2 k^2} |\tilde{\mu}(\mathbf{k})|^2 [1 - \cos(\mathbf{k}\cdot\mathbf{d})].$$

(17.1) Operating localization rate for a Gaussian spatial kernel. The reference mass m_0 fixes the normalization of λ. A rigid body, the same shape in both branches, and the applicability of effective nonrelativistic dynamics are assumed.

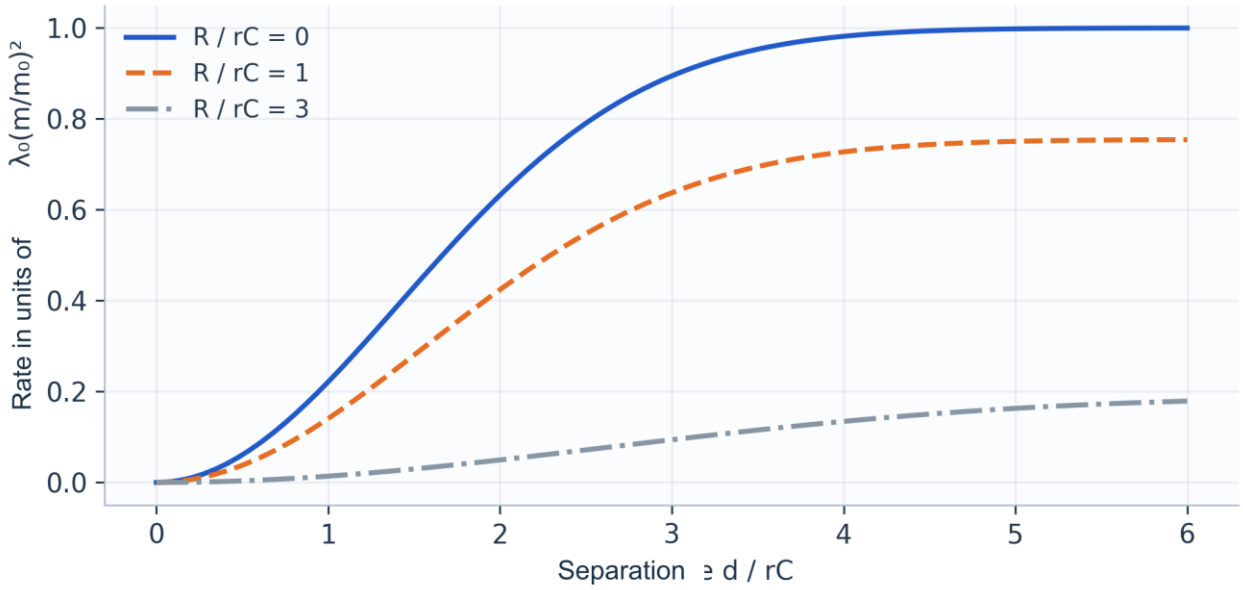


Figure 46. The influence of the finite size of a homogeneous sphere at the same total mass. The radius R changes the mass form factor, so the compact law cannot be transferred to any bodies.

What correlations are physically permissible?

Drawing a correlation function freely is not enough. Let some field act at several points. The variance of any weighted sum of its values must be non-negative. This requirement simultaneously limits all elements of the correlation matrix. Checking only adjacent pairs does not guarantee the consistency of the entire system. In a computational model, such a violation may remain invisible until a sufficiently large number of spatial points are considered.

For a homogeneous stationary Gaussian field, the spectral method of specifying is convenient: the spatial correlation is obtained as a transformation of the non-negative spectral density. The Gaussian kernel satisfies this condition. A more complex form, for example several correlation scales, can be constructed as a sum of admissible components with non-negative weights. However, the introduction of each additional scale increases the freedom of adjustment. Such a model should benefit from new observations, and not only better describe the points used in tuning.

Even the admissibility of correlations solves only part of the problem. For the proposed quantum evolution, it is necessary to verify trace conservation and positivity of the density matrix, including its expansion by an auxiliary system. The correct ensemble equation does not yet specify the physical mechanism for the occurrence of a separate measurement result. Also, relativistic consistency and the law of conservation of energy of the complete system do not automatically follow from it. These requirements should be kept separate so that the success of one mathematical test does not replace the others.

$$\sum_{i,j} a_i^{*} C(\mathbf{r}_i - \mathbf{r}_j) a_j \geq 0$$

for any $\{a_i, \mathbf{r}_i\}$.

(17.2) Condition for positive semi-definiteness of spatial correlation. It eliminates the negative variance of any linear combination of field values.

Prediction for a new object

The most meaningful check is built with a series set aside in advance. For example, the parameters are estimated from two mass distributions and several trajectories, and then the visibility for a third shape is calculated. Before opening a new series, the prediction range, calibration parameters and comparison rule are fixed. If, after receiving the result, you are allowed to freely change the intensity or spatial kernel, the test will lose its meaning: the third body will turn into another material for tuning.

The choice of such a body must take into account the distinguishability of the models. Two almost identical samples can give almost proportional responses for all mechanisms considered. Their agreement will be a weak test. It is more useful to find geometries for which the mass localization model and admissible environmental models predict different changes. For example, changing shape while maintaining mass can have different effects on the spatial form factor and optical scattering. Which difference will be useful should be shown by the calculation of the specific material and installation.

The comparison of the possibilities of various experiences has well-known antecedents. Nimmrichter and Hornberger proposed to evaluate macroscopicity through the ability of experiment to limit certain modifications of quantum mechanics [46]. For this program, a practical guideline follows from this: the scale of the body itself is not a measure of the scientific strength of the experience. What is more important is which parameter range it tests and how independently it does so from previous observations.

Shared parameters and independent environmental conditions

For computational verification, two compact objects with the mass ratio 1 to 1.4 were selected. Compactness here means the smallness of each size relative to all tested correlation lengths. This condition allows the use of a point limit of the mass kernel. Absolute mass is not assigned: the example explores shape identification and parameter transfer between two responses. Its amplitude can be converted into a constraint on the fundamental intensity only after setting the real mass and checking the form factor.

Separations are measured in units of reference length ℓ = 100 nm. The first object corresponds to a duration T_1 = 1 s, the second - T_2 = 0.8 s. Each has its own constant and quadratic components of normal coherence loss. Between the objects, the amplitude A, length r_C and reading contrast c remain common. This division of

parameters expresses a specific assumption: the detector calibration is common, and the local conditions of the two series may differ. It does not follow from the word “universality” and must be checked for each device separately.

The amplitude A is related to the initial intensity through $A = \lambda(m_{ref}/m_0)^2$, where m_{ref} is the mass of the first object. The multiplier for the second object is $1.4^2 = 1.96$. Therefore, the same A and r_C do not mean the same curves. In the second response, the mass fraction is stronger, the duration is slightly shorter, and the background is different. It is the agreed difference between the curves, and not their external coincidence, that serves as the subject of joint verification.

The likelihood is formed by the product of the binomial probabilities of all settings and an individual calibration series. General quantities enter into all factors once; local coefficients act only on the data of their object. If instead one independently fits A for each curve and then compares the two rounded numbers, much of the joint calibration information will be lost. In particular, the overall contrast shift creates a correlated movement of both estimates.

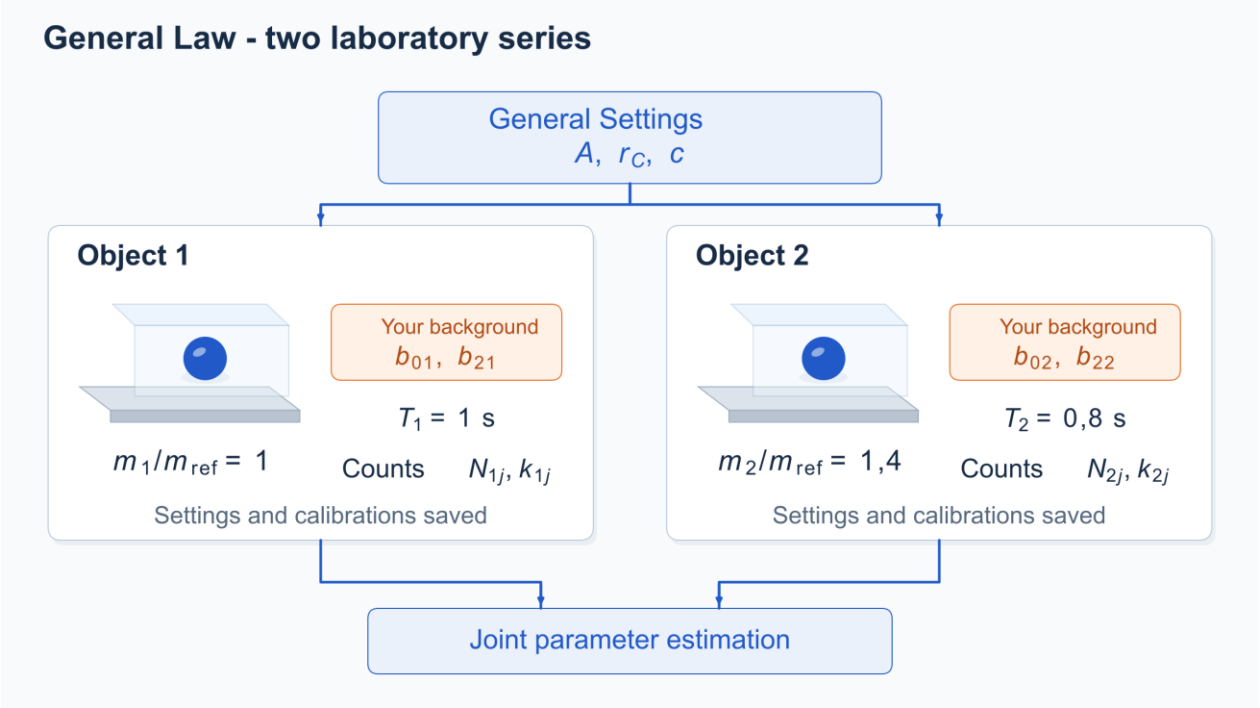


Figure 47. The general law is verified by joint processing of two synthetic series for compact objects with the mass ratio 1:1.4. The common ones are A, r_C and reading contrast c; the normal background coefficients b_{0g} and b_{2g} belong to their object. The durations are T_1=1 s and T_2=0.8 s. The mass multiplier of the second response is 1.4^2=1.96, so universality does not mean matching rates or decay curves. The generality of c is a separate calibration assumption for this example. The absolute masses and the achieved experimental sensitivity are not specified; deferred series uses the same objects in new modes.

In the fixed sample set, maximum likelihood is achieved at A = 0.15334 s^{-1} and r_C = 1.25ℓ. The true generator values were 0.12 s^{-1} and ℓ. The discrepancy is normal for a finite sample: the task of the analysis is to estimate the distribution of the error, and not to necessarily match the rounded estimate with the entered number. The

profile area and actual coverage are presented below; this data is completely synthetic.

The joint hypothesis is further compared to a model in which objects have separate A_1 and A_2 but the same spatial scale. The improvement statistic for amplitude separation is 0.0558. In 200 independent calibration simulations of the general model, the tail fraction is equal to 0.811. In this training set there is no reason to reject the general parameter. This goodness-of-fit tests only the specified models and the accuracy of a given sample; it does not prove universality in all material systems.

In the control set, the amplitudes are deliberately made different: $A_1 = 0.12\ \mathrm{s^{-1}}$ and $A_2 = 0.24\ \mathrm{s^{-1}}$. The resulting statistic is 6.268 and the corresponding calibration tail is 0.0100. The calculation shows how a given procedure recognizes a violation of an obligation. These values cannot be translated into an accurate estimate of the extremely small p: with 200 calibration repetitions, the tail resolution is limited to approximately one-two-hundredth.

The delayed series changes the distances and durations for the same two objects. No new background coefficients are introduced into it. Therefore, the transfer of the geometric dependence and accumulation time is checked, and not the work on a third unknown device. A true prediction for a new body shape would require its measured density and a separate calibration of the local environment. This distinction allows a small example to be used in its entirety without attributing to it more experiment than what is accomplished.

$$\mathcal{L} = \mathcal{L}_{\mathrm{cal}}(c) \prod_{g=1}^{2} \prod_{j} \binom{N_{gj}}{k_{gj}} p_{gj}^{\,k_{gj}} (1-p_{gj})^{N_{gj}-k_{gj}}$$

(17.3) Overall likelihood. The subscript g denotes the object, j the setting. Parameters A, r_C and c are general; the coefficients b_{0g} and b_{2g} are local.

Energy and boundaries of description

Spatial localization is usually associated with a change in momentum distribution. In chapter 11 this connection is discussed through heating. Its methodological consequence is important here: the parameters selected from interference should also be used to calculate energy observations. If an unrelated intensity is introduced for each group of data, a single physical hypothesis disappears. Instead, we get several separate descriptions, which are mistakenly given a common name.

Dissipative variants of CSL have already been developed; in particular, Smirne and Bassi proposed an extension that eliminates the unbounded growth of the mean energy in the corresponding [54] model. Therefore, finding a heating problem does not mean that there is only one way to solve it. But choosing the dissipative option changes the set of parameters and predictions. It requires a new calculation, and not a verbal clause added to the old localization formula.

In this part of the book, the Gaussian model is treated as a limited effective hypothesis. It allows us to formulate a joint experimental question, but does not replace the fundamental field theory. The transition to such a theory would require

further determination of energy transfer, causal structure, and relationships with other types of matter. The absence of these elements should be designated as open work; it would be premature to fill the gap with the names of new entities.

Two hypotheses with different physical commitments

The spatial hypothesis of this chapter and the temporal hypothesis of the next chapter are considered as two independent problems. In the first, the law of connection with the mass distribution is fixed and the spatial kernel is checked. In the second, the phase interaction operator of the two-level sensor is fixed and the time correlator is checked. The symbols λ, r_C, σ and τ_c therefore do not denote the four already combined parameters of one fundamental theory.

For a spatial experiment, the observed probability is obtained after propagating the selected mass state, taking into account the normal environment, and applying the registration model. In the compact stationary limit, this path gives an exponential with $A[1 - \exp(-d^2/(4r_C^2))]$. For a time sensor, the probability is obtained from the accumulated relative phase under the influence of $H(t) = \hbar\delta\omega(t)\sigma_z/2$ and the given control. The operator σ_z denotes the difference between two internal states; by itself it tells nothing about the distance between mass branches.

The two tasks can only be combined by adding a physical transfer model. For example, a random spatial field can interact with the difference between two mass densities, and its value along moving branches creates δω(t). Then the phase correlator depends simultaneously on the spatial spectrum, motion and mass distribution. Even with a factorized spectrum, the observed temporal amplitude depends on the object and its trajectory. The simple equality λ = σ or the transfer of the spin correlation time to the mass model has no basis.

The two existing numerical series retain independent parameters: the binomial spatial analysis tests the general mass law, and the controlled two-level sensor is a stationary time correlator. In the last sections of this chapter, a limited general transfer model is constructed that makes the mathematical connection of these problems explicit. It does not transform separate calculations into a single experiment and does not establish the fundamental nature of the field.

When universality fails a test

Rejection of a selected version of a hypothesis becomes justified when there is no general parameter domain capable of describing a predetermined set of tests within independently specified uncertainties. This statement necessarily refers to a specific kernel, the law of connection with mass and the range of applicability. It does not exclude any conceivable modification of quantum mechanics. At the same time, such a result cannot be discounted by talking about the infinite number of possible other models: the tested version indeed failed.

If all observations are consistent with the absence of an additional effect, the conclusion takes a different form. An upper limit on the intensity in the studied range

of spatial scales is obtained. A family that allows arbitrarily low intensity cannot be completely excluded in this way. However, boundaries may prevent a particular model from performing the task for which it was introduced. To do this, it is necessary to separately calculate what minimum intensity is required for its own mechanism of macroscopic localization.

The positive result also has successive levels. First, an unexplained general dependence is established, then resistance to expansion of environmental models, then predictive transfer between objects. Only after this there is a basis for discussing the fundamental origin. No single step replaces the next one. This sequence makes the program rigorous while maintaining its main ambition: to test whether different material systems have one additional regularity.

General law of spatial and temporal correlations

Let us construct a limited general model in which the relationship between two descriptions can be calculated. Let Z(x,t) be a real classical Gaussian field with zero mean, stationary in the laboratory system. It interacts with the mass density operator $\hat{\mu}(x)$ through the random Hamiltonian given below. The parameters $\lambda \geq 0$, $r_C > 0$ and $\tau_c > 0$ determine the intensity, spatial length and correlation time. The reference mass m_0 is fixed. Here λ has dimension s^{-1}, Z has dimension s^{-1}, and the field covariance has dimension s^{-2}.

The product of a Gaussian spatial kernel and an exponential time correlator is admissible: its space-time spectrum is non-negative. For each field realization, the self-adjoint Hamiltonian generates a unitary propagator U_Z. Therefore, the averaged mapping $\mathcal{E}_T(\rho) = E[U_Z \rho U_Z \dagger]$ preserves the trace and is completely positive, including in the presence of an auxiliary system. This is a random unitary model of an ordinary field. It does not derive an objective choice of one branch and is not a new theory of collapse; the difference between ensemble attenuation and individual localization is preserved [28].

For the phase calculation, we define two narrow branches with densities $\mu_+(x,t)$ and $\mu_-(x,t)$. Their movement and shape are considered given; noise transitions between branches and changes in trajectories under the influence of the field are negligible here. The difference $\Delta\mu_t = \mu_+ - \mu_-$ turns the field into a relative frequency $\delta\omega(t)$. The control is given by a real function y(t), and the accumulated phase is equal to $\Phi_y = \int_0^T y(t)\delta\omega(t)dt$. If the exchange of branches is already included in the density, you cannot additionally change the sign of y: this would be double counting of one effect.

Gaussianity gives the exact equality in this phase approximation $\nu_y = E[\exp(-i\Phi_y)] = \exp(-\chi_y)$, where χ_y is half the phase dispersion. The standard method of controlled Gaussian dephasing is outlined in the work of Cywiński et al. [58]. Here its input correlator is calculated from the mass distributions. The double convolution J(t,s) takes into account both geometries at different times; One instantaneous distance d(t) for a colored field is usually not enough.

For point branches, J contains four spatial correlations: two between identical branches at moments t and s and two between different branches, taken with a minus sign. For an extended body, the same convolution with full density is used. Therefore, motion, rotation and internal mass redistribution change the time response even with constant λ, r_C and τ_c. A simple substitution of the total mass is only permissible in the verified compact limit.

The internal spin with the same mass densities in the two states has $\Delta\mu_t = 0$ and does not feel this connection. Spin reading requires a conditional spatial movement or a physical difference in mass distributions. The ideal echo further assumes a real inversion of the interaction difference; turning an isolated spin by itself does not provide it. The final time of movement is taken into account by given trajectories, and not by an instantaneous change of sign.

$$\widehat{H}_Z(t) = \frac{\hbar}{m_0}\int d^3x\,\widehat{\mu}(\mathbf{x})Z(\mathbf{x},t)$$

$$G(\mathbf{r}) = e^{-r^2/(4r_C^2)}$$

$$\mathbb{E}[Z(\mathbf{x},t)Z(\mathbf{x}',s)] = \frac{\lambda}{2\tau_c}e^{-|t-s|/\tau_c}G(\mathbf{x}-\mathbf{x}').$$

(17.4) Complete definition of the field and its relationship with mass. The spatial kernel is dimensionless and normalized by the condition G(0) = 1; its volume integral is not equal to unity.

$$\delta\omega(t) = \frac{1}{m_0}\int d^3x\,\Delta\mu_t(\mathbf{x})Z(\mathbf{x},t)$$

$$J(t,s) = \int d^3x\,d^3x'\,\Delta\mu_t(\mathbf{x})\Delta\mu_s(\mathbf{x}')G(\mathbf{x}-\mathbf{x}')$$

$$K(t,s) = \mathbb{E}[\delta\omega(t)\delta\omega(s)] = \frac{\lambda}{2\tau_c m_0^2}e^{-|t-s|/\tau_c}J(t,s).$$

(17.5) Spatial convolution has the dimension of mass squared. When the branches move, the phase correlator K(t,s) in the general case is not a function of the time difference alone.

$$\chi_y(T) = \frac{\lambda}{4\tau_c m_0^2}\int_0^T dt\int_0^T ds\,y(t)\,y(s)e^{-|t-s|/\tau_c}J(t,s).$$

(17.6) General two-time visibility functional. The sign of individual terms may be negative, but the total χ_y is non-negative as half of the variance.

$$\frac{J(t,s)}{m^2} = \sum_{a,b\in\{+,-\}} s_a s_b G(\mathbf{r}_a(t)-\mathbf{r}_b(s))$$

$$s_+ = 1,\ s_- = -1.$$

(17.7) Four correlations for point branches of the same mass m. The formula allows you to directly substitute given trajectories.

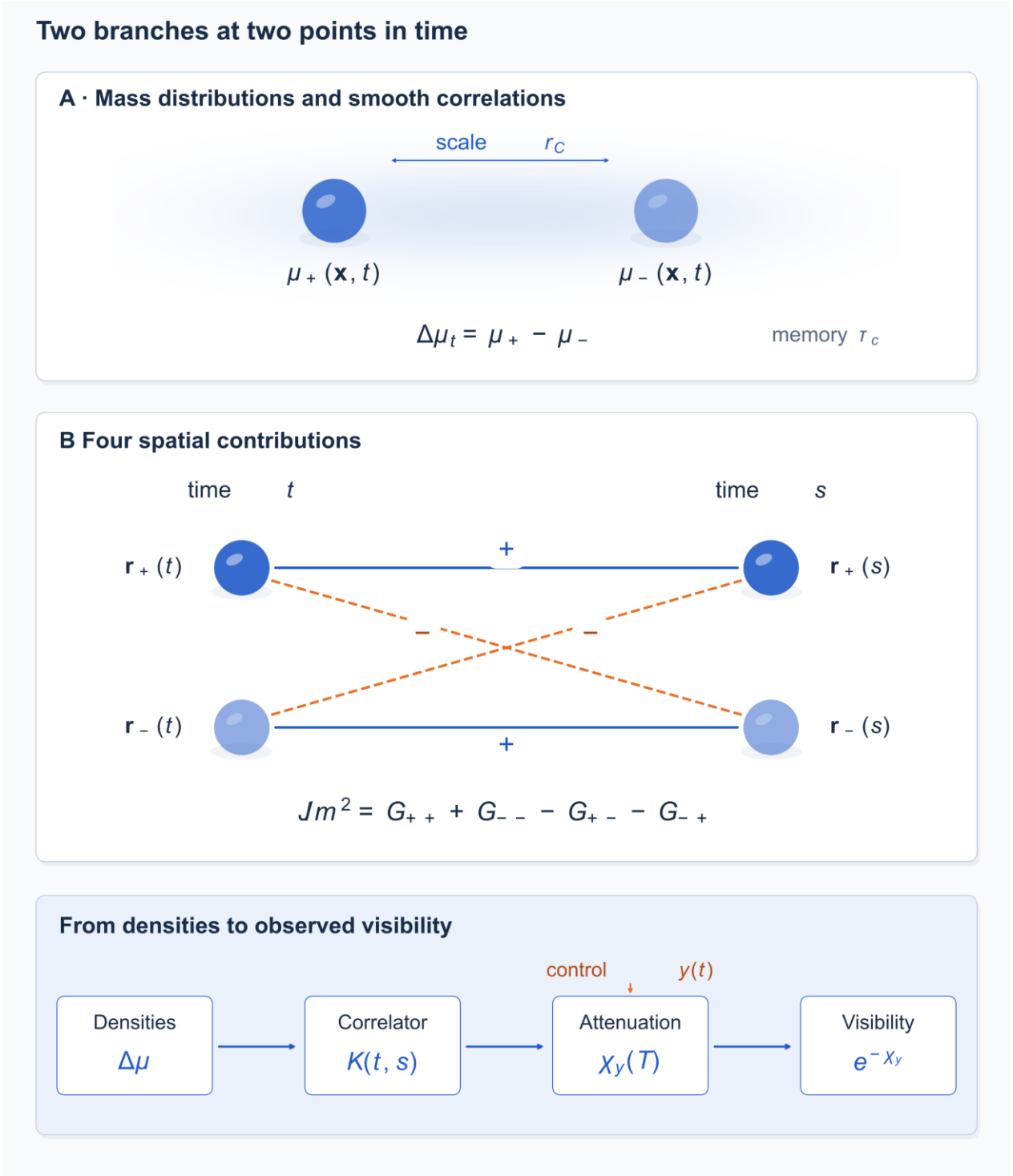


Figure 48. In the constrained random unitary model, the Gaussian field is related to the difference in the mass densities of the two branches. The top panel denotes smooth spatial and temporal correlation scales rather than rigid field cells. The lower geometry reveals four terms J(t,s): two correlations of branches of the same name with a plus sign and two cross ones with a minus sign. The four markers show two branches at different times, and the lines represent correlation terms, not forces or signal transfer. Geometry and control determine K(t,s), χ_y and visibility. The model describes ensemble dephasing and does not prove objective branch selection. If the mass densities of internal states coincide, Δμ=0. A spin turn by itself does not invert mass coupling; the exchange of branches cannot be simultaneously taken into account in the densities and the repeated change of sign of y.

Normalization of Ramsey and echo in one transfer model

Let us consider two stationary point branches of mass m at a distance d. Then J = $2m^2[1 - G(d)]$, and the relative frequency has an exponential correlator $K(t,s) = \sigma_g^2 \exp(-|t-s|/\tau_c)$. Its amplitude is no longer free: it is determined by geometry and mass. If $\eta_g = m/m_{ref}$ and $A = \lambda(m_{ref}/m_0)^2$, then $\sigma_g^2 = \Gamma_g/\tau_c$, where $\Gamma_g = A\eta_g^2[1 - \exp(-d^2/(4r_C^2))]$. Different objects receive different σ_g with the same field.

Normalization is checked by a white-noise time limit. The function $\exp(-|u|/\tau_c)/(2\tau_c)$ has a unit integral along the entire time axis and tends to δ(u). Therefore χ_y tends to $\lambda\int_0^T y^2(t)J(t,t)dt/(2m_0^2)$. For fixed branches and $y^2 = 1$, the result is $\Gamma_g T$. For identical rigid bodies shifted by d, J = 2[I(0) − I(d)], where I is the convolution of two densities with G. The Fourier transform G gives exactly the coefficient $\lambda r_C^3/(\pi^{3/2}m_0^2)$ of the spatial formula of this chapter: there is no additional factor of two.

With finite memory, Ramsey corresponds to y = 1, and the ideal Hahn echo corresponds to a sign change in T/2. Substitution into the two-time integral gives the closed-form expressions below. For $T \ll \tau_c$, the initial indicators are equal to $\Gamma_g T^2/(2\tau_c)$ and $\Gamma_g T^3/(12\tau_c^2)$, respectively. For fixed T and pulse sequence, when $\tau_c \to 0$, both tend to $\Gamma_g T$: an ideal echo does not eliminate this white component.

To proceed to registration events, it is enough to specify the analysis phase φ, the calibrated contrast c and the standard background indicator χ_{env}, statistically independent of Z. For a symmetric two-output readout, the binomial probability p_y is obtained, written below. General field parameters are included in it through the calculated χ_y; geometry and control must be known for each platform. Thus, the transfer tests a specific distribution of events, rather than the superficial similarity of decay times. The binomial law requires independent implementations in iterations; with residual field correlation between cycles, a joint temporal likelihood is required.

The numerical illustration uses A = 0.12 s^{-1}, r_C = 100 nm, τ_c = 0.8 s and T = 1 s for both masses. The table shows only the contribution of a given field: c = 1 and $\chi_{env} = 0$. The quadrature of the complete two-time integral and the closed formulas coincide with an absolute error of less than 3×10^{-17}. When $\tau_c = 8\times10^{-5}$ c the ratios $\chi_R/(\Gamma_g T)$ and $\chi_E/(\Gamma_g T)$ are equal to 0.99992 and 0.99976. The calculation is reproduced in the file calculations/spacetime_v02.py; its results are stored side by side in JSON.

An additional check of two equal point parts of a rigid body located at $\pm r_C$, with a common shift $d = r_C$, gives the geometric factor 0.0734893 instead of the compact 0.2211992. Direct convolution and Fourier integral are consistent. For the triangular separation with the maximum $2r_C$, the transition to the integral of the instantaneous white rate is also tested. These calculations test the selected transfer model and its limits; There are no experimental data here.

Given A and τ_c, even an extremely large separation allows only $\sigma_1 \le 0.3873\ s^{-1}$ and $\sigma_2 \le 0.5422\ s^{-1}$. Therefore, the independent example of the next chapter with $\sigma = 1.2\ s^{-1}$ is not the same field with the same numerical parameters. The general law allows a re-calculation of a consistent example, but does not retroactively merge previous series. Even its successful experimental verification would require a separate distinction between the ordinary field and the proposed fundamental mechanism.

$$\Gamma_g(d) = A\eta_g^2\left[1 - e^{-d^2/(4r_C^2)}\right]$$

$$\sigma_g^2 = \frac{\Gamma_g(d)}{\tau_c}$$

$$A = \lambda\left(\frac{m_{\text{ref}}}{m_0}\right)^2.$$

(17.8) Mapping spatial parameters to temporal phase noise amplitude for stationary compact branches. At d = 0 both quantities are equal to zero.

$$G(\mathbf{r}) = \frac{r_C^3}{\pi^{3/2}}\int d^3k\, e^{-r_C^2k^2}e^{i\mathbf{k}\cdot\mathbf{r}}$$

$$\chi_{y,\tau_c\to 0} = \frac{\lambda}{2m_0^2}\int_0^T dt\, y^2(t)J(t,t).$$

(17.9) Spatial and temporal normalization. For hard shift, the convolution transformation reproduces the previous formula Γ_μ(d), including its coefficient.

$$\chi_R(T) = \Gamma_g\left[T - \tau_c\left(1 - e^{-T/\tau_c}\right)\right]$$

$$\chi_E(T) = \Gamma_g\left[T - 3\tau_c + 4\tau_c e^{-T/(2\tau_c)} - \tau_c e^{-T/\tau_c}\right].$$

(17.10) Accurate phase responses of stationary branches under ideal control. They coincide with the time formulas of chapter 18 after a physically based substitution $\sigma_g^2 = \Gamma_g/\tau_c$.

$$p_y = \frac{1 + ce^{-\chi_{\text{env}}-\chi_y}\cos\varphi}{2}$$

$$0 \le c \le 1,\ \chi_{\text{env}} \ge 0.$$

(17.11) Probability of one registered exit. For N independent repetitions, the number of such outcomes has a binomial distribution; additional detector errors are entered separately, as in chapter 6.

One space-time law for two masses: synthetic calculation at T = 1 s

m/m_{ref}	**d**/r_C	**σ, s⁻¹**	ν_R	ν_E	ν_{white}
1.0	0.6	0.113624	0.995577	0.999137	0.989725
1.0	1.0	0.182153	0.988672	0.997783	0.973805

m/m_{ref}	**d**/r_C	**σ, s⁻¹**	ν_R	ν_E	ν_{white}
1.0	2.0	0.307925	0.967967	0.993676	0.926951
1.0	4.0	0.383735	0.950696	0.990196	0.888872
1.4	0.6	0.159073	0.991349	0.998308	0.979960
1.4	1.0	0.255015	0.977918	0.995658	0.949304
1.4	2.0	0.431096	0.938182	0.987643	0.861849
1.4	4.0	0.537229	0.905652	0.980875	0.793825

$\nu_R = \exp(-\chi_R)$, $\nu_E = \exp(-\chi_E)$; $\nu_{\mathrm{white}} = \exp(-\Gamma_g \mathrm{T})$ — limit $\tau_c \to 0$ for fixed A and r_C. Mass relations are dimensionless.

General parameters acquire testable meaning when mass densities, trajectories, and controls translate them into probabilities of observable events. The constructed model shows such a translation and its white-noise limit. The next chapter explores in more detail what temporal memory reveals about the source of dephasing and what ambiguities persist even under control.

18 Memory and controlled decoherence hypothesis

The disappearance of interference can be studied not only by changing mass and distance. There is one more lever: to change the order of interactions in time. If the environment retains its properties for some time, correctly chosen control can partially cancel the accumulated random phase. This capability allows the measurement of noise memory but requires caution in drawing conclusions about the origin of irreversibility.

Memory as a measurable property

The timing hypothesis states that a selected component of phase fluctuations has a reproducible correlation scale and predicts the results of different control sequences. Here it is tested as an independent sensor model. The transfer of parameters to mass spatial localization is not expected: it would require an additional interaction law, discussed at the end of the previous chapter.

The very idea of applying dynamic decoupling to testing alternative quantum theories had already been proposed by Arenz, Hiller, Fraas and Burgart in 2015 [47]. Therefore, the use of impulses is not an application for the discovery of a new method. The subject of our own program is already here: which damping components are actually distinguishable with finite control accuracy and with a preliminarily limited, but fairly wide class of surrounding influences?

There are also non-Markov models of spatial localization. Bassi and Ferialdi investigated such dynamics, including exponential noise correlation, in 2009 year [55]. The following calculation is simpler than these models: it is an exactly solvable problem of random phase action on a two-level system. It is needed to check the measurement logic. It cannot automatically be declared to be a complete stochastic collapse equation or a solution to a single outcome problem.

A model with one memory timescale

Let us consider two branches of the state, between which a random relative phase accumulates. In the chosen approximation, the impact is described by the Hamiltonian $H(t) = \hbar\delta\omega(t)\sigma_z/2$. The value $\delta\omega$ is measured in reciprocal seconds and has a zero average. A stationary Gaussian process with correlation $K(\tau) = \sigma^2 e^{-|\tau|/\tau_c}$ is assumed. The parameter σ sets the characteristic amplitude of frequency fluctuations, and τ_c sets the time during which the connection between them noticeably weakens.

In this chapter, “memory” means precisely the finite duration of correlations. This usage is not equivalent to any definition of non-Markovian evolution accepted in quantum theory. For example, the absence of return of state distinguishability does not yet make the noise white. For the control problem, the specific correlator and how the system accumulates the phase under its influence are essential.

Terminological classification cannot be used instead of calculating observed dynamics.

Let ideal impulses change the sign of the perceived fluctuation; this is described by the function $y(t)$ with values plus or minus one. The normalized visibility is $\nu_y = \exp[-\gamma_w T - \chi_y(T)]$. Here γ_w is a separate non-negative white phase noise rate, the origin of which has not yet been determined. For the Gaussian phase, the average of the exponential is expressed entirely in terms of its dispersion, which gives the double integral below. Pure dephasing is considered; Energy relaxation should be introduced separately if it is significant.

$$\chi_y(T) = \frac{1}{2}\int_0^T dt \int_0^T ds\, y(t)\, y(s) K(t-s).$$

(18.1) Half the variance of the accumulated random phase. Gaussianity ensures the accuracy of this formula for the selected model; for a general non-Gaussian process it is usually insufficient.

Two ways to accumulate phase

In the Ramsey sequence, the sign of the effect does not change. A slow random frequency shift affects the system all the time and creates a large phase spread between repetitions of the experiment. In Hahn echo, a perfect inversion is performed in the middle of the interval. The almost constant part of the shift in the second half compensates for the contribution of the first. If the fluctuation has changed significantly, compensation becomes incomplete. Therefore, comparison of two sequences contains information about the rate of change in noise.

Substituting these two functions $y(t)$ into the integral gives closed expressions. To make them shorter, let's denote them as $x = T/\tau_c$. Both quantities χ are dimensionless: the product $\sigma^2 \tau_c^2$ does not carry units. The formulas can be verified by direct integration and expansion in a short time. This is a useful independent check of the coefficients, since a missing factor of two changes the estimated sensitivity of the entire protocol.

Using control as a frequency filter is a developed area. Alvarez and Suter proposed reconstruction of the color noise spectrum using sequences of inverting pulses [48]. In the workpiece under consideration, this general idea is deliberately reduced to a single correlation time. Simplicity allows one to clearly see both the useful signal and the degeneracy of the parameters. After this check, you can make the spectrum more complex, keeping the known limiting case as a control.

$$\chi_R(T) = \sigma^2 \tau_c^2 (x - 1 + e^{-x})$$

$$\chi_E(T) = \sigma^2 \tau_c^2 \left(x - 3 + 4e^{-x/2} - e^{-x}\right)$$

$$x = T/\tau_c.$$

(18.2) Accurate attenuation rates for Ramsey and ideal Hahn echo with exponential correlator. The R and E subscripts denote two control methods, not different noise models.

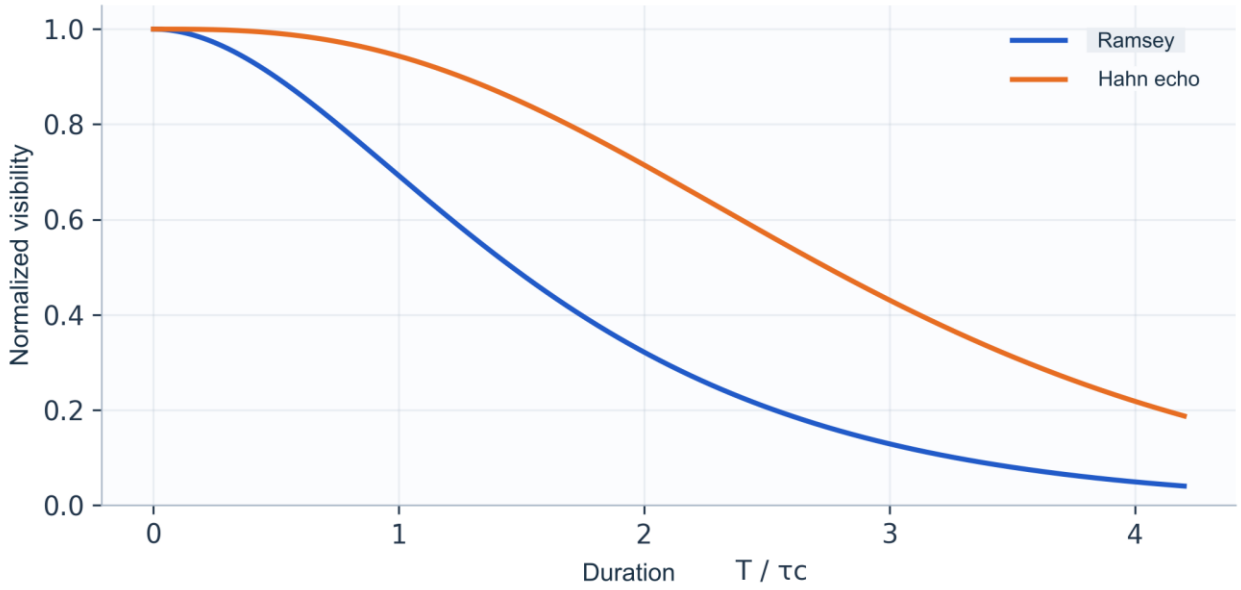


Figure 49. Ornstein-Uhlenbeck Gaussian noise model with σ τc = 1 without additional white contribution. The echo suppresses the influence of slow fluctuations, but does not prove the fundamental origin of the remnant.

What does the visibility ratio show?

From both sequences it is possible to construct a ratio of normalized visibilities. The common white multiplier disappears, and only the expression through the parameters of the correlated component remains. This doesn't mean there is no white noise. It is simply excluded by the selected combination of observations. This distinction between the absence of an effect and insensitivity to it is fundamental for any diagnostic value.

At times much shorter than τ_c, Ramsey's main attenuation is proportional to $\sigma^2 T^2/2$, and echo's is $\sigma^2 T^3/(12\tau_c)$. Therefore, the inversion changes the initial time dependence. For very long times both curves have the same asymptotic slope: $\gamma_w + \sigma^2 \tau_c$. Their ratio tends to be constant. If you measure only this late section, you can establish the overall slope fairly accurately, but still poorly separate its components.

The practical conclusion is that it is necessary to observe the transition region where the experimental time is comparable to the correlation time. If the scale is initially unknown, a survey series with different times is required. The selected parameters should then predict the outcome of another sequence that was not evaluated. Otherwise, a successful description of the two curves may only reflect excessive flexibility in the fit or features of their overall calibration.

$$\ln \frac{\nu_E(T)}{\nu_R(T)} = 2\sigma^2 \tau_c^2 \left(1 - e^{-T/(2\tau_c)}\right)^2.$$

(18.3) Exact exclusion of the total white rate in the idealized model. A consistent normalization of visibility and separately taken into account errors of additional pulses are assumed.

White noise and fundamental ambiguity

Let the correlation $K(\tau) = 2D\delta(\tau)$ act instead of finite memory. Then the double integral turns into $D\int_0^T y(t)^2 dt = DT$. For ideal sign changes, the square y is always equal to one. Neither Ramsey nor echo eliminates such contributions. In the limit of the exponential model, white noise is obtained when τ_c tends to zero and the product $D = \sigma^2\tau_c$ is preserved, and not when the amplitude σ is fixed.

Therefore, an unremovable decay residue in itself does not indicate a fundamental collapse. It can be provided by a fairly quick external process. If two mechanisms produce the same complete statistics of available controlled measurements, new repetitions of the same experiments will not separate them. Discrimination would require either additional physical constraints on the environment or another observable quantity for which the models actually diverge.

Even the apparent plateau of error as the number of pulses increases needs to be verified. It may occur due to control lane limits, accumulation of turning errors, or other channel loss. Reference to the mathematical limit of infinitely fast ideal operations does not justify the derivation for a finite sequence. It is necessary to calculate what each compared model predicts given the actually available form of the control signal.

The control must influence the desired degree of freedom

For a spin qubit, an inverting pulse changes the orientation of the internal state. In a spatial interferometer, a similar operation may require an exchange of trajectories or specially calculated movement of wave packets. These actions are not automatically equivalent. Rotating the spin without changing the mass distribution does not become a test of mass-proportional localization simply because it improves spin coherence. First you need to establish what physical difference exists between the branches of the state being tested.

Real pulses have a finite duration. During a turn, the carrier may change continuously, so the description in one momentary sign becomes an approximation. In addition, the control field is capable of heating an object, changing its trajectory, or introducing its own fluctuations. For each sequence, the overall response and preparation and readout losses should be calibrated. The general normalization of the two types cannot be declared identical only from the symmetry of the ideal scheme.

Experimental noise spectroscopy on a superconducting qubit was demonstrated by Bylander et al [49]. This result confirms the ability to explore the environment through control, but does not automatically transfer the achieved characteristics to a massive spatially separated state. Separating these concerns is useful: processing methods can first be tested on an available sensor, and the sensitivity to the proposed mass mechanism can be calculated for a different, physically appropriate degree of freedom.

Calculation of a rectangular pulse of finite duration

Let's look at control that actually takes time. In the middle of a sequence of duration T, a rectangular pulse is applied around the x axis. It lasts t_p = fT, and its angular velocity is Ω = π(1 + ε)/t_p. Here f is the fraction of time inside the pulse, ε is the relative error of the angle. Before and after it, the system freely evolves along (T − t_p)/2. This definition preserves the same total Ramsey and echo time: the impulse is included in the budget, rather than added to it unnoticed.

During rotation, phase noise continues to operate. The complete Hamiltonian contains both Ωσ_x and [δω(t) + Δ]σ_z. These operators do not commute. Therefore, replacing the influence with a single sign y = ±1 inside the pulse is no longer accurate. The calculation extends the entire Bloch vector, including the transverse component and the temporary change in the longitudinal one. General methods for taking into account arbitrary control and the finite shape of pulses were developed, in particular, by Green and co-authors [67].

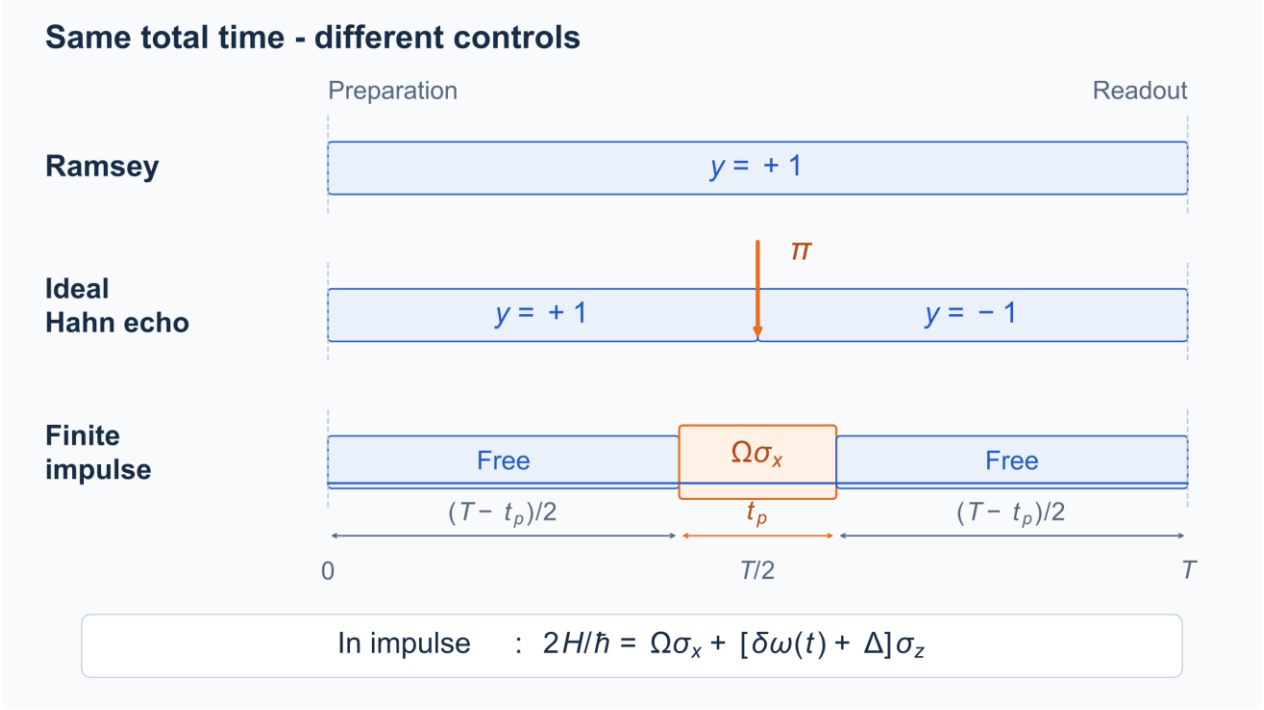


Figure 50. Ramsey, ideal Hahn echo and rectangular pulse echo are compared at one total time T. In the finite-pulse protocol, the pulse occupies t_p within this interval, and both free sections have a duration of (T−t_p)/2. In the pulse, the transverse control Ωσ_x and the phase action [δω(t)+Δ]σ_z act simultaneously; a continuous blue line marks the continuation of noise exposure. Their noncommutative dynamics are calculated from the full Hamiltonian, rather than by arbitrarily smoothing the scalar sign of y. The scheme does not assert the suppression of the white component by an ideal echo and does not transfer the result of the spin test to mass localization without a separate communication model.

For a stationary Ornstein–Uhlenbeck process, the calculation can be performed without randomly enumerating trajectories. The Bloch vector, conditional on the noise value, is expanded in terms of orthonormal Hermite polynomials. The OU operator is diagonal along n: each mode decays at a rate of n/τ_c. Multiplication by noise relates neighboring modes with coefficients σ√n and σ√(n + 1). At each section

of constant control, a finite linear system is obtained; its solution is found by the matrix exponential.

Used σ = 1.2 s⁻¹, τ_c = 0.8 s and zero true white rate. The experiment times are 0.12; 0.20; 0.35; 0.60; 1.00; 1.60; 2.40 and 3.20 s. Initial state - +x; registration contrast c = 0.96. The calculation with 36 Hermite modes is compared with 24 modes: the maximum difference in the Bloch components is less than $3\cdot10^{-15}$. The instantaneous limit coincided with the analytical formulas of Ramsey and Hahn echo up to $2\cdot10^{-15}$. These tests validate the solution of the selected model rather than the description of a specific experimental sensor.

The resulting average probabilities are then deliberately processed by the ideal instant echo formula. σ, τ_c and non-negative γ_w were selected; the original readout contrast was assumed to be known. Random counting noise was not added at this step: it is necessary to isolate the systematic bias created by the incorrect description of the pulse. The residual after fitting therefore measures the misfit of the models and is not a p-value.

The table shows the gradual appearance of false white rate even at an error-free angle π. At f = 0.01 the displacements are small, but at f = 0.25 the reconstructed γ_w is already close to 0.00762 s⁻¹, although its true value is zero. Increasing the number of repetitions will not eliminate this effect: it will only more accurately reveal the difference between the finite pulse and the ideal analysis. The allowed duration depends on the required output accuracy. For a given set of times, for f ≤ 0.03, the error in the predicted probability after a perfect fit is less than $3\cdot10^{-5}$; it is impossible to transfer this numerical limit to another σ, τ_c or pulse shape.

$$H(t)=\frac{\hbar}{2}[\Omega(t)\sigma_x+(\delta\omega(t)+\Delta(t))\sigma_z]$$

(18.4) During a square pulse, Ω is constant; outside the pulse it is zero. For calculations without detuning Δ = 0. In cases with angle error, Δ = 0.15 s⁻¹ is additionally considered only within the pulse.

$$\dot{\mathbf{r}}_n=-\frac{n}{\tau_c}\mathbf{r}_n+(\Omega L_x+\Delta L_z)\mathbf{r}_n+\sigma L_z\left(\sqrt{n}\,\mathbf{r}_{n-1}+\sqrt{n+1}\,\mathbf{r}_{n+1}\right).$$

(18.5) Equations for Hermite modes of the conditional Bloch vector. L_a performs a cross product with the unit axis vector a. The observed mean vector is r_0; initially r_0 = (1,0,0), the remaining modes are zero.

Perfect fit to finite pulse data

f = t_p/T	Estimate σ, s⁻¹	Estimation τ_c, s	False γ_w, s⁻¹
0.00	1.20000	0.80000	0.000000
0.01	1.19998	0.80002	0.000012
0.03	1.19979	0.80021	0.000111
0.10	1.19767	0.80212	0.001242
0.25	1.18731	0.80826	0.007619

Average synthetic probabilities; ε = 0 and there is no detuning. The value in the first line about $2.4 \cdot 10^{-8}$ s⁻¹ is the numerical remainder of the optimization at true zero.

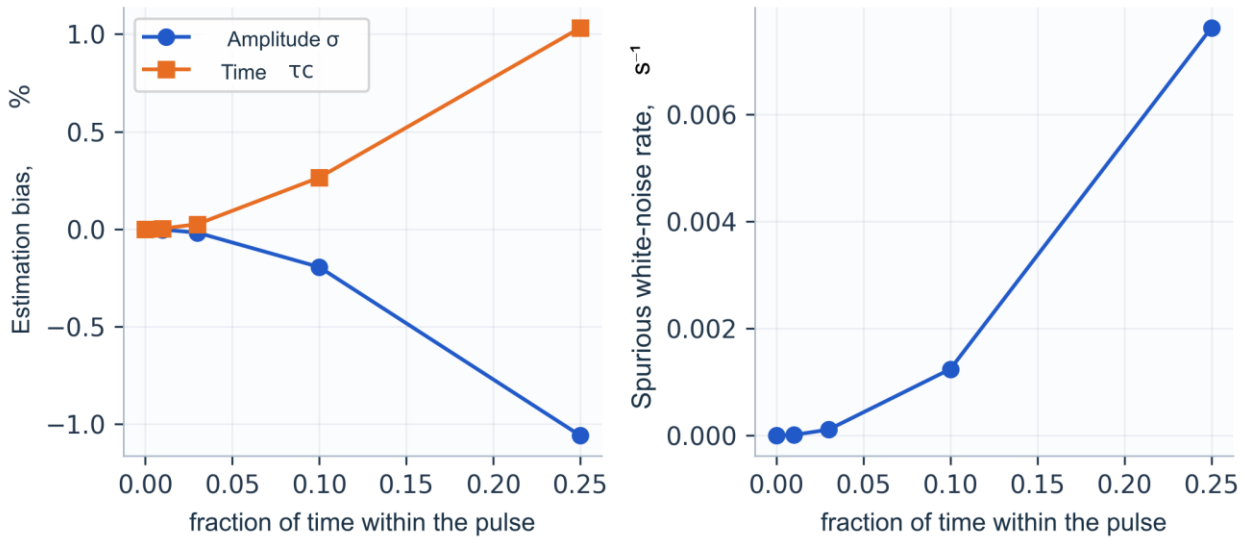


Figure 51. Bias of ideal estimates under finite rectangular impulse. True white rate is zero; the growth of the restored γ_w is caused by a mismatch of control models. Synthetic calculation of the OU sensor with σ = 1.2 s⁻¹ and τ_c = 0.8 s.

How a readout error creates an additional mechanism

The physical action of the impulse and the recording of the result must be modeled separately. In the following control case f = 0.03, angle error ε = 0.03, and during the pulse there is a detuning 0.15 s⁻¹. With a correct overall reading, the ideal fit gives γ_w around 0.000151 s⁻¹. Now an additional contrast reduction has been introduced only for echo by 1.5%. It can be represented by a symmetric registration error that occurs after the control sequence. This reduction is physically permissible, but is not present in the erroneously used general calibration.

The ideal model then returns σ ≈ 1.13873 s⁻¹, τ_c ≈ 0.88009 s, and γ_w ≈ 0.03619 s⁻¹. The correlation time is overestimated by approximately 10%, and the white component appeared entirely from a technical discrepancy. In this example, the residual maximum probability error after fitting reaches 0.00514. With a large

enough sample, the model itself can be rejected based on the quality of its description; with a small sample, its flexibility may be sufficient to produce plausible but biased parameters.

The control procedure follows from the model: separately measure the response after each control sequence, save the number of operations and evaluate the dependence of the reading on the mode. Times missing during selection become an additional check. If the finite pulse is included in the propagation, and the difference between c_R and c_E is described by its own calibration, resampling the average data gives σ = 1.19999964 s⁻¹, τ_c = 0.80000065 s and the white rate 1.63·10⁻⁷ s⁻¹. These results are consistent with the entered values within the numerical error of this calculation. For random outcomes, you will need to repeat the same test with finite statistics.

The example sets the conditional boundary of the method. The presence of a residue with frequent management does not determine its origin. A useful remainder is one that survives independent calibration, correctly calculated pulse action, and prediction of new regimes. This requirement directly links experimental accuracy with the strength of fundamental inference.

Two sensors expand verification

One sensor reports how noise changes over time at its location. Two sensors additionally make it possible to study joint fluctuations. For clarity, let us assume the same local correlators and cross-correlation $K_{AB}(\tau) = c(R)K(\tau)$, where R is the distance between the sensors and $|c(R)| \le 1$. The common and difference phases then experience different attenuation. Their comparison can exclude the independent white component, but only if the independence of this component is explicitly stated.

In the simplest model of coherence between the states 00 and 11, as well as between 01 and 10, they have the following visibilities. Multiqubit spectroscopy of self- and cross-spectra of Gaussian noise has already been developed by Paz-Silva, Norris and Viola [50]. This formula is a special case study that shows the meaning of additional information. It does not cover arbitrary quantum environments or all possible types of interqubit communication.

The working hypothesis of finite memory is rejected in the selected range if a single correlator does not predict the delayed sequences and spatial correlations after accounting for calibration. However, failure of the single-exponential form does not reject all processes with memory. The next comparison would be multi-scale or non-Gaussian noise. For the latter, there are protocols using higher order spectra [51]; simply changing the value of τ_c may not be enough.

$$\nu_{\pm}(T) = \exp\!\left[-2\gamma_w T - 2(1 \pm c(R))\,\chi_y(T)\right].$$

(18.6) The plus sign corresponds to the common phase of two identical sensors, the minus sign corresponds to the difference. Equal control, Gaussianity, and independent white local noise are assumed for each sensor.

From two coherences to joint counts

To make two views observable, preparation and reading are specified. For the general phase, the state $\Phi^+ = (|00\rangle + |11\rangle)/\sqrt{2}$ is prepared; for difference - $\Psi^+ = (|01\rangle + |10\rangle)/\sqrt{2}$. It is assumed that the preparation has already been calibrated, there is no direct interaction between the sensors during accumulation, and the influence of control signals has been taken into account. Under these conditions, pure dephasing leaves the populations unchanged and multiplies the corresponding off-diagonal pair by v_+ or v_-.

In each series, X⊗X and Y⊗Y are measured. For Φ^+ their means are v_+ and $-v_+$; for Ψ^+ - v_- and v_-. Therefore, the combinations $[\langle XX\rangle - \langle YY\rangle]/2$ and $[\langle XX\rangle + \langle YY\rangle]/2$ give the two required coherences. These are specific two-channel correlators: for each repetition a pair of signs is stored, and its product takes the values ±1. The random coincidence of individual local averages is not enough here.

When measuring XX, the probabilities of identical signs ++ and −− are equal to $(1 + v)/4$ each, and of different signs +− and −+ - $(1 - v)/4$. Therefore, the variance of the estimated correlator from N events is equal to $(1 - v^2)/N$. Two independent measurement bases reduce the variance of the corresponding average combination to $(1 - v^2)/(2N)$ if N repetitions are performed in each. The resource distribution between bases must be explicitly indicated: the same particle cannot be considered twice measured in incompatible bases.



Figure 52. The preparation $\Phi^+=(|00\rangle+|11\rangle)/\sqrt{2}$ is sensitive to the overall phase, and $\Psi^+=(|01\rangle+|10\rangle)/\sqrt{2}$ - to the difference. Readings XX and YY are performed in different repetitions: for Φ^+ the means are v_+ and $-v_+$, for Ψ^+ - v_- and v_-. Each entry contains a joint pair of characters; the correlator is assembled from four joint event numbers. In the numerical example of the book, 4000 events are allocated for each of the four series, in total 16 000. Calibrated preparation, accounted management and lack of direct interaction during accumulation are assumed. Difference coherences do not eliminate arbitrary technical noise, and joint correlators cannot be replaced by local means. Volumetric sensors are conceptual images of functional modules.

The numerical example uses the same σ and τ_c, time T = 1 s, local white rate γ_w = 0.03 s^{-1} and cross-correlation c(R) = 0.4. It turns out χ_R = 0.494443, v_+ = 0.235878 and v_- = 0.520310. The logarithmic difference restores c(R) = 0.4. For 4000 events for each of the four preparation × basis sets, the linear estimate of the standard error c is about 0.0251 if χ is known exactly. A total of 16 000 events are required.

This budget does not yet include the uncertainty of χ, imperfect preparation, mutual interference, and the difference between the two detectors. Their inclusion will increase the error and may change the optimal distribution of replicates. The value of the example lies in the completed chain from the state to the four probabilities and the correlation estimate. General multiqubit spectroscopy is significantly broader than this symmetrical classical model [50].

$$v_+ = \frac{\langle XX\rangle_\Phi - \langle YY\rangle_\Phi}{2}$$

$$v_- = \frac{\langle XX\rangle_\Psi + \langle YY\rangle_\Psi}{2}$$

$$c(R) = \frac{\ln v_- - \ln v_+}{4\chi_y}.$$

(18.7) The last equality uses the same control, the known χ_y and the independent equal white component. The logarithm cannot be applied to a negative noise estimate of visibility without a separate statistical model.

The form of control is included in the law of observations along with the noise correlator. The completed example shows both the usefulness of echo and the cost of incorrect calibration. For spatial measurements, the same problem arises: to determine what information is carried by the initial events and what differences in mechanisms remain after the joint assessment of all unknown quantities.

19 The limit of distinguishability and a minimal set of observations

To describe a measured curve well does not mean to determine the mechanism that generated it. Sometimes several physical explanations give equal probabilities for all available outcomes. Sometimes the difference exists but is lost in preparation and registration errors. Before discussing new physics, it is necessary to establish what information experiment actually contains and where the possibilities of a selected set of observations end.

What does the apparatus actually measure?

Visibility, decoherence rate, and noise spectrum are usually not recorded directly. The detector produces events, coordinates, voltage readings or state discrimination results. The transition from them to physical parameters uses a measurement model. If this model is inaccurate, further mathematical rigor will not correct the original error. Therefore, the analysis starts with the probability of the observed data, including preparation, loss, and readout, rather than with a nice curve already constructed.

In the simplest two-output experiment, the true probability depends on visibility and the controlled phase. Let ε_0 denote the probability of writing one instead of zero, and ε_1 the reverse error. The observed probability then has the form below. With N independent repetitions, the number of units follows a binomial distribution. Unknown readout errors can simulate visibility reduction and are therefore assessed from individual calibration data or in conjunction with physical parameters.

Independence of repetitions is also an assumption. Slow drift can connect neighboring events, and the selection of registered particles can change the composition of the observed sample. Therefore, the order of measurements, the conditions of each run, and the reasons for excluding data are stored. A lost object cannot automatically be considered a manifestation of localization: loss of registration and loss of phase coherence represent different observable events and require different parts of the probabilistic model.

$$p_{\mathrm{true}} = \frac{1 + V\cos\phi}{2}$$

$$p_{\mathrm{obs}} = \varepsilon_0 + (1 - \varepsilon_0 - \varepsilon_1)\,p_{\mathrm{true}}.$$

(19.1) Example of a two-source readout model. The formula does not describe any installation; it shows how detector errors change the relationship between quantum visibility and the frequency of detected events.

Fully specified experiment with initial readings

The following example is an artificial computational experiment. Its initial events are derived from a given binomial generator rather than extracted from a laboratory

measurement. A real replication of the published interference series is discussed in chapter 12. These two materials solve different problems: replication connects the presentation with external observations, and simulation allows you to test a procedure against a known truth and determine the frequency of its errors.

Selected two compact objects from chapter 17. For each, eight settings are made d/ℓ = 0; 0.6; 1.0; 1.6; 2.3; 3.2; 4.5; 6.0, where ℓ = 100 nm. The setting accounts for 1600 of registered two-output events. Additionally, there are 5000 calibration events in which the readout contrast is checked against a known state with zero accumulation time. The total volume of the training series is equal to 30 600 events. The null setting does not measure the spatial mechanism, but limits the constant background along with the calibration.

The model assumes symmetric binary readout and independent repeats. The probability of the “plus” outcome is at the maximum of the interference phase. The contrast c is multiplied by the coherence loss exponent. The coefficients b_{0g} and b_{2g} describe a given background family; the index g distinguishes objects. The quadratic term is an effective approximation over a chosen range, not a universal law of the medium. The presence of a more complex acceptable background is checked separately.

In the generator c = 0.95, b_{01} = 0.04 s^{-1}, b_{02} = 0.06 s^{-1}, b_{21} = 0.008 s^{-1} and b_{22} = 0.012 s^{-1}, if the distance squared is expressed in terms of ℓ^2. In the main signal series A = 0.12 s^{-1}, $r_C = \ell$. Zero series have A = 0; weak signal - A = 0.035 s^{-1}. The time of the first series is 1 s, the second - 0.8 s. The mass ratios are fixed to 1 and 1.4. The geometry in this example is known exactly; its additional uncertainty would require separate input calibrations.

The calculations use a = −ln c and the scaled quadratic factors $B_2g = 36b_{2g}$. This change in coordinates improves the numerical conditioning without changing the physical model. a, two b_{0g}, two B_2g and A are estimated together. All rates are non-negative. Optimization ranges are preset: $10^{-5} \le a \le 0.3$; $0 \le b_{0g} \le 0.3$ s^{-1}; $0 \le B_2g \le 1.4$ s^{-1}; $0 \le A \le 0.7$ s^{-1}. These boundaries are part of the teaching procedure and are maintained in all ensembles.

The length is searched on the finite grid r_C/ℓ = 0.50; 0.65; 0.80; 1.00; 1.25; 1.60; 2.00; 2.50. For each value, all other parameters are re-selected, after which the highest likelihood is selected. The grid is fixed before confirming sets are generated. It is not depicted as a continuous search without restrictions: other optima may exist between nodes, and a more dense search would require a new calibration of the procedure. Such a limited protocol is convenient because the scope of its verification is completely defined.

The original entry consists of N and k for each setting. In independent trials, the order of identical two-outcome events adds no information to the binomial likelihood, so these numbers are sufficient statistics. In the present experiment, time and order would also be preserved to test for drift; By definition, there is no drift in this generator. The archive contains all k sets, generator parameters and a fixed seed

20261113. A separate demo set uses seed 20261214 and was not selected for significance.

In this set, the calibration gave 4863 a plus outcome from 5000. The complete two series are presented in the table. Maximization by initial samples preserves the natural dependence of variance on probability. If you first turn them into visibility and logarithmic rates, and then assign the same error to all points, you get a different procedure. Its calibration cannot be automatically borrowed from true binomial analysis.

$$p_{gj} = \frac{1 + c\exp\{-T_g[b_{0g} + b_{2g}(d_j/\ell)^2 + A(m_g/m_{\mathrm{ref}})^2 f_j(r_C)]\}}{2}$$

$$f_j(r_C) = 1 - e^{-d_j^2/(4r_C^2)}.$$

(19.2) Conditional probability model of the registered outcome. It does not include particle loss; fixed N means the number of trials already registered. In a separate calibration, $p_{\mathrm{cal}} = (1 + c)/2$.

One pre-fixed synthetic set

d/ℓ	k₁ from 1600	k₂ from 1600
0.0	1539	1528
0.6	1518	1519
1.0	1515	1493
1.6	1476	1472
2.3	1456	1408
3.2	1401	1340
4.5	1381	1294
6.0	1293	1231

Same curve for different mechanisms

Chapter 10 shows that spatial localization of a certain type can be reproduced by random impulses from the medium. Chapter 18 gave a temporal analogue: white external dephasing and additional irreversible rate can add up to one inseparable parameter. This is not a flaw in the numerical algorithm. If the probabilities coincide, the algorithm has no information to select a physical origin.

It is necessary to distinguish between exact and practical degeneration. With exact degeneracy, no increase in the number of repetitions of the same protocol solves the problem. In practice, the models diverge slightly, but there is less error available.

Then additional statistics sometimes help. However, systematic calibration uncertainty need not decrease with the number of events. A million repetitions of one incorrectly measured distance does not turn it into the correct distance.

Useful work begins with finding explicit parameter transformations that preserve all predictions. If the increase in fundamental intensity can be completely compensated by a decrease in the unknown white background, the direction of indistinguishability has been found. The next experiment should be chosen so that compensation stops working. This could be a different mass, a different spatial profile, an independent measurement of the environment, or an energetic observation. Its value is determined by the violation of a specific degeneration.

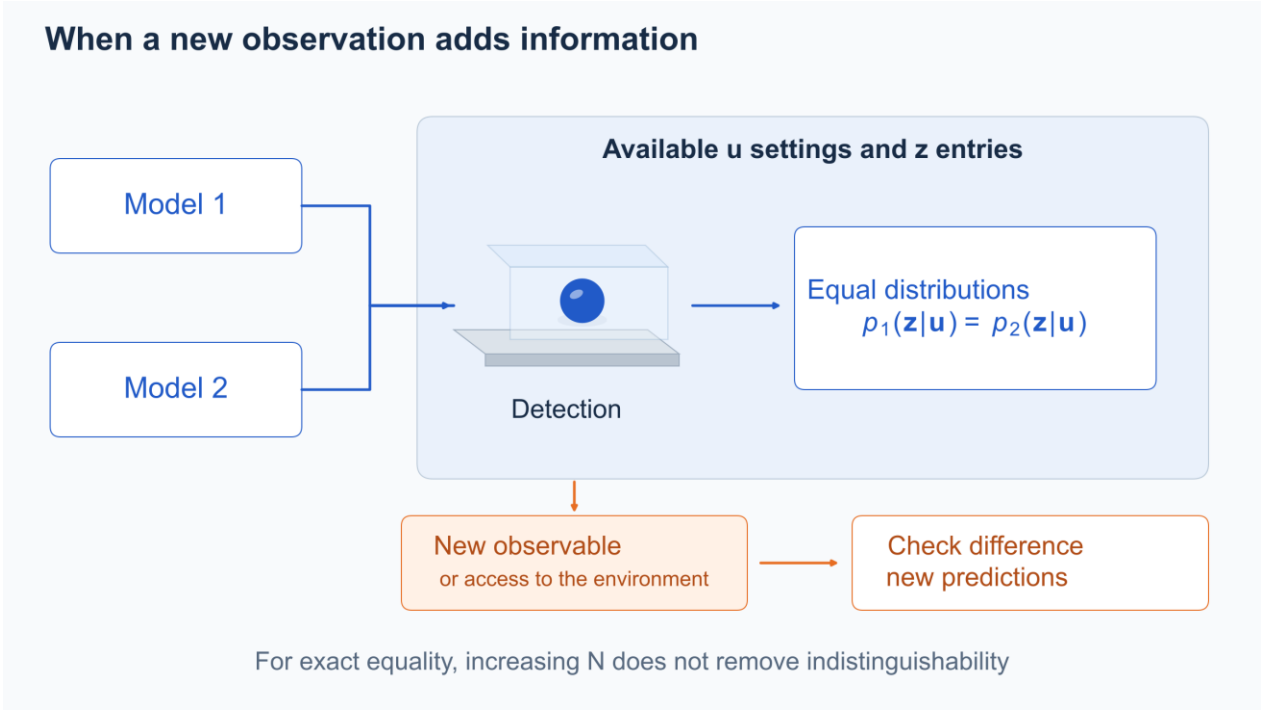


Figure 53. The frame defines the available settings and registration. Accurate operational indistinguishability requires equality of distributions across the entire allowed protocol family; in a process with memory - for full multi-temporal statistics, not just one final channel. With such equality, an increase in the number of events does not create missing information. Additional observation or independent access to the environment is only useful when specific models predict different distributions for them. The blocks “Model 1” and “Model 2” indicate explanations rather than individually observed mechanisms.

Local and global distinguishability

Let the vector of parameters be denoted by $\boldsymbol{\theta}$, and the calculated average observations by $\mathbf{g}(\boldsymbol{\theta})$. Derivatives of predictions with respect to parameters form the sensitivity matrix J. If its columns are linearly independent, small changes in different parameters affect the data in different ways. Under ordinary smoothness conditions, the full column rank serves as a sufficient regular criterion for local identifiability. It shows that in a sufficiently small neighborhood there is no continuous direction of compensation.

A local result does not exclude another solution far from the found one. A nonlinear model may have several separate parameter regions with the same predictions. Therefore, an analytical search for symmetries, studies of likelihood profiles, and numerical launching from different initial regions are necessary. Even a successful numerical search is not proof of global uniqueness in the entire continuous space. Its scope and resolution must be indicated.

The zero intensity boundary is especially important. If the additional mechanism is turned off, its correlation length may not affect the data at all. It makes no sense to estimate it at such a point with the usual symmetric confidence interval. In addition, the insufficient rank of derivatives does not always prove complete nonlinear non-identifiability: there are special points at which the first derivative vanishes. Therefore, rank testing complements model research, but does not replace it.

$$J_{ka} = \frac{\partial g_k}{\partial \theta_a}$$

$$\mathcal{J} \simeq J^T \Sigma^{-1} J.$$

(19.3) Sensitivity matrix and information matrix in the Gaussian approximation with a fixed known covariance Σ. For raw counting data, information is calculated from the corresponding likelihood.

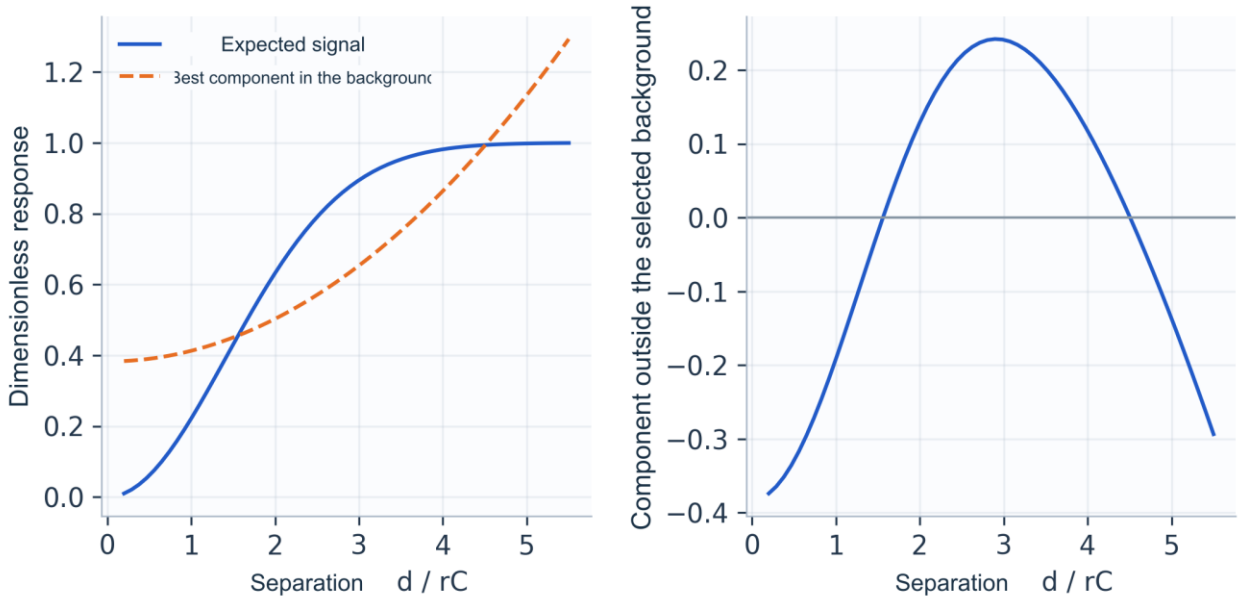


Figure 54. Projection of a signal onto the space of a constant and quadratic background with equal weights. Only the part not absorbed by this background remains for differentiation; expanding the environmental model can reduce it.

How to exclude a known background shape

The contrast of chapter 10 can be summarized. Let us imagine the set of estimated rates as the sum of a known family of background dependencies, the signal being tested, and the error. The columns of the F matrix define valid background shapes, such as constant and squared separation. The vector **s** describes the shape of a single signal at a fixed correlation scale. It is required to construct weights **w**, for which

$\mathbf{w}^T F = 0$. Then the corresponding combination of data does not depend on the coefficients of the selected background.

With a known positive definite covariance Σ, the problem has an explicit solution: the part that lies in the space of background dependencies is subtracted from the signal. The remainder is then weighted by the inverse covariance. Below is this design for linearly independent columns F. For dependent columns, the independent basis is first selected or a well-defined generalized inversion is used. Direct inversion of an almost singular matrix can create artificially enormous sensitivity.

Only the recorded background is reduced. If in reality there is an additional spatial dependence, it may remain in contrast entirely. Therefore, two calculations are useful: a basic one with a physically based model and a stability check with an extended family of permissible deviations. If, after reasonable expansion, the signal disappears, the result should be considered dependent on background assumptions. The very fact of using linear algebra does not make the diagnosis independent of the model.

$$\mathbf{s}_\perp = \mathbf{s} - F(F^T \Sigma^{-1} F)^{-1} F^T \Sigma^{-1} \mathbf{s}$$

$$\mathbf{w} \propto \Sigma^{-1} \mathbf{s}_\perp .$$

(19.4) Project the signal outside the selected background subspace in the error metric. Weights should be determined by model and calibration prior to testing on a confirmation sample.

Maximum contrast does not equal the best experiment

In an ideal calculation, one can find the distance at which the absolute contrast is maximum. Actual sensitivity also depends on the number of events, losses, registration errors, and the cost of each run. With greater separation, visibility may become too low and rate uncertainty too great. Then the point with the largest theoretical signal will be less useful than the point with less effect but a more reliable reading.

In the Gaussian linear approximation for a known signal, the following ratio of the expected effect to the statistical error is obtained. It refers to fixed shape parameters and known covariance. If the scale of correlation is searched among many options, the search itself must be taken into account. If a covariance is imprecisely estimated, its uncertainty is also carried over into the result. For real design, it is preferable to calculate the expected initiating events and evaluate the complete analysis procedure on artificial samples.

Bayesian design of interferometric collapse tests considering pressure, thermal radiation and number of measurements was studied by Laing and Bateman [19]. This is an existing example of how experimental geometry is linked to parameter information. In this program, the selection criterion should be supplemented with robustness to an uncertain background: a good experiment should remain distinguishable over a permissible change in calibration, and not just at one most convenient point in the model.

$$Z_{\exp} = A\sqrt{\mathbf{s}_{\perp}^{T}\Sigma^{-1}\mathbf{s}_{\perp}}.$$

(19.5) The expected signal to noise ratio in the specified linear Gaussian approximation. This is a design tool, not a ready-made detection value in real data.

The minimum set is not specified by one number

The number of measurements and the number of independent observations are two different things. A thousand repetitions with one setting refines one probability. Several different settings can produce a new dependency structure, but only if their predictions are not copies of each other. Therefore, the rule “four parameters, four points are enough” is unreliable. It does not take into account unknown calibration, degeneracy, and the need to check the quality of the model itself.

For a space-time program, a reasonable minimum set is determined by the problem. What is needed are observations that constrain the environment, at least slightly different geometries, a memory-sensitive time sequence, and an independent series to test the transfer. However, these categories do not guarantee success on their own. Before the experiment, a coupled model should be built and it should be determined which parameters remain uncertain. Sometimes one well-chosen additional mode is more useful than a dozen similar options of the previous one.

It is also necessary to measure the input parameters. An error in mass, distance, or duration changes the theoretical prediction itself. Such quantities cannot always be considered absolutely known and all uncertainty cannot be placed only on the vertical axis of the graph. The coupled model can include calibration parameters with individual data. Then the real cost of the inference is visible: what accuracy of geometry and environment is enough for the difference of interest not to disappear.

Testing on held-out data

Once a model is selected, testing is required on data not used to adjust its shape. A delayed series can change mass, distance, temperature, or control sequence. Conditions are chosen in advance so that competing models produce different predictions. A simple random division of almost identical repetitions into two parts tests the reproducibility of the estimate, but is usually a weaker test of the transfer of a physical law to a new regime.

Before opening a confirmatory series, all the rules are fixed: the range of parameters, calibration corrections, the criterion of disagreement and acceptable options for the medium model. This does not prohibit subsequent exploration of the unexpected. It only separates the prediction made in advance from the explanation found after viewing the result. If a new feature requires a model change, the next independent series must check the already changed version.

Different statistical approaches answer different questions. The frequency procedure evaluates the behavior of the rule when repeating experiments; Bayesian updates the distribution of parameters given initial assumptions. The strong dependence of the output on the chosen a priori range should be shown. Neither a

high model comparison coefficient nor a low probability in one null model automatically means that all physical alternatives have been taken into account.

A parameter profile and results from the held-out run

For the given readings, the comparison statistics with A = 0 is 57.369. A full length search is included in both this number and the zero calibration of chapter 21. The best estimate of A is 0.15334 s^{-1}. However, the maximum point does not show the width of the uncertainty. If an increase in A is accompanied by a change in r_C and background coefficients, the predictions may change little. This can be seen in the profile likelihood, where for each fixed A the background and the entire length grid are re-optimized.

For the demo set, the profile area along A extends from 0.090 to 0.275 s^{-1} on the grid step 0.005 s^{-1}. The threshold of the profile difference is equal to 4.2681 and was obtained by separate modeling at A = 0.12 s^{-1} and the specified background. This is a point calibration in a given internal mode. It does not prove uniform 95 percentage coverage for all possible A, backgrounds and continuous r_C. An actual test of coverage on an independent ensemble is given in chapter 21.

The deferred protocol uses d/ℓ = 0.85; 1.35; 2.05; 2.85; 4.80 and durations reduced by 0.65 times. For each object, there are 800 events to configure; Additionally, an independent registration calibration is maintained. All predictions are calculated using the parameters of the training series. New readings are not involved in re-adjusting A, r_C or the background. This tests the transfer over distance and time, not just the stability of the random division of repetitions of the previous setting.

The total discrepancy between the delayed samples and the forecast in Pearson form is 13.484. Its reference distribution is built by simulating the full path: a new training set, a new selection, and new delayed events. Therefore, the error of the predicted parameters is not considered zero. The tail fraction is equal to 0.392 for 1000 repetitions in the nominal model. In this example, the forecast is consistent with the new series. This is a spot check of the selected generator; extending the background class can change the output.

At the beginning of the second series, the measured probability for the first object is 762/800 = 0.9525; the forecast is approximately 0.95675. For the last setting of the second object, 672/800 = 0.8400 is observed with a forecast of about 0.85109. The difference between individual points is natural for the final counting data. The point of the general criterion is to evaluate the entire sequence according to a predetermined rule, without retroactively selecting the most successful or most divergent point.

If disagreement arose, the next step would depend on its structure. The overall calibration shift is different from the time scale error; Selective divergence of large distances indicates a different part of the model. After verification, the deferred data can be used to develop the next version of the description, but then another independent series will be required. A reproducible procedure makes this transition

explicit and allows one to separate the explanation of what has already been seen from a truly new prediction.

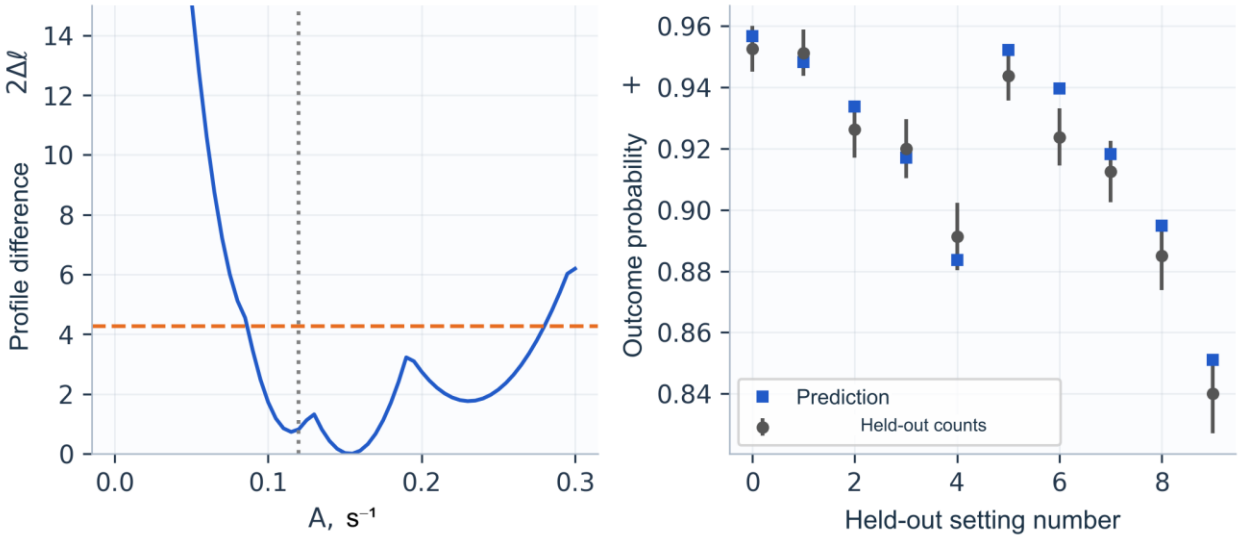


Figure 55. Amplitude profile and prediction of delayed binomial events. On the left is the log-likelihood difference after a full grid search r_C; on the right is the forecast and independent readings of new settings. The vertical dotted line marks the entered A, the horizontal dotted line marks the calibrated threshold. The bars on the right show one binomial standard error of the frequencies, without the error of the predicted parameters; the general criterion takes it into account by separate modeling. All events are synthetic.

The limits of physical inference

After a complete analysis, the result should be formulated at the level that the observations support. It is possible to limit parameters, detect a discrepancy with known background, favor one parameterization over another, or successfully predict a new series. These statements vary in strength. They cannot be quietly replaced by a general statement about the new nature of reality.

The limit of discernibility is also a positive scientific result. If it is proven that the chosen class of measurements does not distinguish between the two hypotheses, there is no reason to repeatedly repeat a useless comparison. You can specify which assumption needs to be added and which observation can test that assumption. This turns the mathematical constraint into a guide for the next experiment.

The results of the analysis performed should be read as a map of conditions: in one area the parameters are definable, in another only their total contribution is distinguishable, in the third everything is hidden by calibration. Such a map is more honest than one maximum sensitivity figure and is more useful for choosing equipment. It explains which uncertainty needs to be reduced first in order for the next measurement to actually add knowledge.

20 Experimental apparatus and the full data pipeline

A research program gains experimental meaning when each observation is associated with an understandable method of recording. Below are proposed protocol concepts for which response calculations, a list of calibrations and feasibility criteria can be compiled. Their purpose is to link testable hypotheses to devices. Real technical parameters should emerge from the analysis of the selected laboratory and measured equipment.

Three different roles of the experimental platform

Not every useful installation must directly search for a new fundamental effect. The first role of the platform is to test control and statistical analysis methods on a known signal. The second is to limit the environmental influences that can simulate the desired dynamics. The third is to create a physical state that is truly sensitive to the modification being tested. These roles can be performed by different devices. They are connected by an agreed calculation, and not by mandatory external similarity.

For example, a well-controlled internal qubit is useful for investigating pulse errors and reconstructing time correlations. The spatial interferometer allows direct investigation of coherence between branches with different mass distributions. The mechanical sensor is capable of providing information about force noise and energy exchange. The resulting numbers cannot be directly compared as equal "decoherence levels". Each platform requires its own transfer model that relates the general parameters of the hypothesis to the recorded events.

The preparation of such models should precede the selection of a beautiful hardware design. First, it is determined which two explanations remain indistinguishable. Then we look for an observable quantity that destroys this degeneracy. After this, the ability to measure it is assessed. This procedure allows you to stop the development of an unsuccessful concept at the computational stage, when months have not yet been spent on a device that lacks the necessary physical sensitivity.

Spatial interferometer with changing geometry

The first concept is designed to test the geometric localization law. A system is envisioned in which multiple spatial configurations of the coherent state can be monitored and the resulting distribution of events recorded. The central object of the calculation is the complete history of the state from preparation to reading. In the idealized regime of two narrow held packets, a rate dependent on their distance is applicable. A more complex interferometer requires propagation of the entire state through the elements of the device.

Particular care should be taken when dealing with near-field interference. It cannot be replaced without verification by a picture of two stationary trajectories and

the maximum distance cannot be substituted into a simple exponential. The proposed protocol must calculate the pattern that the detector actually sees, including the velocity distribution, the passage of elements and the final resolution. The contrast from Chapter 10 then acts as a diagnostic limit of the model, and not a universal formula for any geometry.

The main series changes spatial profile under controlled environmental conditions. Additional runs deliberately vary a known external factor to test the predicted response. The suppression of fullerene interference with increasing gas pressure has already been observed and quantitatively compared with the theory of decoherence [26]. For the proposed program, such a dependence serves as an example of meaningful calibration: the model must predict a controlled change in the background before a different mechanism is assigned to its residuals.

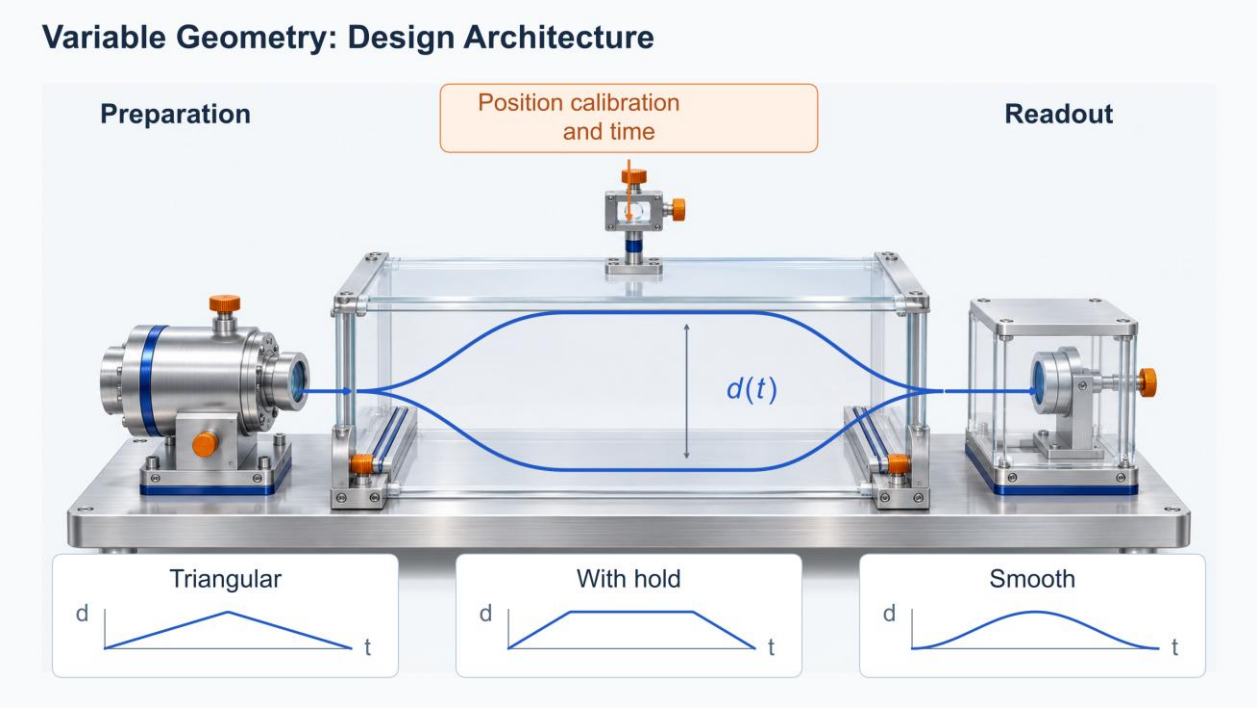


Figure 56. Design functional architecture for variable spatial state profile: preparation, controlled separation and recombination, readout and separate calibration of position and time. The blue lines show the idealized state components, the orange input is the independent control. The boxes compare the shapes of the story d(t), including its beginning and end; maximum separation is not enough. The hardware design is conceptual: no realized masses, vacuum, retention times, or sensitivity are stated here. This two-branch scheme does not replace the full state propagation in the published sodium near-field interferometer.

Thermal and gas background

The pressure measurement itself does not determine the collision background. The composition of the gas, the distribution of velocities, the properties of interaction and the probability of registration of an object after a collision are significant. The theory of such an effect requires a specific scattering model; rigorous derivations of the basic equation were considered, in particular, by Hornberger and Sipe [45]. In a design calculation, you cannot replace an unknown dependence with a single coefficient just because this results in convenient sensitivity.

The thermal state is also heterogeneous in meaning. The temperature of the chamber, the internal excitation of the particle and the effective temperature of its motion describe different quantities. Thermal radiation from heated molecules can indeed reduce interference visibility; This mechanism was studied in experiments with molecules C70 [25]. Therefore, cooling the motion does not relieve the evaluation of internal heating, light absorption, and photon emission throughout the sequence.

The concept includes separate series with changes in the power and duration of illumination, control of the detector background and verification of reproducibility after returning to the original conditions. This reversibility of tuning helps distinguish a stable physical dependence from a slow change in the device. It is advisable to record the impact parameters for each run. A daily average may mask the correlation between laser drift and the order in which different geometries are executed.

Controllable sensor for checking the temporal model

The second concept uses a two-level system with accessible preparation, pulse control and readout. Its first task is to check the entire path from the specified noise to the reconstructed parameters. You can feed a known artificial phase effect into the system, run several sequences, and find out how accurately the analysis returns the input spectrum. Such a test establishes the capabilities of the method, although in itself it is not a search for an additional natural mechanism.

It is useful to separate the series on which the noise model is selected from the series on which the prediction is tested. The second uses different intervals or pulse locations. Additionally, rotation errors and the dependence of reading on the number of operations are measured. If the reconstructed memory time begins to change along with the technical shape of the pulse, the control model is first examined. It would be premature to attribute such a change to a universal property of matter.

To move from this bench to testing mass localization, it is necessary to physically relate the internal state to various mass distributions. Then the calculation must include the movement of the object, spatial separation, its inverse registration and additional noise of the control field. The sensitivity of a conventional spin echo cannot be transferred to this problem by simply changing the notation. The possibility of such a connection and its accuracy constitute an independent stage of feasibility testing.

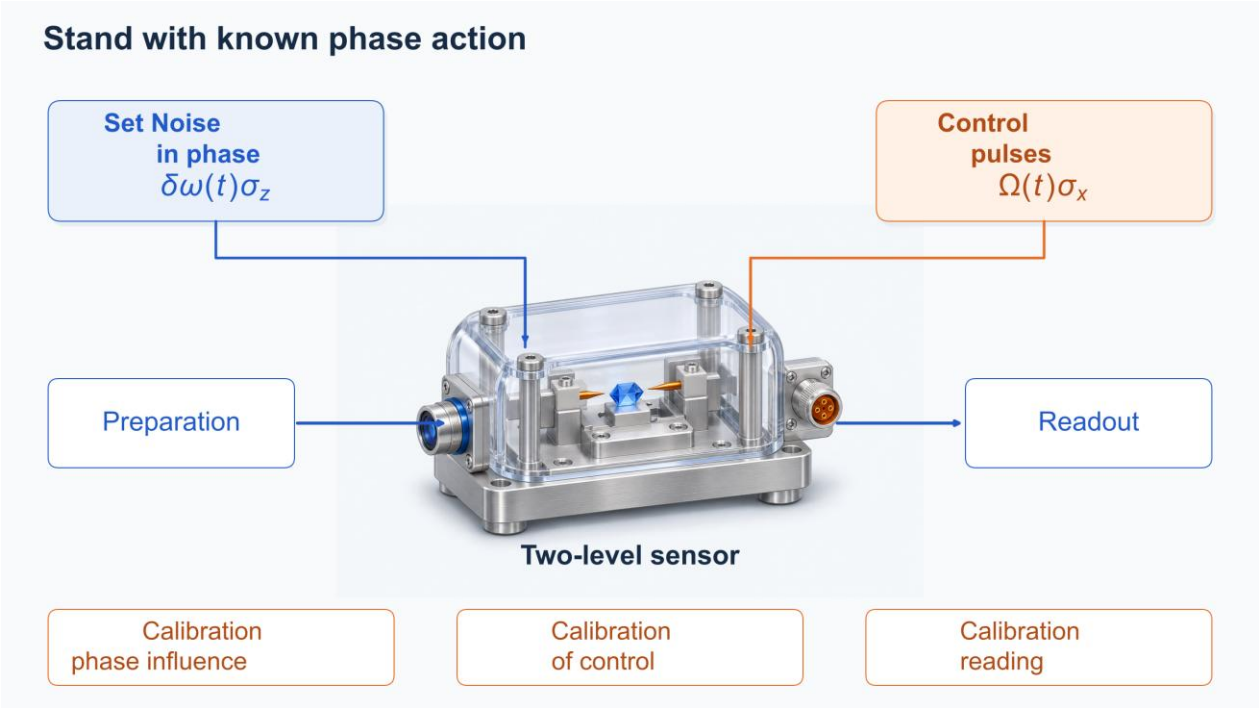


Figure 57. The training stand separates the known artificial phase action according to σ_z from the transverse pulse control according to σ_x. Preparation and readout form the main tract; impact, impulse and registration are verified by independent calibrations. The illustration shows the functional channels and conceptual sensor and does not show the implemented electrical wiring or the achieved performance of a particular device. Returning the entered parameters validates the method; it does not indicate the discovery of fundamental noise. To transition to mass localization, a physical connection of internal states with different mass distributions is additionally required.

Training stand with testable error

The calculations of the two previous chapters set up a complete training stand of three levels. At the first level, the physical state and the law of influence are known. On the second one, a detector is specified and initial events are generated. The third uses a fixed analysis that does not have access to the hidden values of the generator. This organization allows processing errors to be detected without first requiring the existence of a new natural mechanism.

For the spatial bench, the settings, N, k and the results of the general calibration are saved. The test starts with a zero split and a known signal, continues with a full length search, and ends with a prediction of a different geometry. For a temporal test bench, the analytical Ramsey and echo are first played, then the finite duration, erroneous angle, and readout inconsistency are entered. In both cases, it is known when the remainder is caused by an artificially introduced technical reason. This makes a false physical interpretation an observable result of program testing.

The statistical budget is not equal to the duration of the laboratory work. In the spatial example, 30 600 is the number of recorded events. With efficiency η and cycle time t_{cycle}, the expected build time would be of the order of $\mathrm{N}t_{\mathrm{cycle}}/\eta$ if the losses are independent and the cycle is the same. In a real installation, both multipliers depend on preparation, mass, geometry and sampling requirements. Therefore, there

is no absolute time assigned for this training stand. It is calculated only after selecting an agreed device specification.

The published platform and its reproduced data are discussed in chapters 7, 9 and 12. Its real parameters cannot be replaced by the dimensionless coefficients of the training example. In particular, the near-field distribution does not automatically reduce to a single binary maximum or to a pair of stationary packets. The connection between the two descriptions is methodical: initiating events, calibration, likelihood, error checking, and prediction. The transmission physical model remains its own for each installation.

The practical development sequence therefore has measurable stops. The algorithm must first return the known input signal and the intended false alarm rate. The response of real calibration runs is then checked. After this, the physical model of the experiment of interest is compared. If the generator does not reproduce already at the first level or the detection turns out to be sensitive to an imperceptible choice of grid, increasing the complexity of the equipment does not correct the defect in the procedure.

A reproducible record includes more than an attractive figure. Negative outcomes are retained: an incorrect environmental model, the wrong pulse, or a mismatched calibration. They show which inferences are ruled out even at high formal sensitivity. In the next chapter, these results form a quantitative map of where the selected program applies.

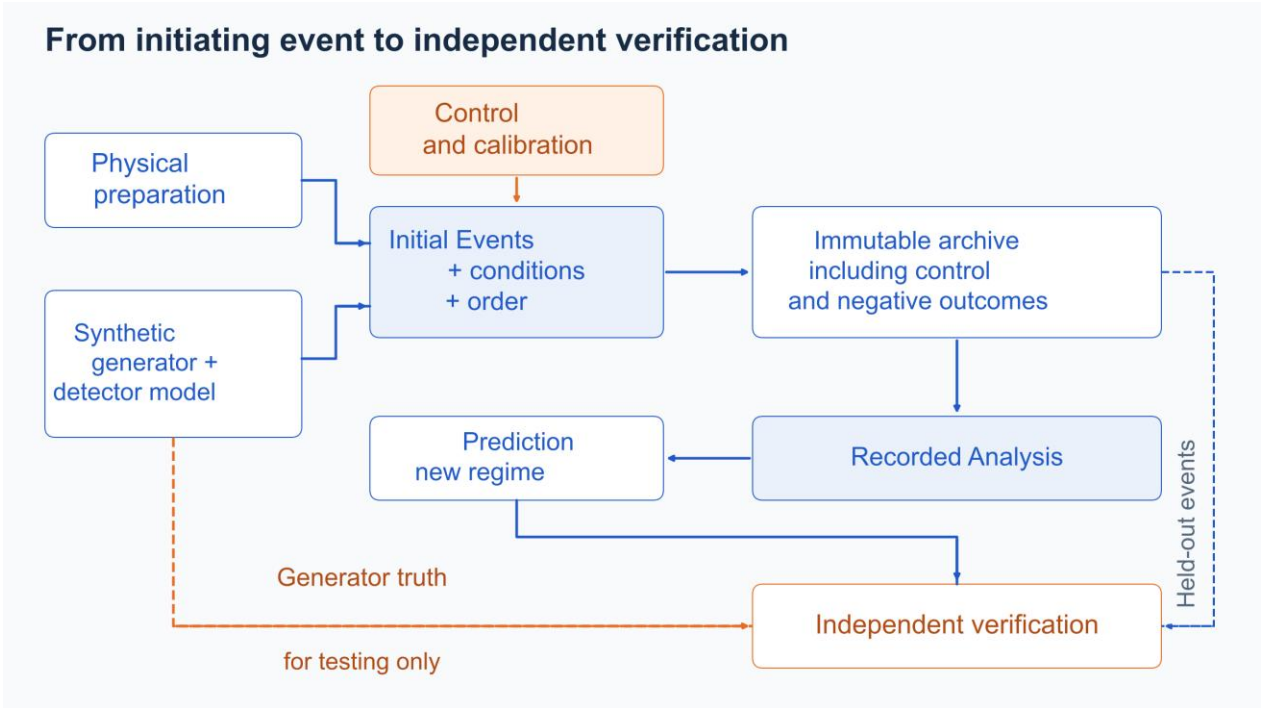


Figure 58. Physical and synthetic preparation are different sources of initial events. Settings, calibrations, measurement order, control and negative results are saved until analysis. The fixed analysis builds a forecast of the new regime; deferred events go directly to the independent check and are not returned to the fit until it is completed. The true parameters of the synthetic generator are available only to the checking module. A logged event is not the same as preparation or dialing time. The real route must also store excluded events and selection reasons; The conditional binomial model is applicable only under its assumptions.

Two sensors and spatial correlations

The third concept is designed to study joint noise. The two sensors are placed in several configurations, and the analysis evaluates not only local spectra, but also mutual dependencies. Changing distance and orientation is useful if different mechanisms predict different spatial laws. For quantum sequences, it is necessary to take into account mutual control and direct communication of sensors. For mechanical channels, the response of each sensitive element is additionally calculated.

Common electronic components, a light source and a mechanical support are capable of creating correlations that are superficially similar to the action of a common field. Therefore, the project includes control rearrangements and changes in the technical communication route while maintaining the geometry under study. If the correlation follows a cable or common amplifier, this is instrument information. If it retains a certain spatial dependence under independent reading methods, there is a stronger basis for further physical analysis.

The relative timing of the channels needs to be calibrated. Delay error changes the phase of the cross spectrum and can bias inferences about propagation or impact memory. At the same time, mutual interference during control must be assessed: the pulse of one sensor can directly disturb another. The control series checks this transmission route. Only after this does it make sense to compare the observed correlation with the core of the universal hypothesis of chapter 17.

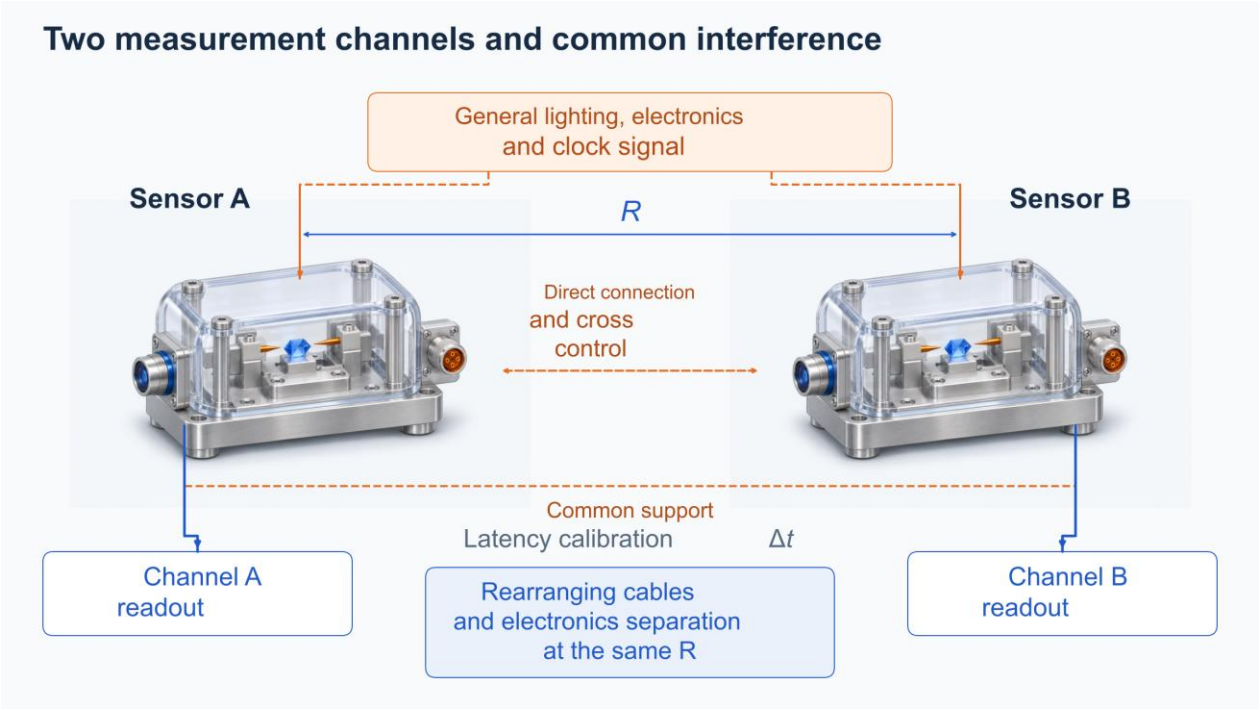


Figure 59. The two sensors have separate acquisition paths and an adjustable distance R. The orange dotted line highlights the common interference technical paths being tested: light, electronics, clock, mechanical support, direct coupling, and cross control. A generic laser, amplifier or clock is not considered error-free by definition. Control re-arrangement of cables and separation of electronics is carried out while maintaining R and orientation. The relative recording delay Δt is calibrated separately from the physical temporal structure of the correlation under study. The hardware images indicate conceptual sensing modules and not a specific experimental implementation.

Mechanical observations and preparation status

Force noise and heating provide additional information about the mechanism that is assumed to be spatially localizing. But what is measured is the motion of a mechanical object, not an abstract force. Therefore, mass, frequency response, attenuation, acquisition characteristics, and possible readout correlation with feedback are required. Given such a correlation, simply adding “object noise” and “instrument noise” may not be correct. All significant cross terms are retained in the working model.

An experiment by Delić et al demonstrated cooling of the motion of an optically confined nanoparticle to the quantum ground state [52]. This result provides concrete support for the discussion of the preparation of massive quantum systems. It does not mean that the spatial superposition with the required division is automatically ready. Between cooling, state creation, state retention, and persuasive sensing, there are separate tasks, each of which affects the resulting sensitivity.

The joint verification concept uses one set of complementary mechanism parameters for interference and mechanical observations. Moreover, each platform has its own model of background forces. The coincidence of numerical residual capacities is not a sufficient indication of a common origin. The full predicted transition between observations, including geometry and frequency band, is tested. It

is precisely this transition that can make the additional channel an independent test of the hypothesis.

A feasibility specification and the choice of the next step

Each concept requires a data sheet with measured or reasonably accessible parameters. It includes the object's mass and shape, distribution of initial states, separation history, cycle time, detection efficiency, and environmental uncertainties. The characteristics that have already been demonstrated in the chosen combination and the characteristics that are only supposed to be combined are recorded separately. The sum of the records of different laboratories does not automatically form the parameters of one feasible experiment.

Extending observation time sometimes motivates space concepts. The MAQRO paper looked at how free fall, vacuum and microgravity could change the capabilities of [53] array interferometry. This is a design rationale and not evidence of implementation of the protocol discussed here. Comparison of ground and space schemes must include the entire cycle of preparation, control and registration. Longer free movement is only useful if the information it creates is stored in an actual measurable result.

The next stage is selected based on the most limiting uncertainty. If readout calibration destroys discriminability, increasing mass does not solve the problem. If it is limited by background thermal radiation, it is more useful to examine the thermal model. If all technical losses are small enough and the signal remains indistinguishable for physical reasons, another observable quantity is required. This choice conserves resources and makes each facility improvement related to a specific scientific question.

The book's numerical examples cover different parts of the specification: the published interference experiment provides a real set of parameters and external replication, the spatial simulation provides a proven inference procedure, and the controlled sensor provides the calculated budget for the model impulse error. Their combined use does not mean that all characteristics are already implemented in one device. The development of a new device requires separate coordination of these three levels.

The completed design links state, environment, control, detector, and inference rule. The calculations performed show at what level the supposed distinguishability disappears and what change actually adds information. The final chapter contrasts these findings with the literature and documents the conditions under which a research program remains meaningful.

21 Results of the computational program and the limits of inference

The program ends with the results of several different tests: reproducing the known experiment, analyzing artificial initiating events, testing an erroneous background, and calculating the final control. Each result has its own area of applicability. Their comparison shows what has already been established within the models and which statements will require new observations.

What belongs to literature and what is done here

The book combines existing physical models and inference methods into a reproducible sequence of calculations. The historical priority of CSL, dynamic decoupling, multiqubit noise spectroscopy, and statistical tests does not carry over to this sequence. The scientific contribution of a particular new protocol is determined by the difference between its premises and results from the closest published works, and not by the number of combined directions.

Important immediate predecessors of the statistical part are the studies of Schrinski and co-authors 2019 and 2020 years [65, 66]. They use original measurements and their uncertainties to test parameterized modifications of quantum mechanics. The work of Laing and Bateman examines Bayesian inference and experimental control selection in near-field interferometry with background mechanisms [19]. The idea of inferring events or taking pressure into account is therefore not a new result of this book.

The actual completed part here has an educational and methodological status: a fully reproducible binomial protocol is defined, independent error ensembles are performed, transfer to delayed distances is shown, the influence of finite impulses is calculated, and a counterexample of erroneous physical attribution is presented. The resulting numbers refer to explicitly specified models. They are not stated for the first time by discovered laws, universal limits of nature, or experimental detection of collapse.

The comparison table shows the place of the given calculations among existing methods. To establish a new scientific result, it is necessary to prove the superiority of a specific protocol over the closest method with the same physical resources or to identify a previously unknown limit of distinguishability. The methodological conclusions presented here are supported by calculations and tests of their applicability.

Immediate predecessors and status of completed work

Support work	An established result	Use in the book
Schrinski et al. 2019 [65]	Conclusion based on input data and uncertainties	Basis of event analysis; separate frequency simulation of own training protocol
Schrinski et al. 2020 [66]	Testing modifications in matter wave interference	Distinguishing between a model limitation and a general claim of classicality
Laing and Bateman 2024 [19]	Bayesian background analysis and control selection	A reference point for physical completeness; Calculation of conditional KL for four instructional designs
Arenz et al. 2015 [47]	Dynamic decoupling in testing alternative theories	Explicit refinement of final control and false remainder
Paz-Silva et al. 2017 [50]	Multiqubit Gaussian noise spectroscopy	Particular two-sensor example with specified probabilities
Green and others 2013 [67]	Freeform control and universal noise	Numerical propagation of a specific rectangular pulse

Reproduced bounds and independent calculations

The calculation program begins with checking the control limits. The spatial kernel reproduces the compact limit and disappears at zero separation. The three-point contrast eliminates the stated constant and quadratic background terms, and its generalization to linear separation and convergence changes the optimal distance. Analytical Ramsey and echo coincide with independent integration and with the instantaneous full propagation limit of the controlled sensor.

For the stochastic time model, the convergence of the Hermite expansion was additionally verified. For the gravitational example, the state matrix, partial transposition spectrum, and analytical threshold are compared. For the statistical part, the original binomial samples and complete selection results are saved. Such tests do not prove the truth of physical hypotheses, but they allow us to eliminate a number of errors in normalization, indices and software implementation.

External replication uses published data and the author's analysis presented in chapter 12: 95 scans, 3895 positions and 10 772 714 registered counts. With the initial fixed calibrations and spatial scale $\hbar/\sigma_q$ = 10 nm, we obtained τ_5 = $2.842065516\cdot10^{15}$ s and μ = 15.453634, which reproduces the published rounded values. Independent trapezoidal quantile interpolation gives μ = 15.451403. The difference around 0.00223 is less than the rounding accuracy given in the article. This is a repetition of the stated procedure and not a new blind analysis of all systematic effects; this part's own simulations have separate assumptions and calibrations.

Full procedure error rate

For the spatial experiment, the likelihood ratio statistics q = 2(ℓ₁ − ℓ₀) was applied. In the alternative, A is non-negative and iterates over the entire predefined mesh r_C; at zero A = 0. If zero, the length is not determined from the data. Therefore, the threshold is taken from a separate null ensemble that has undergone the same selection and search, and not from the usual formula for one internal parameter.

The first ensemble of 1000 sets calibrates the 95th percentile: q_{crit} = 3.48640. The second independent null ensemble yielded 56 exceedances from 1000. The false discovery rate is 5.6%; The 95 Wilson percentage interval for the Monte Carlo estimate is 4.3 %–7.2 %. The difference from the nominal 5% is within the final test statistics. The threshold itself is also estimated from the final ensemble; the specified interval is conditional on its realized value.

When A = 0.12 was introduced s^{-1}, the procedure detected an addition in 1000 cases from 1000. Zero number of gaps in this series does not mean mathematically unity power: the lower limit of the Wilson interval is 99.62%. For the weaker A = 0.035 s^{-1}, 841 out of 1000 was found, that is, 84.1% with the interval 81.7%–86.2%. This gives rise to the quantitative meaning of sensitivity: the same protocol has a different probability of success at different amplitudes.

The profile area along A has a separate calibration. With A = 0.12 s^{-1} and a given background 1000 of simulations, the threshold 4.26806 for the profile difference was determined. At the next independent thousand, the true value entered the region 946 times. The actual coverage is 94.6%; Monte Carlo assessment interval is 93.0 %–95.8 %. This is a test at one internal point, and not a proof of coverage on the entire boundary A = 0 and throughout the entire continuous space.

The calibration follows recording fluctuations and joint background estimation. It does not repeat the unknown history of a real device: geometric drift, temperature unsteadiness and incorrect physical transfer function cannot be considered automatically taken into account here. For other equipment, the threshold must be calculated according to its own model and range of systematic effects. The finite grid r_C is also included in the protocol definition; changing this grid changes the number of available explanations for random variation.

Six ensembles of 1000 sets, as well as a separate demo set, are saved along with the code. Separate null and signal ensembles are used for thresholding, error rate testing, and coverage testing. This excludes quality assessment on the same samples for which the rule was configured. The generator and assay are intentionally identical in control runs; the next episode violates precisely this convenient condition.

Testing on independent ensembles using 1000 sets

Check	Frequency	95 % interval Monte Carlo
False detection with a given background	5.6 %	4,3 %–7,2 %
Detection A = 0.035 s^{-1}	84.1 %	81,7 %–86,2 %
Detection A = 0.12 s^{-1}	100.0 %	99,62 %–100,00 %
Coverage A = 0.12 s^{-1}	94.6 %	93,0 %–95,8 %

The intervals describe the final precision of the Monte Carlo estimate. They are not confidence intervals for the physical parameters of the experiment.

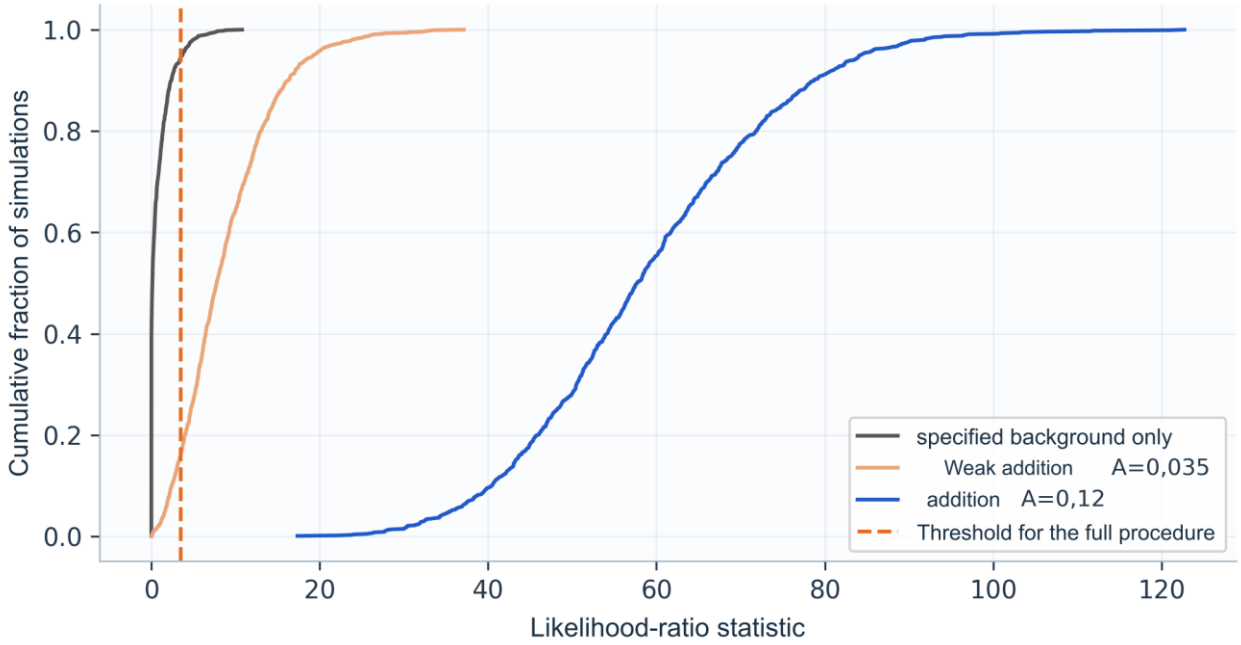


Figure 60. Distributions of full search statistics by scale: given background, weak and strong additives. The threshold is determined by a separate null ensemble. Each validation curve contains 1000 of complete synthetic experiments.

Checking against a background not included in the fit

In the last series, the fundamental amplitude A is zero, but the environment creates two components of random impulses. Their spatial scales are 0.65ℓ and 2.2ℓ, non-negative weights are 0.65 and 0.35; the total amplitude is 0.12 s^{-1}. A mixture of admissible Gaussian impulse processes remains an admissible process. It is not equal to the only Gaussian kernel, which is used in the analyzing alternative, and certainly not included in its quadratic zero background.

However, the same procedure exceeds the previous threshold in 1000 cases from 1000. This is not an error in calculating p in the written null model: that model is indeed incorrect for the new generator. It would be a mistake to call all excesses a detection of objective collapse. There is no such mechanism in the generator. The

result only establishes the insufficiency of the limited background family and the preference for a more flexible form of attenuation.

An even stronger counterexample can be constructed. If the medium is allowed exactly the same Gaussian momentum kernel with the same mass law, its ensemble generator will coincide with the localization dynamics being tested. The predictions of all available system sequences then match, including additional replicates and energy observations, if the match covers the full generator. The minimum KL distance is zero. In this case, the problem is not solved by increasing the number of events or by a smarter optimizer.

The output is possible only after adding physical information for which the models diverge: an independent observation of the medium, a verified limitation of its spectrum, a different law depending on geometry, or a new recording channel. Such a limitation cannot be declared established simply because it is convenient for obtaining sensitivity. Therefore, a positive statistical discovery in the book is formulated as a disagreement with a given background, and the question of fundamental origin remains conditional on the completeness of physical alternatives.

Selecting measurements with consistent discriminability

The design of the next series begins with a given area of interest. It may include specific non-null hypothesis parameters or a range that is not already excluded by other data. Experimental options are compared under the same time budget and taking into account the actual outcome of events. An increase in complexity is justified if it adds independent information or reduces major uncertainty, and not just increases the absolute value of the ideal contrast.

One possible criterion is the minimum difference in probabilistic predictions for all acceptable background options. In the formula below, the setting q denotes the full protocol, θ_* the fixed non-null hypothesis being tested, and η_0 and η_1 the environment parameters. The Kullback-Leibler divergence between the distributions of possible data was used. This is a measurement selection instrument; the mathematical measure itself is not a new physical entity.

If the achieved minimum is zero, there are indistinguishable predictions among the feasible options. This protocol does not ensure uniform discrimination between the selected models. If the infimum only approaches zero, it is necessary to study the limiting region separately. When searching across a range of fundamental parameters, one cannot imperceptibly include zero intensity and then expect positive guaranteed sensitivity to the entire range: at the very zero boundary, the compared models coincide.

$$\Delta(q;\theta_*) = \inf_{\eta_0\in\mathcal{N}_0,\eta_1\in\mathcal{N}_1} D_{\mathrm{KL}}\big(P_q(\cdot|\,\theta_*,\eta_1)\|P_q(\cdot|\,H_0,\eta_0)\big).$$

(21.1) An example of a criterion for stable discrimination with a fixed non-zero hypothesis being tested. The sets of acceptable backgrounds are specified by independent calibration. The criterion should be weighed against the cost and duration of the chosen protocol.

Four designs with the same number of events

The minimum KL-distance criterion was calculated for four pre-listed protocols. All have 5000 calibration and 25 600 main events; the distances and distribution of main events between them change. The fixed non-null hypothesis has A = 0.12 s^{-1} and r_C = ℓ. The null model contains only a constant and quadratic background. In both hypotheses, five parameters of readout and normal attenuation are varied separately.

The main design range is specified in coordinates (a,b_{01},B_{21},b_{02},B_{22}): [0.040;0.065], [0.025;0.065], [0.22;0.36], [0.040;0.085], [0.35;0.52]. These are clearly accepted ranges for training calculations. They are not presented as measured constraints of a particular laboratory. In a real experiment project they would have to be justified by independent calibration. After this, joint numerical minimization is performed based on the background of both hypotheses. Each minimum is tested against six different starting points.

Among the four candidates, the “Emphasis on curvature” option had the largest minimum distance. Its value is 45.334. The wide uniform protocol gave 41.274, and the restriction to short splits only gave 7.627. This is the result of a choice within a finite set for a specific budget, and not a proof of the absolute optimum over all possible controls.

In the version with an emphasis on curvature, the distances are 0; 0.6; 1.3; 2.0; 2.8; 4.0; 6.0 in units of ℓ. 1400 is allocated to them accordingly; 1200; 1800; 2200; 2000; 1800; 2400 events per object. The zero point limits the base visibility, intermediate distances distinguish core bending, and long distances limit quadratic background and saturation. Therefore, the utility distribution does not coincide with the choice of a single point of maximum absolute contrast.

The price of calibration assumptions is tested by expanding the ranges to [0.03;0.09], [0;0.15], [0;0.8], [0;0.15], [0;1.0]. Minimum distances are reduced as the normal background has more ways to simulate the signal. The table shows this change for each design. When an accurate noise simulation is included in the background, the distance becomes zero for all options. This is a separate qualitative limit that cannot be overcome by successful redistribution of the same budget.

KL is the expected log-likelihood difference for given distributions, but its number is not equal to the p-value and is not automatically translated into a number of standard deviations here. The behavior of the full procedure on finite samples is tested for a wide protocol at one nominal point; this is not a test of the power under the worst-case background found by KL minimization. To finally select a new design, it is necessary to repeat these checks with its threshold, calibration and real losses. The performed minimization provides a reasonable design rating and does not replace experimental validation.

An equal budget in this comparison means an equal number of events recorded. If receiving a large split increases preparation time or reduces output, you should replace the event limit with a total time limit. Without such a transfer model, the promise of gains in operating hours would be unfounded. Therefore, the results

presented strictly retain the resource meaning that was specified during the calculation.

Numerical selection among four valid designs

Design	Events	Minimum KL	After expanding the background
Short separations	30600	7.627	0.810
Wide range	30600	41.274	15.058
Emphasis on curvature	30600	45.334	17.167
Focus on saturation	30600	39.933	15.709

The minima are obtained numerically with several starting points; this is not a proof of the global optimality of continuous control.

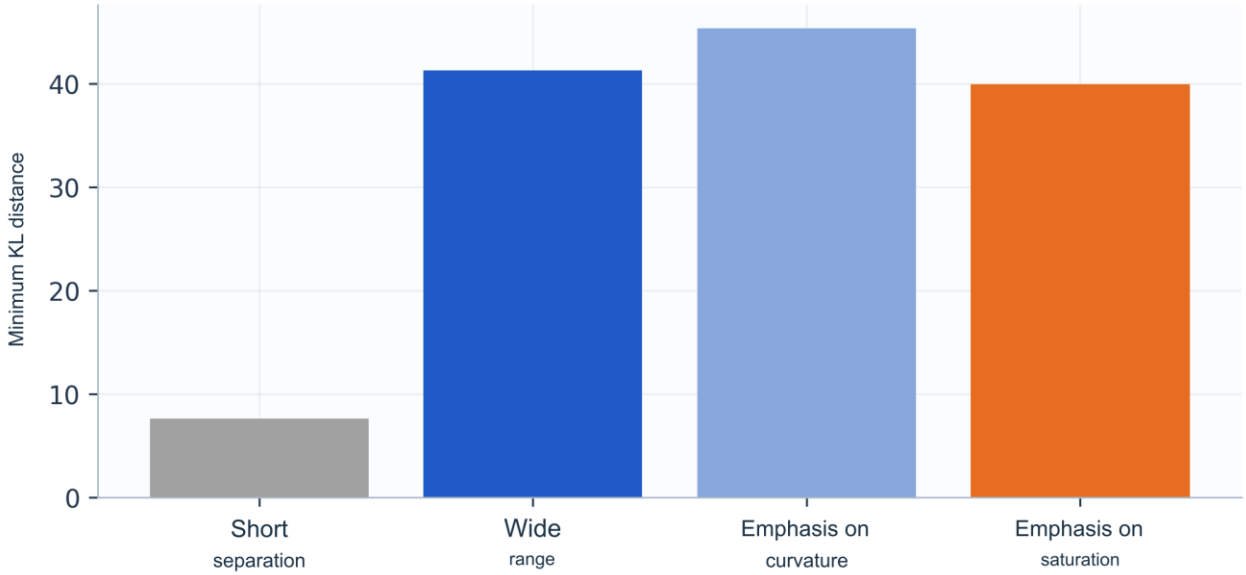


Figure 61. Numerical minimum KL distance of four protocols with the same budget 30 600 of registered events and a limited design background range. The columns compare only the listed options; KL is not a p-value.

Separate the search series from the confirming series

A search series is needed to study the device, detect unknown interference and select an adequate model. It allows changes to hypotheses if their origin is documented. The confirmatory series has a different task: to verify an already recorded prediction. Before opening it, the protocol, range of parameters, processing method, control observations and conditions for recognizing the result as inconsistent with the model are recorded.

The independence of confirmation is enhanced when the physical regime changes. A prediction for a different mass or shape provides more information about universality than additional repetitions of the former object. Predicting a new

sequence tests the temporal model. Playback on another installation experiences transfer beyond the specific environment. Neither of these options guarantees a fundamental discovery, but each closes off some possibility of attributing the result to a local feature.

An unexpected observation retains value even if it fails a predetermined criterion. It can be used to build the next version of the hypothesis. In this case, the result is honestly returned to the search phase. Such a discipline does not prohibit creativity: it makes a distinction between the moment an idea emerges and the moment when an idea first stands up to independent scrutiny.

Formal reasons to reject the hypothesis version

The spatial version is rejected when its fixed kernel and mass relation law do not describe the intended observations under any acceptable general parameters, and the joint verification procedure takes into account errors and multiple comparisons. The time-based single-exponential version is rejected when it does not predict delayed control sequences within reasonable uncertainties. These findings apply to specific versions and not to all possible additional processes.

The proposed detection method may also fail regardless of the truth of the physical hypothesis. If the addition of a valid background mechanism makes the signal precisely unidentifiable, the claim that this set of observations establishes its origin should be abandoned. If the required calibration accuracy is not available on the selected platform, this protocol is deferred. If a computational implementation violates the positivity of a state or unit, the model is first corrected and any bounds derived from the error are invalidated.

Avoiding generality is especially important when transferring between systems. If different platforms require incompatible fundamental parameters after a thorough environment check, you cannot enter a different intensity for each and keep the same name of the hypothesis. A new dependence law can be proposed, but it becomes a new version with its own predictions. It'll need another independent series, not a recycle of previous successes.

Result with or without residual effect

The absence of a significant additional signal leads to parameter limitations. It is necessary to publish the area of scale in which the experiment is truly sensitive, and the conditions on which the boundary is based. A family with arbitrarily weak intensity usually maintains an almost standard limit. Therefore, the formulation of the result must distinguish between exclusion of a specific area and evidence of the absence of any possible deviation.

If a residual is present, alternative explanations and the dependence of the conclusion on the model are first tested. The predicted spatial profile, temporal structure, and interobject transport are then examined. Strong evidence requires agreement between these parts, not just a small error of one amplitude. Particularly

valuable is a result that links two different observations in advance and withstands their joint testing without adding free parameters.

If the remainder disappears after improving the description of the environment, the research does not lose its meaning. The real mechanism was identified, the installation model was corrected, and the conditions for future tests were clarified. This outcome should be retained in the final report, rather than leaving only the last successful curve. A history of excluded explanations helps other groups avoid making the same mistake.

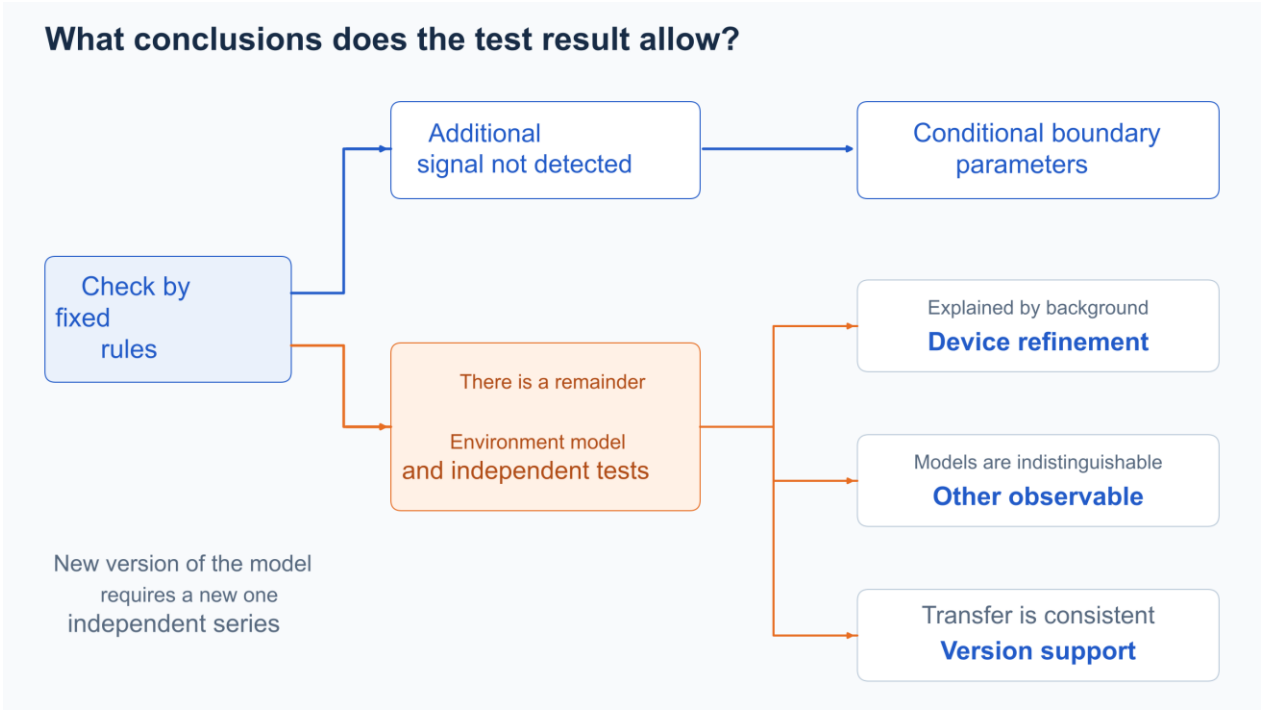


Figure 62. The absence of an additional signal provides a conditional limitation of the parameters in the sensitive area of the experiment. The remainder guides the investigation toward a model of the environment, independent tests, and prespecified transfer. The background explanation clarifies the device; exact indiscernibility requires another observable; a consistent migration supports a specific version only within the tested range. Neither exceeding a statistical threshold nor a small p-value by itself leads to the discovery of collapse. If a surprise is used to change the model, it is checked by the next independent series.

Completed result and next scientific task

The computer program produced several results of different nature. The published interference analysis is reproduced on external data. The illustrative spatial experiment is advanced from binary outcomes to overall parameter estimation, verified false discovery rates, and prediction of new conditions. A temporal example quantifies how finite control and registration error create a spurious white component. The gravity part relates the ideal phase to the noise threshold and measurable evidence.

There is also a negative result that determines the strength of any positive statements: expansion of the admissible background can destroy physical identification, even when the statistical test confidently rejects the original

background. Exact imitation results in channel matching and zero discriminability; the approximate mixture of noise scales shows the fragility of the narrow model on finite data. Both cases are retained in the final set because they limit the meaning of the discovered remainder.

The next independent scientific task should be set in relation to these results. For example, one can look for a measurable constraint in the surrounding field that precludes exact simulation and yet is tested independently of the signal being sought. Another option is to extend full statistical calibration to a continuous range of scales and experimentally established class of systematic effects. Each direction will require its own result and comparison with the literature; completeness of educational calculations does not replace evidence of scientific novelty.

The book thereby brings research logic to an executable procedure. Its outcome is not the promise of necessarily discovering new physics, but the ability to say in advance what distinguishes the chosen experiment, how often the analysis is wrong, and what additional observations might make the conclusion stronger. It is precisely this accuracy that makes further work cumulative: the following result is based on the reproduced calculation and the known limit of its applicability.

A physical inference becomes stronger when its numerical sensitivity and limit are known. In this program, both elements are presented together: completed checks are adjacent to obvious counterexamples of indistinguishability. Further expansion of quantum theory must maintain the same connection between formula, measurement, alternative and independent prediction.

What has been established and where inference ends

The state-to-observation sequence allows us to separate computational correctness from physical sufficiency. The same probabilities in the same basis do not mean the same state. The same ensemble equation does not define a single individual stochastic history. The same measuring channel for all permitted control, on the contrary, means precise operational indistinguishability: increasing the number of repetitions does not create the missing difference.

A spatial example provides a concrete development of this idea. The contrast of the three settings eliminates given constant and quadratic backgrounds, but remains sensitive to nonlinear backgrounds and geometric errors. The real trajectory changes the optimum: with triangular separation and convergence $d_0/rC \approx 3.06018$ instead of 2.09629 for a constant distance. Joint heating measurement helps against individual alternatives, but does not eliminate the exact match of the complete generator with an acceptable random pulse environment.

The connection with actual experiment is provided by the published sodium set: 95 scans, 3895 positions and 10 772 714 counts. Repeating the published author's procedure gives $\mu = 15.453634$, which is consistent with the published rounding. The specification and budget show the scale of time, geometry, gas composition and registration. They also explain why the reproduction number for fixed calibrations does not replace the analysis of all systematic uncertainties.

In a separate statistical experiment, the inference procedure itself is tested. A full search over a predefined scale grid is included in the zero calibration. Independent runs yield 56 false detections on 1000 zero sets at the nominal rate of 5%; the coverage of the profile area at the tested point is 946 out of 1000. For a weak introduced signal, detection occurs in the 841 of the 1000 series. The uncertainty of these shares and the limitation of the tested parameter range are given in chapter 21.

Expanding the background changes the physical meaning of the result. A mixture of ordinary spatial noise can consistently reject an overly narrow null model without objective collapse. The finite control pulse and readout mismatch can create a false white residue when fitting the ideal timing formula. These examples show how much of the inference is provided by the statistical test and how much is provided by the independent limitation of the physical alternative.

The gravitational example is brought from four phases to a mixed state, a witness from three measurement settings and finite statistics. With an explicitly chosen independent dephasing, the entanglement condition is obtained analytically and verified by matrix calculation. A comparison of the unitary interaction with the minimum noise of a given classical channel is carried out in the general domain of applicability. The conclusion about the mediator remains related to the premises of the compared theories, and the resulting numerical requirements remain related to the parameters of the learning experiment.

Further experimental work has clear outcomes: independent calibration of the medium, expansion of the range of geometries, verification of the transfer of general parameters, and comparison of specified dynamics according to the initial events. The book provides mathematical, numerical, and replication steps on which to build this work. A claim about new physics will require observations that stand up to the same detailed comparison with valid alternatives.

Appendix A Symbols and physical units

Common notation

Different sections use models of different levels. The matrix ρ always describes the state of an explicitly chosen system; it doesn't have to be pure. H is the Hamiltonian, $\hbar$ is Planck's constant divided by two π. In formulas with compound systems, the subscripts A and B indicate the subsystems, and Tr is the trace or partial trace when the excluded subsystem is specified.

The distance between branches is denoted by d or Δx. In the gravity example, d might represent the average distance between objects, and s their internal separation; the meaning is specified immediately before the calculation. This distinction is important: interobject distance and superposition size serve different physical roles.

The localization rate Γ has the dimension of inverse time. In the compact spatial model, A is the effective frequency, r_C is the correlation length. The base frequency λ_0 and the effective A are related only in an explicitly specified model and geometric approximation. These designations cannot be used as identical parameters without a mass coefficient.

In the diffusion model, D_{pp} has the dimension of the square of the momentum divided by the time. Therefore, D_{pp} $d^2/\hbar^2$ is the rate, and D_{pp}/m is the rate of change of the kinetic energy of one Cartesian degree of freedom. The transition to full three-dimensional energy requires taking into account all components and the accepted normalization.

In the temporal noise model, δω is the angular frequency, σ is its root-mean-square amplitude, τ_c is the correlation time. The damping exponent χ is dimensionless. The combination $\sigma^2\tau_c^2$ is also dimensionless, so it can multiply the ratio function T/τ_c. This simple check helps detect missing time multipliers.

In a sodium interferometer, d_g denotes the grating period, L is the distance between adjacent gratings, T_{13} is the time of flight from the first to the third. This eliminates confusion with the distance d between gravitating bodies. In the reanalysis, τe is the classicalization time with electron mass normalization, and $\hbar/\sigma q$ is the spatial length of its own convention; their connection with λ and rC is established by comparing the generators.

Checking limiting cases

A correct formula must pass a few simple tests. When the intensity of the added process disappears, the original forecast should be restored. With zero separation of the two spatial branches, the corresponding localizing contribution should disappear. At a sufficiently small distance, the saturated kernel must be consistent with its quadratic expansion.

For a Gaussian spatial kernel, small separation means d/r_C is much less than one. An increase in mass at a constant density increases body size; therefore it can take the system out of compact mode. You cannot simultaneously increase the mass indefinitely and save the formula of a point object without checking the geometry.

For noise with memory, the white noise limit requires specifying which combination of parameters remains constant. If the correlation time is reduced at a fixed variance, the integrated strength of the noise may disappear. If we preserve the area of the correlation function, we obtain a finite Markov contribution. Different limiting procedures correspond to different physical models.

Appendix B A concise glossary

States and measurements

Amplitude is a complex quantity used to calculate probability. If there are coherent alternatives, the amplitudes are added, after which the square of the modulus is taken. Amplitude is not a negative or complex probability of an observed outcome.

Coherence is the presence of phase connections relative to the selected set of alternatives. Its observability depends on the available measurements. In the density matrix, the corresponding connections are expressed by off-diagonal elements in the selected basis.

Decoherence is a reduction in available coherent connections when describing a selected system. In the standard theory, it can arise due to correlations with the environment. The term itself does not establish the fundamental irreversibility of the complete description.

Entanglement is a property of a composite state that cannot be represented as a convex mixture of tensor products of states of subsystems with non-negative weights whose sum is equal to one. The classical correlation of results in one basis alone is not enough to establish entanglement.

Collapse is a word with several uses. It can denote a conditional update of a state after a measurement result or a supposed objective physical process. The book clarifies the meaning: models of objective collapse are considered as separate dynamic hypotheses.

The visibility of interference is a measure of the depth of modulation of the observed pattern. Its reduction may depend on coherence, background counting and reading procedure. Physical interpretation requires a model of these contributions.

Noise and data inference

The Markov description is an approximation in which the chosen evolutionary model does not require explicit consideration of the environment’s memory of the previous history. Its applicability is related to the time scale and nature of the interaction; the word "Markovian" does not automatically mean fundamental.

Colored noise is noise with a nontrivial frequency dependence of the spectral power. It is characterized by temporal correlations. The specific type of spectrum must be specified and verified in the available range.

Identifiability is the ability to distinguish between parameter values based on selected observations. Structural unidentifiability means precise degeneracy of predictions; practical weak discriminability means insufficient accuracy with a non-zero difference.

The null model is the model against which the additional effect is tested. It must include known significant processes and uncertainties. Its rejection does not automatically select one particular alternative.

Systematic uncertainty is uncertainty associated with the calibration, response, conditions, or structure of the model. It does not have to decrease with a simple increase in the number of identical measurements.

Held-out testing is the evaluation of predictions under conditions not used to set up the model. It tests the transferability of parameters and helps detect overfitting, but its interpretation depends on how independent and informative the new conditions are.

The power of a test is the probability of rejecting the null model given a given alternative. It depends on the effect size, measurement design, and background assumptions. There is usually no single power number for all possible signals.

Coverage is the proportion of replicate data sets in which the constructed region contains the true parameter. Numerical verification at one point and with one generator does not prove correct coverage over the entire parameter space.

Profiling is the maximization of the likelihood of nuisance parameters, given a fixed parameter of interest. It takes into account the possibility of compensating for the effect of interest by allowing a change in the background, but does not add mechanisms that are missing in the model.

Kullback-Leibler divergence is a mathematical difference between given distributions, expressed here in nat. It is useful for comparing designs given the alternatives and resources selected; is not itself a p-value or probability of discovery.

Appendix C Reproducing the calculations

The source-materials package

The original public set of sodium measurements is located in data/pedalino_2026; the original archive and metadata are stored separately. For data and third party code, the attribution is CC BY 4.0.

Basic checks cover the spatial kernel, three-point combination, time integrals, and the gravitational example. Absolute and relative tolerances are specified for each. Additional calculations test two bases, instrumentation, stochastic histories, trajectories, and energy observations. The correspondence of the programs to these tasks is given in the accompanying instructions.

replicate_pedalino.py executes the original author's procedure on a working copy of the archive without making any numerical changes to the source code. platform_v02.py independently adjusts individual scans and calculates the conditional environment budget, specification and illustrative localization map. Their results are separated from the synthetic statistics_v02.py sets.

statistics_v02.py reproduces the full binomial procedure, zero runs, inserted signals, coverage, delayed checking and design comparison. control_v02.py calculates finite impulses in stationary Ornstein-Uhlenbeck noise. gravity_v02.py builds mixed state, witness, finite statistics, clock and comparison of gravitational dynamics.

spacetime_v02.py checks the conditional general law of spatial and temporal correlations of the Gaussian mass field: stationary and moving branches, extended body, agreement of the Fourier integral and the white-noise limit. This program is not a simulation of a new fundamental theory of collapse.

Execution procedure

Preparing the computing environment and commands for different operating systems are given in the accompanying instructions for the calculations.

Basic checks and foundations_v02.py are performed first. Next, replicate_pedalino.py is launched, followed by platform_v02.py, which uses the saved density. Space-time, statistical, temporal and gravitational calculations are independent of this order. The full repetition command and information about saved results are given in the instructions. Full Monte Carlo requires more time than constructing deterministic curves.

For random series, the initial state of the generator is fixed in the code. This allows a specific example to be repeated, but does not make the estimated error rate an exact mathematical constant: the final ensemble has its own uncertainty. Therefore, the numerical fractions are accompanied by intervals, and the analytical guarantees are separated from the frequencies in the selected simulation.

What does successful repetition mean?

The coincidence of the analytical expression with an independent numerical calculation verifies the implementation under its assumptions. A match with a published number checks the reproduction of the specified procedure. None of these checks automatically establishes the truth of the chosen physical mechanism.

For the sodium set, source hashes, number of points, checksums and resulting density are stored. For the synthetic experiment, the generation law, settings, thresholds and results of independent series are preserved. For geometric and temporal examples, approximation limits are indicated. In this way, the reader can distinguish between programming error, numerical error, statistical uncertainty, and limitations of the model itself.

Appendix D Technical derivations

Binomial likelihood and joint calibration

Let in the i-th setting from N_i independent binary trials there are k_i “plus” outcomes. Their probability p_i depends on physical and calibration parameters. The number of possible permutations of identical outcomes is equal to the binomial coefficient; multiplying the probabilities of individual trials gives the probability k_i. For independent settings, the product becomes a sum after logarithm. A separate calibration adds its own term ℓ_{cal} rather than fixing the unknown c without error.

For the used model $p_i = (1 + \exp(-z_i))/2$, the linear predictor z_i is written as $X_i\theta$ with fixed r_C. Its first coordinate a = −ln c is included in both the main data and the calibration. The A and local background values determine the remaining columns. The derivative of the probability is equal to $-\exp(-z_i)\,X_i/2$. Substituting the derivative of the logarithm gives the gradient used in the optimization; its independent verification is performed by central difference.

The expected information depends on the probability itself, so the same N does not mean the same accuracy for all settings. The given matrix describes the regular internal mode with a fixed structure of the model. At the boundary A = 0, the dependence on r_C disappears and regular circulation of the complete information matrix is not applicable. Therefore, the zero threshold of the chapter 21 is constructed by simulating the entire search, and not by the symmetric error of a non-existent length estimate.

$$\ell(\theta) = \ell_{\text{cal}}(\theta) + \sum_i [k_i \ln p_i + (N_i - k_i)\ln(1 - p_i)] + \text{const}$$

(A4.1) Terms that do not depend on parameters can be omitted only when comparing the same data.

$$\mathcal{J}_{ab} = \sum_i \frac{N_i}{p_i(1-p_i)} \frac{\partial p_i}{\partial \theta_a} \frac{\partial p_i}{\partial \theta_b}.$$

(A4.2) The calibration line is included in the same amount. For independent Gaussian external calibrations, their information matrix would be additionally added.

Minimum variance when excluding a given background

Consider the linear model y = Fβ + A s + ε, where Eε = 0 and Cov ε = Σ is positive definite. The desired linear estimate $\hat{A} = w^T y$ must be unbiased for any β. This requires $w^T F = 0$ and $w^T s = 1$. The variance is equal to $w^T \Sigma w$. The problem is to minimize the positive quadratic form under linear constraints, therefore, with a non-degenerate admissible direction, the solution is unique.

Its weighted projection onto the columns of F is subtracted from the signal. The resulting $s_\perp$ satisfies $F^T \Sigma^{-1} s_\perp = 0$. Selecting w proportional to $\Sigma^{-1} s_\perp$ automatically

eliminates the background. The normalization $w^T s = 1$ fixes the remaining factor. Since s differs from $s_\perp$ only by a vector from the background subspace, the denominator can be written in terms of $s_\perp$ on both sides. Substituting back into the variance gives the inverse weighted norm of the signal.

For three points $d_j^2 = j\, d_0^2$, j = 1,2,3, columns F are equal to a constant and d^2. The space of admissible contrasts is one-dimensional: the sum of the weights and their scalar product with (1,2,3) must disappear. The vector (1,−2,1) fulfills both conditions. It specifies the unnormalized contrast Q; to estimate A, it must be divided by the dot product with the waveform. For equal independent rate errors σ_R, the dispersion Q is equal to $6\sigma_R^2$.

If $s_\perp = 0$, the signal lies entirely in the allowed background. The inversion denominator disappears, and there is no unbiased finite variance linear estimator of A with these restrictions. A small non-zero value gives a large variance. Replacing the inversion with numerical regularization may improve the stability of the calculation, but does not create physical information: it introduces an additional constraint that should be named.

$$\mathbf{s}_\perp = \mathbf{s} - F(F^T \Sigma^{-1} F)^{-1} F^T \Sigma^{-1} \mathbf{s}$$

(A4.3) Linearly independent columns of F are assumed. Otherwise, an independent basis is first selected.

$$\mathbf{w} = \frac{\Sigma^{-1}\mathbf{s}_\perp}{\mathbf{s}_\perp^T \Sigma^{-1}\mathbf{s}_\perp}$$

$$\mathrm{Var}(\widehat{A}) = \frac{1}{\mathbf{s}_\perp^T \Sigma^{-1}\mathbf{s}_\perp}.$$

(A4.4) The shape s and covariance Σ must be specified before confirmatory testing. Their obscurity requires an additional layer of inference.

From Gaussian phase to Ramsey and echo

For pure dephasing, the random relative phase is $\phi_y = \int_0^T y(t)\delta\omega(t)dt$. If δω is a zero Gaussian process, any such linear combination is also Gaussian. The characteristic function gives $\langle \exp(i\phi_y) \rangle = \exp[-\mathrm{Var}(\phi_y)/2]$. Substituting the variance of the integral immediately leads to the double integral χ_y. Zero mean eliminates deterministic phase; a non-zero mean would have to be taken into account separately.

For Ramsey y = 1. The symmetry of the correlator allows the lower integration triangle to be doubled; the 1/2 multiplier disappears. The internal integral of the exponential is equal to $\tau_c(1 - \exp(-t/\tau_c))$. Subsequent integration over t gives $\sigma^2\tau_c^2[x - 1 + \exp(-x)]$, where $x = T/\tau_c$. The dimensions are checked by the product $\sigma^2\tau_c^2$.

For echo, the interval is divided in half. The contribution of each half is equal to half of the Ramsey construction of the corresponding duration, and the cross contribution changes sign. Denoting h = T/2, the correlation integral between the

halves is obtained as $\sigma^2\tau_c^2(1 - \exp(-h/\tau_c))^2$. Subtracting this contribution from the sum of the two within-half variances gives the expression χ_E in chapter 18. The same operation shows why the total white contribution $\gamma_w T$ is reduced in the logarithm of the visibility ratio.

The proof uses commuting phase interaction and ideal sign switching. Inside a finite transverse pulse, the coupling operator rotates and different moments of time may not commute. Then substituting an arbitrary smoothed scalar y(t) is not a universal fix. That is why the additional calculation uses the full three-component Bloch vector and the Hermite modes of the OU process.

$$\chi_R = \int_0^T dt \int_0^t ds\sigma^2 e^{-(t-s)/\tau_c}, \chi_R - \chi_E = 2\sigma^2\tau_c^2\left(1 - e^{-T/(2\tau_c)}\right)^2.$$

(A4.5) The difference in indicators directly gives the logarithm of the ratio of normalized visibility at the same white rate.

Why does coincidence of channels exclude discrimination?

For a fixed preparation ρ and measurement E, the probability of the outcome is equal to $\mathrm{Tr}[E\mathcal{E}(\rho)]$, where $\mathcal{E}$ is the channel of the selected interval. If two descriptions have the same channel for all valid preparations and controls, they give the same probability of each outcome. Equality does not depend on the number of repetitions: the distributions of the entire independent sample are also the same.

A sequence of measurements requires a stronger condition than the coincidence of one final state matrix. Between stages, the available instruments $\mathcal{J}_a$ operate, and the joint probability is equal to the trace of the composition of channels and instruments. If two mechanisms coincide at each such step for the entire allowed control, the equality of probabilities is proved by sequential substitution. For processes with memory, matching single-step channels is not enough on its own: matching full multi-temporal statistics is required.

The white random pulse medium and the chosen localization ensemble equation can have the same Markov generator on the system. For the same added control, their system channels are the same. An independent measurement of the environment would expand a variety of instruments and could destroy equality, but it does not belong to the original limited set of observations. The same applies to access to the hidden record of individual stochastic histories.

If the probabilities are equal, the log likelihood ratio for any set of outcomes is zero, and the KL distance is also zero. Given equal prior weights, no decision rule will beat random choice in this exact matching problem. The meaningful next question is what physically accessible extension of observations makes the distributions different. It requires a new calculation, and not an increase in the complexity of the previous classifier.

$$P(a_1, \ldots, a_n) = \mathrm{Tr}\left[\mathcal{J}_{a_n}\mathcal{E}_n \cdots \mathcal{J}_{a_1}\mathcal{E}_1(\rho)\right].$$

(A4.6) Composite expression for Markov sequential experiment. Processes with memory require a joint description of the system and memory or an equivalent multi-time process.

References

The list combines primary research and reference reviews. Numerical references in the text lead to bibliographic entries. Author's versions and journal publications of the same work are combined; preprints are indicated separately.

[1] M. Arndt, O. Nairz, J. Vos-Andreae, C. Keller, G. van der Zouw, A. Zeilinger. Wave–particle duality of C60 molecules. Nature 401, 680–682 (1999). Peer-reviewed experimental article.

DOI 10.1038/44348

[2] B.-G. Englert. Fringe Visibility and Which-Way Information: An Inequality. Physical Review Letters 77, 2154–2157 (1996). Peer-reviewed theoretical article.

DOI 10.1103/PhysRevLett.77.2154

[3] W. H. Zurek. Pointer basis of quantum apparatus: Into what mixture does the wave packet collapse. Physical Review D 24, 1516–1525 (1981). Peer-reviewed theoretical article.

DOI 10.1103/PhysRevD.24.1516

[4] W. H. Zurek. Environment-induced superselection rules. Physical Review D 26, 1862–1880 (1982). Peer-reviewed theoretical article.

DOI 10.1103/PhysRevD.26.1862

[5] J. S. Bell. On the Einstein Podolsky Rosen paradox. Physics Physique Fizika 1, 195–200 (1964). Peer-reviewed theoretical article.

DOI 10.1103/PhysicsPhysiqueFizika.1.195

[6] J. F. Clauser, M. A. Horne, A. Shimony, R. A. Holt. Proposed Experiment to Test Local Hidden-Variable Theories. Physical Review Letters 23, 880–884 (1969). Peer-reviewed theoretical article.

DOI 10.1103/PhysRevLett.23.880

[7] B. Hensen et al.. Loophole-free Bell inequality violation using electron spins separated by 1.3 kilometres. Nature 526, 682–686 (2015). Peer-reviewed experimental article.

DOI 10.1038/nature15759

[8] G. Lindblad. On the generators of quantum dynamical semigroups. Communications in Mathematical Physics 48, 119–130 (1976). Peer-reviewed theoretical article.

DOI 10.1007/BF01608499

[9] V. Gorini, A. Kossakowski, E. C. G. Sudarshan. Completely positive dynamical semigroups of N-level systems. Journal of Mathematical Physics 17, 821–825 (1976). Peer-reviewed theoretical article.

DOI 10.1063/1.522979

[10] M. F. Pusey, J. Barrett, T. Rudolph. On the reality of the quantum state. Nature Physics 8, 475–478 (2012). Peer-reviewed theoretical article with the author's version.

DOI 10.1038/nphys2309

[11] N. Gisin. Weinberg’s non-linear quantum mechanics and supraluminal communications. Physics Letters A 143, 1–2 (1990). Peer-reviewed theoretical article.

DOI 10.1016/0375-9601(90)90786-N

[12] U. Sinha, C. Couteau, T. Jennewein, R. Laflamme, G. Weihs. Ruling Out Multi-Order Interference in Quantum Mechanics. Science 329, 418–421 (2010). Peer-reviewed experimental article with the author's version.

DOI 10.1126/science.1190545

[13] H. Everett III. Relative State Formulation of Quantum Mechanics. Reviews of Modern Physics 29, 454–462 (1957). Peer-reviewed theoretical article.

DOI 10.1103/RevModPhys.29.454

[14] D. Bohm. A Suggested Interpretation of the Quantum Theory in Terms of Hidden Variables I. Physical Review 85, 166–179 (1952). Peer-reviewed theoretical article.

DOI 10.1103/PhysRev.85.166

[15] Sebastian Pedalino; Bruno E. Ramírez-Galindo; Richard Ferstl; Klaus Hornberger; Markus Arndt; Stefan Gerlich. Probing quantum mechanics with nanoparticle matter-wave interferometry. Nature 649, 866–870 (2026). Peer-reviewed experimental article.

DOI 10.1038/s41586-025-09917-9

[16] E. Aprile et al.; XENON Collaboration. Challenging Spontaneous Quantum Collapse with the XENONnT Dark Matter Detector. Physical Review Letters 136, 120201 (2026). Peer-reviewed experimental article.

DOI 10.1103/2jm3-4976

[17] Stefan Nimmrichter; Klaus Hornberger; Philipp Haslinger; Markus Arndt. Testing spontaneous localization theories with matter-wave interferometry. Physical Review A 83, 043621 (2011). Peer-reviewed theoretical article.

DOI 10.1103/PhysRevA.83.043621

[18] Bassano Vacchini. Theory of decoherence due to scattering events and Lévy processes. Physical Review Letters 95, 230402 (2005). Peer-reviewed theoretical article.

DOI 10.1103/PhysRevLett.95.230402

[19] Shaun Laing; James Bateman. Bayesian inference for near-field interferometric tests of collapse models. Physical Review A 110, 012214 (2024). Peer-reviewed theoretical article.

DOI 10.1103/PhysRevA.110.012214

[20] Davide Giordano Ario Altamura; Andrea Vinante; Matteo Carlesso. Improved bounds on collapse models from rotational noise of the Laser Interferometer Space Antenna Pathfinder mission. Physical Review A 111, L020203 (2025). Peer-reviewed analysis of existing measurements.

DOI 10.1103/PhysRevA.111.L020203

[21] Gian Carlo Ghirardi; Philip Pearle; Alberto Rimini. Markov processes in Hilbert space and continuous spontaneous localization of systems of identical particles. Physical Review A 42, 78–89 (1990). Peer-reviewed original theoretical article.

DOI 10.1103/PhysRevA.42.78

[22] Lajos Diósi. Models for universal reduction of macroscopic quantum fluctuations. Physical Review A 40, 1165–1174 (1989). Peer-reviewed original theoretical article.

DOI 10.1103/PhysRevA.40.1165

[23] Roger Penrose. On Gravity's role in Quantum State Reduction. General Relativity and Gravitation 28, 581–600 (1996). Peer-reviewed theoretical article.

DOI 10.1007/BF02105068

[24] Matteo Carlesso; Luca Ferialdi; Angelo Bassi. Colored collapse models from the non-interferometric perspective. The European Physical Journal D 72, 159 (2018). Peer-reviewed theoretical article.

DOI 10.1140/epjd/e2018-90248-x

[25] Lucia Hackermüller; Klaus Hornberger; Björn Brezger; Anton Zeilinger; Markus Arndt. Decoherence of matter waves by thermal emission of radiation. Nature 427, 711–714 (2004). Peer-reviewed experimental article.

DOI 10.1038/nature02276

[26] Klaus Hornberger; Stefan Uttenthaler; Björn Brezger; Lucia Hackermüller; Markus Arndt; Anton Zeilinger. Collisional Decoherence Observed in Matter Wave Interferometry. Physical Review Letters 90, 160401 (2003). Peer-reviewed experimental article.

DOI 10.1103/PhysRevLett.90.160401

[27] D. J. Bedingham; H. Ulbricht. Correlated random walks caused by dynamical wavefunction collapse. Scientific Reports 5, 13380 (2015). Peer-reviewed theoretical article with a proposal for experiment.

DOI 10.1038/srep13380

[28] Marco Hofmann; Barbara Drossel. Dephasing versus collapse: Lessons from the tight-binding model with noise. New Journal of Physics 23, 103025 (2021). Peer-reviewed theoretical article.

DOI 10.1088/1367-2630/ac2ae2

[29] Suroj Dey; Peter Barker; Animesh Datta. Testing Spontaneous Collapse Models with Coulomb Mediated Squeezing. arXiv:2604.21705 (2026). Preprint v1 from 23 April 2026.

DOI 10.48550/arXiv.2604.21705

[30] John F. Donoghue. General relativity as an effective field theory: The leading quantum corrections. Physical Review D 50, 3874–3888 (1994). Peer-reviewed theoretical article.

DOI 10.1103/PhysRevD.50.3874

[31] Tobias Westphal, Hans Hepach, Jeremias Pfaff, Markus Aspelmeyer. Measurement of gravitational coupling between millimetre-sized masses. Nature 591, 225–228 (2021). Peer-reviewed experimental article.

DOI 10.1038/s41586-021-03250-7

[32] Sougato Bose, Anupam Mazumdar, Gavin W. Morley, Hendrik Ulbricht, Marko Toroš, Mauro Paternostro, Andrew A. Geraci, Peter F. Barker, M. S. Kim, Gerard Milburn. Spin Entanglement Witness for Quantum Gravity. Physical Review Letters 119, 240401 (2017). Peer-reviewed theoretical proposal for the experiment.

DOI 10.1103/PhysRevLett.119.240401

[33] Chiara Marletto, Vlatko Vedral. Gravitationally Induced Entanglement between Two Massive Particles is Sufficient Evidence of Quantum Effects in Gravity. Physical Review Letters 119, 240402 (2017). Peer-reviewed information-theoretical argument and experiment proposition.

DOI 10.1103/PhysRevLett.119.240402

[34] Joseph Aziz, Richard Howl. Classical theories of gravity produce entanglement. Nature 646, 813–817 (2025). Peer-reviewed theoretical article from October 22 2025.

DOI 10.1038/s41586-025-09595-7

[35] Anirudh Gundhi, Giorgia Infantino, Angelo Bassi. Can classical theories of gravity produce entanglement?. arXiv:2604.19696v3, 7 August 2026 (2026). Preprint.

DOI 10.48550/arXiv.2604.19696

[36] Andrea Di Biagio. Gravity-induced entanglement is not a theory-independent witness of nonclassicality of the gravitational field. Physical Review D 114, 084050, 19 October 2026 (2026). Peer-reviewed theoretical article.

DOI 10.1103/r8ry-sp35

[37] Farhan Hanif, Debarshi Das, Jonathan Halliwell, Dipankar Home, Anupam Mazumdar, Hendrik Ulbricht, Sougato Bose. Testing Whether Gravity Acts as a Quantum Entity When Measured. Physical Review Letters 133, 180201 (2024). Peer-reviewed theoretical proposal.

DOI 10.1103/PhysRevLett.133.180201

[38] Nikolaos Mitrakos, Maria Papageorgiou, T. Rick Perche, Marios Christodoulou. When does entanglement through gravity imply gravitons?. Physical Review D 114, 025019, 24 July 2026 (2026). Peer-reviewed theoretical analysis.

DOI 10.1103/lq47-1hfg

[39] Don N. Page, William K. Wootters. Evolution without evolution: Dynamics described by stationary observables. Physical Review D 27, 2885 (1983). A peer-reviewed theoretical construct of conditional tense.

DOI 10.1103/PhysRevD.27.2885

[40] Ekaterina Moreva, Giorgio Brida, Marco Gramegna, Vittorio Giovannetti, Lorenzo Maccone, Marco Genovese. Time from quantum entanglement: An experimental illustration. Physical Review A 89, 052122 (2014). Peer-reviewed experimental illustration of the model on the polarization of two photons.

DOI 10.1103/PhysRevA.89.052122

[41] Ladina Hausmann, Alexander Schmidhuber, Esteban Castro-Ruiz. Measurement events relative to temporal quantum reference frames. Quantum 9, 1616 (2025). Peer-reviewed theoretical article from January 30 2025.

DOI 10.22331/q-2025-01-30-1616

[42] Dvir Kafri, Jacob M. Taylor, Gerard J. Milburn. A classical channel model for gravitational decoherence. New Journal of Physics 16, 065020 (2014). Reviewed model.

DOI 10.1088/1367-2630/16/6/065020

[43] Jonathan Oppenheim, Carlo Sparaciari, Barbara Šoda, Zachary Weller-Davies. Gravitationally induced decoherence vs space-time diffusion: testing the quantum nature of gravity. Nature Communications 14, 7910 (2023). Peer-reviewed theoretical article.

DOI 10.1038/s41467-023-43348-2

[44] Mike D. Schneider, Nick Huggett, Niels Linnemann. A demonstration that classical gravity does not produce entanglement. Classical and Quantum Gravity 43, 177001, 1 September 2026 (2026). Peer-reviewed theoretical article.

DOI 10.1088/1361-6382/ae6f62

[45] Klaus Hornberger; John E. Sipe. Collisional decoherence reexamined. Physical Review A 68, 012105 (2003). Peer-reviewed theoretical article.

DOI 10.1103/PhysRevA.68.012105

[46] Stefan Nimmrichter; Klaus Hornberger. Macroscopicity of Mechanical Quantum Superposition States. Physical Review Letters 110, 160403 (2013). Peer-reviewed theoretical article.

DOI 10.1103/PhysRevLett.110.160403

[47] Christian Arenz; Robin Hillier; Martin Fraas; Daniel Burgarth. Distinguishing decoherence from alternative quantum theories by dynamical decoupling. Physical Review A 92, 022102 (2015). Peer-reviewed theoretical article.

DOI 10.1103/PhysRevA.92.022102

[48] Gonzalo A. Álvarez; Dieter Suter. Measuring the Spectrum of Colored Noise by Dynamical Decoupling. Physical Review Letters 107, 230501 (2011). Peer reviewed research article.

DOI 10.1103/PhysRevLett.107.230501

[49] Jonas Bylander; Simon Gustavsson; Fei Yan; Fumiki Yoshihara; Khalil Harrabi; George Fitch; David G. Cory; Yasunobu Nakamura; Jaw-Shen Tsai; William D. Oliver. Noise spectroscopy through dynamical decoupling with a superconducting flux qubit. Nature Physics 7, 565–570 (2011). Peer-reviewed experimental article.

DOI 10.1038/nphys1994

[50] Gerardo A. Paz-Silva; Leigh M. Norris; Lorenza Viola. Multiqubit spectroscopy of Gaussian quantum noise. Physical Review A 95, 022121 (2017). Peer-reviewed theoretical article.

DOI 10.1103/PhysRevA.95.022121

[51] Leigh M. Norris; Gerardo A. Paz-Silva; Lorenza Viola. Qubit Noise Spectroscopy for Non-Gaussian Dephasing Environments. Physical Review Letters 116, 150503 (2016). Peer-reviewed theoretical article.

DOI 10.1103/PhysRevLett.116.150503

[52] Uroš Delić; Manuel Reisenbauer; Kahan Dare; David Grass; Vladan Vuletić; Nikolai Kiesel; Markus Aspelmeyer. Cooling of a levitated nanoparticle to the motional quantum ground state. Science 367, 892–895 (2020). Peer-reviewed experimental article.

DOI 10.1126/science.aba3993

[53] Rainer Kaltenbaek et al.. Macroscopic Quantum Resonators (MAQRO): 2015 update. EPJ Quantum Technology 3, 5 (2016). Peer-reviewed publication by the authors of the mission concept.

DOI 10.1140/epjqt/s40507-016-0043-7

[54] Andrea Smirne; Angelo Bassi. Dissipative Continuous Spontaneous Localization (CSL) model. Scientific Reports 5, 12518 (2015). Peer-reviewed theoretical article.

DOI 10.1038/srep12518

[55] Angelo Bassi; Luca Ferialdi. Non-Markovian Quantum Trajectories: An Exact Result. Physical Review Letters 103, 050403 (2009). Peer-reviewed theoretical article.

DOI 10.1103/PhysRevLett.103.050403

[56] L. Leppäjärvi, M. Sedlák. Postprocessing of quantum instruments. Physical Review A 103, 022615 (2021). Peer-reviewed theoretical article.

DOI 10.1103/PhysRevA.103.022615

[57] K. Jacobs, D. A. Steck. A Straightforward Introduction to Continuous Quantum Measurement. Contemporary Physics 47, 279 (2006). Peer-reviewed educational article.

DOI 10.1080/00107510601101934

[58] Ł. Cywiński, R. M. Lutchyn, C. P. Nave, S. Das Sarma. How to enhance dephasing time in superconducting qubits. Physical Review B 77, 174509 (2008). Peer-reviewed theoretical article.

DOI 10.1103/PhysRevB.77.174509

[59] Michał Horodecki, Paweł Horodecki, Ryszard Horodecki. Separability of Mixed States: Necessary and Sufficient Conditions. Physics Letters A 223, 1–8 (1996). Peer-reviewed theoretical article.

DOI 10.1016/S0375-9601(96)00706-2

[60] Tianfeng Feng, Vlatko Vedral, Chiara Marletto. Collapse-based models for gravity do not violate the entanglement-based witness of nonclassicality. Physical Review D 113, 104055 (2026). Peer-reviewed theoretical article.

DOI 10.1103/83rl-nygv

[61] Don N. Page, C. D. Geilker. Indirect Evidence for Quantum Gravity. Physical Review Letters 47, 979 (1981). Peer-reviewed experimental article.

DOI 10.1103/PhysRevLett.47.979

[62] Wassily Hoeffding. Probability Inequalities for Sums of Bounded Random Variables. Journal of the American Statistical Association 58, 13–30 (1963). Peer-reviewed mathematical article.

DOI 10.1080/01621459.1963.10500830

[63] Sebastian Pedalino; Bruno E. Ramírez-Galindo; Richard Ferstl; Klaus Hornberger; Markus Arndt; Stefan Gerlich. Probing quantum mechanics with nanoparticle matter-wave interferometry — Dataset and code. Zenodo, version v1, measurements April 2025 (2025). Open data and code, CC BY 4.0.

DOI 10.5281/zenodo.17502163

[64] Sebastian Pedalino; Bruno E. Ramírez-Galindo; Richard Ferstl; Klaus Hornberger; Markus Arndt; Stefan Gerlich. Supplementary Information to Probing quantum mechanics with nanoparticle matter-wave interferometry. Nature, supplementary material (2026). Supplementary material from peer-reviewed article, CC BY 4.0.

https://static-content.springer.com/esm/art%3A10.1038%2Fs41586-025-09917-9/MediaObjects/41586_2025_9917_MOESM1_ESM.pdf

[65] Björn Schrinski; Stefan Nimmrichter; Benjamin A. Stickler; Klaus Hornberger. Macroscopicity of quantum mechanical superposition tests via hypothesis falsification. Physical Review A 100, 032111 (2019). Peer-reviewed theoretical article.

DOI 10.1103/PhysRevA.100.032111

[66] Björn Schrinski; Stefan Nimmrichter; Klaus Hornberger. Quantum-classical hypothesis tests in macroscopic matter-wave interferometry. Physical Review Research 2, 033034 (2020). Peer-reviewed theoretical article.

DOI 10.1103/PhysRevResearch.2.033034

[67] Todd J. Green; Jarrah Sastrawan; Hermann Uys; Michael J. Biercuk. Arbitrary quantum control of qubits in the presence of universal noise. New Journal of Physics 15, 095004 (2013). Peer reviewed research article.

DOI 10.1088/1367-2630/15/9/095004

[68] Simone Manti; Nicola Bortolotti; Lajos Diósi; Kristian Piscicchia; Catalina Curceanu. Atomic correlation effects in collapse-induced spontaneous radiation. arXiv:2608.07205v1 (2026). Theoretical preprint.

DOI 10.48550/arXiv.2608.07205

List of figures

Explanatory diagrams and quantitative graphs are arranged in order of appearance in the text. The names lead to the corresponding pictures.

1. Interference and path mixture 7
2. Two-path interferometer and two outputs 9
3. Two density matrices 14
4. Two preparations in two bases 16
5. Same first result and different states after it 18
6. Object, device and environment 22
7. Accumulation of correlations with the environment 23
8. Two records and conditional selection of events 25
9. Conditional bars and full set of events 26
10. Two stations and four setting combinations 29
11. Correlations CHSH 30
12. Three paths, eight configurations and general normalization 37
13. Branch separation profiles 41
14. Two physical outputs and three types of recording 42
15. Four scales of one spatial experiment 47
16. Measuring path of sodium experiment 53
17. Conditional constraint map CSL 54
18. Spatial kernel and quadratic approximation 57
19. Same mass and different distributions of matter 59
20. Different individual stories of one ensemble 62
21. Particle inside the medium and measuring path 67
22. Residual gas budget 70
23. General movement and independent shifts of three lattices 72
24. Three-point contrast 78
25. Trajectory and contrast optimum 80
26. Three geometries and two different calibration errors 82
27. Spatial contrast and heating 88
28. Translational and rotational reading 89
29. Two probes: sum and difference channels 91
30. Two ways to check the published set 97
31. Published readings and independent fitting 99
32. Reproduced posterior density 101
33. Three ways to set the gravitational source 106
34. What connections need to be controlled between two small masses 111
35. Four joint alternatives of two masses 115
36. Geometry and gravitational phase 117
37. Three reading settings for one preparation 120

38. Noise and witness to entanglement 121
39. Four outcomes in three settings 123
40. Clock as part of a joint measurement 130
41. Conditional probabilities of quantum clock 133
42. One conditional slice and two sequential readings 134
43. Clock blur 136
44. Direct unitary connection and classical feedback 140
45. Comparison of gravity dynamics 146
46. Finite body size and form factor 150
47. General law and different conditions of two objects 152
48. Two branches at two points in time 157
49. Ramsey and echo with correlated noise 163
50. Ramsey, ideal echo and finite pulse 165
51. Estimation offset due to finite pulse 167
52. Two sensors, four series and common or difference phase 170
53. Limit of available information and new observation 175
54. Signal and background projection 176
55. Parameter profile and deferred check 180
56. Functional experiment architecture with variable partitioning 182
57. Stand with known phase influence 184
58. Full event route from preparation to independent verification 185
59. Two measuring channels and technical paths of common interference 187
60. Calibration of the complete search procedure 192
61. Comparison of four measurement designs 195
62. What conclusions does the test result allow? 197

Author and projects

Email: info@brenev.com

Author website: brenev.com

Mira website: mira.technology

Other projects: haraizen.tech

Telegram: https://t.me/Eudgenee